Synthèse de copolymères biodégradables et étude de leur nanostructuration en vue de l'obtention de matériaux poreux multifonctionnels

Nikola Toshikj

THÈSE POUR OBTENIR LE GRADE DE DOCTEUR DE L'UNIVERSITÉ DE MONTPELLIER

En Chimie et Physico-chimie des Matériaux

École doctorale Sciences Chimiques Balard

Unité de recherche de l'Institut Charles Gerhardt de Montpellier, UMR 5253

Synthèse de copolymères dégradables et étude de leur nanostructuration en vue de l'obtention de matériaux poreux multifonctionnels

Présentée par Nikola TOSHIKJ

Le 10 décembre 2021

Sous la direction
du Dr. Sébastien BLANQUER et du Pr. Jean-Jacques ROBIN

Devant le jury composé de

Christelle DELAITE, Professeur, Université de Haute-Alsace	Rapportrice
Daniel GRANDE, Directeur de Recherches, Université Paris-Est	Rapporteur
Hélène ANGELLIER-COUSSY, Maitre de Conférences, Université de Montpellier	Examinatrice
Christophe SINTUREL, Professeur, Université d'Orléans	Président du jury
Olivia GIANI, Maitre de Conférences, Université de Montpellier	Invitée
Jean-Jacques ROBIN, Professeur, Université de Montpellier	Directeur de thèse
Sébastien BLANQUER, Chargé de Recherches, Université de Montpellier	Co-encadrant de thèse

UNIVERSITÉ DE MONTPELLIER

To my closest and dearest family and friends

Sans la curiosité de l’esprit, que serions-nous? Telle est bien la beauté et la noblesse de la science : désir sans fin de repousser les frontières du savoir, de traquer les secrets de la matière et de la vie sans idée préconçue des conséquences éventuelles.“

Marie Curie

“And once the storm is over, you won't remember how you made it through, how you managed to survive. You won't even be sure, whether the storm is really over. But one thing is certain. When you come out of the storm, you won't be the same person who walked in. That’s what this storm is all about.“

Haruki Murakami

“Пирej е троскотна трева, а некои ја викаат и коштрева. Ама ти колку сакаш кошкај ја, корни ја, куби ја, таа пак не умира. Само малку да се допре до земјата, и пак ќе се фати, ќе оживи, ќе потера. Ништо не ја ништи таа трева.”

Петре М. Андреевски

Remerciements

Je tiens tout d'abord à remercier M. Jean-Jacques Robin et M. Sébastien Blanquer de m'avoir fait confiance et m'avoir donné l'opportunité d'effectuer cette thèse. Votre enthousiasme, encouragement, investissement et soutien scientifique mais aussi amical m'ont guidé durant ce projet. Je vous suis énormément reconnaissant et je n'oublierai jamais ces trois années passées avec vous.

Je tiens à remercier M. Daniel Grande et Mme Christelle Délaite d'avoir accepté à évaluer ce travail de thèse en qualité de rapporteurs. Je remercie également M. Christophe Sinturel, Mme Hélène Angellier-Coussy et Mme Olivia Giani pour avoir accepté à juger ce travail et être impliqués dans cette exercice. Je suis reconnaissant à tous les membres du jury d'avoir contribué avec l'expertise scientifique de chacun aux discussions enrichissantes que nous avons pu échanger lors de ma soutenance de thèse.

Je remercie également M. Patrick Lacroix-Desmazes en tant que responsable de l'équipe ICGM-D2 pour m'avoir accueilli au sein des différents locaux du laboratoire. Un grand merci à tous les permanents de l'équipe pour tout ce que vous avez faits pour nous (« les étudiants ») et pour votre investissement au bon fonctionnement du laboratoire.

Un grand merci aux personnes qui ont collaboré à mes travaux : Michel, un énorme merci pour ton aide précieux avec des innombrables clichés et analyses AFM ; Aurélien, merci pour ton aide avec la NMR ; Sylvain, merci pour le ''shape-memory'' ; Amine, merci pour la DSC ; Aurélie, merci pour les questions administratives. Je tiens à remercier Cansu Akkaya pour les grandes quantités de polymères synthétisés et pour tout ton travail fourni pendant ton stage. C'était bien de travailler avec vous.

Et bien sûr, cette thèse aurait été beaucoup plus difficile sans la présence de mes amis du laboratoire : Loona, Lucie, Paul, Tarek, Thomas, Ding Ding, Laura, Nina, Agnès, Zoé, Michel, Ariella (courage aux noveaux ;)) - Merci pour tous les moments passés dans et dehors du labo, pour votre énergie positive, les soirées, Porquerolles, Berthom, etc etc… ☺ Justine, Bastien, Sofia, Nicole, vous comptez là aussi ;).

Un profond merci à mes amis Angelica, Anatole, Cansu, Léa, Filip, Iva, Aneta, Ema, Nasti, Paul, Sami, Fanny, Maël, Yac, Marina, Martina, Sara…pour tous les souvenirs de Montpellier, pour la soirée de la soutenance et beaucoup beaucoup plus !

Un grand merci à mes amis en Macédoine (Фирма 3.14) : Ana, Sara, Aleksandra, Angela, Anja… qui étaient présents à mon aventure de thèse et à bien d'autres !

En fin, je remercie mes parents et mes grands-mères de m'avoir permis d'étudier toutes ces années ; Merci pour votre énorme soutien. Ви благодарам за сè !

TABLE OF CONTENTS / TABLEAU DES MATIERES

INTRODUCTION

CHAPTER I / CHAPITRE I

CHAPTER II / CHAPITRE II

CHAPTER III / CHAPITRE III

CHAPTER IV / CHAPITRE IV

CHAPTER V / CHAPITRE V

CONCLUSION

INTRODUCTION GENERALE

Introduction générale

La population mondiale compte 7.8 milliards d'habitants en 2021, avec des projections à plus de dix milliards au milieu du 21^{e} siècle. En raison de cette augmentation explosive de la population, le monde est confronté à plusieurs problématiques alarmantes telles que la pollution environnementale, les carences en nourriture, en ressources, en énergies ou encore, les problèmes de santé. La plupart des pays ont vu leur niveau de vie s'élever et leur consommation de produits manufacturés augmenter de façon importante ce qui s'est accompagné par la génération de volumes de déchets importants. En 2020, 367 millions de tonnes de plastiques ont été fabriquées dans le monde, avec un taux de production et de consommation qui continue de croitre. Le devenir de ces matériaux provoque incontestablement un impact nocif sur l'environnement.

Une des stratégies prometteuses pour réduire cet impact sur l'environnement est le recyclage des polymères. Même si des méthodes performantes de recyclage des matériaux ont été mises en œuvre, cette stratégie doit être encouragée encore plus fortement. Cependant, le recyclage de tous les types de polymères reste un défi majeur et ne peut pas être une solution unique à la pollution par les plastiques. C'est la raison pour laquelle, l'utilisation de matériaux dégradables devient indispensable. Les polymères dégradables sont définis comme des matériaux qui sont dégradés et catabolisés dans un environnement naturel, sans libération de substances nocives pour cet environnement. En termes généraux, il existe 5 mécanismes de dégradation des matériaux : i) la dégradation hydrolytique, ii) la dégradation enzymatique, iii) la dégradation oxydative, iv) la dégradation physique et v) la dégradation radiative. Même si une large gamme de matériaux polymères naturels est connue pour être dégradable, certains polymères synthétiques, tels que les poly(ester)s ou les poly(carbonate)s par exemple, peuvent présenter la même caractéristique de dégradation, tout en offrant une polyvalence des propriétés chimiques, physiques ou mécaniques, offrant ainsi un champ d'applications potentielles encore plus large. Étant conscient de la nécessité d'étudier et de développer davantage le domaine des polymères dégradables de synthèse, les polymères étudiés dans cette thèse appartiennent exclusivement de cette classe, ce qui constitue **un premier objectif de ce projet**.

La science des matériaux s'intéresse de plus en plus aux polymères poreux et les principaux efforts des chercheurs portent sur la maîtrise d'une porosité bien définie avec une surface spécifique élevée, une facilité de mise en œuvre, la possibilité de les fonctionnaliser. L'utilisation de matériaux organiques, voire de matériaux naturels et renouvelables, permet d'aboutir à des structures légères, contrairement aux matériaux poreux inorganiques. Ces matériaux structurés à façon peuvent répondre aux défis mondiaux en étant employés dans une large gamme d'applications : séparation/adsorption de gaz, traitement de l'eau, catalyse, stockage d'énergie, optoélectronique, biomédecine....

L'utilisation des polymères poreux remonte aux années 1930-1950s lorsqu'ils ont été employés comme résines échangeuses d'ions. Depuis, un progrès considérable a suivi, conduisant au développement de techniques variées de fabrication des polymères poreux dont les principales approches sont les *direct templating* et *direct synthesis*, l'auto-assemblage de copolymères à blocs (ainsi que des méthodologies légèrement moins employées comme la polymérisation en émulsion en phase interne, la polymérisation interfaciale ou les *breath figures)*. Ainsi, ces approches ont conduit à différentes structurations de polymères poreux présentant des pores aux échelles variées (Figure A). Néanmoins, comme présenté dans la Figure A, uniquement deux techniques permettent un contrôle reproductible du processus de génération de pores : l'auto-assemblage de copolymères à blocs pouvant conduire aux pores nanométriques, et les techniques prometteuses de fabrication additive tridimensionnelle (3D) permettant la création d'objets à taille micrométrique.

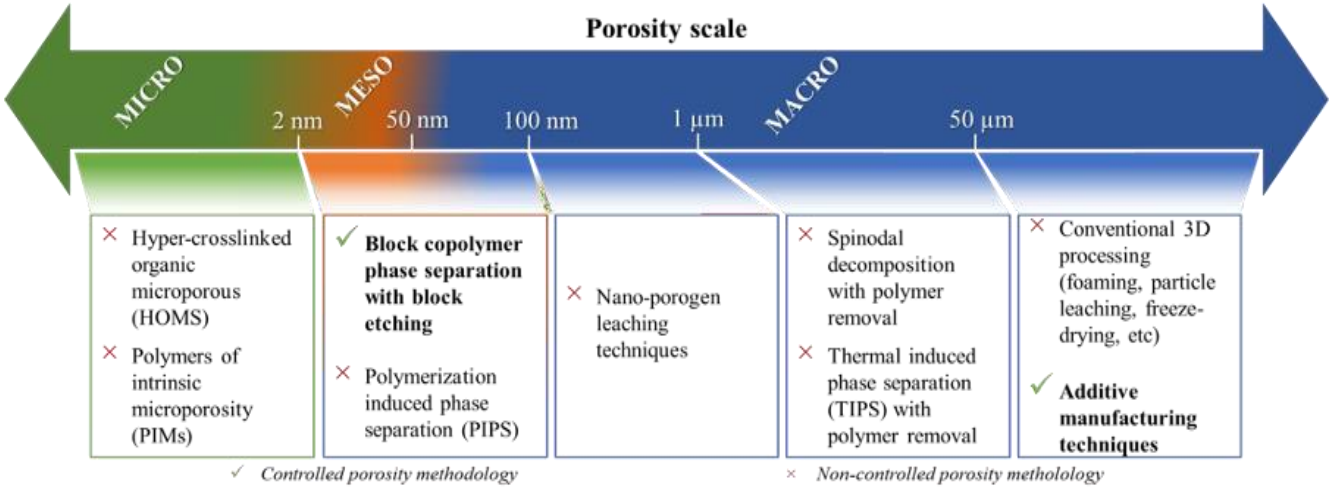

Figure A: Techniques employées pour la génération de matériaux polymères poreux (d'après les définitions IUPAC). Les matériaux poreux peuvent être classés selon la taille des pores : 2 nm de diamètre pour les microporeux, 2 à 50 nm pour les mésoporeux, supérieure à 50 nm pour les macroporeux.

Actuellement, un énorme enjeu est centré sur le développement de structures à porosités hiérarchiques bien définies en combinant les concepts et les méthodologies des différentes approches connues jusqu'à présent. Ces structures hiérarchiques possédant différents niveaux d'organisation sont particulièrement recherchées car elles permettent d'aboutir à une synergie entre les avantages de chaque classe de pores débouchant sur des structures à propriétés innovantes ciblant des applications encore plus avancées. Dans cette perspective, un axe majeur est en développement dans notre laboratoire avec pour objectif d'associer l'auto-assemblage de copolymères à blocs dégradables avec la fabrication additive 3D par photo-polymérisation afin de créer des polymères poreux à porosités hiérarchiques et contrôlées (Figure B).
C'est dans cet esprit que cette thèse s'inscrit, en se focalisant principalement sur l'**étude et la maitrise de la séparation de phases de copolymères à blocs dégradables** afin de générer une nanoporosité contrôlée.

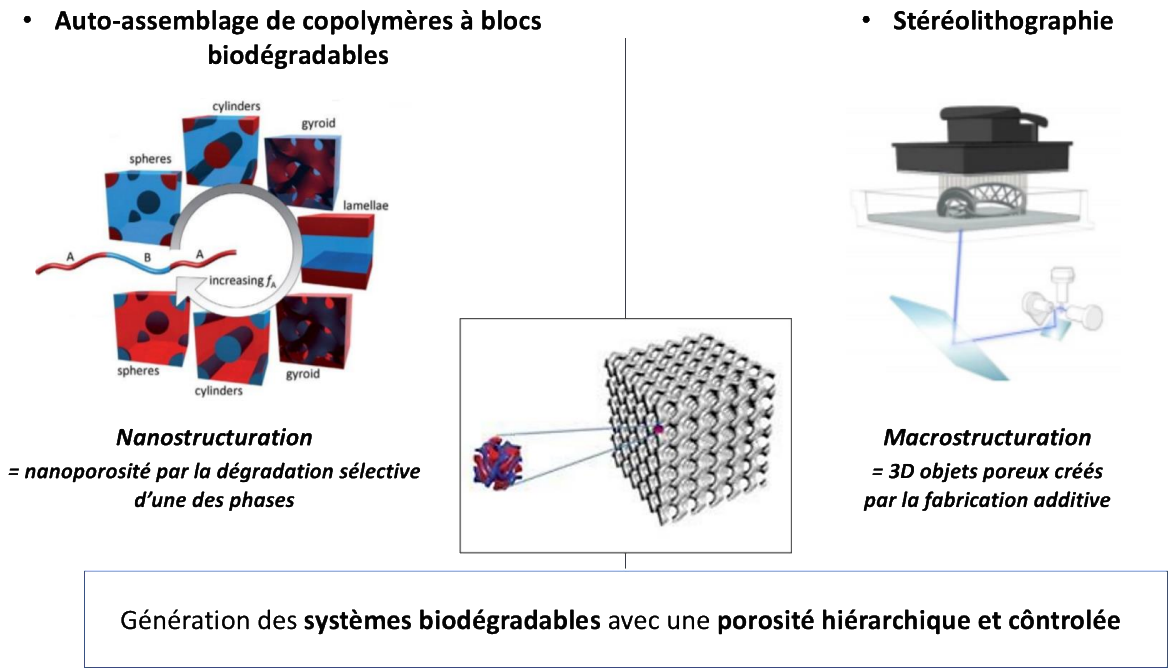

Figure B: Concept général du développement de structures tridimensionnelles à porosités hiérarchiques.

Même si l'auto-assemblage de copolymères à blocs est un outil puissant dans la science des matériaux modernes, des décennies de recherche ont été nécessaires pour fournir une base de compréhension de ce phénomène, en commençant par la caractérisation de différentes morphologies à l'aide de divers paramètres tels que : le critère d'interaction de Flory Huggins (χ), le degré de polymérisation (N), les fractions volumiques de chaque bloc (f) ainsi

que les différentes architectures de chaînes de polymères. Sachant que la séparation de phases des copolymères à blocs totalement dégradables est un domaine encore extrêmement peu exploré, cette étude constitue un défi complet allant depuis les aspects de synthèse jusqu'à l'étude de l'organisation des copolymères.

Dans cet objectif, **deux classes de copolymères triblocs** ont été étudiées et synthétisées : le poly(triméthylène carbonale)-*b*-poly(acide lactique)-*b*-poly(triméthylène carbonate) (PTMC-*b*-PDLLA-*b*-PTMC) et le poly(triméthylène carbonate)-*b*-poly(ε-caprolactone)-*b*-poly(triméthylène carbonate) PTMC-*b*-PCL-*b*-PTMC. Il s'agissait également d'étudier des assemblages de copolymères totalement amorphes ou bien, de copolymères à phase amorphe et semi-cristalline. Par ailleurs, nous avons cherché à stabiliser les systèmes obtenus après structuration afin de faciliter la génération de porosité et permettre une dégradation facilitée du bloc central. De plus, en gardant comme objectif d'utiliser le procédé de fabrication 3D, ces matériaux devaient permettre de coupler l'auto-assemblage des copolymères lors de la fabrication additive (ici, la stéréolithographie) avec la photo-polymérisation.

Le **chapitre I** du manuscrit se concentre sur une étude bibliographique des différents assemblages de copolymères à blocs étudiés jusqu'à présent, conduisant à des systèmes (nano)poreux. Cette étude s'est principalement focalisée sur des systèmes confinés dans des films minces, comme étudié dans la suite du projet. Les conditions permettant d'atteindre une séparation de phases suivie par la création d'une porosité optimale ont été détaillées pour de nombreuses associations de copolymères à blocs. Ce chapitre bibliographique a permis de mettre en évidence une absence d'étude sur l'auto-assemblage de copolymères à blocs entièrement dégradables dans le but de générer une porosité contrôlée.

Le **chapitre II** présente une approche simple et générale de synthèse de copolymères triblocs à partir du poly(acide lactique) comme macroamorceur par la polymérisation par ouverture de cycle (ROP). Les problèmes de faible réactivité du PDLLA du fait de la présence d'un alcool secondaire encombré ont été résolus en déterminant le système catalytique le plus approprié et capable de mener à des copolymères dont les compositions soient parfaitement contrôlées, c'est-à-dire, parfaitement du type tribloc, sans anomalie d'enchainement. En effet,

la synthèse de copolymères avec des architectures chimiques parfaitement contrôlées est un requis primordial pour une séparation de phases efficace.

Par la suite, le **Chapitre III** s'intéresse à l'étude de la séparation de phases dans les systèmes amorphes PTMC-*b*-PDLLA-*b*-PTMC. Des morphologies bicontinues de PTMC et PDLLA auto-assemblées dans des films minces produits par la technique de *spin-coating* ont été atteintes grâce à l'approche *d'annealing* par des vapeurs de solvant sélectif. L'étape de photo-réticulation a permis une stabilité mécanique lors de la dégradation hydrolytique sélective de la phase PDLLA, conduisant ainsi à une matrice poreuse innovante de PTMC.

Le **Chapitre IV** est axé sur l'étude du copolymère tribloc semi-cristallin PTMC-*b*-PCL-*b*-PTMC. Des études approfondies sur l'interrelation entre la cristallinité et la photo-réticulation ont permis l'établissement de propriétés à mémoire de forme au sein de ces matériaux. Simultanément, en jouant sur la cinétique de cristallisation à l'état fondu, un accès à une séparation de phases uniquement thermodynamique a été établie.

Finalement, le **Chapitre V** se focalise sur l'insertion de liaisons clivables dans le copolymère tribloc PTMC-*b*-PCL-*b*-PTMC, avec comme objectif d'apporter une réponse à la dégradabilité difficile du bloc central PCL. Un clivage efficace de ces liaisons est démontré et conduit à des altérations de la morphologie des films minces de ce copolymère ainsi que de leurs propriétés physico-chimiques.

CHAPTER I / CHAPITRE I

Introduction Chapitre I

Ce premier chapitre représente un état de l'art des systèmes auto-assemblés de copolymères à blocs utilisés pour la génération de matrices nanoporeuses. Des assemblages de copolymères à blocs complètement dégradables conduisant à des systèmes poreux n'ont à ce jour pas été rapportés dans la littérature, aussi, ils représentent un des points principaux des recherches menées dans ce projet de thèse. Ce chapitre bibliographique se focalise soit sur des systèmes de copolymères à blocs non-dégradables, soit sur des systèmes dont un seul des blocs n'est pas dégradable, en vue de générer une porosité. L'accent est mis sur l'étude de ces systèmes mis sous la forme de films minces comme cela a été étudié dans cette thèse. Deux points essentiels et inter-dépendants sont développés dans cette étude bibliographique : i/les conditions théoriques et expérimentales conduisant à l'auto-assemblage optimal de copolymères à blocs (di-, tri- ou multiblocs), ii/ les techniques et les procédés expérimentaux de génération de porosité. De multiples paramètres tels que la composition des blocs, le choix du solvant, les conditions d'*annealing*, la génération de pores par des méthodes douces, etc., sont discutés en vue d'aboutir au procédé idéal conduisant à des systèmes possédant des porosités les mieux ordonnées possible.

Ce chapitre rassemble donc les découvertes scientifiques dans le domaine de la nanostructuration et la nanoporosité de films minces obtenus à partir d'auto-assemblages de copolymères à blocs linéaires durant les dernières trois décennies. Ce chapitre I dans son intégralité fera l'objet d'une review scientifique soumise à un journal prochainement.

Chapter I

– The state of the art –

Chemical approaches for the generation of (nano)porous structures from phase-separated block copolymer thin films

Nanopatterns derived from block copolymer self-assembled thin films can find applications in areas such as photovoltaics, wave guides, photonic crystals, neuro-prosthetic technologies. This review offers a state of the art of i/ the methods to promote phase-separation in block copolymer thin-films followed by ii/ the approaches for porosity generation in these systems. Therefore, direct access to organic materials with balanced interfacial engineering and long-range pore size uniformity is reported herein.

1. Introduction

Nanoscale structured materials have demonstrated growing application potential in various domains such as separation and filtration systems, gas storage, catalysis, (bio)sensing, prospective lithography templating, etc. Their exclusive intrinsic properties have been stimulating for intense scientific research by both industrial and academic fields. Hence, top-down (X-ray, ion, electron, and laser etching) and bottom-up approaches (surfactants, colloids, lipids, and block copolymers) have been developed for achieving controlled nanoscale regularity. Among them, porous polymers are an energetic growing branch of the materials science due to the possibility to combine the properties of both polymers and porous surfaces. Hence, advantageous features such as easy processability, lightweight, high surface area, well-defined pores and switching between open and closed porous structures among many others can be pursued. Differing blocks of polymerized monomers connected between them with covalent chemical linkages constitute a special interesting class of polymer materials – the block copolymers (BCPs).

BCPs are well known to possess the ability to generate microphase separation and self-assemble into different morphologies. The self-organization of the BCPs in domains rich in one block from the domains rich in the other block results from the minimization of the contact energy between the two components due to their thermodynamic incompatibility. Phase-separation in macroscopic manner is prevented in these systems because of the covalent bond joining the dissimilar chains. Instead, nanoscopic phase organization is observed. The Mean-field theory suggests a value of the dimensionless combination parameter (χN) equaling to at least 10.5 in order to achieve a well-separated symmetric block copolymer system.[1] In this parameter, N stands for the number of volume segments capable to interact per polymer chains, while χ is the Flory-Huggins interaction parameter interpreting the energy cost upon contact of two block copolymer units. The χ parameters at room temperature of some of the polymers of interest are the following: χ=0.26 for PS-PDMS, χ=0.18 for PS-P2VP, χ=0.09 for PS-PI, χ=0.08 for PS-PEO and χ=0.06 for PS-PMMA.[2–6] Therefore, an attentive selection of the BCP molar mass must be made to meet the basic requirements for phase-separated system in function of the block copolymer nature. Practically, by controlling the BCP architecture, organized materials on the nanometer length scale can be achieved. As a result, depending on the block length ratio and the Flory-Huggins interaction parameter, the minor component can be present as spheres, cylinders, bicontinuous structures or lamellae fixed in the matrix of the majority part.

Therefore, BCPs containing a chemically degradable block or BCPs linked between with cleavable linkages among others, after selective elimination of the minority constituent are considered as serious templates for the preparation of nanoporous organic materials. Depending on the foreseen applications, these materials can be in the form of thin films, bulk monoliths or isoporous membranes. Significant quantity of reported scientific data on these subjects has been made since the initial review of Hillmyer in 2005.[7–12]

However, the simplest, most accessible, and economically attractive route for nanoscale patterning results from thin films of BCP self-assemblies. The self-assembly in thin films offers morphologies at times inaccessible in the bulk counterparts. Also, some etching techniques can result in limited minor block degradation in thicker or bulk samples. In addition, upon pattern transfer, nanoporous thin films can serve as isoporous membranes as well.[9,13,14]

In fact, the formation of nanoporous thin films is fully dependent on three main sections of parameters: molecular parameters (chemical nature of the covalently bonded blocks, the Flory-Huggins interaction parameter, the molar mass, the dispersity, and the volume fraction), their behavior in solution (solvent selectivity, miscibility, and viscosity) and processing parameters (evaporation time after solvent casting/spin-coating, casting conditions and temperature effect). Moreover, the quantity of defects in thin films is related to the values of χ parameter of the corresponding BCP assembly. Block copolymers with higher χ tend to minimize the appearance of defects due to better phase separation and are prone to achieve advanced long-range order. On the contrary, whilst generating phase-separated structures from block copolymers with lower χ, additional techniques to enhance long-range order and promote self-assembly are being highly used and appreciated. Controlling such parameters is a demanding task for reaching high pore density and uniform pore sizes. The latter present the highest objective in the elaboration of nanoscale thin film porous materials. Each self-assembled di- or triblock copolymer system requires specific strategy for successful pore generation while maintaining a stable matrix.

Consequently, the purpose of this review is to present, detail and discuss the chemical techniques and processes implemented till present, together with the optimal experimental conditions for the preparation of nanoporous thin films from self-assembled block copolymers. Specific accent is put on the methods of achieving well-separated self-assemblies leading to porous structures presenting long-range order within a mechanically stable structure, thus promoting potential applications.

2. Ozonolysis of polydienes

2.1 Nanoporous templates by ozonolysis of PS-b-PI

Dating from 1988, pioneering works for the preparation of ordered nanoporous films from BCP precursors were performed by Nakahama *et al*.[15,16] This research group started from synthesizing polyisoprene-*block*-poly((4-vinylphenyl)-dimethyl-2-pro-poxysilane copolymers by anionic living polymerizations. Afterwards, casted films of (PI-*b*-P4VPDM-*b*-PI) and (P4VPDM-*b*-PI-*b*-P4VPDM), whereby crosslinking the siloxane moieties of the PS and further ozonolysis of the PI phase, resulted in nanoporous crosslinked PS.

The ozonolysis was performed by soaking the film in dichloromethane solution containing 0.25 mmol of O_3 (at 40°C for 6 h). Weight measurements of the porous sample pointed towards 70% PI removal compared to the non-porous specimen. Simultaneously, significant decrease in the characteristic PI signals was evidenced by IR spectroscopy. The ozone firstly attacks the double bonds in the PI backbone, thus provoking chain scission, following an electrophilic reaction proceeding by the Creege mechanism.[17] A schematic interpretation of ozone impact on dienes is represented in Scheme I-1.

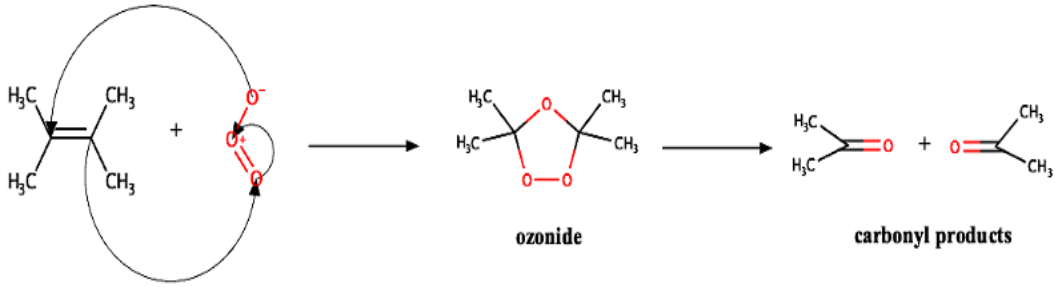

Scheme I-1: Ozonolysis of diene molecules.

In the meantime, ozone exposure crosslinks the PS, thus making the films insoluble. The PS was selected as the nanotemplate matrix due to its easy processability and satisfactory tensile strength below its glass transition, with the possibility to further enhance its mechanical properties by crosslinking, as represented in this case.

Prior to PI etching, lamellar microdomains were predominant in both films upon self-assembly of PI and PS phase. It was demonstrated that the block lengths had direct impact on the microdomain ordering and consequently in the width of the resulting pores. In a study of thin films from PS-PI blends, it was concluded that the phase-separation in this system occurs in the ultimate stages of the "spin-coating" process, where upon solvent quenching the structure is trapped in a non-equilibrium phase-separated morphology.[18] Depending on the mass fractions of the two parts, circular, non-circular or bicontinuous phase-separated morphologies were evidenced. Thus, to promote PS/PI phase-separation, the solvent annealing is preferred over thermal quenching due to the PI instability at temperatures above PS glass transition point.

Therefore, Hashimoto *et al*. in 1997 evidenced gyroid three-dimensional continuous nanochannels after ozonolysis of thin films of binary mixture of PS-*b*-PI block copolymer and PS homopolymer containing 62 wt. % of PI.[19] Blending PS homopolymer within the copolymer structure proved to enhance and control microdomain ordering. The films were casted from toluene solutions, since the latter is a neutrally good solvent for both blocks. Afterwards, ozonolysis was performed for 24 h. Later, they were immersed in ethanol for 24 h to remove cleavage-reaction carbonyl residues, demonstrating 100 % PI removal by NMR technique and weight measurements. Tsiang *et al*., further investigated the efficiency of ozonolysis when cleaving various minor block morphologies whilst preparing nanoporous thin films from PS-*b*-PI precursors.[20] The highest removal rate of the minor block after 24 h ozonolysis was reported for i/ isomeric PI precursors possessing the biggest content of 1,4-PI units among the two others (1,2-PI and 3,4-PI) and ii/ for lamellar PI microdomains. In fact, 90 % degree of ozonization (which corresponds to the effective removal of double bonds) was reported for this morphology, 80 % for the bicontinuous, 70 % for the cylindrical and 50 % for the spherical microdomains (Figure I-1). These values depended on the volume and the contact area of the domain accessible to ozone. Microscopy studies such as scanning electron microscopy (SEM), transmission electron microscopy (TEM) and atomic force microscopy (AFM) demonstrated porous PS with holes ranging from 20 to 30 nm, depending on the initial morphology, after extraction of the cleaved PI chains with ethanol.

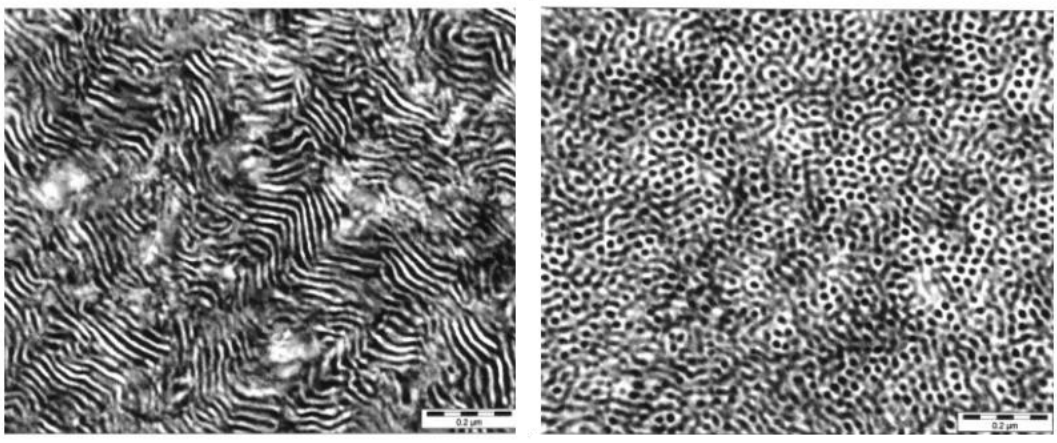

Figure I-1: TEM images of ozonated samples presenting initial lamellar (left) and bicontinuous morphology (right).[20]

2.2 Nanoporous templates by ozonolysis of PS-*b*-PB

In another study, Mansky *et al.* elaborated PS-*b*-PB block copolymers serving as precursors for the creation of porous PS thin films as lithographic templates.[21] Thin films of asymmetric PS_{23k}-*b*-PB_{10k} presented periodic arrays of PB cylinders oriented perpendicularly to the substrate. This orientation was achieved by spreading a drop of dilute polymer solution in toluene on the surface of de-ionized water bath, followed by evaporation of the solvent. If the polymer thin film was produced by spin-coating followed by solvent evaporation, PB cylinders parallel to the surface were obtained due to a minimized energy of PB blocks at the substrate and the free surface. In this case, enhanced perpendicular orientation could be achieved *via* thermal annealing at 115 °C for 12 to 24h, a temperature above the T_g (PS), giving mobility to the polymer chains. Successful removal of the minor PB block was performed by exposing the thin films to room temperature oxygen atmosphere containing 2% ozone for 4 h. Hence, butadiene fragments were removed by placing the sample in deionized water. TEM analysis of unstained films showed cylindrical pores of 13 nm with lattice constant of 27 nm.

2.3 Ozonolysis for the preparation of porous redox-responsive materials

PI etching from poly (ferrocenylmethyl methacrylate)-*block*-poly(isoprene) copolymers synthesized by anionic polymerization led to stimuli-responsive nanoporous materials.[22] The two blocks demonstrated excellent phase-separation properties, previously enhanced by slow dichloromethane evaporation from thin films followed by thermal annealing (155°C for 1h) in N_2 atmosphere. Diverse PI volume content in the di- and triblock copolymer architectures led to spherical, cylindrical, or lamellar morphologies that translated into controlled pores after PI ozone etching and ethanol extraction. The ferrocene component imparted redox mediated surface charge switching capability of the resulting nanoporous structure, potentially useful in separation methods or smart devices.

3. UV-degradation

Covalently linked poly(styrene)-*block*-poly(methyl methacrylate) diblock copolymers, synthesized *via* anionic polymerization (AP) or atom transfer radical polymerization (ATRP) have been widely investigated since the 2000s for the generation of nanoscopic templates.[23,24] Detailed investigations of their self-assembly and photonics technologies[25] inducing PMMA removal by UV irradiation, led to high-density storage,[26–29] optical[30,31] and antireflection coating[32] materials, as well as nanoporous membranes[33,34] from this widely available and easy processable block copolymer system.

3.1 Generation of porosity in PS-*b*-PMMA based systems *via* UV-etching

PS-*b*-PMMA are attractive block copolymers due to the different response of blocks to UV light.[35] Thus, while PMMA acts as negative photoresist, in the meantime, the PS network stands for positive photoresist. Therefore, an exposure to deep UV light causes PMMA degradation that generates the nanoporosity, but also simultaneously PS crosslinking which then chemically and mechanically stabilizes the PS phase. PS-*b*-PMMA spin-coated thin films are most often exposed to mercury UV lamps with emission length of 254 nm. More precisely, efficient PS crosslinking can be achieved with an irradiation of 25 $J.cm^{-2}$ while 3.4 $J.cm^{-2}$ is widely sufficient for chain scission of PMMA homopolymer.[36] However, it is important that the irradiation intensity is adequate enough so that the scission occurs precisely in the junction spot between the two blocks. Consequently, PMMA can be easily removed by solvent rinsing. A selective solvent for PMMA extraction can be acetic acid followed by deionized water cleanse.

Generally, hexagonally close packed pores with diameters ranging from 14 to 50 nm and separation distances from 24 to 89 nm were obtained after PMMA UV-etching and extraction. [37] For instance, nanoporous films derived from PS-*b*-PMMA presenting 15 to 25 nm pores were proven effective in the size-exclusion of biomacromolecules, such as ferritin (with diameter of 12 nm).[38] Moreover, large distribution of pore sizes with differing pore spacings could be achieved with thinner films (≈ 42 nm).[39] On the other side, films too thick could potentially lack long-range order and demonstrate elongated pores. Hence, UV-etching as a method for generation of nanoporous structures remains performant uniquely on submicrometer thick films.

Regarding the pore functionalization, Ito *et al.* used the electrostatic cyclic voltammetry technology on PS-*b*-PMMA thin films immobilized on gold substrates to evidence carboxyl (-COOH) groups present on the cylindrical pore surface.[40] They suggested that the surface carboxyl groups were probably formed during UV irradiation of the sample, in the presence of oxygen traces. Moreover, a covalent functionalization of these groups through EDC-mediated amidation was developed, resulting in pores with amine terminated molecules.[41] Such functionalization opened perspectives to chemical sensing and catalysis of these nanoporous PS thin films.

3.2 Methods for enhancing phase-separation phenomena in PS-*b*-PMMA thin films

Prior to minor block removal, the varying experimental conditions leading to optimized phase-separation phenomena of PS-*b*-PMMA are important to be discussed. Generally, out of particular interest are block copolymers presenting cylindrical self-assembled microdomains given that the elimination of the minor component can lead to nanopore arrays suitable for the foregoing applications. Cylindrical orientation normal to surface can be achieved in different ways depending on the nature of the material. In case of PS-*b*-PMMA nanometer range thin films, microdomain alignment can be ensured by the means of compensating interfacial interactions by anchoring a random copolymer as neutral substrate surface prior to spin-coating of the thin film.[42] On the other side, micrometer range thicker films can present aligned domains via the application of external electric fields.[43]

The random copolymer brushes method as a way of controlling polymer-surface interactions[42] is further detailed. PS-*r*-PMMA, prepared by free-radical polymerization with broad molar mass distribution is end-grafted on native silicon oxide layer. For that purpose, firstly the copolymer solutions in toluene (1% w/v) are spin-coated onto clean silicon wafers, leading to 60 nm thick films. Afterwards, the polymer coated silicon substrates are subjected to thermal annealing at 140 °C, a temperature over the T_g of both PS and PMMA, thus permitting terminal OH groups to be grafted to the native oxide layer of silicon. Once the non-grafted polymer is removed by toluene rinsing, the remaining layer presents a thickness of 5 nm. The interfacial energies of both PS and PMMA with the brushes is balanced for PS mole fraction of 0.6. The optimal conditions for achieving random-copolymer neutrality are profoundly detailed in the study by Ham *et al.*, defining more specific data for achieving cylindrical and lamellae microdomain orientations.[44]

The impact of electric fields in microdomain ordering in block copolymer systems has been also investigated.[45,46] In the case of 10-30 μm PS-*b*-PMMA thick films, an alignment of the microdomains normal to the field lines, resulting from the different interfacial interactions between the copolymer and the electrode surfaces has been reported for a precise field strength of 11.5 $V.\mu m^{-1}$.[43] The possibility to achieve such microdomain orientation advantageously did not depend on the film thickness, unlike the previous method.

Furthermore, thermal annealing has been used for promoting long-range ordering and microphase separation in PS-*b*-PMMA thin films. In the case of PS-*b*-PMMA (of 67 000 $g.mol^{-1}$) thin films, the optimal thermal annealing conditions of 24 h exposure at 165 °C resulted in structures with improved quality thus optimized long-range order and uniformity.[39] Higher temperatures up to 200 °C led to films with improved microdomain ordering with reduced 1 h annealing periods. On the contrary, short annealing times at the same temperature resulted in low long-range order and irregular pore shapes, due to the insufficient mobility of the chains. On the other side, solely spin-coating of the block copolymer solution on glass substrates, without employing thermal annealing, resulted in short-range phase-separation.[32] The access to fully developed cylindrical PMMA microdomains in PS matrix was restricted in this case, due to the fast solidification of both blocks at room temperature (below their glass transition points).

3.3 Physico-chemical parameters influencing the phase-separation phenomena in PS-*b*-PMMA thin films

The film thickness, the block copolymer molar mass, the solvent annealing, and the type of substrate for spin-coating were reported to influence the ordering of the microdomain phase-separation in PS-*b*-PMMA thin films. In a study concerning the first parameter,[47] in thin films developed from asymmetric PS-*b*-PMMA block copolymers (of 46 100 $g.mol^{-1}$, with PMMA block of 21 000 $g.mol^{-1}$ and lattice spacing (L_0) of 36 nm) it was evidenced that perpendicular orientation of PMMA domains was achieved only for two precise values of film thickness (t): when $t \sim L_0$ and $t \sim L_0/2$. Such demonstrated values signify that phase-organization in PS-*b*-PMMA systems is possible even in ultrathin films (below the lattice spacing value), allowing applications in advanced lithographic processes.

Due to their modest Flory-Huggins interaction parameter of 0.06 (at room temperature),[48] high-molar mass of PS-*b*-PMMA (M_n > 35 000 g.mol^{-1}) are required in order to achieve well-separated morphologies. Meanwhile, it was established that the copolymer molar mass also impacted the size of the phase-separated microdomains.[37] The lateral ordering of the domains (achieved by an electric field herein) decreased with increasing molar mass of the copolymer. Therefore, the upper limit, where the long-range ordering was lost, is evidenced for PS-*b*-PMMA with 295 kg.mol^{-1}. Depending on the molar mass of the block copolymer, cylindrical microdomains ranging from 12 to 40 nm can be aimed with separation distances from 20 nm to 80 nm, respectively. Hence, it can be concluded that the microdomain size increases proportionally with the number of segments N in the polymer. The different molar mass of the block copolymers was not an obstacle to successfully orient the microdomain perpendicularly to the surface.

Well-ordered hexagonally packed PMMA cylinders in thin films of symmetric PS-*b*-PMMA can be also developed when the nature of the solvent for vapor annealing and its duration are precisely defined.[49] For example, in the study of Yu *et al.*, only films of 19, 26 and 38 nm thickness (which is less than half of the lamellar repeat spacing (t~ $L_0/2$)) led to hexagonally packed cylinders of PMMA with diameter of 43 nm. The films needed to be exposed to solvents with vapors selective of the PMMA phase, such as chloroform and acetone for 60 h ($\chi_{chloroform\text{-}PMMA}$=0.39, $\chi_{acetone\text{-}PMMA}$=0.18; where the smaller value corresponds to a bigger the affinity between the polymer and the solvent).–This formation of controlled microphase separated domains is due to the enhanced mobility of the PMMA phase upon penetration of acetone or chloroform. Film thickness bigger than $L_0/2$ and prolonged exposure of solvent vapors led to perpendicular lamellar microphase morphology or additional metastable structures.

The substrate roughness also influenced the orientation of microdomains.[50] Thus, when asymmetric cylinder forming PS-*b*-PMMA thin films (with f_{PMMA}=0.3) were spin-coated on gold substrates covered with nanoscale grains and under controlled thermal annealing conditions (190 °C for 150h), vertical orientation of the cylindrical PMMA domains was evidenced. On the other side, in the same annealing conditions, the high affinity of PMMA to oxide-coated Si substrate led to cylindrical microdomains oriented perpendicularly to the surface, which then explains the reason why this substrate is preferred for spin-coating PS-*b*-PMMA thin films.

3.4 Alterations of microdomain spacing by PS-*b*-PMMA blending with PMMA homopolymers or PS-*b*-PMMA short chain block copolymers.

In a research reported by Jeong *et al*.,[51] promoting microdomain orientation in 300 nm films was achieved by simple addition of PMMA homopolymer in asymmetric PS-*b*-PMMA copolymers, thus making the use of electric fields not mandatory. A volume fraction of added PMMA homopolymer and copolymer (f_{PMMA}) equal to 0.26 in 71 kg.mol^{-1} PS-*b*-PMMA was sufficient to promote large degrees of long-range order and enhance the perpendicular orientation of the domains. Likewise, further modification on the microdomain size can be done *via* blending of PS-*b*-PMMA block copolymers with larger amounts (10 to 20 wt %) of PMMA homopolymers or with another PS-*b*-PMMA block copolymers with shorter chains prior to spin-coating.[52] Interestingly, blending with both low and high molar mass PMMA homopolymers lead to an increase in size of the cylindrical domains. Higher molar mass *P*MMA had the tendency to segregate in the middle of the cylindrical microdomains, while lower molar mass PMMA presented uniform distribution in the microdomain. On the other side, blends with short PS-*b*-PMMA lead to decrease in cylindrical domain size. The latter can be due to the positioning of the symmetric diblock copolymer at the domain's interfaces, leading in a decrease of the interfacial tension and increase of the stretching free energy.

3.5 Homopolymer addition as a method for decreasing pore size

Controlling PMMA UV-degradation and specifically microdomain ordering upon homopolymer addition opened the possibilities to reduced pore sizes, unachievable in traditional PS-*b*-PMMA systems. Therefore, generation of sub-10 nm porosity in PS-*b*-PMMA thin films can be attained upon adding homopolymers of PMMA,[53] PEO[54] or PLA[55] to the block copolymer prior to spin coating followed by homopolymer removal.

3.5.1 PMMA Homopolymer addition

In the case of PS-*b*-PMMA/PMMA blends, there are two ways to prepare nanoporous structures. The first method succeeds in complete removal of the PMMA phase (homopolymer and PMMA block in copolymer) by UV irradiation followed by acetic acid rinsing, while the second method solely removes PMMA homopolymer by acetic acid solvent rinsing (Figure I-2).[56] Interestingly, by the second approach, the pore diameters can be decreased down to 6-8 nm, with an increase in the microdomain spacing.

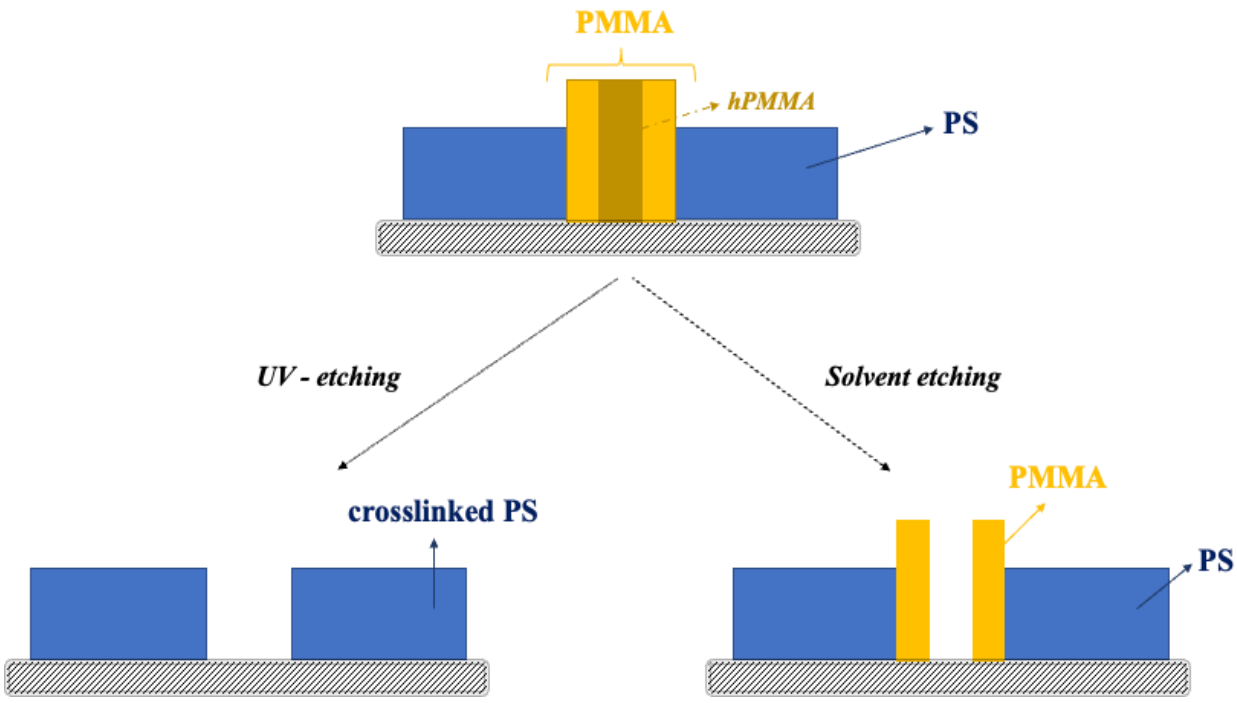

Figure I-2: Schematic representation for obtaining nanoporous templates, by the two distinct approaches from PS-*b*-PMMA/PMMA blends.

In the beginning of the study, firstly the PS-*b*-PMMA/hPMMA mixtures were spin-coated on neutralized surface with random PS-*r*-PMMA copolymer brushes (with f_{PS}=0.6). Following the reasoning presented in the aforementioned 3.4 section, microphase separation in another study by Jeong *et al.*, occurred when the homopolymer molar mass was considerably higher than the one of the corresponding block.[56] Thus, films of PS-*b*-PMMA containing 10 wt % PMMA homopolymer in the mixture, resulted in 6 nm pores upon PMMA homopolymer removal and array of nanopores of 22 nm upon removal of both PMMA homopolymer and block of the copolymer. Nevertheless, the pores produced in this way demonstrated thermal

instabilities. Upon annealing at temperatures higher than glass transition points of PS and PMMA, the pores were replaced by islands or holes on the surfaces. Even at room temperature most of them disappeared after several months. Ozone crosslinking of the PS matrix, performed upon exposure of the thin films to a low flow rate (0.6 $cm^3.min^{-1}$) of ozone/air (20:80) at 17 °C for 30 min, was proposed as a method for the material stabilization.[57] Therefore, the crosslinked PS matrix allowed easy removal of the homopolymer, leading to thermally stable pores even upon annealing at high temperatures. The PMMA homopolymer was removed once the sample was immersed in acetic acid for 4h. Afterwards, the pores were stabilized by annealing at 170 °C for 4h. In this case, lasting nanopores with diameters from 6 to 18 nm were achieved with their size increasing with the initial amount of PMMA homopolymer in the mixture. Upon additional UV-treatment, the PMMA copolymer part was further removed, leading to a material with pore sizes up to 32 nm.

The inner morphology of the generated pores can be well visualized through transmission electron microtomography (TEMT) imagery.[53] Thus, complete PMMA removal from 70 nm thin films of PS-*b*-PMMA/PMMA mixtures led to ideal cylindrical pores spanning the entire film thickness. On the other side, while only the PMMA was removed by acetic acid extraction, the generated pores were of funnel-shaped morphology, with smaller diameter on top and larger diameter on the bottom of the film. The latter is due to the bigger extension of the PMMA chains while they are being pulled out of the bottom of the film.

Microfiltration membranes (MF) with ultrahigh virus selectivity[33] can be produced upon transferring 300 nm thick films of PS-*b*-PMMA/PMMA onto supporting MF polysulfone membrane *via* buffered HF solution. These membranes with 15 nm narrow pores, resulting after PMMA removal on the top of a supporting layer, demonstrated high sensitivity and flux for the separation of human pathogens. In another case,[34] the top separation layer consisting of 160 nm thick films of PS-*b*-PMMA block copolymers led to 17 nm nanopores upon PMMA removal *via* UV and acetic acid treatment. Herein, the pores were oriented perpendicularly to the surface near the top and the bottom of the film, while inside the film, parallel and perpendicular orientations of the pores were observed. Such orientation proved much more efficient filtration of viruses than the previous one. The nanoporous membrane, with the polysulfone bottom layer acting as mechanical support and thanks to crosslinking of the PS phase, demonstrated excellent resistance to organic solvent and harsh conditions such as high temperatures and strong acidic or basic environment.

3.5.2 PEO Homopolymer addition

Initial studies of blending PEO structures within PS-*b*-PMMA BCP were reported on Au-PEO nanoparticle blends.[58] The latter were evidenced to enable the direction of self-assembly *via* solvent annealing in high relative humidity atmosphere. Thereupon, Park *et al.*, reported PEO homopolymer blends (5 wt % in respect to the BCP) within PS-*b*-PMMA, which enhanced the perpendicular to substrate cylinder orientation (Scheme I-2).[54]

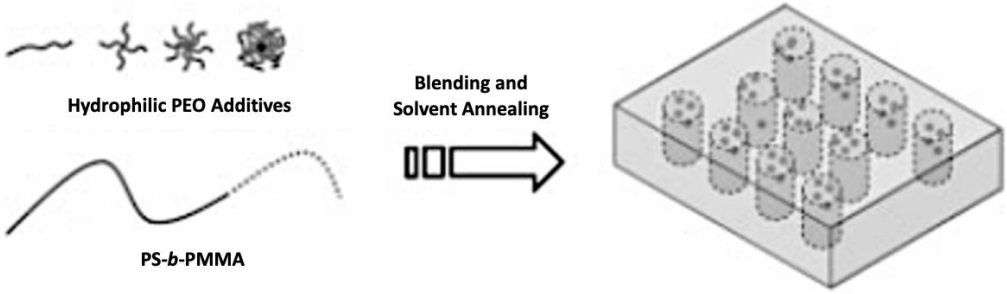

Scheme I-2: PEO blending and solvent annealing under high relative humidity approach for achieving highly ordered PMMA cylinders in PS matrix.[54]

Thus, high molar mass PEO with branched architectures enhanced this type of microdomain separation with high lateral ordering, while low molar mass linear PEO did not produce any effect. In fact, the normal to surface PMMA orientation was stimulated by the hydrophilic PEO interaction with water vapor under high humidity solvent vapor annealing (SVA) conditions (detailed in the 4.1.4 section). Because PEO and PMMA are highly compatible and miscible, the PMMA hydrophilicity consequently increased. Thus, in the absence of PEO, parallel to surface PMMA orientation was observed in this study. UV-treatment and acetic acid rinsing resulted in ordered nanoporous thin films.

3.5.3 PLA homopolymer addition

Moreover, in the case of PLA homopolymers, depending on the molar mass of the additional homopolymer and the system composition, the specific core/shell morphology could be achieved.[55] Blends of PS-*b*-PMMA (of 101 kg.mol^{-1} with f_{PMMA}=0.3 and PLA of 16 kg.mol^{-1}) were spin-coated onto modified silicon wafers and solvent-annealed in THF atmosphere (good solvent for PMMA and PLA). Precisely, this composition resulted in PMMA cylinders

containing the PLA phase thus minimizing the surface energies between the most incompatible PS/PLA pair.[59] PLA hydrolysis (presented in the following part of the review) resulted in 6 nm porous domains. UV-etching of PMMA gave access to second level of porosity, with pore diameters larger than those present in usual PS-*b*-PMMA system.

3.6 Ozone crosslinking as a method for decreasing pore size

Apart PMMA block UV-degradation or acetic acid solvent rinsing of the added homopolymer, ozone crosslinking of PS-*b*-PMMA thin films has been also reported for achieving pores with reduced sub-10 nm diameter.[60] Upon ozone exposure, the PS phase is being crosslinked while PMMA remains intact. Thus, covalent coupling of the adjacent polymer chains provokes volume shrinkage upon crosslinking. Therefore, PS-*b*-PMMA thin films reduced in size upon ozonation at 17°C for defined time periods, followed by thermal annealing which induced the shrinkage. Pore sizes of 3 and 8 nm were obtained for exposure time to ozone of 4 and 30 min, respectively.

3.7 PS-*b*-PMMA-*b*-PEO triblock copolymer system

Back in 2006, Hawker *et al.* investigated the behavior of ABC triblock copolymer system synthesized *via* controlled living radical polymerization, with PS as the major constituent while PMMA and PEO were the minor components.[61] Thin films demonstrating phase-separated morphologies were produced by spin-coating benzene polymer solutions on silicon substrates followed by solvent annealing in benzene atmosphere with elevated relative humidity (70 to 90 %). High level of humidity (> 70%) was afterwards reported as being essential for achieving phase-separated structures with high degree of lateral ordering in PEO-containing BCPs.[62] Moreover, the obtained morphologies depended directly on the molar mass of the minor block components. Hence, the structured core-shell arrangement, resulting from the decreased miscibility between PMMA and PEO upon increasing of their molar mass, was achieved for BCPs containing PMMA of 6 kDa and PEO of 5 kDa. Effective UV-cleavage of PMMA was possible uniquely for this type of arrangement, thus leading to well-controlled hexagonal array of porous cylinders with diameter between 10 and 15 nm. On the other side, when PEO and PMMA were miscible and appear as cylinders in the PS matrix, the photochemical degradation of PMMA was not complete and no template was achieved.

4. Hydrolysis of polyesters

Hydrolysis of poly(lactic acid) (PLA) is one of the widely used methods for production of nanoporous structures, especially for nanolithographic templating. Hillmyer *et al.*, initially reported PS mesoporous monoliths from PS-*b*-PLA block copolymers synthesized by two steps polymerization procedures – anionic polymerization of styrene followed by controlled ring opening polymerization (ROP) of D,L-lactide.[63,64] Initially, PLA degradation as a method for obtaining nanoporous systems, was made on monolithic samples. Afterwards, the same protocol was adapted on thin films. Thus, the method consisting of immersing the samples in 0.5 M NaOH aqueous methanol solution at 65°C, proved effective in both cases.[63,65] The samples being placed at a temperature above the T_g(PLA) but below the T_g(PS) resulted in main-chain cleavage of the PLA chains by surface erosion mechanism due to the unstability of the ester bonds in basic conditions.[66,67] Meanwhile the PS stayed intact while the PLA degradation product (sodium lactate) being soluble in the solution, is completely removed without damaging the matrix. A brief visualization of PLA degradation mechanism is presented on scheme I-3.

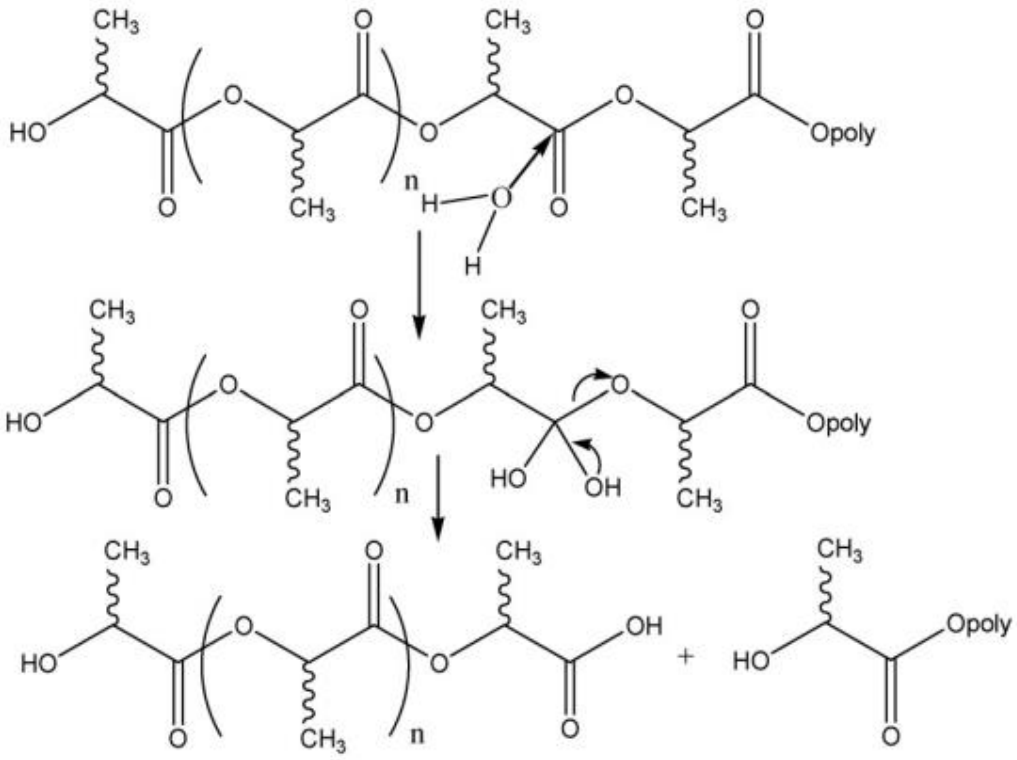

Scheme I-3: PLA hydrolysis in alkaline conditions.[69]

Not long ago, Sarkar *et al.* demonstrated effective PLA etching with another reagent, the trifluoroacetic acid (TFA), proven efficient for the pores generation in 2 mm PS-*b*-PLA thick films.[68]

However, prior to PLA etching, particular attention was devoted to the study of microdomain ordering in the PS-PLA system. The PS-*b*-PLA block copolymer belongs to a segregation regime with intermediate strengths between the two components, with the Flory-Huggins interaction parameter $\chi_{PS\text{-}PLA}$ equal to 0.14 at 110 °C. In monolithic samples, sinusoidal shear alignment of the melt-state PS-*b*-PLA gave macroscopic ordering of cylinder-oriented PLA domains parallel to the flow direction and oriented in plane of the sample. The cylindrical morphology in the bulk state was possible for PS-*b*-PLA block copolymers presenting f_{PLA} ranging from 0.21 to 0.43.

Nevertheless, contrary to monolithic samples, self-assembly of block copolymers in thin films is more complex and strongly affected by the presence of two interfaces: the air/film and the film/substrate ones. The methods for enhancing phase-separation, the conditions influencing this phenomenon, as well as the resulting porosity are reviewed in the following part.

4.1 Phase-separation and generated porosity in PS-*b*-PLA thin films

Thin films of PS-*b*-PLA can be easily prepared by spin-coating or casting procedures. Once again, among the various phase-separated morphologies, cylinder forming block-copolymers (*C*) have been of particular attention while targeting specific applications such as: membranes, templates for nanowire arrays or pattern transfer to another bottom-line substrate. Nanoporous films with cylindrical holes can be obtained by selective etching procedure of the previously oriented normal to surface (*C)* macrodomains.

In terms of characterization, nanoporous PS thin films can be examined *via* GI-SAXS and microscopy techniques such as AFM, TEM and SEM. Film thickness can be measured by ellipsometry methods. Successful PLA removal can be also evidenced through Raman spectroscopy, by the disappearance of the relevant PLLA bands at 870 and 1770 cm^{-1}, assigned to the C-COO and C=O stretching modes, respectively.[70] Imaging the free surface is possible after removal of the sacrificial block and the internal structure of the film is visible *via* cross-sectional analysis.

However, there is an information lacking about the structure of the sample, notably the topology of porosity. Hence, in 2011, Sinturel *et al.*, adjusted the Environmental Ellipsometric Porosimetry (EEP) for optimized investigation of porosity in polymer thin films.
Nevertheless, the main challenge stayed in firstly controlling the polymer interface interactions and inducing direct cylindrical microdomain ordering normal to surface *($C_{\perp}$)*, beneficial to the applications listed above.

4.1.1 Effect of thermal annealing on the PS-PLA phase-separation

Hillmyer *et al.* reported thin films with PLA cylinders oriented normal to surface at polymer-air interface during thermal annealing.[71] In their study, chlorobenzene solutions of 92 kg.mol^{-1} PS-*b*-PLA (with PLA volume fraction of 0.36) were spin-coated (2000 rpm) on silicone substrates with native oxide layer. Following, the films were thermally annealed up to 240 °C (above the transition temperatures of both blocks and the order-disorder temperature (T_{ODT}) for PS-PLA of 170 °C, as suggested by SAXS)[72] for times up to 48 h. Due to the strong similarities in the surface energies between PS and PLA, the preferential wetting at the polymer-air interface was avoided resulting in the most energetically favorable $C_{\perp}$ orientation.[73] The thermal annealing gave mobility to the crystallizing PLA-block parts, driving them to assemble into the most thermodynamically favorable shape. By these means, perpendicular to surface orientation of PLA cylinders was achieved, independently on the film thickness and while using variety of substrates (single-crystal, polycrystalline, hydrophilic, and hydrophobic ones). These films were further used to prepare porous templates by combined two-step PLA degradation: firstly, immersion of the film in NaOH solution followed by short (10 s) O_2-reactive ion etching (RIE) to make the pores span the entire film thickness. The RIE is a dry-etching method employing chemically reactive plasma for materials removal when deposited on specific wafers.[74] It has been demonstrated to influence the surface properties of polymer films, which is useful in the nanopatterning approach.[75,76]

4.1.2 PS-matrix crosslinking toward porous structure stabilization when employing thermal annealing

However, pore collapse was noticed in some cases when porous films were heated up to 200°C. Preferential crosslinking of the PS matrix prior to PLA removal was depicted as an idea to outpace this problem. Thus, enhanced stabilization of nanoporous structures from microphase separated PS-*b*-PLA thermally annealed thin films was reported in a study dating from 2005 by Russell *et al.*,[77] where thermally crosslinkable benzocyclobutene (BCB) groups were statistically incorporated in the PS matrix by previous random copolymerization. Thin films from (PS-*r*-BCB-*b*-PLA) were prepared by spin-coating of 1 wt % chlorobenzene polymer solution on gold substrates. The PLA volume fraction in the block copolymer systems were of 0.24 and 0.36. The thermal crosslinking of BCB groups was performed at 200 °C preceded by thermal annealing of the thin films at 170°C. The crosslinking did not alter the cylindrical normal to surface orientation of PLA domains, as evidenced by AFM. The PLA hydrolysis in basic conditions was performed by immersion of the film in 0.5 M NaOH water/methanol solution (50/50 v/v) at room temperature for 7 h, followed by washing cycles with methanol and water to remove the remaining base. Thus, after minor component etching, thanks to the matrix crosslinking, the resulting porous structure did not collapse even in benzene or THF exposure for 3 days. Furthermore, the degradation of PLA resulted in the presence of hydroxyl groups on the crosslinked cavities, as the first example of functionalized porosities from PS-*b*-PLA thin films.

4.1.3 Impact of solvent choice on the PS-PLA phase-separation

Nevertheless, because the PLA phase is being sensitive to thermal annealing, possibly leading to structures presenting defects, possible degradation and morphology disorganization, other approaches for microdomain ordering were pursued. In a study reported by Ho *et al.*, the effect of solvent evaporation upon spin-coating of thin films from PS-*b*-PLLA was investigated. They stated perpendicular cylinders of PLLA in PS-*b*-PLLA thin films obtained *via* selective choice of appropriate solvents for the polymer solution.[72] Two main conditions were attested to strongly influence the microdomains ordering: the solvent miscibility between the blocks and the effect of the solvent evaporation rate. The desired $C_{\perp}$ orientation was achieved by spin-coating of 1.5 wt % polymer solutions from PS-selective solvent with intermediate evaporation rate such as chlorobenzene (vapor rates of 12 mmHg at RT).

They noticed that selective solvents (chlorobenzene) promote phase-segregation, while neutral solvents (1,2-dichloro ethane) diminish it. Furthermore, the perpendicular morphology was favored by the regulated permeation of the solvent in the block copolymers during its evaporation. Thus, the perpendicular morphology is easier to be achieved for thinner samples due to the formation of the perpendicular hexagonally packed cylinder domains ($HC_{\perp}$) on the entire film thickness, in the direction of the maximum solvent-concentration gradient (Figure I-3A). Simple hydrolytic removal of the $HC_{\perp}$ PLA phase led to nanopatterned templates with cylindrical nanochannels spanning the entire film thickness as evidenced by field emission scanning electron microscopy (FESEM) images.

A mechanism for cylinder orientation upon solvent evaporation from 8 wt % toluene solution casted PS-*b*-PLA films was proposed from Phillip *et al*.[78] They suggested that open atmosphere fast drying of the so-casted films was required for perpendicular orientation of the cylinders, while slow evaporation gave parallel orientation (Figure I-3B). This statement allows the conclusion that the perpendicular cylinder orientation is kinetically trapped non-equilibrium structure.

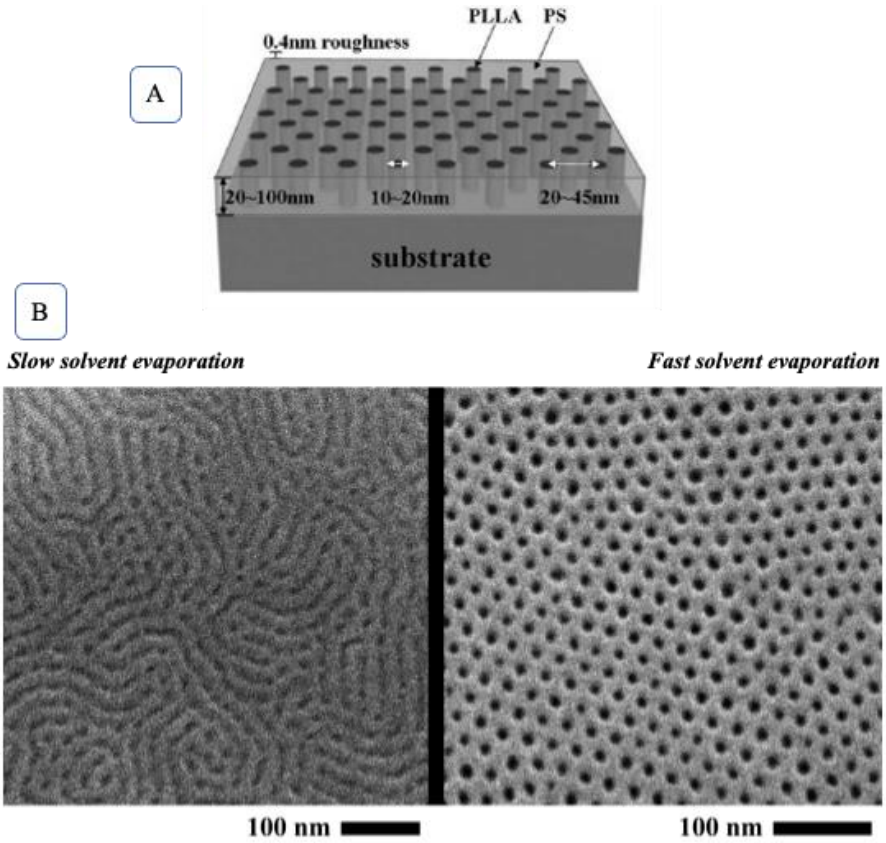

Figure I-3: (A) Illustration of PS–*b*-PLLA nanopattern prepared by spin coating of thin-films,[72] (B) Influence of the speed of solvent evaporation on the resulting nanoporous thin films after PLA etching - Fast evaporation is required for perpendicularly oriented cylinders.[78]

4.1.4 Solvent vapor annealing as the ideal method for enhancing phase-separation in PS-b-PLA thin films

Russel *et al.* had previously introduced and developed the theory of solvent vapor annealing (SVA) as an approach for ordered morphologies in PS-*b*-PEO thin films.[79]

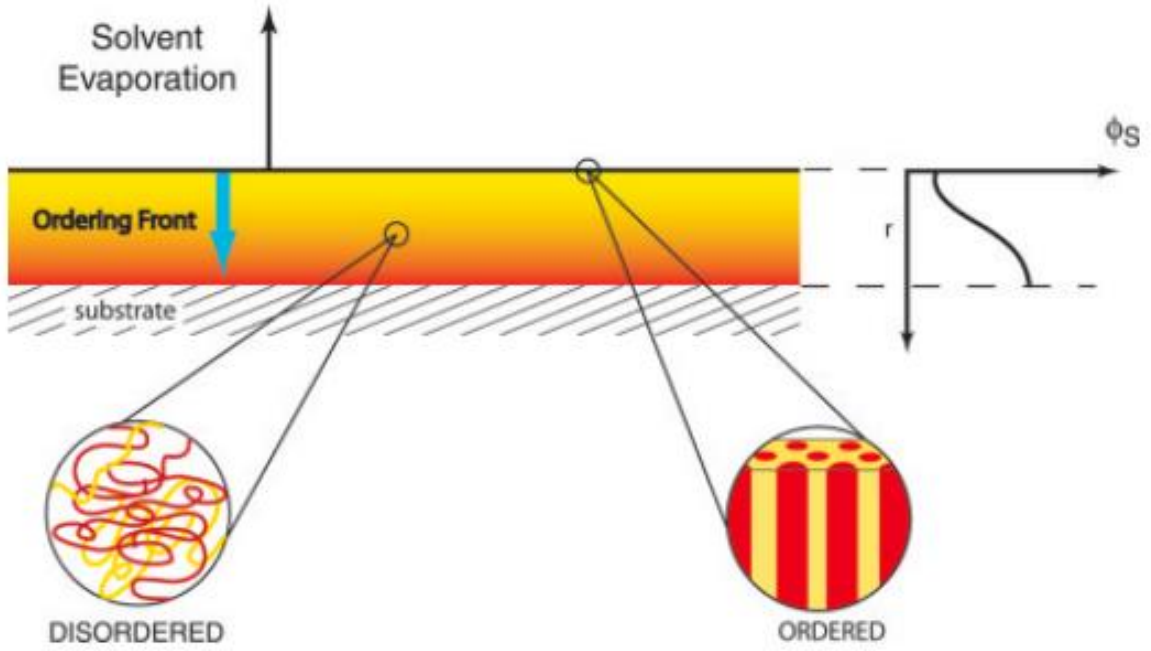

Figure I-4: Schematic representation of the effect of solvent evaporation (solvent annealing) on the microphase separation in block copolymer thin films, as established by Russel *et al*.[79]

Due to the lowest solvent concentration on the thin film surface, the BCP undergoes ordering into phase separated structures. However, going to the bottom of the film, the solvent concentration staying high, the film is still in its disordered state. As the solvent evaporates, a gradient of its concentration is established, proportional to the depth of the film (*r*) and oriented normal to the surface. Hence, an ordering front starts propagating upon solvent evaporation, going from top to the bottom of the film, resulting in ordered arrays of cylindrical microdomains (Figure I-4).[79]

Following this study, the influence of vapors of various solvents was studied on spin-coated thin films from PS-*b*-PLA.[80] By these means, the thermodynamic self-assembly of the blocks is combined with lyotropic transitions taking place whilst the film is transforming from the swollen to the dry state.[81] Firstly, thin films were made by spin-coating of 20 $mg.ml^{-1}$ chlorobenzene solutions of 90 $kg.mol^{-1}$ PS-*b*-PLA (with f_{PLA} of 0.34), presenting cylinder type morphology in the bulk state. Afterwards, the films were placed in closed desiccator with saturated solvent vapor pressure at 20°C. The influence of the type of the solvent and the annealing time were investigated in these cylinders forming BCP. The optimal well-ordered perpendicular normal to surface PLA morphology was obtained with vapors of THF (neutral solvent for both blocks) during 4 h. For instance, longer SVA periods of 7 h led to parallel to surface orientation of the microdomains due to fast reorganization kinetics because of the elevated vapor pressure of THF in the chamber (176 mmHg). PLA selective solvent (acetone) gave no organized morphologies, while PS selective solvent (chlorobenzene) granted cylinder domains perpendicular to surface after long annealing times of 60 h.

In a following study, Leighton *et al.* fully optimized and discussed the SVA conditions for ultra-fast ordered morphologies and nanolithography applications from PS-*b*-PLA, independently of the block copolymer synthesis, molar mass or composition.[82] Baruth *et al*. even managed to produce purpose-built chamber for controlled solvent vapor annealing of block copolymer thin films.[83] This progress represents a major scale-up example allowing to control the key SVA parameters (solvent evaporation rate and purity, solvent concentration in the film, exposure time, vapor pressure, humidity and temperature, *etc*.). In another strategy, Cummins *et al*.[84] combined the SVA with temperature, resulting in solvothermal vapor annealing (SVTA) as a way for ordered lamellar microdomains in PS-*b*-PLA block copolymers.

4.1.5 PS-matrix stabilization upon PLA hydrolysis

Vayer *et al*. presented simple and beneficial additional step for stabilization of the thin film prior to PLA etching.[80] Thus, UV exposure of annealed films (at wavelength of 365 nm, 40W) for 1 h gave strengthened and crosslinked films that avoided delamination upon PLA hydrolysis. High degree of long lateral ordering persisted upon PLA hydrolysis, resulting in hexagonally cylindrical pores spanning the entire film thickness (Figure I-5).

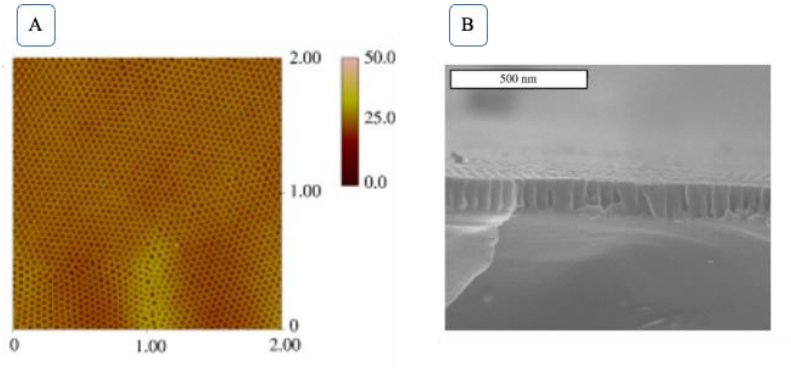

Figure I-5: AFM (A) and SEM (B) imaging of SVA annealed, UV-crosslinked and hydrolyzed PS-*b*-PLA thin film.[80]

Furthermore, the combination of UV-matrix reinforcement and PLA hydrolysis led to composite ultrafiltration membranes (UF) upon coating PS-*b*-PLA thin films on microporous substrate, as reported by Cussler *et al*.[85]

4.2 PS-*b*-PLA/PS-*b*-PEO mixtures for nanoporous structures with advanced properties

Nanoporous thin films made from blends of PS-*b*-PLA and PS-*b*-PEO have proved to be effective in the physical immobilization of biomacromolecules.[70,86] The three-step strategy for this purpose is presented in Figure I-6.

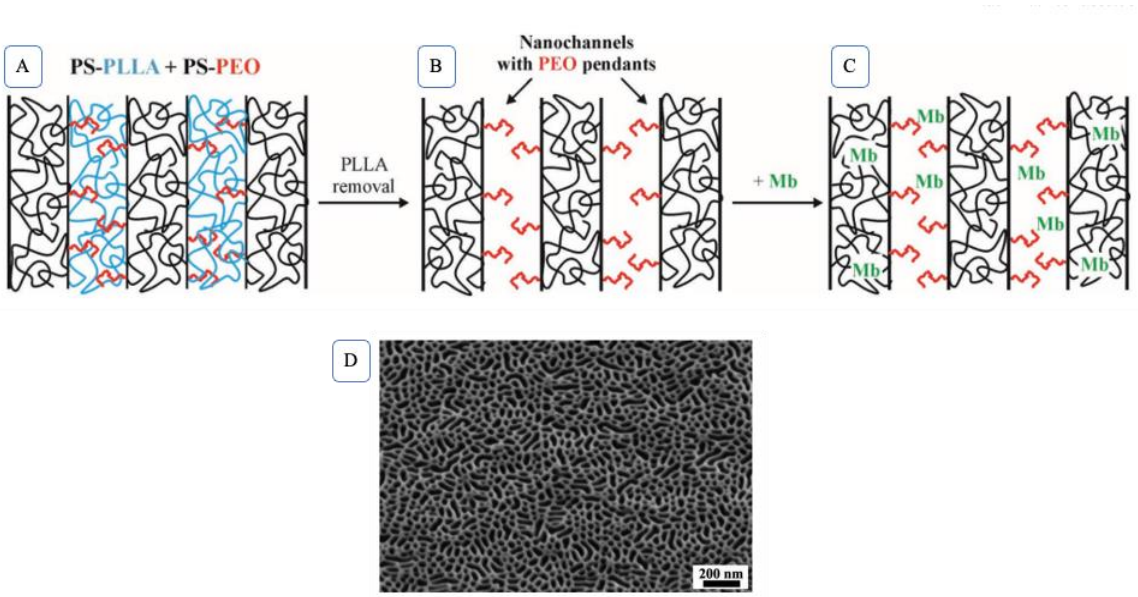

Figure I-6: (A) Nanostructured thin film of PS-*b*-PLA/PS-*b*-PEO blends presenting lamellar morphology, subjected to hydrolysis (B) resulting in nanometric PS channels with pendant PEO groups, later used for physical adsorption of myoglobin molecules (C); (D) FESEM image of PS-PLLA/PS-PEO blend thin films after hydrolysis.[86]

Hence, in the study of Malafonte *et al*.,[86] solutions of 1% (w/w) PS-*b*-PLLA/PS-*b*-PEO (with 90/10 w/w ratios) mixtures in 1,2-dichloroethane have been used for preparation of thin films by drop casting or spin-coating procedures (3000rpm, 30s). Short thermal annealing by heating the films up to 200 °C followed by cooling down to room temperature was used to improve the solid-state morphology. Both PS-*b*-PEO and PS-*b*-PLA possessed similar molar mass and PS volume fraction close to 0.5, thus leading to lamellar microdomain morphology oriented perpendicularly to the substrate (glass or silicon). Due to the favorable miscibility between the PLLA and PEO phases,[87] the thin films consisted of alternating lamellae of PS with PLLA and/or PLLA/PEO. The selective PLA hydrolysis led to nanoporous hydrophobic PS domains, as evidenced by FESEM imaging (Figure I-6D).

Pendant PEO-chains remained on the pore walls together with carboxylic and hydroxyl groups generated upon the ester-cleavage of PLA. The as generated thin films with elongated 20 nm pores were used for selective immobilization of enzymes such as horseradish peroxidase (HRP) or proteins such as myoglobin. The hydrophilicity of the pendant PEO chains enabled increased contact between the PS and the aqueous protein solution, thus further enhancing the adsorption on the PS support.

4.3 PI-*b*-PLA block copolymer as templates for nanoporous thin films

Likewise, phase separation in PI-*b*-PLA thin films has been investigated, the main reason being the high thermodynamic incompatibility between the two blocks. Their interaction parameter $\chi_{PI\text{-}PLA}$ presents a value of 0.3 at 25°C. In the study of Cavicchi *et al*.,[88] thin films of PS-*b*-PI (with f_{PLA} =0.77) were spin coated from chloroform solutions on silicon wafers bearing surfacic native oxide. Strong unfavorable interactions between the two segments led to cylindrical microdomains of PLA in PI matrix upon simple solvent evaporation from thin films.

Solvent annealing with vapors of good solvent for both blocks was investigated for further enhancing phase separation. On the contrary, thermal annealing was not possible due to the thermal sensitivity of PI block. Hence, films swollen at higher concentrations (38%) of chloroform resulted in cylindrical microdomains oriented perpendicular to the surface, as evidenced by grazing incidence small-angle X-ray scattering (GISAXS) and SEM. This alignment resulted from the enhanced polymer chains mobility and mediated interfacial interactions.

Moreover, the PI phase is known to be crosslinkable, as a possible way to enhance matrix stabilization. Therefore, PI crosslinking was performed by using sulfur monochloride vapors (S_2Cl_2), while PLA degradation by using 1M tetra butyl ammonium fluoride (TBAF) solution in THF. Unfortunately, after hydrolysis the films were difficult to be characterized because they no longer adhered to the surface and were found floating in the TBAF/THF solution.[89]

4.4 PS-*b*-PI-*b*-PLA block copolymer as templates for nanoporous thin films and nanoporous membranes

If solvent annealing was needed to induce an ordered morphology in PI-*b*-PLA thin films, spontaneous alignment was achieved upon casting films of PS-*b*-PI-*b*-PLA block copolymers. The automatic perpendicular alignment of PLA cylinders[90] is a result of the interphase emplacement of PI due to the low surface energy of this component, resulting in net delimitation contact between PS and PLA. The instant core-shell cylindrical morphology, with the degradable PLA phase in the core part, is a strong potential for large-area nanostructures because additional techniques (thermal or solvent vapor annealing) for boosting long-range order are not needed in this case.

Therefore, Hillmyer *et al.* in 2013, reported UF membranes from these phase-separated structures (with $f_{PS} = 0.62$, $f_{PLA} = 0.25$ and $f_{PI} = 0.13$), presenting good hydraulic flux properties and size-selectivity of PEO solutes.[91] Moreover, the added PI block that stayed on the pore walls after hydrolysis, was reported to enhance the mechanical tenacity of the membrane while simultaneously conferring more pronounced hydrophilic character.

Moreover, filtration membranes with enhanced mechanical properties such as improved flexibility and toughness were produced by the incorporation of an additional crosslinkable high-modulus PS block[92] resulting in PS-*b*-PI-*b*-PS-*b*-PLA precursors.[93] The tetrablock terpolymer architecture did not complicate the microdomain ordering, nor PLA etching. Membranes with 100 nm thick selective layer and 15 nm pore sizes with narrow distribution were obtained. Thus, the resulting nanoporous material from ABAC crosslinked block copolymer precursors, presented greater mechanical properties compared to the non-crosslinked nanoporous composite membranes of PS or PS-PI. Furthermore, the same triblock terpolymer was afterwards studied in the aim to achieve precisely controlled nanoporous thin films via SVA.[94]

5. PS-*b*-PDMS systems prone to HF-etching or reactive ion-etching for production of porous structures or nanolithographic templates

Polystyrene-*block*-polydimethylsiloxane (PS-*b*-PDMS) have been firstly synthesized and have begun to be studied since the 1970s.[95] Recent advances demonstrate their controlled synthesis by sequential anionic living polymerization.[96] This BCP leads to a powerful segregation between the two blocks and enhanced PDMS surface activity, both phenomena resulting from the strong non-polar nature of this block.[97,98] Hence, PS-*b*-PDMS demonstrates a Flory-Huggins interaction parameter (χ=0.26 at 25°C) significantly larger than the other block copolymer associations.[2] Thus, even in low-molar mass PS-*b*-PDMS (of 7 kg.mol^{-1}), phase-separated (lamellar) domains were evidenced.[99] In fact, the behavior of this BCP in the bulk state has been thoroughly investigated.[100–102] Politakos *et al*. managed to define the precise volume fraction of PDMS (f_{PDMS} presenting a narrow value of 0.41) to obtain the curious double gyroid (DG) morphology in bulk PS-*b*-PDMS samples of high χN values. In the meantime, cylindrical or alternating lamellae morphologies were present for the boundary values of f_{PDMS} (0.39 and 0.45 respectively).

5.1 Self-assembly phenomena in PS-*b*-PDMS thin films

Ross and Jung were the first authors to examine the behavior of strongly segregated PS-*b*-PDMS in nanometer range structures.[103] Thin films of commercial PS-*b*-PDMS (of 45 kg.mol^{-1} and f_{PDMS}=0.34) were produced by casting 1.5 wt % polymer solutions in toluene onto Si substrates with native oxide layers. Further, the films were solvent-annealed in toluene vapors (preferential solvent for PS: δ_{PS}= 18.5, $\delta_{toluene}$=18.3) for various durations to facilitate phase-separation. PDMS cylinders were reported to align parallelly or perpendicularly to the surface under intermediate vapor pressures for annealing times of 4 and 15 h, respectively. In some cases, to enhance lateral ordering of the BCP, the substrates were previously modified by grafted brush layers of hydroxy-terminated PS or PDMS homopolymers with low molar mass. PDMS-brushed surface also promoted parallel alignment. Borah *et al*. introduced the possibility to functionalize the Si-surface with ethylene glycol molecules to boost in-plane orientation of the PDMS cylinders.[104]

However, Ross *et al.* later demonstrated favored solvent vapor annealing in acetone atmosphere for PS-*b*-PDMS of lower molar mass (16 kg.mol^{-1}).[105] They explained that less good solvent for both blocks such as acetone, does not sufficiently swell the low molar mass block copolymer, thus maintaining a high segregation strength between the two components.

In another study, the same research group investigated the use of controlled mixed solvent vapors to tune the cylinder-forming PS-*b*-PDMS into expanded range of morphologies, even leading to a perforated lamellar structure.[106] Furthermore, they managed to produce PDMS structures with concentric ring shape under confinement in shallow circular trenches.[107] Additionally, for PS-*b*-PDMS of 45 kg.mol^{-1}, Gotrik *et al.* evidenced further control of the morphology and dimension of the self-assembled domains by use of mixed solvent vapors of toluene and n-heptane.[108]

Moreover, blending of PS homopolymers with PS-*b*-PDMS could alter the phase-separation and provokes specific morphology transitions.[109] The blend solutions were made by mixing PS-*b*-PDMS and PS with different weight ratios in toluene and stirred for 24 h. Thin films were produced by spin-coating (2000 rpm, 40s) on Si-wafers, followed by solvent annealing in toluene atmosphere with controlled vapor (at 30°C for 24 h). Different blending ratios resulted in morphologies such as spherical, concentric lamellar or multihelical. Thomas *et al.* introduced another morphology in the PS-*b*-PDMS system upon surface reconstruction of solvent annealed thin films presenting a perpendicular orientation to the substrate. The surface modification, provoked by immersion of the films in dodecane followed by short O_2-RIE to remove the PDMS surface layer, resulted in an interesting core-shell morphology. Templated self-assembly techniques such as graphoepitaxy have been also implemented for directed self-assembly of PS-*b*-PDMS systems, resulting in uniform 20 nm line arrays of the domains.[110]

5.2. Generation of porous structures from PS-*b*-PDMS precursors

Depending on the choice of etching technique, self-assembled PS-*b*-PDMS can lead to two different types of nanoporous structures. Thus, HF-etching selectively removes PDMS leading to nanoporous PS-matrix, while on the other side, O_2-reactive ion etching (RIE) particularly degrades the PS-phase.

5.2.1 O_2 reactive ion-etching (O_2-RIE)

On the other side, under specific oxidative conditions, the PDMS block is transformed into SiO_2 while the PS matrix is selectively degraded.[111] O_2-RIE is performed by firstly exposing the annealed films to CF_4 plasma for short periods (10 s) followed by O_2 plasma exposure for PS-removal. Inorganic nanoporous templates such as silicon oxy-carbide nanorings or nanolithography masks can be therefore obtained.[65,111–113]

Meanwhile, uniquely short CF_4 plasma treatment enables better visualization of the phase-separation morphology because it selectively removes the PDMS layer segregated to the surface of thin films. Such phenomena results from the lower surface tension value of PDMS (γ =19.9 mN.m^{-1}) compared to the one of PS (γ = 40.7 mN.m^{-1}).[110,114]

5.2.2 HF-etching

Ndoni *et al*. were the first to produce nanoporous PS monoliths from PS-*b*-PDMS *via* selective PDMS etching.[115] Molar excess of anhydrous hydrogen fluoride (HF) was employed to selectively and completely remove the PDMS phase-separated domains, resulting in spherical voids in the PS matrix. Anhydrous HF as strong protonating acid,[116] quantitatively cleaves the Si-O while transforming it to Si-F bond (Scheme I-4). The reaction products (dimethyldifluorosilane, trimethylfluorosilane, water and the excess of HF) were needed to be removed by vacuum.

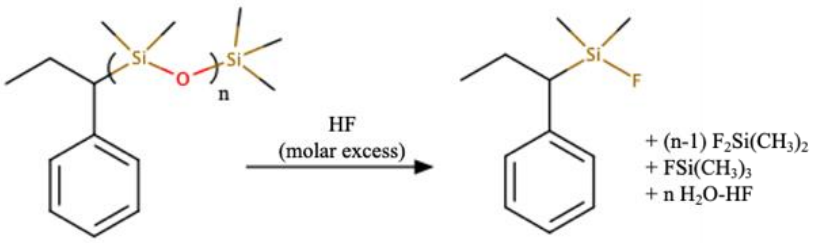

Scheme I-4: Cleavage of Si-O bonds in PS-*b*-PDMS using HF.

Gyroid-structured PS monolith as well as porous PS-nanofibers were equally developed from PS-*b*-PDMS precursors by the same HF-etching conditions.[117,118] Moreover, the equal approach could lead to nanoporous PI and PB materials with enhanced mechanical properties due to their crosslinkable abilities.[119,120]

Selective PDMS etching in nanoporous block copolymers thin films was initially reported in 2008 by Ndoni *et al*.[121] Polydimethylsiloxane-*b*-poly(tertbutyl acrylate)-*b*-polystyrene (PDMS-*b*-P*t*BA-*b*-PS), synthesized via combination of living anionic and RAFT polymerizations was used as precursor. After solvent annealing, the casted samples were subjected to selective PDMS etching using a previously reported HF equipment for cleaving synthetic peptide resins.[122] In the meantime, the P*t*BA block was deprotected, leading to hydrophilic poly(acrylic acid) (PAA) group covering the pore walls. Pores with radii of 6 and 14 nm, depending on the differing BCP precursors, were evidenced by SEM and GISAXS. Water uptake measurements were performed to confirm the hydrophilicity of the porous structure. In another study, Cheng *et* al., employed the same cleaving reagent in the aim to produce nanochannels from PS-*b*-PDMS/PDMS blends.[109]

Nevertheless, a serious issue with this approach represents the hazard nature of the HF cleaving agent. Anhydrous HF is an extremely toxic reagent, whose inhalation can cause serious damage to the human respiratory system and even lead to life-threatening consequences.[123] Serious precautions should be overtook when handling this reagent, thus this research group attempted less-hazardous trifluoroacetic acid (TFA) for PDMS cleaving. For that purpose, the films were placed in large-molar excess TFA solution and stirred for 3 h before being washed with methanol and dried under argon. Unexpectedly, quantitative PDMS removal was evidenced in these conditions together with simultaneous P*t*BA deprotection. Thus, an alternative route was presented for PDMS removal.

6. Nondegradative approaches for pores generation from self-assembled block copolymer thin films

Wang *et al.* introduced a simple and efficient strategy where nondegradative swelling of the minor block led to nanoporous structures.[124] The big advantage of such approach is the maintenance of the structural performances of porous block copolymer thin films because the polymer chains stay undamaged during the process. The nondegradative block method for generation of porosity also includes elimination of added salts, homopolymers or additives from the block copolymer self-assemblies.

Herein, the most studied block copolymer pair was poly(styrene)-poly(vinyl pyridine) (Scheme I-5). Both PS-P2VP and PS-P4VP pairs possess high affinity for phase separation due to their elevated Flory-Huggins interaction parameter. In fact, the high degree of dipole polarization of the P4VP block leads to big repulsive interactions between this amphiphilic segment and the hydrophobic PS block,[125] thus giving extremely important values for their interaction parameter ($\chi_{PS\text{-}P4VP}$ >>1).[126] For comparison, the $\chi_{PS\text{-}P2VP}$[6] is about 0.18 at room temperature, because of the emplacement of the charged nitrogen atom furthest away from the main chain in P4VP unit compared to the P2VP unit.

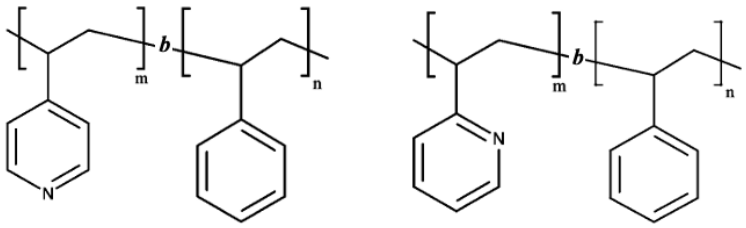

Scheme I-5: Chemical structures of PS-*b*-P4VP (left) and PS-*b*-P2VP (right) block copolymers.

The specific conditions influencing the self-assembly in PS-*b*-PVP systems and the nondegradative methods for achieving nanoporous structures from this precursor are further discussed.

6.1 Swelling

Selective minor block swelling as a nondegradative strategy for generation of nanoporous templates was adapted for both PS-*b*-P2VP and PS-*b*-PMMA BCP thin films. Moreover, the SNIPS (solvent - non-solvent induced phase separation) method, as the optimal strategy for production of ultrafiltration membranes, includes BCP swelling and is applicable to wide variety of di- and triblock copolymers, is briefly presented herein.

6.1.1 Impact of P2VP swelling in PS-b-P2VP block copolymer thin films

The Wang research group[124] initially studied 110-600 nm thick films of amphiphilic PS-*b*-P2VP block copolymers in the aim to produce porous membranes. Rapid perpendicular alignment of spin-coated films of this block copolymer (even for high molar mass of 362 000 $g.mol^{-1}$) was achieved within 40 s exposure to saturated vapors of chloroform. The low boiling point (61.2 °C) of this solvent, neutral for both blocks, favored a higher rate of cylinder growth, while their length spanning the entire film thickness is a result of the strong immiscibility between PS and P2VP blocks[125] The selective swelling-induced pore generation process is a result of the immersion of so-annealed thin films in hot ethanol (at 50°C for 3h) followed by air drying and results in uniform straight nanopores spanning the entire film thickness, as confirmed by GISAXS. The hexagonal pores result from the deformation of the PS matrix and the overflow of P2VP chains from the cylindrical microdomains upon immersion in the selective ethanol solvent. In addition, the pore size could be controlled by varying the swelling temperature and the BCPs molar mass or further tuned by inner deposition of metal oxide thin layers. In a following very similar study, porous membranes from PS-*b*-P2VP-*b*-PI triblock terpolymers were developed with higher permeability than the previous one.[127] In fact, the rubbery PI component modified the two glassy blocks towards materials with enhanced mechanical properties but also accelerated swelling rates due to its softening effect on the PS phase. In another case, whilst employing PS-*b*-P2VP-*b*-PEO block copolymers, water in addition to ethanol can be used for the swelling process due to its selectivity for PEO.[128]

6.1.2 Impact of PMMA swelling in PS-b-PMMA block copolymer thin films

In addition to UV-etching, the generation of porosity in PS-*b*-PMMA systems can be also obtained by non-degradative and simple swelling of the BCP thin film, without the need

to extract the PMMA block.[129] In fact, upon immersion of previously thermally annealed 30 nm BCP thin film in acetic acid, the PMMA phase migrates to the film surface. Therefore, the structure being reorganized due to the preferential interactions of PMMA with this selective solvent, is causing the PMMA phase to swell, which upon drying leads to nanopores generation. In addition, the surface of the thin film changes from hydrophobic to hydrophilic due to the presence of PMMA domains. Since no chemical reactions were employed, the whole process is fully reversible upon heating at temperatures over the glass transition point of the block leading to recovering of the original cylindrical domains in the film. Interestingly, the pores produced by PMMA swelling, in this case, are of similar size as those made by UV-PMMA photodegradation. In addition, UF membranes were also developed by this strategy.[130] The diameter of hexagonally packed pores herein depended on the duration of the acetic acid treatment. Swelling for 20 min plateaued the pore size to average 17.5 nm. Composite UF membranes were fabricated upon transferring the as-produced porous films onto macroporous PVDF membranes with the aid of 5 wt.% HF solution. Ultimately, these UF membranes were tested and proved their efficiency for selectivity and rejection of Au nanoparticles (NPs) at 2 bar pressures. Also, they possessed good mechanical stability with resistance to strong basic and acidic conditions. In a following study reported by Ryu *et al.*,[131] the influence of additional P*t*BA block was studied in the elaboration of 200 nm UF thin films from PS-*b*-PMMA-*b*-P*t*BA triblock copolymer. Microdomains consisting of PMMA and minor P*t*BA blocks presented identical orientation achieved *via* thermal annealing (170°C, 2 days) as in the previous case. Likewise, acetic acid swelling-deswelling process of the so-oriented microdomains with defined duration created controlled porosity. Moreover, hydrolysis of the *t*BA units on the pore walls resulted in functionalization of the pore surfaces with poly(acrylic acid) units, thus conveying pH-responsive properties of the membrane.

6.1.3 Isothermal BCP self-assembly/phase-inversion process (SNIPS) to produce advanced UF membranes

In order to overcome limitations such as defects or lack of sufficient long-range order in the UF membranes, a combination of block-copolymer self-assembly with the most industrially common technique for membrane preparation – the non-solvent induced phase separation (NIPS), has been developed by Abetz *et al.*, thus leading to novel membranes for higher purposes.[132–134]

Advantageously, the experimental procedure of membrane preparation starting from a BCP solution in various solvent mixtures is composed of four straightforward steps:

1. Manual doctor-blade casting of 200 μm thick film of 12-25 wt.% block copolymer solution on a conditioned nonwoven support
2. Solvent evaporation at room temperature for short period (10 to 60 s)
3. Immersion of the film into non-solvent bath of defined temperature and time
4. Drying at ambient conditions

In such a way, the membrane preparation process is composed of two related parts: firstly, block copolymer self-assembly (S) takes place, upon solvent evaporation where microphase separation occurs and starts to propagate, a process driven by an established concentration gradient. Secondly, the surface structure being fixed, the highly swollen polymer precipitates by the non-solvent-solvent exchange (NIPS). Therefore, the porous structure results from liquid-liquid demixing process while the top layer represents the self-assembly of the block copolymer in ordered structure. In other words, the porous matrix of the as-prepared isoporous asymmetric membrane is constituted by the polymer-rich phase while the polymer-poor phase induces pores formation. If a highly volatile solvent is used in the casting solution, the obtained material results in a highly ordered thin layer on the top-surface (Figure I-7C). Meanwhile, a supporting and mechanically stable non-ordered sponge-like layer of the same block copolymer occupies the bottom part (Figure I-7C). In addition, the as prepared isoporous asymmetric membrane sits on top of a porous support, thus ensuring their stability, conformability, and cost, all while avoiding additional processing steps such as etching, removal or transfer.

Recently, Abetz *et al.* published an exhaustive review treating this subject.[135] Briefly, we can find various di- or triblock copolymer associations for the preparation of SNIPS membrane, such as : PS-*b*-P4VP,[136] PS-*b*-P2VP,[137] PS-*b*-PEO,[138] PS-*b*-PHEMA[139] *etc*), triblock copolymer associations (like PI-*b*-PS-*b*-P4VP,[140] PI-*b*-PS-*b*-PDMA,[141] PS-*b*-PNaSS-*b*-PS[142] or PS-*b*-P2VP-*b*-PEO[143]) but also BCP with low χ as PS-*b*-PNIPAM,[144] hence demonstrating the broad future perspective of this approach toward ideal UF membranes.

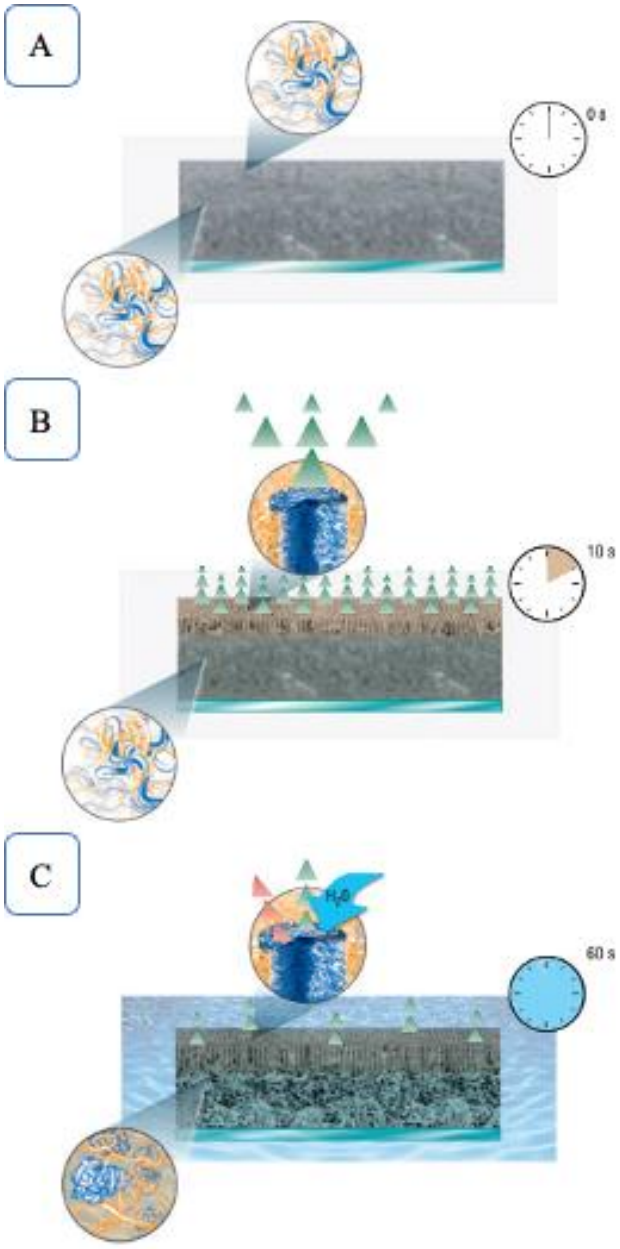

Figure I-7: Schematic representation of the SNIPS process on the formation of isoporous membranes from PS-*b*-P4VP precursors as established by Abetz *et al*.[132]

6.2 Dissolution and extraction of additives from PS-*b*-P4VP self-assembled block copolymer thin films

Another approach for generating nanoporous membranes and templates was developed by extraction of a supplemental third component low molar mass additive from block copolymer thin films with ordered morphologies.

6.2.1 P4VP-PDP via H-bonding

Ikkala *et al*. back in 1998, introduced the concept of polymeric supramolecular nanostructures where methane sulfonic acid (MSA) and pentadecylphenol (PDP) molecules were complexed to the P4VP unit of microphase-separated PS-*b*-P4VP *via* hydrogen bonding.[145] The creation of self-organized structures-in-structures allowed altering of the block copolymer morphology from spherical to cylindrical. Afterwards, the same group demonstrated PS mesoporous polymers with hollow cylinders after oligomeric PDP extraction via methanol washing.[146] Subsequently, the same concept was adjusted for obtaining nanoporous structures from thin films of PS-P4VP supramolecular complexes. As a matter of fact, the addition of an extra component in block copolymer thin films helps adjusting the interfacial interactions thus leading optimized phase-separated morphologies. For instance, if lamellae-*within*-cylinders, lamellae-*within*-spheres or lamellae-*within*-lamellae morphologies were obtained for bulk self-assemblies of supramolecular PS-*b*-P4VP(MSA)$_{1.0}$(PDP)$_{1.0}$[147], the bicontinuous double gyroid morphology was evidenced in thin films of poly(tert-butoxystyrene)-*b*-polystyrene-*b*-poly(4-vinylpiridine) triblock copolymers with less than stoichiometric amount of added PDP.[148] Thin films of PtBOS-*b*-PS-*b*-P4VP triblock copolymer alone adopted a triple lamellar morphology. On the other hand, thin films of PtBOS$_{46}$-*b*-PS$_{46}$-*b*-P4VP$_8$ (PDP)$_x$ presented the core-shell gyroid morphology where the P4VP(PDP) complexes formed the core channels with x values of 0.3 to 0.8, as observed by SAXS and TEM (Figure I-8).

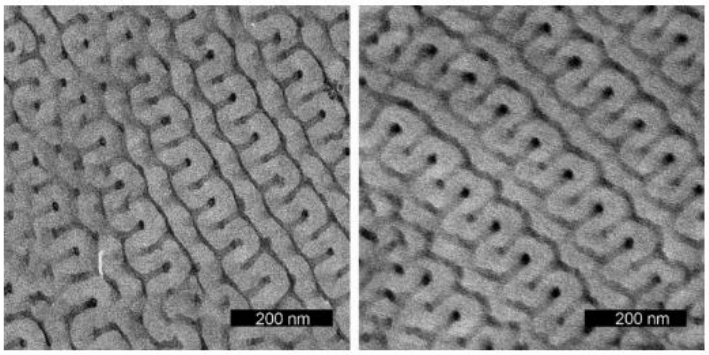

Figure I-8: Core-shell gyroid morphology observable in PtBOS$_{46}$-*b*-PS$_{46}$-*b*-P4VP$_8$ (PDP)$_x$ (with x=0.3-0.8) thin films.[148]

To prepare nanoporous structures from this precursor, initially the P*t*BOS$_{46}$-*b*-PS$_{46}$-*b*-P4VP$_8$ triblock copolymer is dissolved with different amounts of PDP in chloroform solution and

stirred for couple of hours so that the supramolecular complex can form through hydrogen bonding. Afterwards, the solution is poured in a petri dish and solvent annealed for 1 week under chloroform atmosphere followed by brief 10 min thermal annealing at 130 °C. The porosity was created by stirring the film in ethanol at room temperature for 3 days, allowing removal of the amphiphilic PDP component. The total porosity of the sample was 10.4 %, which corresponds to the initial concentration of PDP additives, with average pore diameter of 12.5 nm.

6.2.2 P4VP-HABA additive supramolecular self-assembly

Sindorenko *et al.* meanwhile reported PS-*b*-P4VP thin films with successful supramolecular assembly (SMA) between the PVP unit and 2-(4'-hydroxybenzeneazo)benzoic acid (HABA) molecules.[149] Cylindrical nanodomains of PVP-HABA associates in PS matrix oriented perpendicular to the surface were achieved by solvent vapor annealing in 1,4-dioxane saturated vapors for 30 min at room temperature from chloroform solution deposited films. Stamm and Liu further studied the supramolecular assembly of the same system under a solvent mixture annealing atmosphere.[150] Previously, the key step for forming the SMA was the drop-by-drop addition of PS-P4VP to the HABA solution (1/1 molar of HABA/4-vinyl pyridine monomer unit). The addition was performed at the boiling point of the common chloroform in an ultrasonic bath. Afterwards, the solution was kept overnight to complete the H-bonding. The heating proved essential for the formation of SMA, as evidenced by FTIR. The thin films were produced via dip coating process on Si-substrates. The cylindrical microdomain alignment did not change upon varying substrates (PS brush, Au, Ni, or indium tin oxide (ITO) coated glass) due to the self-adaptive nature of the supramolecular PVP-HABA assembly. Finally, selective solvent (methanol) rinsing for 2 min destroyed the SMA and washed away the HABA molecules, resulting in nanoporous membranes with 8 nm hollow channels and PVP brushes decorating the pore walls. The films proved successful for electrodeposition of Ni thus creating a dense array of metallic nanodots.

Additional approaches for the generation of nanoporous structures include elimination of added homopolymers or metal salts complexes with P4VP units from thin films of PS-*b*-P4VP, as described in the parts 6.3 and 6.4.

6.3 Elimination of P4VP homopolymers from PS-*b*-P4VP/P4VP self-assembled thin films

Producing nanoporous structures from blends of PS-*b*-P4VP/P4VP was achieved by simple extraction of the added homopolymer from the thin film by ethanol washing.[151] For the preparation of films, blends of PS-*b*-P4VP and P4VP homopolymer were dissolved in THF (selective solvent for PS) where the weight fraction of P4VP (block and homopolymer) varied between 0.03 and 0.55. The films were prepared by spin-coating the solution (3000 rpm, 60 s) on various substrates (silicon, mica, or glass) without any additional annealing step. Instead, they focused on studying the nanophase separation of P4VP domains, which were oriented vertically to the surface upon solvent evaporation from the spin-coated films. The solubilization of P4VP homopolymer in the P4VP block promoted nanophase separation and enabled obtaining structures with varied nanoporosities, as the size of the P4VP nanodomains increased with the amount of added P4VP homopolymer. The as generated nanopore systems, possessing pores traversing the entire material and with diameter smaller than the wavelength of visible light, presented potential for antireflective (AR) coatings.

6.4 Elimination of metal-salt complexes from PS-*b*-P4VP self-assembled thin films

Sageshima *et al*. investigated nanophase-separated hybrids upon mixing PS-*b*-P4VP and iron (III) chloride in a selective solvent with coordination capacity.[152] For this purpose, PS-*b*-P4VP, previously synthesized by RAFT polymerization, was mixed with $FeCl_3$ in pyridine, further solvent-casted on a hot plate at 50°C and left for 24h. Thermal annealing at 165 °C for 60 h led to hexagonally packed cylinders with interdomain spacing of 42 nm as observable by TEM. In fact, the addition of metal salt and the ensuing complexation phenomena provoked morphology transition from spherical to cylindrical confirmed in particular by SAXS.

Thin sections of the polymer film were produced by microtoming technique. Later, they were immersed in water, thus inducing the porosity in these samples. Because the metal salt is soluble in water, it was easily and rapidly removed from the polymer structure (30 s). TEM-images demonstrated pores with diameters between 19 and 25 nm. Since the P4VP chains stayed on pore walls and further possessed the coordination ability, these nanoporous films presented potential as catalyst or photonic devices and photovoltaic films.

7. Cleavable linkages

The production of nanoporous materials from amphiphilic phase-separated block copolymers, via usual (previously discussed) techniques such as chemical etching, reactive ion-etching, ozonolysis, or UV degradation occasionally meets constraints due to the harsh conditions. The removal of one block in such circumstances can lead to side chain hydrolysis or undesired degradation. For example, even though Hillmyer and co-workers produced nanoporous films from PS-*b*-PEO block copolymers by chemical etching (HI-cleavage), harsh conditions were required due to the poor degradability of PEO.[153]

A possible solution for alike problems could be the introduction of cleavable group or labile linker between the building units of the diblock copolymer, thus creating a "smart" system. The consecutive cleaving reaction, carried out under mild conditions, could allow removal of one of the blocks by an easy washing procedure, thus leaving after a stable nanoporous structure. This approach is an attractive pathway to generate nanoporous templates since it enables using different polymer sequences. Moreover, pore walls bearing promising functional groups could be made by thoughtful choice of both the type of juncture and the cleavage conditions. However, according to this way, the building polymer units must be monofunctional to react with the linker.

The cleavable groups, acting as linkages between the two building blocks can be divided in three separate categories depending on their nature: irreversible, reversible, and supramolecular linkages. Most of the phase-separated polymers containing these linkages are present in the form of thin films. The mastered synthesis, self-assembly studies and easy PEO washing promoted the PS-*b*-PEO as the reference material from this approach (Figure I-9).

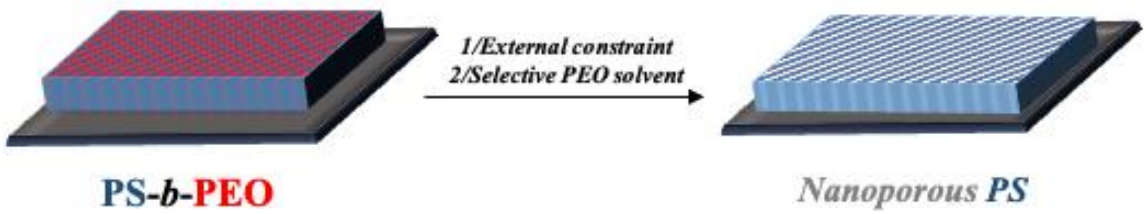

Figure I-9: Model for generation of nanoporous thin film structures from PS-*b*-PEO precursors bearing a cleavable linkage.

Hence, various procedures for generation of nanoporous materials from "smart" block copolymer systems (most generally PS-*b*-PEO) bearing cleavable junctions are afterwards discussed.

7.1 Irreversible linkages

7.1.1 UV light sensitive junctions – o-nitrobenzyl (ONB) carbamates and esters

The most often used cleavable linkages in block copolymer systems are the photolabile groups due to their direct receptivity to light stimuli, where the removal is handled in neutral conditions without the need of any additional chemical reagent. Among them, *o*-nitrobenzyl derivatives (ONB) in the form of ONB esters, carbamates and carbonates have been profoundly used as protecting groups in the chemistry of carboxylic acids, amines and alcohols, respectively.[154] Recently, they have also been employed as agents for reaction induced phase-transitions of BCPs in solvent and for copolymers with hydrophilic/hydrophobic pH-stimuli responsiveness.[155,156] Their advantage in generating nanoporous structures from BCP systems lies in the easy control of the photo-degradative process which later on allows facile minor block removal. Thus, light can be generated outside of the system, localized in time and space with its wavelength controlled during the reaction.[157] Upon light absorption, in the case of ONB derivatives, photolytic cleavage of the chemical bond (Scheme I-6) occurs by an intramolecular Norrish-type II reaction mechanism.[158]

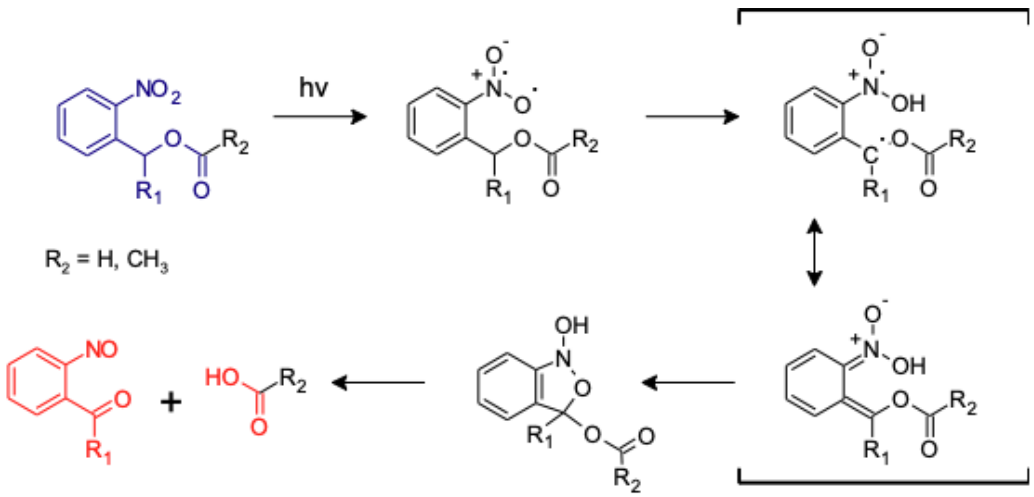

Scheme I-6: Photosensitivity of ONB ester derivatives.[159,160]

Therefore, carbamates, carbonates, and esters ONB derivatives are transformed into an acetal intermediary, immediately being converted into an aldehyde plus additional released carboxylic acids, amines, or alcohols. Moreover, in the case of carbamates, decarboxylation process leads to the release of amines. As a result, possible aldehyde or amine decorated pores could be observed in the nanoporous templates.[159,161]

The initial block copolymer system containing a photo-cleavable junction was synthesized by Kang *et al.* in 2008.[162] PEO functionalized with ONB was prepared and used as macroinitiator for ATRP of styrene giving $PS_{23.7k}$-*hv*-PEO_{5k}. For the preparation of thin films, 0.5 wt.% polymer solution in benzene (doped with KI to enhance phase separation) was spin-coated (3000 rpm, 50s) on Si substrates. Afterwards, the sample was annealed in benzene/water atmosphere with relative humidity of 85% for 2h. Vertically aligned PEO cylinders in PS matrix with long-range order were evidenced by AFM imaging. Exposure of the film to UV-light (350 nm) for 2 h followed by washing with MeOH/H_20 (8:1) mixture (selective solvent for PEO) resulted in successful photolytic cleavage of the ONB and selective extraction of PEO giving a nanoporous structure, as observed by TEM. This study on nanoporous templates from PS-*hv*-PEO precursors was the starting point for many others that followed thereafter. Fustin *et al.* synthesized PS-*hv*-PEO block copolymers *via* an attractive "one-pot" ATRP-CuAAC "click" reaction process.[163] The essence of the approach was the development of ATRP initiator containing both the ONB ester junction and an alkyne group for the "click" reaction. CuBr and PMDETA were employed as catalytic system (Figure I-10).

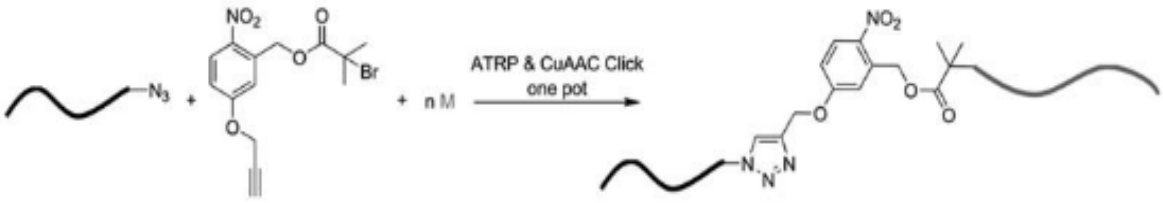

Figure I-10: General approach for synthesis of photocleavable block copolymers *via* "one-pot" ATRP-CuAAC "click" approach.[163]

Thenceforth, the same research group performed a detailed investigation on the production of nanoporous templates from these precursors.[164] Generation of nanopores under mild conditions, the control and accessibility of pore wall functions and patterning of the thin films were discussed. Similarly to the previous case,[162] PS_{176}-*hv*-PEO_{113} thin films displayed HP cylinders of PEO in PS matrix after spin-coating and annealing in benzene/water vapors.

ONB cleavage was performed by exposure of the thin film to UV-light (300 nm) for 20 min. The PEO phase was extracted by immersing the film in MeOH/H2O (9/1) mixture for 16 h. UV-Vis and FTIR spectroscopies were used to confirm the PEO removal, while TEM and SEM proved the pore creation. Moreover, SEM imaging demonstrated pores spanning the entire film thickness. Microscopy images of the thin films before and after ONB cleavage and PEO extraction are represented on Figure I-11.

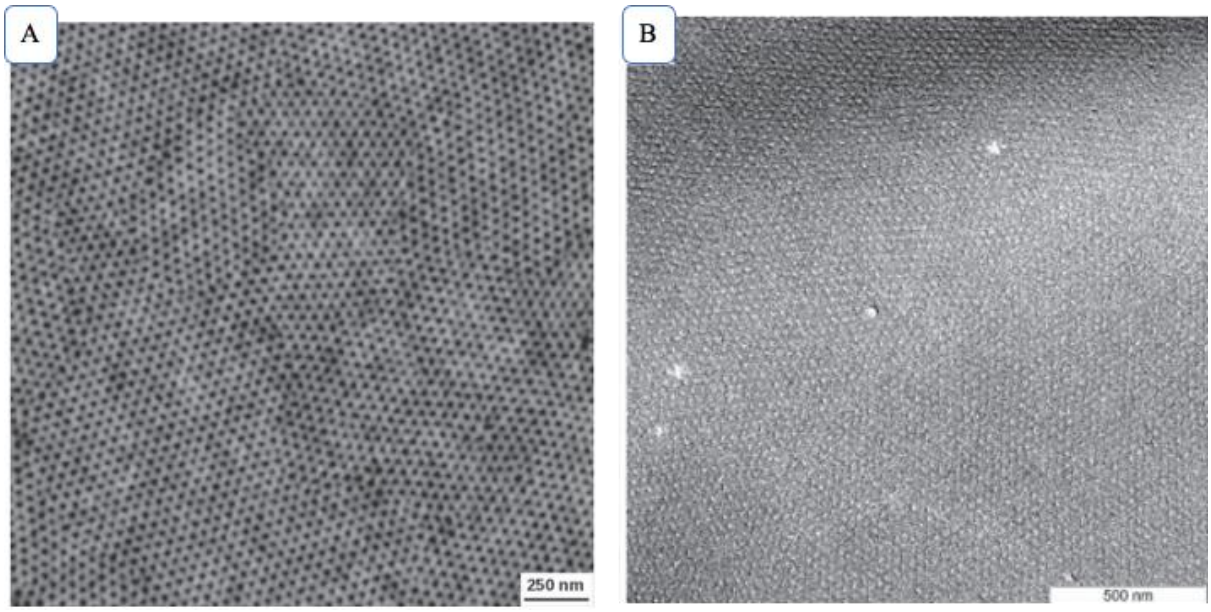

Figure I-11: AFM height image of annealed PS-*hv*-PEO thin films (A) and TEM image of nanoporous PS thin film stained with RuO_4 (B).[164]

The accessibility of the cleavage resulting -COOH group decorating the pore walls was demonstrated by reaction with fluorescent dye bearing diazomethane moieties (PDAM), known to be extremely reactive with carboxylic groups. The reaction was monitored by a spectro-fluorometer, where an increase in the signals occurs upon thin film immersion in the PDAM solution. In the final step of the study, the thin films were patterned with photolithographic mask giving materials with porosities on macro- and nanolevels. Furthermore, the same research group presented amine-decorated nanoporous PS from PS-*hv*-PEO block copolymers connected with the ONB carbamate junction.[161]

On the other side, Theato *et al.* developed a RAFT-click chemistry approach for the synthesis of PS-*hv*-PEO bearing a ONB ester junction.[165] After ONB cleavage and PEO extraction, nanoporous PS thin films with 15-20 nm pores presenting long-range order were obtained. Previous annealing of the thin films under H_2O/THF atmosphere (20 °C, 2.5h) seemed to further enhance the phase-separation. The nanoporous thin films were used as nanoscale template to produce silica nanodot arrays.

Further ameliorations of the PS-*hv*-PEO system for nanoporous template generations have been afterwards reported. Ma *et al.* proposed an approach for strengthening the nanoporous structure and achieving further stability towards pore collapse by crosslinking the PS matrix,[166] by reversible photo-crosslinking of the coumarin group For that purpose, the coumarin group was introduced beside the photo sensitive ONB derivative in the PS-*hv*-PEO block copolymer structure.[167] Therefore, upon UV-exposure of PS-*hv*-PEO thin films to UV-light, degradation and crosslink arise simultaneously, as demonstrated by UV-vis absorption and FTIR. In a recent study, Altinpinar *et al.* indicated that 4 h UV exposure of PS_{27k}-*hv*-PEO_{5k} thin films followed by 50 min washing with water were the optimal conditions for successful generation of pores.[168] Moreover, the in-situ scanning force microscopy (SFM) topography provided further information on the stability of nanoporous thin films upon PEO removal and suggested the occurrence of irreversible morphology changes of the thin film surface upon the washing procedure. Ito *et al*. reported the effects of modification of a gold surface by thiolate self-assembled monolayers (SAMs) for spin-coating of PS-*hv*-PEO thin films on the self-assembly and the generated porosity.[169] Cysteamine SAM surface equilibrated the interactions between PS and PEO thus enhancing vertical orientation of PEO microdomains. Moreover, these molecules enabled investigation of the thin film properties by electrochemical methods due to the short alkyl chains allowing electrode reactions. Thus, cyclic voltammetry (CV) was employed for analysis of the porous structure. Ultra-dense 12-19 nm nanopores were achieved thanks to the underlying substrate.

In addition to PS-*b*-PEO, Theato *et al.* reported nanoporous poly(pentafluorophenyl (methyl)acrylate) (PPFP(M)A) thin films with amine-decorated pore walls from initial PPFP(M)A-*hv*-PEO block copolymer precursors prepared by RAFT polymerization.[170] Moreover, they developed iron oxide nanorings rom ester-functionalized nanopores originating from the photocleavable polystyrene-*b*-poly(maleimide pentafluorophenyl ester-*co*-styrene)-*b*-poly(ethylene oxide) bearing an ONB junction.[171]

7.1.2 Acid cleavable junctions

7.1.2.1 Trityl ether

Trityl ether (TTE) has been frequently used as protective group in many domains of carbohydrate and synthetic chemistry due to its resistance to strong nucleophiles, bases and radicals.[172] It has been reported recently in innovative polymer synthesis.[173] TTE is well known to be labile in Bronsted or Lewis acid (in ambient temperature) conditions because of the stabilized cation by the resonance effect of the surrounding aromatic rings (Scheme I-7).

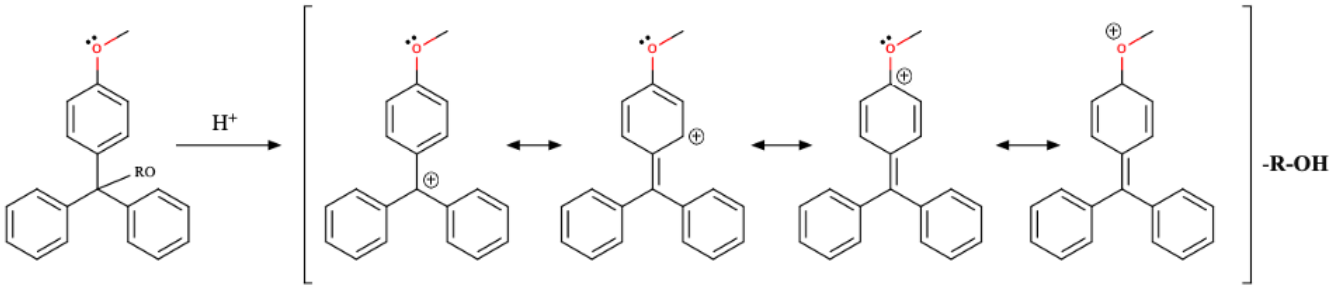

Scheme I-7: Acid-labile property of the trityl ether groups.

The group of Venkataraman *et al*. introduced for the first time the cleavable trityl ether linkage in block copolymer systems.[174] Methoxy terminated poly(ethylene glycol)-trityl ether-TEMPO was used as a macroinitiator for nitroxide-mediated radical polymerization (NMP) of styrene. By dissolving the polymer in toluene containing trifluoroacetic acid, successful cleavage of the trityl ether after 20 min of stirring was validated. NMR and SEC indicated that the cleavage occurred precisely at the trityl ether junction. Following, the same group proceeded the study for generation of nanoporous thin films.[175] Trityl ether cleavage in such case resulted by exposure of the thin films to TFA vapors for 4 h.

Because TFA acts both as a cleaving agent and PEO-selective solvent, the generation of porosity was achieved in one-step when the films were immersed in the acid solution. Previously the spin-coated $PS_{19.6k}$-*TTE*-PEO_{5k} thin films were annealed in benzene atmosphere under N_2 for 48h. Potassium iodide was added in the initial polymer solution to enhance phase-separation. The complexation of PEO with salt promoted the unfavorable interactions between PS and PEO. Moreover, it created sharp interface between the two domains thus helping the site-specific scission. However, before TFA exposure, the crown-ether complex between PEO and the salts must be broken to enable physical access of the acid to the juncture. Therefore, the films were immersed in mixture of methanol and water (10/1 v/v) causing PEO swelling. In the case of unsalted films, the solvent annealing was performed in atmosphere with 70-90% relative humidity. High relative humidity conditions are reported to promote phase-separation and ordering of hydrophilic PEO. In both cases, PEO cylinders with long-range order and

normal to the surface were achieved later resulting in defect-free 12 nm pores. PEO removal was confirmed by IR spectroscopy. SAXS data corroborated the SFM and pointed out towards controlled porosity. The only restraint in this method could be the low reactivity of the functional tertiary alcohol group remaining on the pore walls after TTE cleavage.

Amphiphilic PEG-*b*-PMMA bearing trityl ether juncture were reported by Qi *et al*.[176] PEG-macroinitiator bearing TTE-Br end-group was used for ATRP of MMA. 0.7 % (w/v) polymer solution in toluene was used for spin-coating (3000 rpm, 30 s) on silicon wafers and produced thin films. Phase-separation was pursued by using the direct immersion annealing technique. The latter includes immersion of the film in a mixture of solvents, one of them being a non-solvent for the blocks while other acts as a good solvent (in this case n-heptane and toluene respectively). Nevertheless, phase-separated morphology was not quite discernible on these films. The cleavage was stimulated by exposing the films to saturated TFA vapors for 30 s followed by methanol/water washing. Fast Fourrier Transform (FFT) on reproduced AFM-images post-cleavage showed some cylindrical pores lacking long-range ordering.

7.1.2.2 Acetal Linkages

Another acid-sensitive group is the acetal function, whose hydrolysis mechanism to aldehydes and ketons with the release of primary alcohols have been thoroughly investigated thus far.[177] Hawker designed PS-*act*-PEO copolymers interconnected with an acetal junction for the creation of nanoporous templates.[178]

In a first step, commercially available mono hydroxyl terminated PEO was end-functionalized with 2-chloroethyl vinyl ether using pyridinium *p*-toluenesulfonate as a specific catalyst for the synthesis of acetal from alcohol and alkyl vinyl ether. The obtained acetal terminated PEO was further reacted with sodium azide thus making PEO-acetal-N_3. Finally, an alkyne functionalized alkoxyamine was clicked with this modified PEO giving a macroinitiating group for nitroxy mediated polymerization of styrene (PS-*act*-PEO). 30-40 nm thin films of PS-*act*-PEO were produced by spin-coating of the polymer solution onto Si-wafers. 36-48 h solvent annealing in THF saturated vapors with elevated 90% RH atmosphere enhanced the microphase separation of hexagonally packed cylinders with long-range order, as observable by SEM (Figure I-12A and 12B). Exposure of the films to TFA vapors for 4 h followed by methanol washing resulted in complete removal of the PEO phase giving nanoporous thin films with -OH decorated pore walls (Figure I-12C 12D).

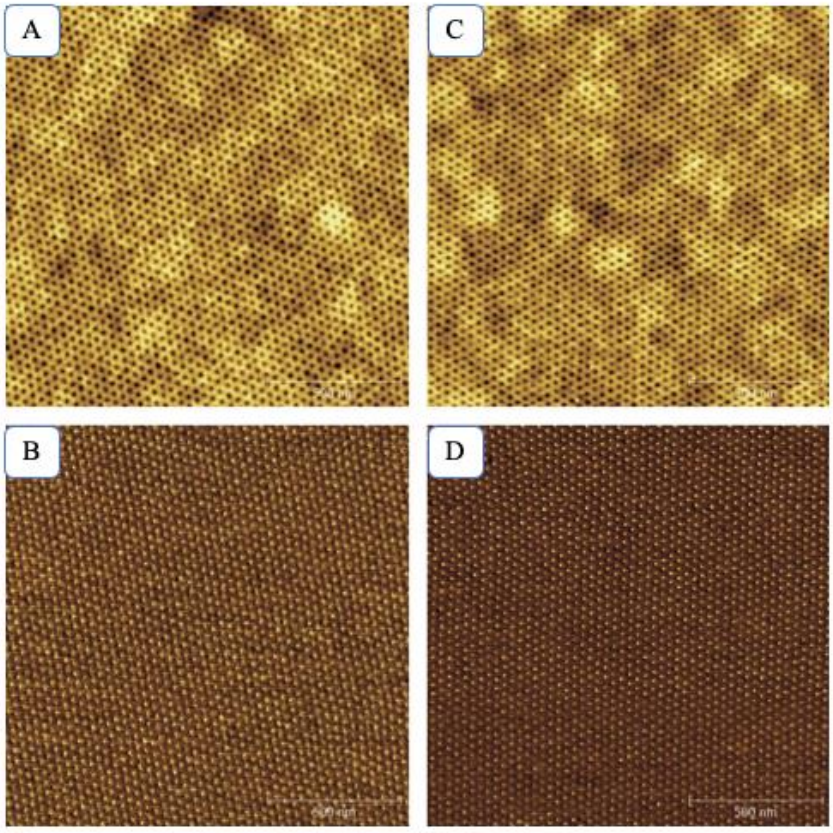

Figure I-12: AFM height (A) and phase (B) images of solvent-annealed PS-act-PEO BCP thin films leading to nanoporous thin films upon TFA vapor exposure, represented by AFM height (C) and phase (D) images.[178]

Using a similar approach for "click" synthesis, acetal cleavage and PEO extraction, Coulembier and co-workers reported for the first time nanostructured thin films from poly(3-hexylthiophene)-*act*-poly(ethylene oxide).[179]

Grande *et al.*, on the other side, developed PS porous catalytic supports from PS-*b*-DLLA block copolymer precursors bearing an acetal linkage.[180] An acetal-containing difunctional initiator was used for ATRP polymerization of styrene, followed by ROP polymerization of D,L-lactide. Thin films were produced by spin coating (400 rpm for 15s followed by 40s at 2000 rpm) polymer solutions in THF on Si wafers. Afterwards, they were annealed for various periods in closed chamber with saturated THF vapors. The best orientation of hexagonally close-packed PLA cylinders in PS matrix was achieved for 24 h exposure to THF vapors of the PS_{178}-*b*-PLA_{130} block copolymer. Acid-cleavage of the acetal junction was performed by immersing the thin films in a mixture of ethanol/TFA (4/1) for 4 h. PLA removal

was confirmed *via* ^{1}H-NMR and SEM techniques. The SEM micrographs also demonstrated that most of the obtained pores ranged from 1 to 2 μm with a slight minority in the 100-200 nm range. Aldehyde functions decorating the pore walls were used for reductive amination with tetraethylenepentamine, thus promoting amine-functionalized nanoporous PS. Furthermore, *in situ* generated gold nanoparticles were immobilized onto such functionalized nanopores, leading to possible heterogeneous supported catalysis applications.

7.1.2.3 Hemi-Acetal Ester Linkages

Close to acetal function, the unstability of the hemi-acetal ester (HAE) was also investigated as cleavable function. Hence, HAE incorporated between poly(isobutyl vinyl ether) and PMMA was investigated for creating nanoporous patterns.[181] α-halophenyl acetic acid was used as hetero-bifunctional initiator for the living cationic polymerization of isobutylvinyl ether (IBVE) and the living radical polymerization of MMA. Firstly, the HAE junction was formed *via* click-reaction between the -COOH group of the initiator and the vinyl ether. Besides, the HAE is also qualified as *activable* by convenient Lewis acid catalyst ($SnBr_4$ in this case) for debuting the polymerization of IBVE. Therefore, the as-obtained poly(IBVE) possessed an α-end carbon-halogen bond acting as macroinitiator for the radical polymerization of MMA with Ru catalyst, thus yielding PIBVE-HAE-PMMA. Thin films of the block copolymer were produced by casting from 5 wt % toluene solutions. It must be noted that slow solvent evaporation of 10 days is required to achieve microphase separated morphology of PIBVE cylinders in PMMA. Furthermore, the HAE is known to be irreversibly *cleavable* in acidic conditions giving an aldehyde and carboxylic acid functions (Scheme I-8). Therefore, the porosity was generated by immersion of the thin films in 0.1 v/v % TFA solution in n-heptane, resulting in selective HAE cleavage and PIBVE washing. However, the porous structures were unable to be detected by TEM microscopy. The only information of the porosity

was given by SAXS analysis that demonstrated hollow cylinders with preserved morphology after minor phase removal.

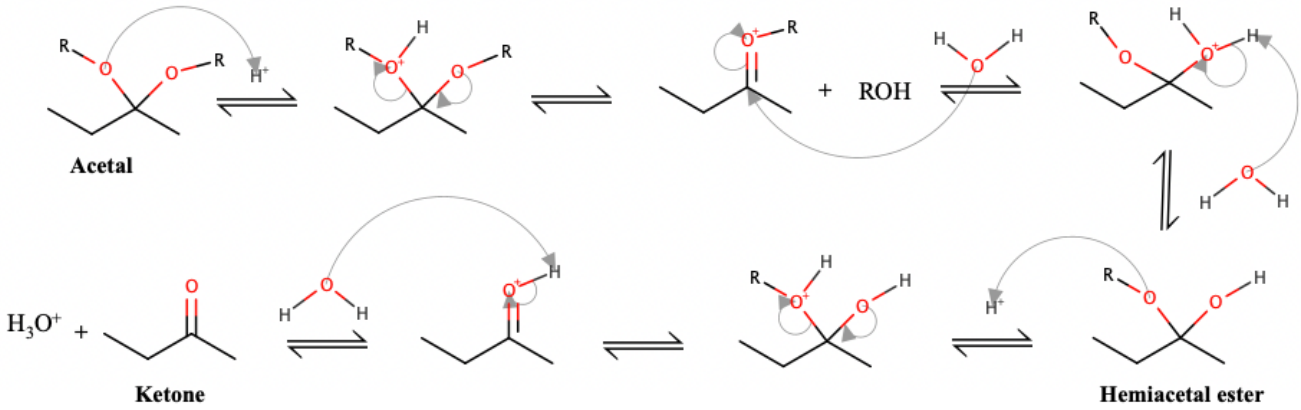

Scheme I-8: Acid-catalyzed hydrolysis of acetals and HAE.

7.2 Reversible linkages

Oxyimines, Hetero Diels-Alder adducts, and disulfide bridges are reversible and breakable junctions under certain experimental conditions (solvent, temperature, pH) and have also been developed as non-covalent linkers in PS-*b*-PEO diblock copolymer systems. Once disrupted, they leave alone the minor block to be washed with a selective solvent (water or ethanol) before giving nanoporous templates.

7.2.1 Hetero Diels-Alder Linkages

PS-*b*-PEO BCPs synthesized *via* the combination of RAFT and hetero Diels-Alder (DA) cycloaddition were reported in a study reported by Glassner *et al.*[182](Scheme I-9A). 2 wt % polymer solution in chloroform was used to drop-cast the films onto silicon wafers. The DA linkage undergoes retro action once heated at 90 °C during 15 h both in solid state and solution (Scheme I-9B).

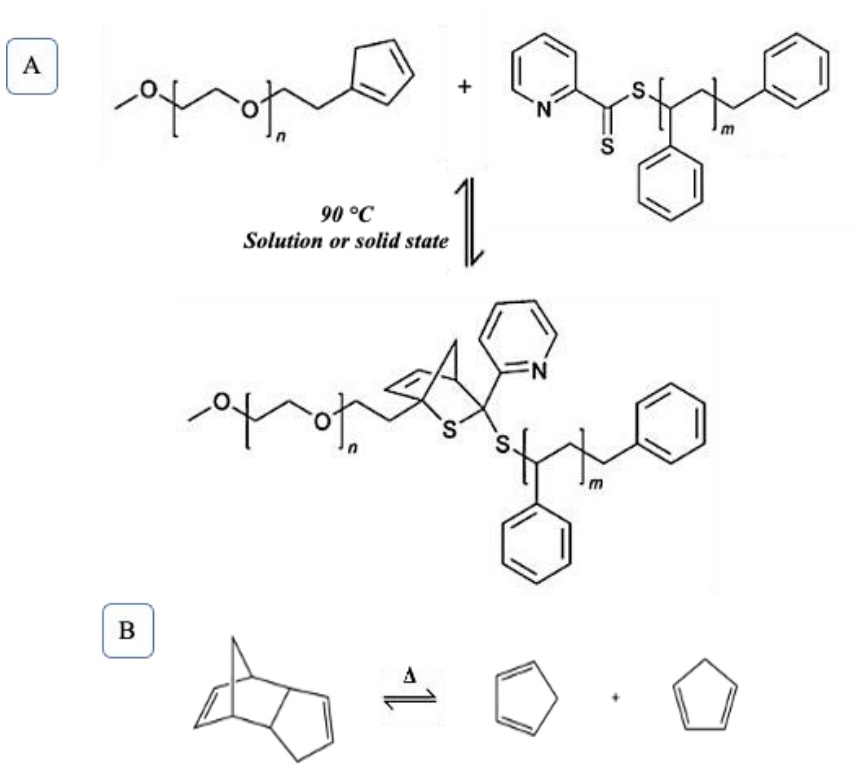

Scheme I-9: Schematic interpretation of the synthesis of PS-PEO BCP by RAFT-hDA approach (A)[182] and the thermoreversible nature of hetero-DA unit (B).

This reaction can be easily monitored *via* UV-Vis spectroscopy because of the dithioesters coloration when C=S double bond $\pi \rightarrow \pi^*$ transition occurs (molecular transition corresponding to an electron promotion from π-bonding orbital to antibonding π-orbital*).[183] Therefore, after thermocleavage of the junction, PS-*b*-PEO results in nanoporous film just by washing with water. Shorter PS blocks and 50 wt % of PEO in the block copolymer can increase the totality of pores with range from 40 to 200 nm, as evidenced in the SEM images.

7.2.2 Disulfide bonds

Another nanoporous PS matrix with pore sizes of 20 nm can be obtained after disulfide bridge removal.[184] PS-*b*-PEO block copolymers were synthesized by RAFT polymerization of styrene from PEO macroinitiator already containing the disulfide bond. Spin-coating of 0.7 wt % polymer solution in benzene followed by annealing in water/benzene vapors enhanced the lateral ordering and gave PEO cylinders perpendicular to surface. PEO cylinders resulted in pores after immersion of the films in 0.1M D, L-dithiothreitol (DTT) solution in ethanol and washing multiple times with the same solvent.

In fact, redox stimulus, provoked by DTT is enough to cleave the junction, leaving free thiol moieties on the pore walls due to hydrogen exchange and intramolecular cyclization (Scheme I-10).

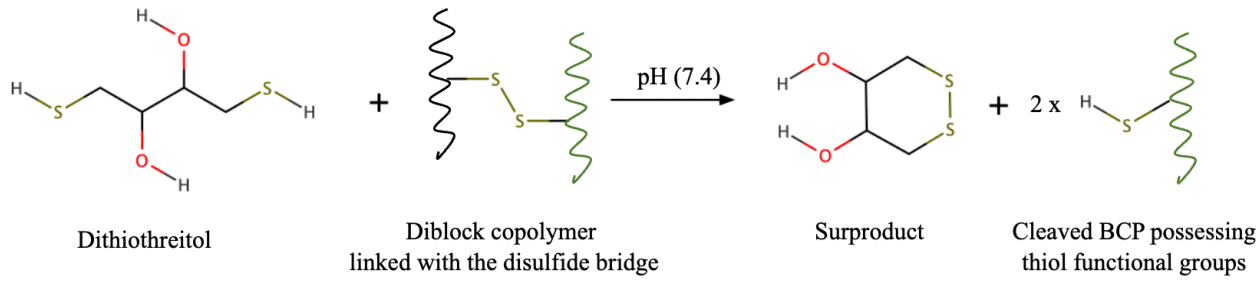

Scheme I-10: Reduction mechanism of the disulfide bond.

The thiol-moieties were then be used to produce highly ordered gold nanotubes by immersion of the nanoporous thin film in ethanol solution containing $HAuCl_4$. Despite confirming the gold loading of the pores, GISAXS analysis corroborated AFM and TEM results of generated pores.

Moreover, successful cleavage of disulfide bridge was reported in bulk channel-die thermally annealed samples of PS-*S*-*S*-PLA block copolymers, representing a rare example of the applicability of cleavable linkages for obtaining porous monoliths.[185] The material was immersed in ethanol solution containing triphenylphosphines at 65°C for 5 days. Ethanol washing resulted in 20 nm pores.

7.2.3 Oxy-imine junctions

Additional interesting porous PS with functionalized cavities can be obtained from PS-*b*-PEO precursors bearing an oxy-imine junction.[186] Firstly, PEO-based macroinitiator bearing the oxy-imine group was used for ATPR polymerization of styrene. Classic spin-coating and solvent annealing procedure gave 20 nm dispersed PEO cylindrical domains in PS matrix with high degree of lateral ordering. Dynamic covalent oxy-imine groups are known to be sensitive and reversible in acidic conditions. Therefore, once the block copolymer film was immersed in trifluoroacetic acid (TFA) solution and washed with water, the PEO cylinders were removed thus leaving a PS matrix with oxy-amine functionalized pores. The availability of the oxy-amine pore groups was confirmed by reforming the oxy-imine linkage through covalent (with an aldehyde group) and non-covalent (with gold ions) interactions.

7.2.4 Anthracene junctions

The anthracene junction is another type of reversible linkage cleavable either by UV at 280 nm or by heating at 170 °C for 4 h. Actually, PS-*b*-PMMA with this junction was the first reported block copolymer system bearing a photocleavable linkage.[187] Penelle *et al.* reported the synthesis by successful UV-coupling of anthracene end-functionalized PS and PMMA even though long reaction times were needed (150 h) and side reactions occurred. Later, the same research group investigated the creation of nanoporous templates from this precursor.[188] At the beginning, spin-coated thin films were annealed in supercritical CO_2 to obtain sufficient mobility for phase separation (thanks to the plasticizing effect of the CO_2). UV cleavage of the thin films remained limited to 70% due to the presence of anthracene dimers side reactions while thermal cleavage (heating above 130 °C) resulted in complete split of the junction. PMMA was washed off with acetic acid, thus giving 47 nm porous PS matrix.

7.3 Supramolecular linkages

Supramolecular block copolymers usually contain blocks linked between in highly directional non-covalent manner with either metal ± ligand complexes, ionic interactions, or hydrogen bonds (Figure I-13). They have been attracting more and more attention in polymer science due to their adjustive, eco-friendly and self-healing properties.[189] In order to achieve a nanoporous thin film from these precursors, washing with selective solvent containing an external stimuli component (protic solvent or counter ion for example) offers easy generation of porosity because it simultaneously disrupts the supramolecular linkage and extracts the minor block. Furthermore, metal complexes can enhance the electrochemical and photochemical properties of the material, while ionic or H-interactions strengthen block interaction *via* targeted reactive groups and further enhance phase separation.

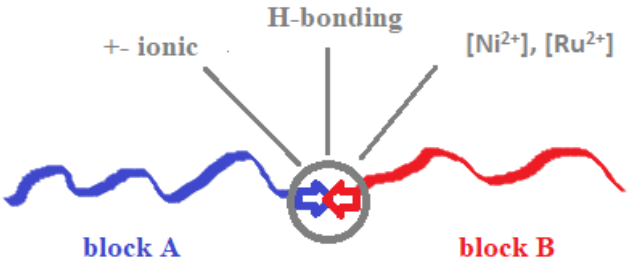

Figure I-13: Types of supramolecular linkages in block copolymer precursors for generation of porous thin films.

Once again, a major part of nanoporous materials from (metallo-) supramolecular self-assembled block copolymers are obtained using PS-*b*-PEO. The three-step procedure starts with spin-coating of thin films, followed by disruption of the metal ± ligand complexes and finally washing off the minor block with a selective solvent.

7.3.1 Metal-ligand complexes and ionic bonds

Ruthenium (II) and Nickel (II) terpyridine bis-complexes have been reported as supramolecular linkers between the PS and PEO blocks, thus giving PS-[Ru]-PEO and PS-[Ni]-PEO block copolymers.[190,191]

THF could be a better option as spin-coating solvent than benzene due to its ability to better solubilize charged metal ligand complexes. On the other side, the latter is often used in covalently linked PS-*b*-PEO. Another common feature includes exposure of the thin films to deep UV irradiations (1.8 $J.cm^{-2}$) towards strengthening the PS matrix before PEO removal. In the case of PS-[Ru]-PEO, the ruthenium terpyridine bis-complexes can be disturbed by using an aqueous $Ce(SO_4)_2$ solution at pH=1, while for the PS-[Ni]-PEO, $MeOH/H_2O$ (9/1 v/v) solution containing 0.005 M of KCN was implemented. In fact, Ce (IV) ions oxidize Ru (II) to Ru (III), while an excess of cyanide disrupts the supramolecular complex linkages and releases the PEO block that is further washed off by the selective solvent (water). The simplest way to evidence PEO removal from the thin films is FTIR analysis, where the intensity of the bands at 2900 cm^{-1} and 1100 cm^{-1} strongly decreases once this block is successfully extracted. The same phenomena resulting to generation of porosity was evidenced *via* imaging techniques such as SFM, TEM and AFM.

Besides, porous PS materials can be equally made from ionically bonded PS-*b*-PEO block copolymers. Proton transfer occurs upon mixing PS-SO_3H and PEO-NMe_2 homopolymers, *via* acid-base reaction in benzene solution between their respective end groups.[192] Therefore $PS^{-+}PEO$ is obtained. Evenly distributed PEO cylinders in PS matrix were achieved when using 1/1 SO_3H/ $N(Me)_2$ molar ratio. 0.05M NaCl water/methanol (1/1 v/v) solution was sufficient to disrupt the ionic bonding and therefore remove the PEO phase by solvent extraction. Recently the ionic junctions have also been reported as a method for enhancing phase-separation in diblock copolymer systems.[193] The electrostatic interactions of the counter ions in the triazolium unit employed as a bond linking two distinct polymer chains led to an increased T_{ODT} compared to the one of a neutral BCP.

The availability of the functional groups present of the pore walls can be confirmed by fluorescent dye grafting in the case of $PS^{-+}PEO$ and PS-[Ni]-PEO precursors. Therefore, terpyridine free ligands or sulfonate groups can be evidenced on the pore walls opening the pathway for further applications such as selective catalysis, sensors and membranes.

7.3.2 Hydrogen-Bonding junctions

The concept of supramolecular AB diblock copolymers build on H-bonding favorized associations of incompatible polymer chains was primarily introduced by Gong *et al*.[194,195] Thereupon, the novelty of synthesizing non-covalently linked PS-*b*-PMMA and their implementation for the generation of nanoporous systems was reported by Montarnal *et al*.[196] Therefore, the PS-*supra*-PMMA BCPs investigated in this study were synthesized through the combination of RAFT polymerization and supramolecular coupling. In the first place, two RAFT transfer agents consisting of symmetrical (SOA) and asymmetrical oligoamides (AOA) yielded PMMA-SOA and PS-AOA homopolymers. The latter were afterwards used as hydrogen-building blocks by efficient supramolecular coupling in chloroform, due to the high association constant of the SOA and AOA building units in this solvent. Such behavior was confirmed through SEC upon mixing of the two homopolymer precursors.

In addition, the amides were chosen over other chemical functions due to their superior thermal and chemical stability especially needed during the thermal annealing of PS-PMMA systems. Hence, efficient thermal annealing (1 h at 180 °C) of PS_{30k}-*supra*-$PMMA_{15k}$ led to hexagonal arrays of PMMA in PS matrix, as observable by SAXS experiments.

On the other side, under similar annealing conditions, PS_{30k}-*supra*-$PMMA_{30k}$ self-assembled into a disordered morphology, thus emphasizing the necessity to find a perfect balance for promoting ordered self-assemblies between the supramolecular junction and the ratios of the blocks (Figure I-14). Nanoporous materials in this case were achieved by using simple polar solvents that break the supramolecular junction and wash off the PMMA phase. For this purpose, the films were immersed in 3 wt % $CHCl_3$ in H_2O/MeOH solution for 10 min. Such approach led to vertically oriented 14 nm pores spanning the entire film thickness.

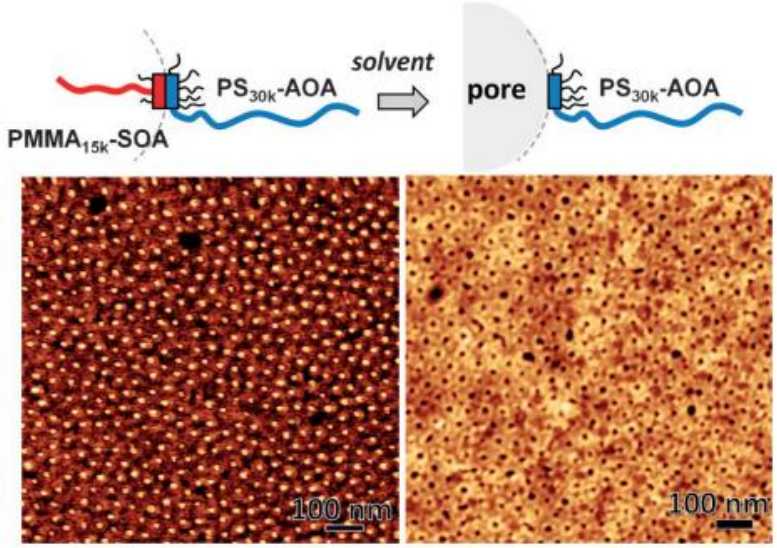

Figure I-14: AFM phase images of PS-*supra*-PMMA BCP thin film before (left) and after disruption of the H-bond junction and PMMA washing (right). [196]

8. Conclusion and Outlook

This review broadly displays that self-assemblies of block copolymers represent a fitting approach for the generation of nanoporous templates. However, three important steps need to be ensured to achieve a stable porous structure.

Foremost, the block copolymer synthesis must be perfectly mastered so that any unfortunate impact on the following stages is avoided. Due to the huge recent advances in BCP synthesis, most noticeably in controlled radical polymerization techniques, this step should not represent an obstacle for the future.

In the second place, the nano-world guidelines should be respected to achieve the optimal phase-separated morphologies for each BCP thin film association. Through this report, we can evidence an optimized control of the self-assembly process in the nanometer range thick films, especially in the recent published works. The different annealing techniques have been adjusted to suitably correspond to almost each BCP pair. Nevertheless, there is research still to be done in terms of microdomain orientation control and pursuing long-range order toward defect-free nanostructures.

Third, the removal of the sacrificial component should be operated with considerable precautions to preserve the integrity of the porous matrix. From one side, opportune solution for harmless chemical etching techniques and matrix stabilization should be pursued. On the other side, the cleavable linkages approach is expected to be accustomed to wider range of BCP, others than PS-*b*-PEO.

Regardless, simultaneous ameliorations of the previously discussed points could be possibly accompanied by the quest for different and innovative BCP precursors than the ones reported thus far. For example, the renewable polysaccharides have been demonstrated to self-assemble in BCP systems with polystyrene in the studies of Borsali and co-workers, which makes them eventual sacrificial block for the generation of nanoporous templates.[197–199] Moreover, some of the degradable block copolymers present encouraging values for their Flory-Huggins interaction parameter, but their self-assembly needs yet to be studied.

The connection between the mechanical resistance of thin films and their possible application is also important to be mentioned. It is known that the nanometer range thickness of the porous thin films can be limitational for their employment in functional devices. Hence, there is a necessity to support these thin films on silicon or polysulfone membranes, possessing satisfactory robustness. The use of porous monoliths may not be the ideal alternative, since chemical etching can possibly damage the matrix, or the latter can present non-uniform pores resulting in reduced performances. The development of integral asymmetric SNIPS membranes is becoming proficient; however, their applications are restricted to the UF purposes. Taking in account the recent developments in the domain of 3D printing,[200–202] the fashionable association of this approach and the BCP self-assembly could open the pathway to structures presenting controlled and stable cavities on multiple levels of porosity, thus opening the pathway of the BCP self-assemblies to a far-reaching range of possible applications.

References

[1] M. De La Olvera Cruz, *J. Chem. Phys.* **1989**, *90*, 1995.
[2] T. Nose, *Polymer (Guildf).* **1995**, *36*, 2243.
[3] T. L. Bucholz, Y. L. Loo, *Macromolecules* **2006**, *39*, 6075.
[4] D. P. B. Copolymers, Y. Ren, T. P. Lodge, M. A. Hillmyer, *Society* **2000**, 866.
[5] A. E. Curzon, *J. Phys. D. Appl. Phys.* **1991**, *24*, 1616.
[6] M. R. Hammond, E. Cochran, G. H. Fredrickson, E. J. Kramer, *Macromolecules* **2005**, *38*, 6575.
[7] D. Grande, J. Penelle, P. Davidson, I. Beurroies, R. Denoyel, *Microporous Mesoporous Mater.* **2011**, *140*, 34.
[8] Q. Liu, Z. Tang, B. Ou, L. Liu, Z. Zhou, S. Shen, Y. Duan, *Mater. Chem. Phys.* **2014**, *144*, 213.
[9] M. A. Hillmyer, *Adv. Polym. Sci.* **2005**, *190*, 137.
[10] D. A. Olson, L. Chen, M. A. Hillmyer, *Chem. Mater.* **2008**, *20*, 869.
[11] R. Poupart, D. Grande, B. Carbonnier, B. Le Droumaguet, *Prog. Polym. Sci.* **2019**, *96*, 21.
[12] C. G. Gamys, J. M. Schumers, C. Mugemana, C. A. Fustin, J. F. Gohy, *Macromol. Rapid Commun.* **2013**, *34*, 962.
[13] J. N. L. Albert, T. H. Epps, *Mater. Today* **2010**, *13*, 24.
[14] P. C. Shaw, T. M.; Trolier-McKinstry, S.; McIntyre, *Annu. Rev. Mater. Sci* **2000**, *30*, 263.
[15] J. S. Lee, A. Hirao, S. Nakahama, *Macromolecules* **1989**, *22*, 2602.
[16] J. S. Lee, A. Hirao, S. Nakahama, *Macromolecules* **1988**, *21*, 274.
[17] S. Rakovsky, G. Zaikov, *J. Appl. Polym. Sci.* **2004**, *91*, 2048.
[18] K. Dalnoki-Veress, J. A. Forrest, J. R. Stevens, J. R. Dutcher, *Phys. A Stat. Mech. its Appl.* **1997**, *239*, 87.
[19] T. Hashimoto, K. Tsutsumi, Y. Funaki, *Langmuir* **1997**, *13*, 6869.
[20] S. Matsumura, A. R. Hlil, C. Lepiller, J. Gaudet, D. Guay, Z. Shi, S. Holdcroft, A. S. Hay, *J. Polym. Sci. Part A Polym. Chem.* **2008**, *46*, 7207.
[21] P. Mansky, C. K. Harrison, P. M. Chaikin, R. A. Register, N. Yao, *Appl. Phys. Lett.* **1995**, *2586*, 2586.
[22] C. Rüttiger, H. Hübner, S. Schöttner, T. Winter, G. Cherkashinin, B. Kuttich, B. Stühn, M. Gallei, *ACS Appl. Mater. Interfaces* **2018**, *10*, 4018.
[23] A. T. Thurn-albrecht, J. Schotter, G. A. Kästle, N. Emley, T. Shibauchi, K. Guarini, C. T. Black, M. T. Tuominen, T. P. Russell, *Science (80-.).* **2000**, *290*, 2126.
[24] T. Thurn-Albrecht, R. Steiner, J. DeRouchey, C. M. Stafford, E. Huang, M. Bal, M. Tuominen, C. J. Hawker, T. P. Russell, *Adv. Mater.* **2000**, *12*, 787.
[25] X. Li, R. D. Dupuis, T. Wernicke, *Photonics Res.* **2019**, *7*, SUVP1.
[26] K. Naito, H. Hieda, M. Sakurai, Y. Kamata, K. Asakawa, *INTERMAG Eur. 2002 - IEEE Int. Magn. Conf.* **2002**, *38*, 1949.
[27] G. S. W. Craig, P. F. Nealey, *J. Photopolym. Sci. Technol.* **2007**, *20*, 511.
[28] R. Ruiz, H. Kang, F. A. Detcheverry, E. Dobisz, D. S. Kercher, T. R. Albrecht, J. J. De Pablo, P. F. Nealey, *Science (80-.).* **2008**, *321*, 936.
[29] C. Park, J. Yoon, E. L. Thomas, *Polymer (Guildf).* **2003**, *44*, 6725.
[30] B. A. C. Edrington, A. M. Urbas, P. Derege, C. X. Chen, T. M. Swager, N. Hadjichristidis, M. Xenidou, L. J. Fetters, J. D. Joannopoulos, Y. Fink, E. L. Thomas, **2001**, 421.
[31] C. S. Wu, P. Y. Tsai, T. Y. Wang, E. L. Lin, Y. C. Huang, Y. W. Chiang, *Anal. Chem.*

2018, *90*, 4847.
[32] W. Joo, M. S. Park, J. K. Kim, *Langmuir* **2006**, *22*, 7960.
[33] S. Y. Yang, I. Ryu, H. Y. Kim, J. K. Kim, S. K. Jang, T. P. Russell, *Adv. Mater.* **2006**, *18*, 709.
[34] S. Y. Yang, J. Park, J. Yoon, M. Ree, S. K. Jang, J. K. Kim, *Adv. Funct. Mater.* **2008**, *18*, 1371.
[35] B. G. Rånby, J. F. Rabek, *Principles and applications*, New York, Wiley, **1975**.
[36] C. Wochnowski, M. A. S. Eldin, S. Metev, *Polym. Degrad. Stab.* **2005**, *89*, 252.
[37] T. Xu, H. C. Kim, J. DeRouchey, C. Seney, C. Levesque, P. Martin, C. M. Stafford, T. P. Russell, *Polymer (Guildf).* **2001**, *42*, 9091.
[38] Y. Li, T. Ito, *Anal. Chem.* **2009**, *81*, 851.
[39] K. W. Guarini, C. T. Black, S. H. I. Yeung, *Adv. Mater.* **2002**, *14*, 1290.
[40] Y. Li, H. C. Maire, T. Ito, *Langmuir* **2007**, *23*, 12771.
[41] Y. Li, T. Ito, *Langmuir* **2008**, *24*, 8959.
[42] P. Mansky, Y. Liu, E. Huang, T. P. Russell, C. Hawker, *Science (80-.).* **1997**, *275*, 1458.
[43] T. Thurn-Albrecht, J. Derouchey, T. P. Russell, H. M. Jaeger, *Macromolecules* **2000**, *33*, 3250.
[44] S. Ham, C. Shin, E. Kim, D. Y. Ryu, U. Jeong, T. P. Russell, C. J. Hawker, *Macromolecules* **2008**, *41*, 6431.
[45] C. Liedel, C. W. Pester, M. Ruppel, V. S. Urban, A. Böker, *Macromol. Chem. Phys.* **2012**, *213*, 259.
[46] E. Field, B. Copolymer, M. Introduction, E. Interaction, C. Varia-, **1991**, 6546.
[47] I. A. Zucchi, E. Poliani, M. Perego, *Nanotechnology* **2010**, *21*.
[48] T. P. Russell, R. P. Hjelm, P. A. Seeger, *Macromolecules* **1990**, *23*, 890.
[49] X. Yu, J. Peng, L. Cui, H. Wang, B. Li, Y. Han, *Macromolecules* **2004**, *37*, 7301.
[50] H. C. Maire, S. Ibrahim, Y. Li, T. Ito, *Polymer (Guildf).* **2009**, *50*, 2273.
[51] U. Jeong, D. Y. Ryu, D. H. Kho, J. K. Kim, J. T. Goldbach, D. H. Kim, T. P. Russell, *Adv. Mater.* **2004**, *16*, 533.
[52] J. Peng, X. Gao, Y. Wei, H. Wang, B. Li, Y. Han, *J. Chem. Phys.* **2005**, *122*.
[53] W. Joo, S. Y. Yang, J. K. Kim, H. Jinnai, *Langmuir* **2008**, *24*, 12612.
[54] S. Matsumura, A. R. Hlil, C. Lepiller, J. Gaudet, D. Guay, Z. Shi, S. Holdcroft, A. S. Hay, *J. Polym. Sci. Part A Polym. Chem.* **2008**, *46*, 7207.
[55] T. H. Nguyen, M. Vayer, C. Sinturel, *Appl. Surf. Sci.* **2018**, *427*, 464.
[56] U. Jeong, H. C. Kim, R. L. Rodriguez, I. Y. Tsai, C. M. Stafford, J. K. Kim, C. J. Hawker, T. P. Russell, *Adv. Mater.* **2002**, *14*, 274.
[57] U. Jeong, D. Y. Ryu, J. K. Kim, D. H. Kim, X. Wu, T. P. Russell, *Macromolecules* **2003**, *36*, 10126.
[58] S. C. Park, B. J. Kim, C. J. Hawker, E. J. Kramer, J. Bang, J. S. Ha, *Macromolecules* **2007**, *40*, 8119.
[59] G. Biresaw, C. J. Carriere, *J. Polym. Sci. Part B Polym. Phys.* **2002**, *40*, 2248.
[60] U. Jeong, D. Y. Ryu, J. K. Kim, D. H. Kim, T. P. Russell, C. J. Hawker, *Adv. Mater.* **2003**, *15*, 1247.
[61] J. Bang, S. H. Kim, E. Drockenmuller, M. J. Misner, T. P. Russell, C. J. Hawker, *J. Am. Chem. Soc.* **2006**, *128*, 7622.
[62] J. Bang, B. J. Kim, G. E. Stein, T. P. Russell, X. Li, J. Wang, E. J. Kramer, C. J. Hawker, *Macromolecules* **2007**, *40*, 7019.
[63] A. S. Zalusky, R. Olayo-Valles, C. J. Taylor, M. A. Hillmyer, *J. Am. Chem. Soc.* **2001**, *123*, 1519.
[64] A. S. Zalusky, R. Olayo-Valles, J. H. Wolf, M. A. Hillmyer, *J. Am. Chem. Soc.* **2002**, *124*, 12761.

[65] M. S. She, T. Y. Lo, H. Y. Hsueh, R. M. Ho, *NPG Asia Mater.* **2013**, *5*, e42.
[66] H. Tsuji, Y. Ikada, *J. Polym. Sci. Part A Polym. Chem.* **1998**, *36*, 59.
[67] T. Maharana, B. Mohanty, Y. S. Negi, *Prog. Polym. Sci.* **2009**, *34*, 99.
[68] A. Sarkar, M. Stefik, *Mater. Chem. Front.* **2017**.
[69] J. Lunt, *Polym. Degrad. Stab.* **1998**, *59*, 145.
[70] F. Auriemma, C. De Rosa, A. Malafronte, R. Di Girolamo, C. Santillo, Y. Gerelli, G. Fragneto, R. Barker, V. Pavone, O. Maglio, A. Lombardi, *ACS Appl. Mater. Interfaces* **2017**, *9*, 29318.
[71] R. Olayo-Valles, M. S. Lund, C. Leighton, M. A. Hillmyer, *J. Mater. Chem.* **2004**, *14*, 2729.
[72] R. M. Ho, W. H. Tseng, H. W. Fan, Y. W. Chiang, C. C. Lin, B. T. Ko, B. H. Huang, *Polymer (Guildf).* **2005**, *46*, 9362.
[73] R. Olayo-Valles, S. Guo, M. S. Lund, C. Leighton, M. A. Hillmyer, *Macromolecules* **2005**, *38*, 10101.
[74] X. Chen, L. Zhang, *Sensors Actuators, B Chem.* **2018**, *254*, 648.
[75] V. Luque-Agudo, M. Hierro-Oliva, A. M. Gallardo-Moreno, M. L. González-Martín, *Polym. Test.* **2021**, *96*.
[76] K. Asakawa, T. Hiraoka, *Japanese J. Appl. Physics, Part 1 Regul. Pap. Short Notes Rev. Pap.* **2002**, *41*, 6112.
[77] J. M. Leiston-Belanger, T. P. Russell, E. Drockenmuller, C. J. Hawker, *Macromolecules* **2005**, *38*, 7676.
[78] W. A. Phillip, M. A. Hillmyer, E. L. Cussler, *Macromolecules* **2010**, *43*, 7763.
[79] S. H. Kim, M. J. Misner, T. Xu, M. Kimura, T. P. Russell, *Adv. Mater.* **2004**, *16*, 226.
[80] M. Vayer, M. A. Hillmyer, M. Dirany, G. Thevenin, R. Erre, C. Sinturel, *Thin Solid Films* **2010**, *518*, 3710.
[81] C. Sinturel, M. Vayer, M. Morris, M. A. Hillmyer, *Macromolecules* **2013**, *46*, 5399.
[82] A. Baruth, M. Seo, C. H. Lin, K. Walster, A. Shankar, M. A. Hillmyer, C. Leighton, *ACS Appl. Mater. Interfaces* **2014**, *6*, 13770.
[83] G. Nelson, C. S. Drapes, M. A. Grant, R. Gnabasik, J. Wong, A. Baruth, *Micromachines* **2018**, *9*.
[84] C. Cummins, P. Mokarian-Tabari, P. Andreazza, C. Sinturel, M. A. Morris, *ACS Appl. Mater. Interfaces* **2016**, *8*, 8295.
[85] W. A. Phillip, B. O'neill, M. Rodwogin, M. A. Hillmyer, E. L. Cussler, *ACS Appl. Mater. Interfaces* **2010**, *2*, 847.
[86] A. Malafronte, F. Auriemma, C. Santillo, R. Di Girolamo, R. Barker, Y. Gerelli, C. De Rosa, *Adv. Mater. Interfaces* **2020**, *7*, 1.
[87] M. Baiardo, G. Frisoni, M. Scandola, M. Rimelen, D. Lips, K. Ruffieux, E. Wintermantel, *J. Appl. Polym. Sci.* **2003**, *90*, 1731.
[88] K. A. Cavicchi, K. J. Berthiaume, T. P. Russell, *Polymer (Guildf).* **2005**, *46*, 11635.
[89] K. A. Cavicchi, T. P. Russell, *Macromolecules* **2007**, *40*, 1181.
[90] T. Kubo, R. F. Wang, D. A. Olson, M. Rodwogin, M. A. Hillmyer, C. Leighton, *Appl. Phys. Lett.* **2008**, *93*, 2013.
[91] S. E. Querelle, E. A. Jackson, E. L. Cussler, M. A. Hillmyer, *ACS Appl. Mater. Interfaces* **2013**, *5*, 5044.
[92] K. A. Cavicchi, A. S. Zalusky, M. A. Hillmyer, T. P. Lodge, *Macromol. Rapid Commun.* **2004**, *25*, 704.
[93] E. A. Jackson, Y. Lee, M. A. Hillmyer, *Macromolecules* **2013**, *46*, 1484.
[94] E. A. Jackson, Y. Lee, M. R. Radlauer, M. A. Hillmyer, *ACS Appl. Mater. Interfaces* **2015**, *7*, 27331.
[95] J. C. Saam, D. J. Gordon, S. Lindsey, **2011**, *2011*, 1964.

[96] P. Georgopanos, T. Y. Lo, R. M. Ho, A. Avgeropoulos, *Polym. Chem.* **2017**, *8*, 843.
[97] X. Chen, J. a Gardella, **1992**, 6631.
[98] X. Chen, J. A. Gardella, P. L. Kumler, *Macromolecules* **1992**, *25*, 6621.
[99] T. H. Andersen, S. Tougaard, N. B. Larsen, K. Almdal, I. Johannsen, *J. Electron Spectros. Relat. Phenomena* **2001**, *121*, 93.
[100] I. Erukhimovich, M. O. de la Cruz, **2004**, 2419.
[101] J. Jenczyk, M. Woźniak-Budych, M. Jarek, S. Jurga, *Eur. Polym. J.* **2018**, *98*, 384.
[102] S. K. Varshney, D. N. Khanna, C. Fibres, P. Bajaj, S. K. Varshney, A. Misra, H. Chu, *Science (80-.).* **1980**, *18*, 295.
[103] Y. S. Jung, C. A. Ross, *Nano Lett.* **2007**, *7*, 2046.
[104] D. Borah, M. Ozmen, S. Rasappa, M. T. Shaw, J. D. Holmes, M. A. Morris, *Langmuir* **2013**, *29*, 2809.
[105] Y. S. Jung, J. B. Chang, E. Verploegen, K. K. Berggren, C. A. Ross, *Nano Lett.* **2010**, *10*, 1000.
[106] Y. S. Jung, C. A. Ross, *Adv. Mater.* **2009**, *21*, 2540.
[107] Y. S. Jung, W. Jung, C. A. Ross, *Nano Lett.* **2008**, *8*, 2975.
[108] K. W. Gotrik, A. F. Hannon, J. G. Son, B. Keller, A. Alexander-Katz, C. A. Ross, *ACS Nano* **2012**, *6*, 8052.
[109] M. H. Cheng, Y. C. Hsu, C. W. Chang, H. W. Ko, P. Y. Chung, J. T. Chen, *ACS Appl. Mater. Interfaces* **2017**, *9*, 21010.
[110] R. G. Hobbs, R. A. Farrell, C. T. Bolger, R. A. Kelly, M. A. Morris, N. Petkov, J. D. Holmes, *ACS Appl. Mater. Interfaces* **2012**, *4*, 4637.
[111] S. Archambault, C. Girardot, M. Salaün, M. Delalande, S. Böhme, G. Cunge, E. Pargon, O. Joubert, M. Zelsmann, *Adv. Etch Technol. Nanopatterning III* **2014**, *9054*, 90540O.
[112] C. C. Chao, R. M. Ho, P. Georgopanos, A. Avgeropoulos, E. L. Thomas, *Soft Matter* **2010**, *6*, 3582.
[113] Y. S. Jung, C. A. Ross, *Small* **2009**, *5*, 1654.
[114] B. M. D. O'Driscoll, R. A. Kelly, M. Shaw, P. Mokarian-Tabari, G. Liontos, K. Ntetsikas, A. Avgeropoulos, N. Petkov, M. A. Morris, *Eur. Polym. J.* **2013**, *49*, 3445.
[115] S. Ndoni, M. E. Vigild, R. H. Berg, *J. Am. Chem. Soc.* **2003**, *125*, 13366.
[116] H. H. Hyman, R. A. Garber, *J. Am. Chem. Soc.* **1959**, *81*, 1847.
[117] T. C. Lin, K. C. Yang, P. Georgopanos, A. Avgeropoulos, R. M. Ho, *Polymer (Guildf).* **2017**, *126*, 360.
[118] G. B. Demirel, F. Buyukserin, M. A. Morris, G. Demirel, *ACS Appl. Mater. Interfaces* **2012**, *4*, 280.
[119] F. Guo, J. W. Andreasen, M. E. Vigild, S. Ndoni, *Macromolecules* **2007**, *40*, 3669.
[120] M. S. Hansen, M. E. Vigild, R. H. Berg, S. Ndoni, *Polym. Bull.* **2004**, *51*, 403.
[121] F. Guo, K. Jankova, L. Schulte, M. E. Vigild, S. Ndoni, *Macromolecules* **2008**, *41*, 1486.
[122] R. B. Merrifield, *J. Am. Chem. Soc.* **1963**, *85*, 2149.
[123] E. Bajraktarova-Valjakova, V. Korunoska-Stevkovska, S. Georgieva, K. Ivanovski, C. Bajraktarova-Misevska, A. Mijoska, A. Grozdanov, *Access Maced. J. Med. Sci.* **2018**, *6*, 2257.
[124] J. Yin, X. Yao, J. Y. Liou, W. Sun, Y. Sen Sun, Y. Wang, *ACS Nano* **2013**, *7*, 9961.
[125] W. Zha, C. D. Han, D. H. Lee, S. H. Han, J. K. Kim, J. H. Kang, C. Park, *Macromolecules* **2007**, *40*, 2109.
[126] C. J. Clarke, A. Eisenberg, J. La Scala, M. H. Rafailovich, J. Sokolov, Z. Li, S. Qu, D. Nguyen, S. A. Schwarz, Y. Strzhemechny, B. B. Sauer, *Macromolecules* **1997**, *30*, 4184.
[127] Z. Wang, Y. Wang, *Macromolecules* **2016**, *49*, 182.
[128] L. Guo, Z. Wang, Y. Wang, *Macromolecules* **2018**, *51*, 6248.
[129] T. Xu, J. Stevens, J. A. Villa, J. T. Goldbach, K. W. Guarini, C. T. Black, C. J. Hawker,

T. P. Russell, *Adv. Funct. Mater.* **2003**, *13*, 698.
[130] H. Ahn, S. Park, S. W. Kim, P. J. Yoo, D. Y. Ryu, T. P. Russell, *ACS Nano* **2014**, *8*, 11745.
[131] S. Park, T. Jun, H. R. Yoon, S. Jo, J. H. Kim, C. Y. Ryu, D. Y. Ryu, *ACS Appl. Polym. Mater.* **2019**, *1*, 584.
[132] K. V. Peinemann, V. Abetz, P. F. W. Simon, *Nat. Mater.* **2007**, *6*, 992.
[133] Z. Zhang, M. M. Rahman, C. Abetz, A. L. Höhme, E. Sperling, V. Abetz, *Adv. Mater.* **2020**, *32*.
[134] J. Hahn, J. I. Clodt, C. Abetz, V. Filiz, V. Abetz, *ACS Appl. Mater. Interfaces* **2015**, *7*, 21130.
[135] V. Abetz, *Macromol. Rapid Commun.* **2015**, *36*, 10.
[136] S. Rangou, K. Buhr, V. Filiz, J. I. Clodt, B. Lademann, J. Hahn, A. Jung, V. Abetz, *J. Memb. Sci.* **2014**, *451*, 266.
[137] A. Jung, S. Rangou, C. Abetz, V. Filiz, V. Abetz, *Macromol. Mater. Eng.* **2012**, *297*, 790.
[138] M. Karunakaran, S. P. Nunes, X. Qiu, H. Yu, K. V. Peinemann, *J. Memb. Sci.* **2014**, *453*, 471.
[139] S. Schöttner, H. J. Schaffrath, M. Gallei, *Macromolecules* **2016**, *49*, 7286.
[140] W. A. Phillip, R. M. Dorin, E. M. V Hoek, U. Wiesner, **2011**, 2892.
[141] R. A. Mulvenna, J. L. Weidman, B. Jing, J. A. Pople, Y. Zhu, B. W. Boudouris, W. A. Phillip, *J. Memb. Sci.* **2014**, *470*, 246.
[142] S. Nehache, M. Semsarilar, A. Deratani, D. Quemener, *Polymers (Basel).* **2018**, *10*.
[143] A. Jung, V. Filiz, S. Rangou, K. Buhr, P. Merten, J. Hahn, J. Clodt, C. Abetz, V. Abetz, 610.
[144] G. Zhu, C. Yang, Y. Yin, Z. Yi, X. Chen, L. Liu, *J. Memb. Sci.* **2019**, *589*, 117255.
[145] R. Moser, W. Reynolds, F. Schraub, **1998**, *280*.
[146] H. Tubes, M. Materials, C. Hollow, P. Brushes, **2001**, 117.
[147] S. Valkama, T. Ruotsalainen, A. Nykänen, A. Laiho, H. Kosonen, G. Ten Brinke, O. Ikkala, J. Ruokolainen, *Macromolecules* **2006**, *39*, 9327.
[148] G. G. Du Sart, I. Vukovic, Z. Vukovic, E. Polushkin, P. Hiekkataipale, J. Ruokolainen, K. Loos, G. Ten Brinke, *Macromol. Rapid Commun.* **2011**, *32*, 366.
[149] A. Sidorenko, I. Tokarev, S. Minko, M. Stamm, *J. Am. Chem. Soc.* **2003**, *125*, 12211.
[150] X. Liu, M. Stamm, *Nanoscale Res. Lett.* **2009**, *4*, 459.
[151] W. Lee, X. Zhang, R. M. Briber, *Polymer (Guildf).* **2010**, *51*, 2376.
[152] S. P. Albu, A. Ghicov, J. M. Macak, R. Hahn, P. Schmuki, *Langmuir* **2007**, *28*, 1.
[153] H. Mao, M. A. Hillmyer, *Macromolecules* **2005**, *38*, 4038.
[154] E. W. Yankee, D. J. Cram, **1964**, *3002*, 6333.
[155] Z. Tajmoradi, H. Roghani-Mamaqani, M. Salami-Kalajahi, *Stimuli-transition of hydrophobicity/hydrophilicity in o-nitrobenzyl ester-containing multi-responsive copolymers: Application in patterning and droplet stabilization in heterogeneous media*, Vol. 205, **2020**.
[156] O. Bertrand, J. M. Schumers, C. Kuppan, J. Marchand-Brynaert, C. A. Fustin, J. F. Gohy, *Photo-induced micellization of block copolymers bearing 4,5-dimethoxy-2-nitrobenzyl side groups*, Vol. 7, **2011**, pp. 6891–6896.
[157] J. M. Schumers, C. A. Fustin, J. F. Gohy, *Macromol. Rapid Commun.* **2010**, *31*, 1588.
[158] C. G. Bochet, *J. Chem. Soc. Perkin 1* **2002**, *2*, 125.
[159] A. Romano, I. Roppolo, M. Giebler, K. Dietliker, Možina, P. Šket, I. Mühlbacher, S. Schlögl, M. Sangermano, *RSC Adv.* **2018**, *8*, 41904.
[160] A. Romano, I. Roppolo, E. Rossegger, S. Schlögl, M. Sangermano, *Materials (Basel).* **2020**, *13*, 1.

[161] C. G. Gamys, J. M. Schumers, A. Vlad, C. A. Fustin, J. F. Gohy, *Soft Matter* **2012**, *8*, 4486.
[162] M. Kang, B. Moon, *Macromolecules* **2009**, *42*, 455.
[163] J. M. Schumers, J. F. Gohy, C. A. Fustin, *Polym. Chem.* **2010**, *1*, 161.
[164] J. M. Schumers, A. Vlad, I. Huynen, J. F. Gohy, C. A. Fustin, *Macromol. Rapid Commun.* **2012**, *33*, 199.
[165] H. Zhao, W. Gu, E. Sterner, T. P. Russell, E. B. Coughlin, P. Theato, *Macromolecules* **2011**, *44*, 6433.
[166] X. Ma, X. Sui, Z. Zhang, C. Li, N. Zhang, A. Chen, Q. Xie, L. Gao, *RSC Adv.* **2015**, *5*, 98105.
[167] S. R. Trenor, A. R. Shultz, B. J. Love, T. E. Long, *Chem. Rev.* **2004**, *104*, 3059.
[168] S. Altinpinar, W. Ali, P. Schuchardt, P. Yildiz, H. Zhao, P. Theato, J. S. Gutmann, *Polymers (Basel).* **2020**, *12*, 1.
[169] T. Ito, H. Coceancigh, Y. Yi, J. N. Sharma, F. C. Parks, A. H. Flood, *Langmuir* **2020**, *36*, 9259.
[170] H. Zhao, W. Gu, M. W. Thielke, E. Sterner, T. Tsai, T. P. Russell, E. B. Coughlin, P. Theato, *Macromolecules* **2013**, *46*, 5195.
[171] H. Zhao, W. Gu, R. Kakuchi, Z. Sun, E. Sterner, T. P. Russell, E. B. Coughlin, P. Theato, *ACS Macro Lett.* **2014**, *3*, 204.
[172] M. S. Shchepinov, V. A. Korshun, *Chem. Soc. Rev.* **2003**, *32*, 170.
[173] M. Ciftci, Y. Yagci, *Macromol. Rapid Commun.* **2018**, *39*, 1.
[174] S. Yurt, U. K. Anyanwu, J. R. Scheintaub, E. B. Coughlin, D. Venkataraman, *Macromolecules* **2006**, *39*, 1670.
[175] M. Zhang, L. Yang, S. Yurt, M. J. Misner, J. T. Chen, E. B. Coughlin, D. Venkataraman, T. P. Russell, *Adv. Mater.* **2007**, *19*, 1571.
[176] Y. Qi, A. Nathani, J. Zhang, Z. Song, C. S. Sharma, S. K. Varshney, *E-Polymers* **2020**, *20*, 111.
[177] E. H. Cordes, *Prog. Phys. Org. Chem.* **2007**, *4*, 1.
[178] K. Satoh, J. E. Poelma, L. M. Campos, B. Stahl, C. J. Hawker, *Polym. Chem.* **2012**, *3*, 1890.
[179] G. Grancharov, V. Gancheva, P. Petrov, J. De Winter, P. Gerbaux, P. Dubois, O. Coulembier, *RSC Adv.* **2016**, *6*, 33468.
[180] R. Poupart, A. Benlahoues, B. Le Droumaguet, D. Grande, *ACS Appl. Mater. Interfaces* **2017**, *9*, 31279.
[181] M. Ouchi, A. Konishi, M. Takenaka, M. Sawamoto, *Polym. Chem.* **2012**, *3*, 2193.
[182] M. Glassner, J. P. Blinco, C. Barner-Kowollik, *Polym. Chem.* **2011**, *2*, 83.
[183] B. Liu, C. H. Lim, G. M. Miyake, *J. Am. Chem. Soc.* **2017**, *139*, 13616.
[184] J. H. Ryu, S. Park, B. Kim, A. Klaikherd, T. P. Russell, S. Thayumanavan, *J. Am. Chem. Soc.* **2009**, *131*, 9870.
[185] B. Le Droumaguet, R. Poupart, D. Grande, *Polym. Chem.* **2015**, *6*, 8105.
[186] J. Rao, S. De, A. Khan, *Chem. Commun.* **2012**, *48*, 3427.
[187] J. T. Goldbach, T. P. Russell, J. Penelle, *Macromolecules* **2002**, *35*, 4271.
[188] J. T. Goldbach, K. A. Lavery, J. Penelle, T. P. Russell, *Macromolecules* **2004**, *37*, 9639.
[189] T. F. A. De Greef, E. W. Meijer, *Nature* **2008**, *453*, 171.
[190] C. Mugemana, J. F. Gohy, C. A. Fustin, *Langmuir* **2012**, *28*, 3018.
[191] C. A. Fustin, B. G. G. Lohmeijer, A. S. Duwez, A. M. Jonas, U. S. Schubert, J. F. Gohy, *Adv. Mater.* **2005**, *17*, 1162.
[192] H. Yu, F. Stoffelbach, C. Detrembleur, C. A. Fustin, J. F. Gohy, *Eur. Polym. J.* **2012**, *48*, 940.
[193] Y. Luo, D. Montarnal, N. J. Treat, P. D. Hustad, M. D. Christianson, E. J. Kramer, G.

H. Fredrickson, C. J. Hawker, *ACS Macro Lett.* **2015**, *4*, 1332.
[194] M. E. SantosMiranda, C. Marcolla, C. A. Rodriguez, H. M. Wilhelm, M. R. Sierakowski, T. M. BelleBresolin, R. Alves de Freitas, *Polym Int* **2006**, *55*, 961.
[195] X. Yang, F. Hua, K. Yamato, E. Ruckenstein, B. Gong, W. Kim, C. Y. Ryu, *Angew. Chemie - Int. Ed.* **2004**, *43*, 6471.
[196] D. Montarnal, N. Delbosc, C. Chamignon, M. A. Virolleaud, Y. Luo, C. J. Hawker, E. Drockenmuller, J. Bernard, *Angew. Chemie - Int. Ed.* **2015**, *54*, 11117.
[197] C. Houga, J. Giermanska, S. Lecommandoux, R. Borsali, D. Taton, Y. Gnanou, J. F. Le Meins, *Biomacromolecules* **2009**, *10*, 32.
[198] I. Otsuka, N. Nilsson, D. B. Suyatin, I. Maximov, R. Borsali, *Soft Matter* **2017**, *13*, 7406.
[199] I. Otsuka, M. Osaka, Y. Sakai, C. Travelet, J. L. Putaux, R. Borsali, *Langmuir* **2013**, *29*, 15224.
[200] H. N. Chia, B. M. Wu, *J. Biol. Eng.* **2015**, *9*, 1.
[201] J. Z. Manapat, Q. Chen, P. Ye, R. C. Advincula, *Macromol. Mater. Eng.* **2017**, *302*, 1.
[202] J. Huang, Q. Qin, J. Wang, *Processes* **2020**, *8*.

CHAPTER II / CHAPITRE II

Introduction Chapitre II

La recherche scientifique dans le domaine des polymères, durant les dernières décennies, a fixé comme un objectif majeur l'aptitude à contrôler et maîtriser avec une haute précision la synthèse des architectures macromoléculaires avancées. Du fait de leur caractère biocompatible et dégradable, les poly(esters) et poly(carbonates) aliphatiques sont, à nos jours, parmi les structures macromoléculaires les plus étudiées à l'échelle académique mais aussi industrielle.[1,2] Le poly(ester) le plus produit actuellement est le poly(acide lactique) (PLA) avec une production de 190 000 tonnes en 2019.[3] En même temps, le marché global de production d'un autre poly(ester) - la poly(ε-caprolactone) (PCL) avoisinait une production de 86 400 tonnes en 2017.[4]

La synthèse des PCL et PLA se fait par polymérisation par ouverture de cycle (Ring Opening Polymerization (ROP) pour le terme anglais) d'esters cycliques. La ROP est une voie bien utile pour l'obtention de polymères avec des masse molaires et puretés élevés tout en gardant un contrôle de la polymérisation, ce qui mène à des structures de faible dispersité et introduit des groupements terminaux accessibles. C'est donc aussi la raison pour laquelle cette technique est utilisée pour la production de poly(carbonates) fonctionnels. De plus, ce type de polymérisation s'est avéré pratique notamment dans l'optimisation de polymères dégradables pour des applications médicales, pharmaceutiques, agricoles et environnementales.[5,6]

La force motrice d'une réaction de ROP est définie par la relaxation de la contrainte imposée par la géométrie du cycle monomère. Ainsi, un monomère est polymérisable par ouverture de cycle lorsque son enthalpie standard de polymérisation est négative et son entropie standard de polymérisation est positive, indépendamment de la température. Cette réaction de ROP peut être effectuée en masse, en solution ou encore en émulsion ou dispersion. La ROP met en jeu non seulement des monomères cycliques mais également un couple catalyseur/amorceur qui est nécessaire pour démarrer la polymérisation.

Ainsi, la macromolécule résultante contiendra des extrémités de chaine qui proviennent soit de l'amorceur soit du monomère et qui donc présentent des sites potentiels de fonctionnalisation. Par conséquence, le choix de l'amorceur et du catalyseur ainsi que le mécanisme réactionnel vont directement influencer la structure macromoléculaire finale et les groupements fonctionnels générés.[7,8]

Les amorceurs les plus utilisés dans la ROP sont à base de molécules possédant des groupes alcool, principalement des alcools primaires, même si quelques études ont montré des amorçages de polymérisation à partir d'alcools secondaires ou encore à partir de fonctions amines.[9,10] Les trois mécanismes les plus courants de la ROP sont les voies anionique, cationique et coordination-insertion.

Les composés organométalliques sont de nos jours encore, les systèmes catalytiques les plus classiques et les plus employées dans la ROP. De nombreuses réactions catalysées par ces systèmes métalliques sont hautement spécifiques, ce qui nécessite une sélection judicieuse du métal et du ligand afin d'arriver à la structure souhaitée de polymère. Le fait que les alcoxydes métalliques possèdent des orbitales p ou d disponibles leur permet de réagir comme centres de coordination. Le catalyseur métallique le plus utilisé en ROP est l'octanoate d'étain, suivi par tri-isopropoxyde d'aluminium, et dans une moindre mesure, les complexes de lanthanide. Même si le premier est le seul système organométallique approuvé par la FDA (Food and Drug Administration),[6] des inconvénients tels que la nécessité de travailler en température, les résidus métalliques dans la structure du polymère ou encore le risque important de réactions de transestérification inter et intramoléculaires, limitent l'avenir des catalyseurs organométalliques au profit de l'organocatalyse comme futur système catalytique pour la ROP.

L'utilisation de l'organocatalyse en ROP a débuté dans les vingt dernières années. Elle présente de considérables avantages comparés aux systèmes de catalyse métalliques classiques, tels que : une grande disponibilité de réactifs organiques, une sensibilité plus faible à l'oxygène et à l'humidité, une activation à température ambiante, une toxicité potentiellement plus faible et plus respectueuse de l'environnement.[11,12] En outre, l'organocatalyse peut avoir un très grand intérêt dans la copolymérisation par ouverture de cycle (ROCOP pour Ring-Opening Copolymerization en anglais). Ainsi, cette voie catalytique est de plus en plus utilisée pour des applications à haute valeur ajoutée comme le domaine biomédical, les emballages alimentaires ou les dispositifs de micro-électronique (Figure II-A).[13–15]

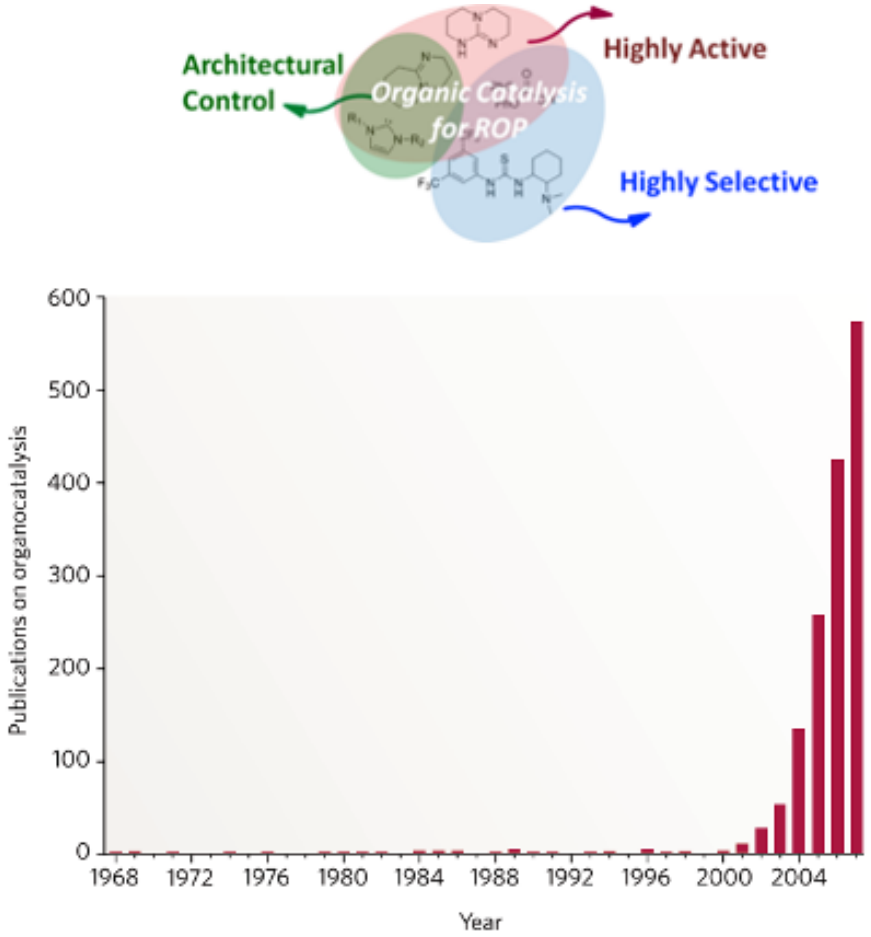

Figure II-A : Les avantages de la ROP par organocatalyse illustrés par la forte croissance des publications scientifiques.[11,16]

Les organocatalyseurs les plus employées dans les réactions de ROP peuvent être différenciés en deux catégories principales : des catalyseurs acides (de type acide de Brønsted ou Lewis) et des catalyseurs basiques (i/ de type guanidines, amidines et dérivés pyridine, ii/dérivés phosphorés et iii/ de type carbènes N-hétérocycliques).[15–18] Ainsi, dans le cas où un catalyseur organique est utilisé pour la ROP, le mécanisme réactionnel dépend du choix du couple amorceur/catalyseur. La première étape réactionnelle d'amorçage, qui est définie par le catalyseur, conduit à des mécanismes réactionnels différents. Il existe cinq cas réactionnels possibles : i) mécanisme par monomère activé lors d'une activation électrophile de l'espèce cyclique (le monomère) ; ii) mécanisme par monomère activé lors d'une activation nucléophile du monomère ; iii) mécanisme zwittérionique par activation nucléophile du monomère ; iv) mécanisme par bout de chaîne activé se produisant lors d'une activation basique de l'amorceur et v) mécanisme issu d'une activation bi fonctionnelle du monomère et de l'amorceur.[15–18]

Dans l'étude présentée dans ce Chapitre, des systèmes catalytiques organométalliques et organiques ont été examinés et comparés en vue de la synthèse d'homopolymères et copolymères à blocs à base de poly(esters) et poly(carbonates) dégradables.

D'après la littérature, il apparait que la réactivité du PLA en tant que macroamorçeur pour la synthèse des copolymères triblocs à architectures contrôlées présente un défi scientifique dû à la nature des groupements alcools présents en bout de chaîne. En effet, il s'agit d'alcools secondaires portés par un carbone disubstitué qui subissent aussi un encombrement stérique par les groupements méthyles, ce qui réduit leur réactivité lors de l'étape d'amorçage. Ainsi, nous avons essayé de surmonter ce problème par le choix d'un système catalytique optimisé tout en gardant comme objectif la production de copolymères triblocs à structures propres et contrôlées. Pour aboutir à des copolymères présentant ces caractéristiques, il fallait avoir un parfait contrôle du processus réactionnel à cause du risque de réactions secondaires de transestérification très présent lorsqu'il s'agit de poly(esters). Ainsi, la production des architectures copolymères triblocs parfaitement définies représentait un des objectifs essentiels de ce projet de thèse, d'autant plus qu'il s'agissait d'un pré-requis indispensable pour une étude fine du phénomène de séparation de phases traitée, notamment, dans le chapitre III.

L'ensemble des travaux de ce Chapitre II a été publié sous forme d'un article scientifique dans *European Polymer Journal*.[19]

Références

[1] K. Fukushima, K. Nozaki, *Macromolecules* **2020**, *53*, 5018.

[2] R. P. Brannigan, A. P. Dove, *Biomater. Sci.* **2017**, *5*, 9.

[3] E. Balla, V. Daniilidis, G. Karlioti, T. Kalamas, M. Stefanidou, N. D. Bikiaris, A. Vlachopoulos, I. Koumentakou, D. N. Bikiaris, *Polymers (Basel).* **2021**, *13*.

[4] Global Caprolactone Market is Prophesied to Fetch More than US$ 11 Bn by 2025, *https://www.globenewswire.com/en/news-release/2019/01/15/1691447/0/en/Global-Caprolactone-Market-is-Prophesied-to-Fetch-More-than-US-11-Bn-by-2025-QY-Research-Inc.html*, (accessed September 30, 2021).

[5] O. Nuyken, S. D. Pask, *Polymers (Basel).* **2013**, *5*, 361.

[6] C. Jérôme, P. Lecomte, *Adv. Drug Deliv. Rev.* **2008**, *60*, 1056.

[7] S. Penczek, J. Pretula, S. Slomkowski, **2021**, 1.

[8] Dubois, P., Coulembier, O. and Raquez, J.M. eds., **2009**. *Handbook of ring-opening polymerization*. John Wiley & Sons.

[9] T. Brossier, G. Volpi, V. Lapinte, S. Blanquer, *Polymers (Basel).* **2021**, *13*, 1.

[10] P. Baheti, O. Gimello, C. Bouilhac, P. Lacroix-Desmazes, S. M. Howdle, *Polym. Chem.* **2018**, *9*, 5594.

[11] A. Nachtergael, O. Coulembier, P. Dubois, M. Helvenstein, P. Duez, B. Blankert, L. Mespouille, *Biomacromolecules* **2015**, *16*, 507.

[12] D. W. C. MacMillan, *Nature* **2008**, *455*, 304.

[13] L. Mespouille, O. Coulembier, M. Kawalec, A. P. Dove, P. Dubois, *Prog. Polym. Sci.* **2014**, *39*, 1144.

[14] D. Bourissou, S. Moebs-Sanchez, B. Martín-Vaca, *Comptes Rendus Chim.* **2007**, *10*, 775.

[15] M. K. Kiesewetter, E. J. Shin, J. L. Hedrick, R. M. Waymouth, *Macromolecules* **2010**, *43*, 2093.

[16] A. P. Dove, *ACS Macro Lett.* **2012**, *1*, 1409.

[17] W. N. Ottou, H. Sardon, D. Mecerreyes, J. Vignolle, D. Taton, *Prog. Polym. Sci.* **2016**, *56*, 64.

[18] N. E. Kamber, W. Jeong, R. M. Waymouth, R. C. Pratt, B. G. G. Lohmeijer, J. L. Hedrick, **2007**, *Chem. Rev.* 2007, 107, 12, 5813–5840

[19] N. Toshikj, J. J. Robin, S. Blanquer, *Eur. Polym. J.* **2020**, *127*, 109599.

Chapter II

A simple and general approach for the synthesis of degradable triblock copolymers by organocatalytic ROP from poly(lactide) macroinitiators

Keywords

Degradable block copolymers; organocatalysis; poly(ε-caprolactone); poly(lactide); poly(trimethylene carbonate); block PLA first route.

Abstract

To overcome the present limitations in the synthesis of degradable triblock copolymers with PLA as central building block, three different reactional mechanisms (coordination-insertion, anionic and cationic) have been involved, while employing the transition from organometallic to organic catalysis. Even though activated chain-end mechanism with stannous octanoate is well known for the successful ROP catalytic reactivity, the synthesis of PLA based triblock copolymers according to this route revealed not negligible transesterification reactions. In the same way, the activated chain-end mechanism through nucleophilic activation (TBD) presented either no reactivity or weak control over the anionic polymerization process. Herein, we therefore propose an activated monomer mechanism as general and simple route for obtaining controlled PTMC-*b*-PDLLA-*b*-PTMC and PCL-*b*-PDLLA-*b*-PCL triblock copolymers by using cationic organocatalysis (MSA). ^{1}H, ^{13}C-NMR and DOSY-NMR spectra confirmed the well-controlled polymer architecture of the B-A-B triblock copolymer.

1.Introduction

Degradable polymers are knowing growing interest, especially due to the eco-friendly concerns but also for the huge potential in biomedical applications. Consequently, in the past couple of years, degradable aliphatic polyesters and polycarbonates have gained noticeable attention and are becoming the gold standard of degradable synthetic materials. More particularly, poly(lactide)s (PLA) have received the highest interest due to their tuneable degradability, high mechanical strength and rigidity. Poly(ε-caprolactone)s (PCL) polyesters have also been used for their elastic properties and likewise show remarkable drug permeability. Finally, amorphous poly(trimethylene carbonate) (PTMC) presents high flexibility and controlled bioresorption through surface erosion and is largely used for biomedical applications such as soft tissue engineering. All these polymers can be synthesized by ring opening polymerization of the corresponding cyclic monomers: lactide (LA), epsilon-caprolactone (ε-CL) and trimethylene carbonate (TMC) respectively. Block copolymerizations of their respective monomers have also been widely investigated in the goal to easily adjust the properties of the resulting copolymers. Those can generate microphase separation, essentially by controlling the composition and microstructure of the copolymers. In that context, copolymers based on PLA (with different D and L-lactide enantiomers rates), PCL and PTMC generating A-B diblocks and A-B-A triblocks are the most current block copolymers encountered in the literature.[1-3] The development of such block copolymers has resulted in new biomaterials with combination of soft and hard blocks and has therefore significantly influenced their degradability kinetics, the elasticity and the physico-chemical behaviour.

The most current polymerization routes in ROP are cationic, anionic and coordination-insertion where the control of the molar mass and dispersity greatly depends on the monomer/catalyst couple. However, it has to be noticed that the reactivity of the various monomers over specific catalytic systems is generally different, thus making sometimes difficult to synthesize the copolymers in one pot. The choice of the catalyst, the type of macroinitiator depending on the first synthesized block and the feeding order of monomers for sequential block copolymerization are the crucial parameters to claim for a controlled and effective copolymerization.

A wide variety of organometallic catalysts have been used for the synthesis of degradable copolymers.[4-6] However, elevated temperature is usually necessary for the polymerization, which considerably increases the risk of transesterification.[7] Furthermore, the presence of metal in the final polymer is nowadays more and more banned, principally for environmental and biomedical applications. Hence, organocatalysis gained a growing interest in ring opening copolymerization. Curiously, the synthesis of degradable block copolymer while using an organocatalyst is poorly reported.[8, 9] One of the reasons of this lack can be explained by the divergent reactivity of monomers according to the catalytic mechanism employed, notably in the case of electrophilic or nucleophilic activations.[10,11] To overcome this orthogonal activation, Wang *et al.* have recently developed the "traceless switching organocatalysis",[10] which was the first efficient approach to generate degradable multiblock copolymers with organocatalysis. The principle is based on the use of two orthogonal catalytic systems by switching the initial electrophilic activation of the first block synthesis by using nucleophilic catalyst to initiate the second one.

Table II-1: List of the reported attempts to synthesize a block copolymer with PLA macroinitiator.

Block copolymer type	**Activation process**	**Active reagents (catalyst or initiator)**	**Effect on block copolymerization**	**References**
PLLA-PDTC	Initiation	Al(O-*sec*-Bu)$_3$ Zn(Et)$_2$ Bu$_2$Sn(OMe)$_2$	Presence of transesterification	[12]
PDLLA/PCL	Initiation	Potassium poly(ethylene glycol)ate macroinitiator	No reaction	[13]
PLLA/PCL PDLLA/PCL	Catalysis	Al(OiPr)$_3$	Presence of transesterification	[14]
PLLA/PCL	Catalysis	Al(OiPr)$_3$	Presence of transesterification	[15]
PLLA/PCL	Catalysis	K[(N(SiMe)$_3$]$_3$	No reaction	[16]
PLLA/PCL	Catalysis	Sn(Oct)$_2$	Presence of transesterification	[17]

PDLA/PTMC PLLA/PTMC	Initiation	$Al(OiPr)_3$ + Schiff base ligand	Block copolymerization without transesterification	[18]
PLLA/PCL	Initiation	$Al(OiPr)_3$ + Schiff base ligand	Block copolymerization without transesterification	[19]
PLLA/PTMC PLLA/PCL	Catalysis + protective additive	$Sn(Oct)_2$ + α-Methyl styrene	Block copolymerization without transesterification	[20]
PLLA/PCL	Initiation	Dimethyl(salicylaldiminato) aluminum	Block copolymerization without transesterification	[21]
PLLA/PCL PDLLA/PCL	Initiation	$Ti(OiPr)_2$ supported by aminodiol ligand	Block copolymerization without transesterification	[22]

Degradable block copolymerization through PLA macroinitiator faces serious limitations that have often been highlighted in the literature. Indeed, degradable copolymers with PLA first route are barely reported in opposition to PLA last route.[13, 14] Table II-1 reports various attempts of block copolymerization using PLA first route and subsequently used as macroinitiator for copolymerization of the second monomer. From the Table II-1, it is apparent that most of the attempts using traditional organometallic catalyst routes showed remarkably low reactivity or else generated significant transesterification. Till now, the only successful way of copolymerizing with PLA macroinitiator has been achieved by either using specific additives or modifying the metal complex by bulky ligands, which then act as initiator and therefore present a serious limitation for the generation of triblock copolymers.[23] Therefore, universal and controlled catalytic route to synthesize degradable block copolymer B-A-B from PLA macroinitiator as central block remains a considerable challenge, especially by using an organocatalytic strategy. Although, block copolymerization with PLA macroinitiator would allow to generate new type of degradable multiblocks that might be interesting to create new materials with rigid blocks surrounded by soft blocks which would display specific phase separation behaviour and interesting properties.

Consequently, in this article, we propose to investigate different catalytic systems from coordination-insertion, anionic and cationic mechanisms to synthesize degradable block copolymer B-A-B from PDLLA macroinitiator. Hence, bishydroxy terminated PDLLA are first prepared and then used as macroinitiator for the copolymerization of PCL and PTMC *via* step and sequential copolymerization to lead to PTMC-*b*-PDLLA-*b*-PTMC and PCL-*b*-PDLLA-*b*-PCL copolymers (Figure II-1). The three classical mechanisms of ring opening polymerization have been investigated to generate these block copolymers: i/ coordination insertion has been tested using stannous octanoate, ii/ nucleophilic activation with guanidine molecules such as TBD, iii/ electrophilic activation with methyl sulfonic acid catalyst.

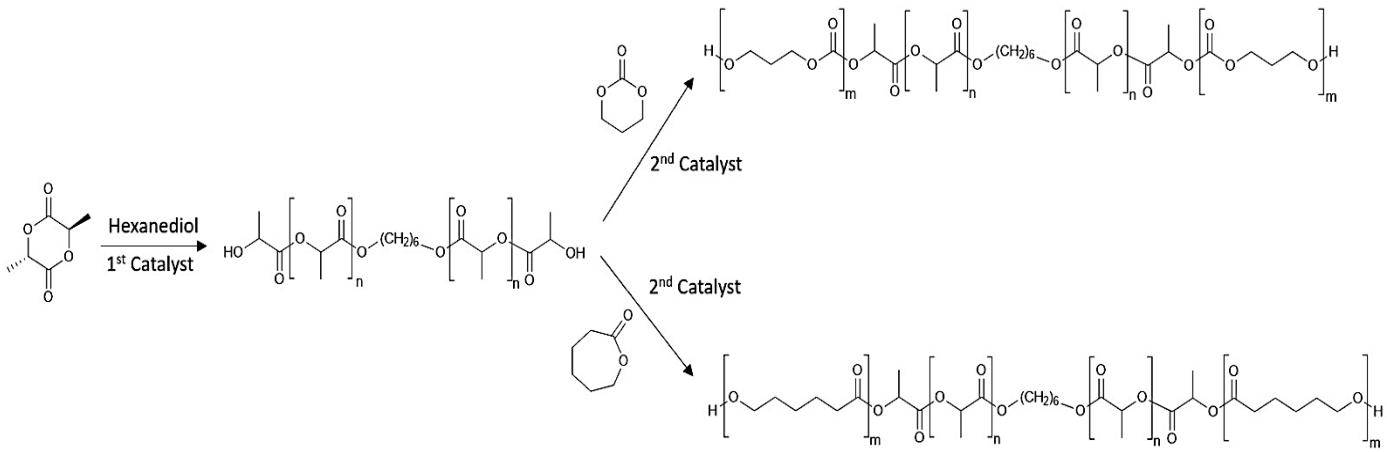

Figure II-1: Synthesis of triblock PTMC-*b*-PDLLA-*b*-PTMC and PCL-*b*-PDLLA-*b*-PCL copolymers *via* PDLLA first route.

2.Experimental section/Methods

Materials

The monomers, DL-LA was purchased from Corbion (The Netherlands), ε-CL (99 %) was obtained from Santa Cruz Biotechnologies (Germany), while TMC was obtained from Foryou Medical (China). The initiator (1,6 hexane diol, 99 %) and the catalysts (MSA, TBD, $Sn(Oct)_2$) were purchased from Sigma-Aldrich (France) and used as received. Anhydrous dichloromethane was retrieved from solvent purificator Inert PureSolv™ (USA) and anhydrous toluene (99.8 %) was purchased from Sigma Aldrich (France) were used as polymerization solvents.

Synthetic procedures

All the syntheses were performed in two-necked round bottom flasks (100 ml), previously dried in an oven at 130°C, and equipped with a magnetic stirrer and a thermometer.

General procedure of homopolymerization of DL-LA **-** DL-lactide (DL-LA) (1,05 g, 14,5 mmol, 100 eq) was solubilized in dichloromethane (DCM) (10,5 ml, $[DL\text{-}LA]_0$ = 0.7 mol/L). The initiator 1,6 hexane-diol (8,61 mg, 0,073 mmol, 1 eq) and the catalyst, 1,5,7-triazabicyclo [4.4.0] dec-5-ene (TBD) (1,42 mg, 0,051 mmol, 1.4 eq) were then added into the solution. The reaction mixture was stirred for 2 minutes at room temperature until the complete conversion of DL-LA, determined by ^{1}H-NMR. Afterwards the catalyst was neutralized by an excess of acetic acid and the reaction mixture was concentrated under vacuum. The polymer was then precipitated in cold methanol and dried in vacuum oven for 24 hours. Conversion rate was >98 % and yield reaction around 95 %.

General procedure for PTMC-b-PDLLA-b-PTMC and PCL-b-PDLLA-b-PCL triblock copolymers syntheses by step copolymerization using PDLLA macroinitiator - Previously synthesized PDLLA macroinitiator (1,05 g, 0,138 mmol, 1 eq) was introduced in a flask; with TMC monomer (1,43 g, 13,8 mmol, 100 eq) or ε-CL (1,57 g, 13,8 mmol, 100 eq). The quantity of monomer and macroinitiator used were based on the desired proportions between the blocks and was fixed for this study at 50-100-50. Some cycles of vacuum and dry argon were performed before injecting the anhydrous solvent ($[TMC/\varepsilon\text{-}CL]_0$=1 mol/L). The reactions with MSA (0,026 g, 0,276 mmol, 2 eq) or TBD (0,0162 g, 0,1932 mmol, 1,4 eq) as catalyst were performed in anhydrous dichloromethane at room temperature while for stannous octoate ($Sn(Oct)_2$) (0,1 wt. % to initiator) as catalyst the used solvent was anhydrous toluene with reaction temperature of 100°C. After full reaction, an excess amount of triethylamine (3 eq in respect to catalyst) was added when using MSA, in order to neutralize this one. Likewise, when using TBD as catalyst, an excess amount of acetic acid (3 eq to TBD) was used in order to neutralize it. Finally, the polymers were slowly poured in cold methanol, the precipitated polymers were filtered and washed several times in the same solvent and dried in vacuum oven for 24 hours.

General procedure of sequential one-pot synthesis of PTMC-b-PDLLA-b-PTMC and PCL-b-PDLLA-b-PCL triblock copolymers - Following the procedure for the synthesis of PDLLA homopolymer reported above, once the conversion of the previous reaches >99 % after 2 min of reaction, MSA (2.5 eq to TBD) was firstly added in the reaction mixture in order to quench the TBD catalyst and then TMC or ε-CL monomer was added to carry on the second polymerization step. The reactions were performed at room temperature for 17 h for the synthesis of PTMC-*b*-PDLLA-*b*-PTMC triblock copolymer and 6h for the synthesis of PCL-*b*-PDLLA-*b*-PCL triblock copolymer. After complete conversion of the monomers, the MSA was quenched with an excess of trimethylamine (3 eq to MSA). Finally, the polymers were slowly poured in cold methanol, filtered, and then washed several times in the same solvent and at last, dried in an oven in vacuum for 24 hours.

Instruments

Size exclusion chromatograms were recorded using a triple detection (GPC Varian 390-LC viscometer detector, Varian 390-LC refractive index detector and UV detector (at 254 nm)) from Agilent Technologies. The analyses were performed in tetrahydrofuran (THF) at a flow rate of 1.0 mL/min at 30 °C. An Agilent PLgel 5 µm guard column and two columns 5 µm PLgel Mixed D were used. Data acquisition and calculations were performed using Cirrus Multi GPC/SEC software. Universal calibration was performed with PS standards from Agilent Technologies (EasiVial) using the intrinsic viscosities given by the supplier.
Nuclear Magnetic Resonance Spectrometry - ^{1}H and ^{13}C NMR spectra were recorded on a 400MHz Bruker Aspect Spectrometer while DOSY spectra were recorded on a 600MHz Bruker Aspect Spectrometer. $CDCl_3$ was used as deuterated solvent. Chemical shifts were given in parts per million (ppm): for ^{1}H and DOSY NMR the reference peak was residual $CDCl_3$ at 7.26 ppm and for ^{13}C NMR at 77 ppm.

3. Results and Discussion

Synthesis of triblock copolymers with PLA as a central block remains as a challenge due to the absence of simple and universal catalytic approach for their preparation (Table II-1). In addition, despite the significant rising of studies devoted to ring opening polymerization by organocatalysis, block copolymerization has been very poorly studied with this type of catalysts.

Therefore, we investigated the synthesis of degradable triblock copolymer B-A-B *via* PDLLA first route using coordination- insertion mechanisms with an organometallic catalyst, cationic and anionic mechanism with an organocatalyst.

To start, DL-LA, ε-CL and TMC have been firstly homopolymerized in order to control the reactivity of each monomer using the selected catalysts. Theoretical degree of polymerization was initially fixed to 100 for all the homopolymers synthesized using hexanediol as a bifunctional initiator. Monomer conversion and degree of polymerization were determined by ^{1}H-NMR (details in SI).

Table II-2: Comparison of the conversion rate for the homopolymerization of the studied monomers using 1,6 hexanediol as initiator.

Catalysts	**Mechanism**	**T (°C)**	**Conversion of TMC**	**Conversion of DL-LA**	**Conversion of ε-CL**
MSA	Cationic	30 °C	100 % after 17 h	10 % after 17 h	100 % after 6 h
TBD	Anionic	25 °C	100 % after 1 h	100 % after 2 min	17 % after 24 h
$Sn(Oct)_2$	Coordination-insertion	100 °C	100 % after 24 h	100 % after 24h	100 % after 24 h

Table II-2 shows the conversion rate of each monomer as a function of the polymerization mechanism. Monomer conversion has been determined by ^{1}H-NMR spectra by comparing the integrated areas of characteristic peaks of the monomers with those of protons from the growing polymer chains. Degree of polymerization was determined from the ratio of the peak integrals of the characteristic protons from the polymer chain with the peak integrals of the characteristic protons from the last unit of the polymer chain or with the characteristic integral peak from the hexanediol initiator. Homopolymerization of each monomer resulted in bishydroxy-terminated homopolymers but the reactivity was not identical since total conversion were not reached in similar times. Indeed, the polymerization of PDLLA *via* cationic mechanism using MSA catalyst was relatively low with 10 % of conversion after 17 h (Figure II-S1). Nucleophilic activation with TBD at room temperature was faster for homopolymerization of DL-LA than for TMC (Figure II-S2). In the case of ε-CL, homopolymerization reached a plateau at 17 % of conversion after 6 h of reaction (Figure II-S3). In contrast, $Sn(Oct)_2$ successfully resulted in bishydroxyterminated homopolymers, with a conversion rate similar for all the monomers after 24 hours of reaction.

However, we notice diverse reactivity of each monomer in the earlier steps of polymerization (at 1, 3, 6 and 10 hours) as represented in SI. It has to be noted that according to our experimental conditions, no transesterification has been detected for all the studied catalysts.

In order to explore the possibility to generate block copolymers with various activation mechanisms, step copolymerization was performed. This approach consisted in polymerization and purification of the first block by precipitation and elimination of residual reactive species such as initial catalyst. As previously presented, nucleophilic activation was the most efficient way to homopolymerize DL-LA and was consequently used to synthesize the first PDLLA block with terminal OH groups. This initial bis-hydroxyl PDLLA block was used to start the copolymerization of the second blocks. The synthesis of triblock PTMC-*b*-PDLLA-*b*-PTMC and PCL-*b*-PDLLA-*b*-PCL copolymers was therefore obtained in solution by using the three studied catalysts. Conversion rate of the second blocks was measured by ^{1}H-NMR (Figure II-2A). In addition, molar fraction of each block was evaluated by ^{1}H-NMR from the ratio of characteristic proton peak integrals for each polymer chain (Figure II-S4). For all the copolymers PTMC-*b*-PDLLA-*b*-PTMC and PCL-*b*-PDLLA-*b*-PCL, the targeted ratio was fixed at 50-100-50.

$Sn(Oct)_2$ catalyst has been already investigated for diblock copolymer PLLA-*b*-PCL with PLLA first route and lead to transesterification (Table II-1). Bero and Kaspercky demonstrated the strong analytical potential of ^{13}C-NMR spectroscopy to determine chain microstructure irregularities that can be due to random transesterification on the same diblock copolymer.[24,25] Later, this study has been widely used as reference to demonstrate the presence of transesterification for any type of block copolymers based on poly(lactide).[19-21] In full awareness of such risk, we investigated the coordination/insertion approach to synthesize the triblock copolymers with PDLLA first route. A full conversion after 24 h have been found for the triblock PCL-*b*-PDLLA-*b*-PCL and monomer sequencing in the triblock was characterized by ^{13}C-NMR. Figure II-2C shows the carbon spectra of the triblock, and the expanded carbonyl carbon region from 169-174 ppm. Carbonyl peaks from PDLLA are characterized by a sharp multiplet at 169.5 ppm due to the stereochemistry from the sequential units of L and D lactide. However, the presence of various peaks in between the carbonyl peaks of PDLLA block at 169.5 ppm and the carbonyl peaks of PCL block at 173.5 ppm are also clearly visible and confirm the random monomer sequencing (triads assigned in Figure II-2C), and therefore demonstrate the presence of significant transesterification.

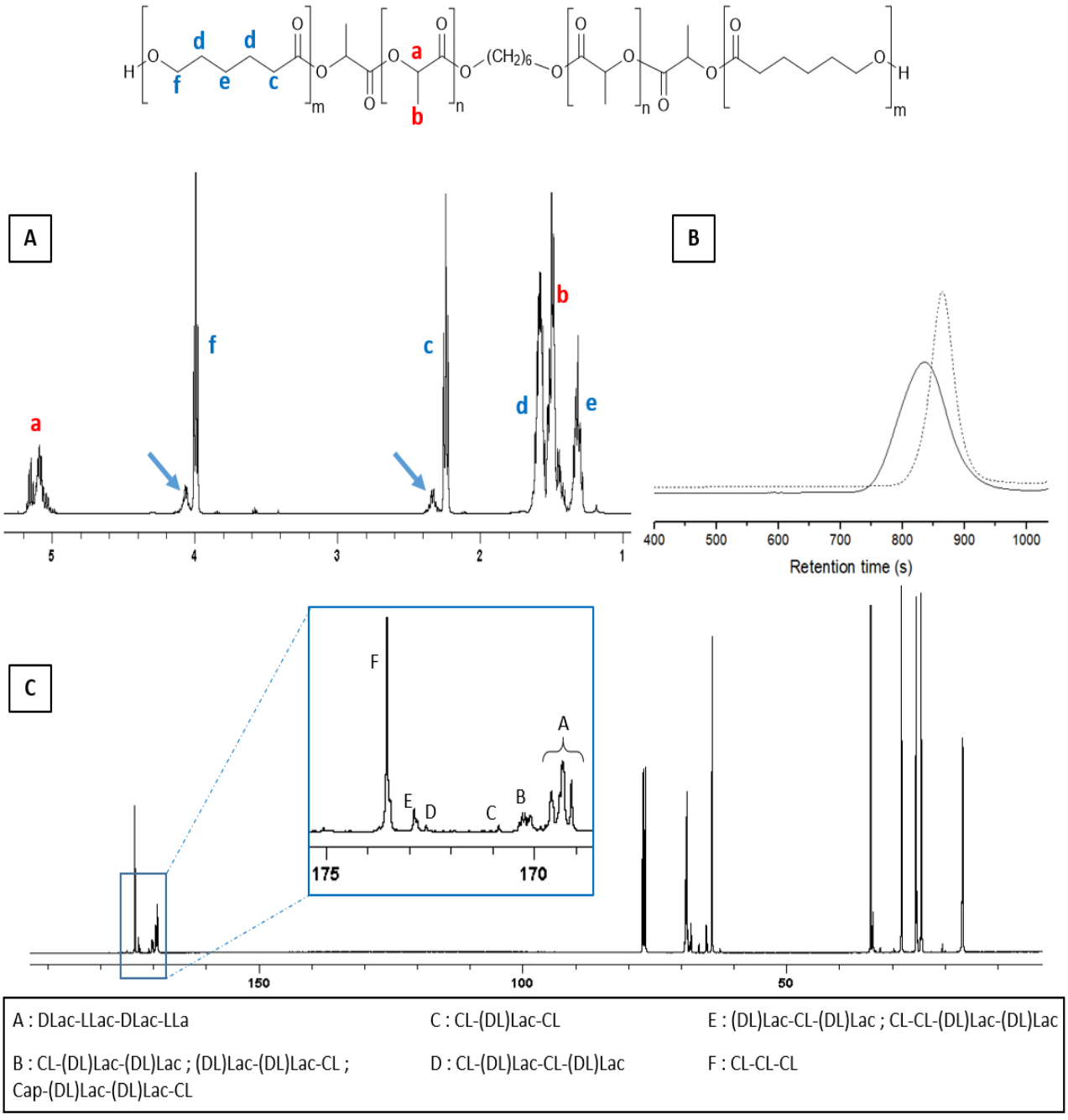

Figure II-2: NMR analyses of the copolymer PCL-PDLLA-PCL formed upon $Sn(Oct)_2$ catalysis. A/ ^{1}H-NMR spectrum in $CDCl_3$ of the copolymer with the assigned signals. The arrows represent the characteristic peaks of random sequence of copolymer coming from the transesterification, B/ SEC chromatograms of the initial homopolymer PDLLA (dots) and the PCL-PDLLA-PCL copolymer (solid line), C/ ^{13}C-NMR spectrum in $CDCl_3$ of the copolymer with expanded carbonyl region. Peak assignments are listed below the graph.

In addition, ^{1}H NMR spectrum also allows to determine the presence of transesterification by the apparition of characteristic peaks at 2.4 ppm and 4.15 ppm (represented by the blue arrows in the Figure II-2A). Consequently, ε-CL monomers were incorporated within the PDLLA chain by transesterification during the reaction of copolymerization. Such transesterification also influenced the chromatogram where the detected copolymer showed a wide signal with dispersity of 2.3 (Figure II-2B). In parallel, synthesis of triblock PTMC-*b*-PDLLA-*b*-PTMC by $Sn(Oct)_2$ showed extremely low reactivity compared to the homopolymerization of TMC, with conversion rate that reached only 33 % after 72 h of reaction (Figure II-3A). By contrast, TMC was nicely homopolymerized by anionic mechanism with TBD and the attempt to synthesize PTMC-*b*-PDLLA-*b*-PTMC also showed the same reactivity with a total conversion after 1 h of reaction. However, DOSY NMR analyses showed different diffusion coefficients between the PTMC homopolymer and the synthesized copolymer which thus means a mixture of PDLLA and PTMC homopolymers (Figure II-3B). Furthermore, diffusion coefficient of the initial PDLLA was exactly similar to that of PDLLA block after copolymerization which therefore confirms that PDLLA did not act as initiator. To corroborate this result, SEC analysis of the synthesized block copolymer PTMC-*b*-PDLLA-*b*-PTMC was performed (Figure II-3C and Table II-3). From the SEC, it was expected to detect chain extension approximately double that of initial PDLLA block size. However, the chromatogram from the copolymer shows a wide Gaussian curve leading to huge dispersity calculated around 11.9 while the initial PDLLA was around 1.24 (Table II-3). In addition, calculated Mw was around 44000 g.mol^{-1} instead of 17400 g.mol^{-1} for the expected copolymer which probably means homopolymerization of PTMC. In summary, it was not possible to synthesize PTMC-*b*-PDLLA-*b*-PTMC triblock copolymer *via* anionic mechanism.

As previously mentioned for the homopolymerization of ε-CL with anionic organocatalysis using TBD, the copolymerization of ε-CL using PDLLA macroinitiator shows a total absence of reaction after 72 h where the monomer ε-CL is still present as observed by ^{1}H-NMR where no characteristic peaks from PCL appeared. As a result, no PCL-*b*-PDLLA-*b*-PCL triblock could be obtained from anionic catalysis (Figure II-S5).

Finally, step copolymerization was also studied using cationic catalysis with MSA. For both synthesized PTMC-*b*-PDLLA-*b*-PTMC and PCL-*b*-PDLLA-*b*-PCL triblocks, complete conversion was reached after 17 h and 6 h, respectively. ^{13}C-NMR spectroscopy was used to

determine the sequential distribution of copolymers. Surprisingly, carbon spectrum of PCL-*b*-PDLLA-*b*-PCL in the carbonyl region did not show the presence of triad peaks that would have come from the transesterification (Figure II-4).

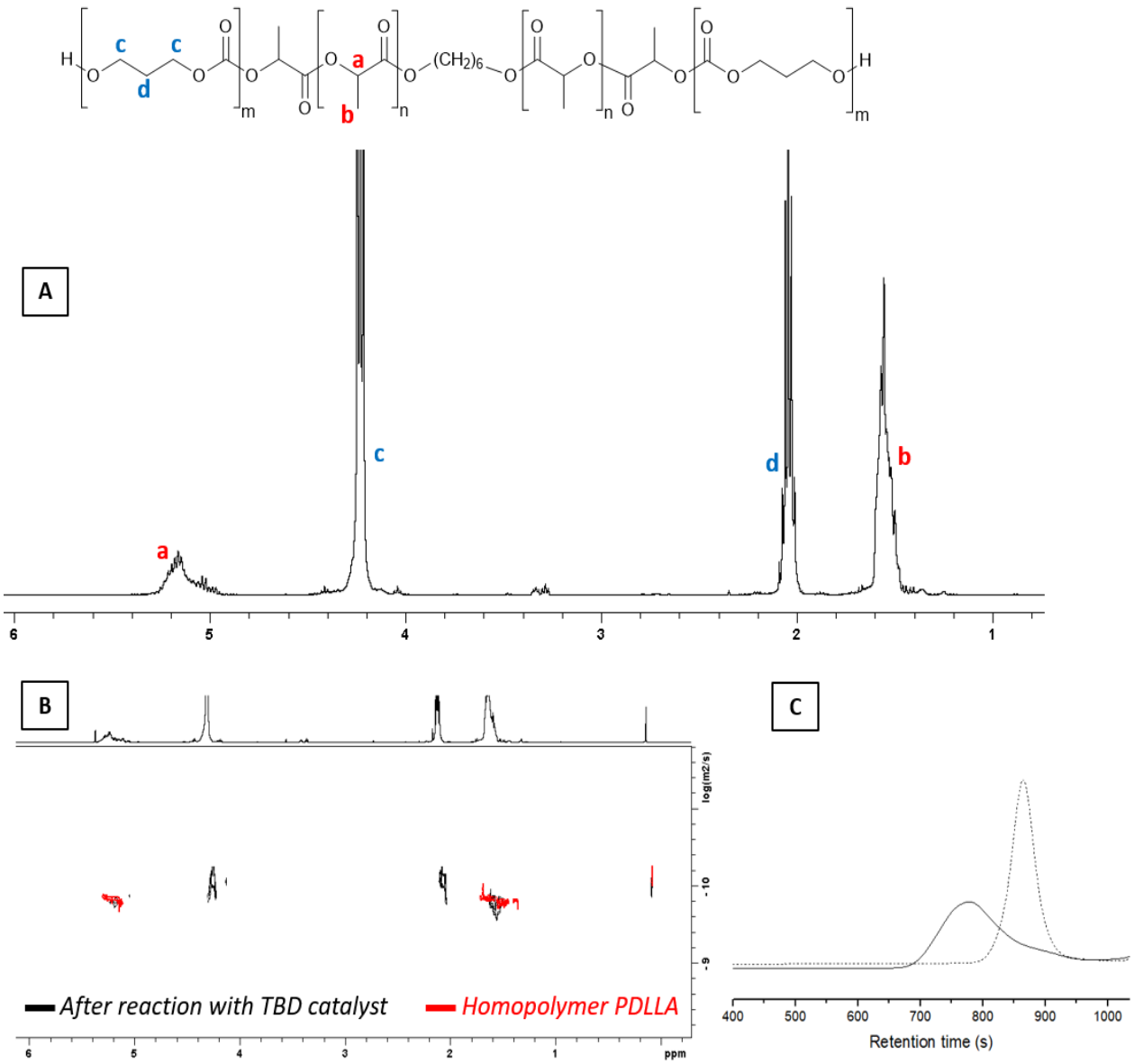

Figure II-3: Spectroscopy analyses after copolymerization of TMC using PDLLA macroinitiator through anionic activation with TBD. A/ ^{1}H NMR spectrum in $CDCl_3$ of the copolymer with the assigned signals, B/ 2D DOSY ^{1}H-NMR spectrum shows the different diffusion coefficient after reaction, the peaks of PDLLA and PTMC blocks in black, and the peak of the initial homopolymer PDLLA in red, C/ SEC chromatograms of initial homopolymer PDLLA (dots) and after copolymerization (solid line).

Table II-3: Molar mass and dispersities of synthesized copolymers measured by SEC.

Catalysis approach	Block copolymer *	Mn th (g.mol^{-1})	Mn SEC (g.mol^{-1})	Mw SEC (g.mol^{-1})	*Đ*
TBD step copolymerization	PTMC-*b*-PDLLA-*b*-PTMC	17400	3900	43900	11,9
MSA step copolymerization	PTMC-*b*-PDLLA-*b*-PTMC	17400	17200	27000	1,34
MSA step copolymerization	PCL-*b*-PDLLA-*b*-PCL	17400	14800	17000	1,31
MSA sequential copolymerization	PTMC-*b*-PDLLA-*b*-PTMC	17400	12200	16000	1,23
MSA sequential copolymerization	PCL-*b*-PDLLA-*b*-PCL	17400	13300	14900	1,37

*Initial PDLLA block was synthesized by TBD activation and led to:
Mn,th = 7200 g.mol^{-1}; Mn,SEC = 9880 g.mol^{-1} and Mw,SEC = 11370 g.mol^{-1}.

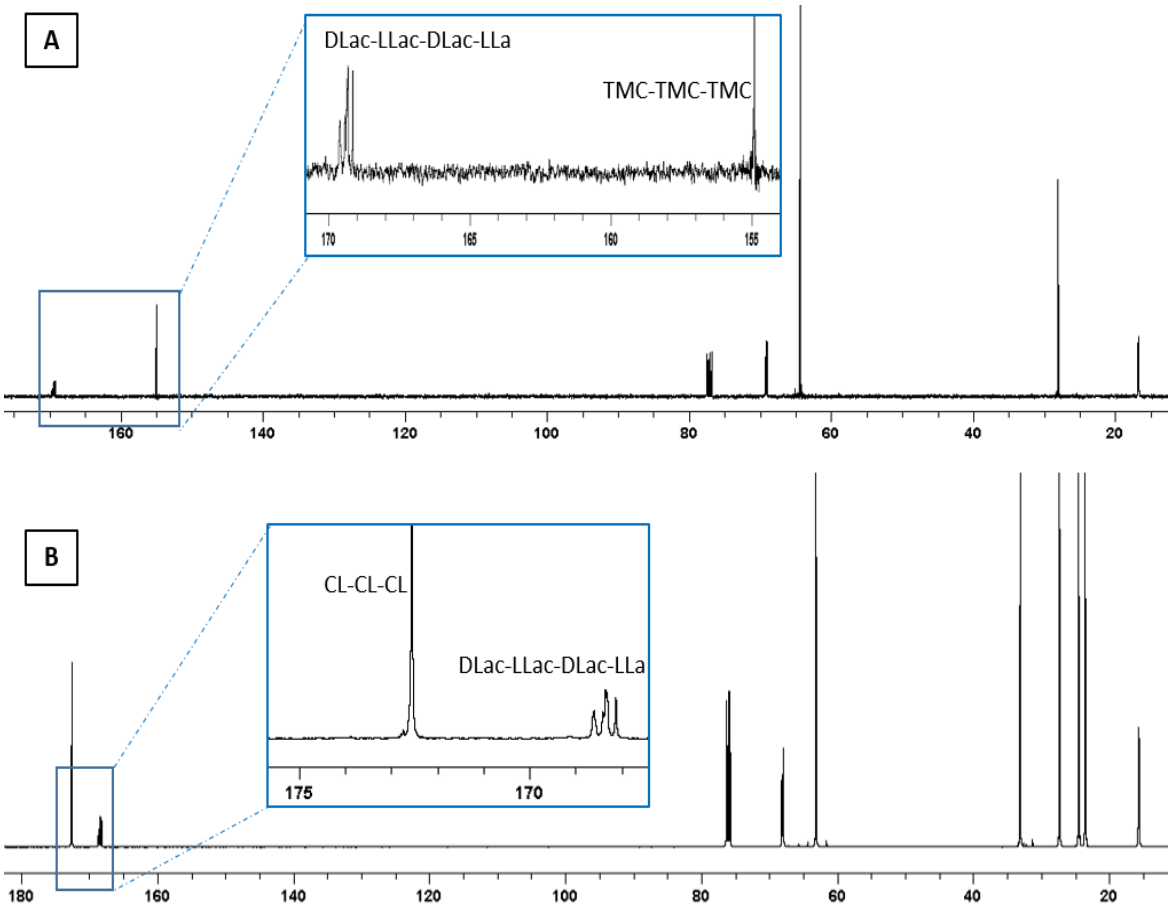

Figure II-4. ^{13}C-NMR spectra in $CDCl_3$ for each triblock PTMC-*b*-PDLLA-*b*-PTMC (A) and PCL-*b*-PDLLA-*b*-PCL (B) obtained by cationic activation using MSA catalyst, with expanded carbonyl region. Specific assignment signals are specified.

Same result was observed for the PTMC-*b*-PDLLA-*b*-PTMC triblock copolymer in the carbonyl carbon region from 153-170 ppm, which includes the carbonyl region of PDLLA block and PTMC block at 154 ppm (Figure II-4). Carbon NMR indicated that the transesterification processes did not occur when MSA was used as catalyst. DOSY-NMR spectra for both copolymers (Figure II-5A and II-5C) clearly identifies a uniform diffusion coefficient which confirms the formation of block copolymerization for both investigated copolymers. For SEC chromatograms for both triblock copolymers, the curves noticeably shifted toward lower retention times compared to those of corresponding PDLLA macroinitiators (Figure II-5B, II-5D and Table II-3).

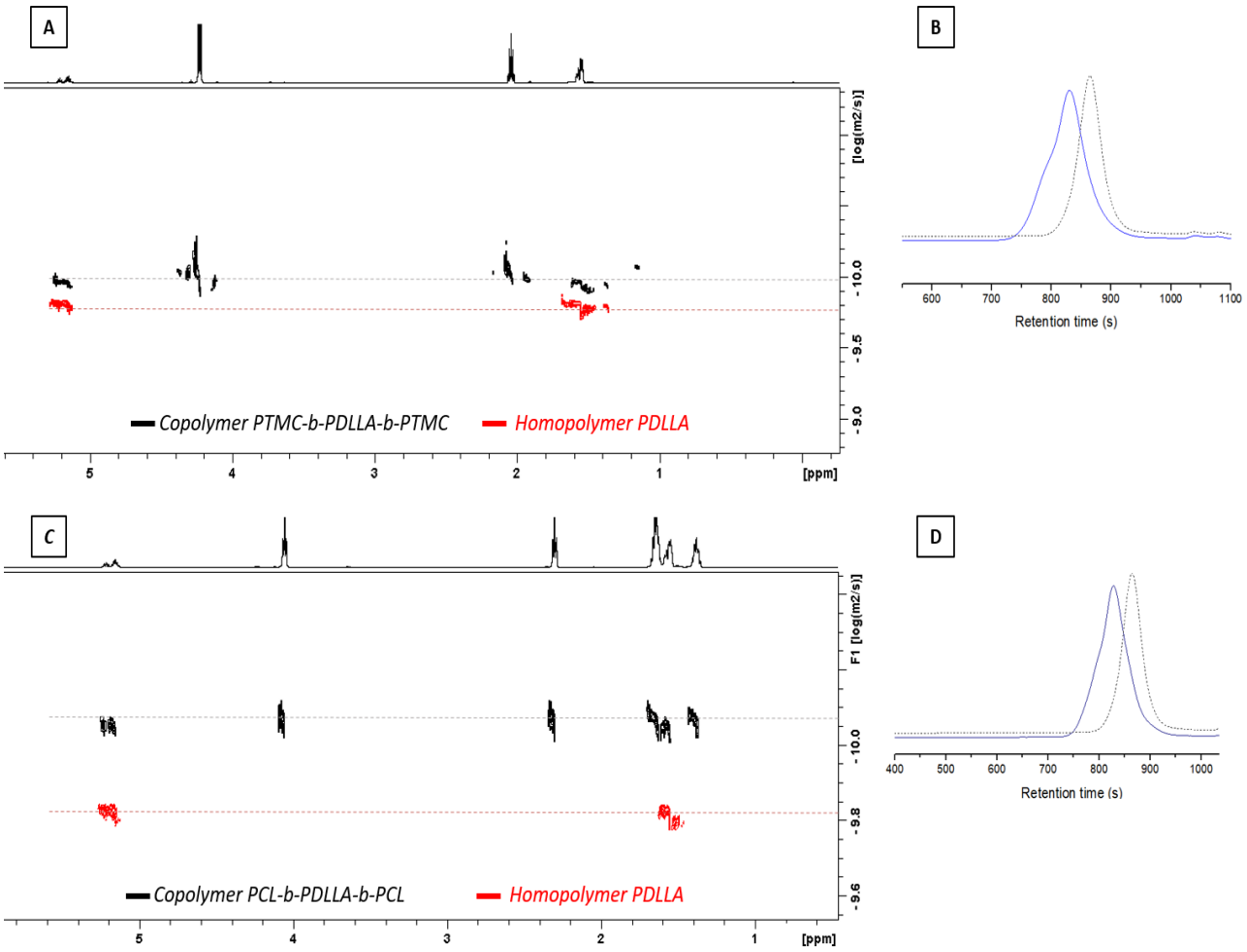

Figure II-5. A/ 2D DOSY ^{1}H-NMR spectrum of PTMC-*b*-PDLLA-*b*-PTMC, diffusion coefficients (black for block copolymer and red for the initial PDLLA homopolymer, B/ SEC chromatograms of initial homopolymer PDLLA (dots) and PTMC-*b*-PDLLA-*b*-PTMC (solid line), C/ 2D DOSY ^{1}H-NMR spectrum of PCL-*b*-PDLLA-*b*-PCL, diffusion coefficients (black for block copolymer and red for initial PDLLA homopolymer), D/ SEC chromatograms of initial homopolymer PDLLA (dots) and of PCL-*b*-PDLLA-*b*-PCL (solid line).

Clearly, the reactivity of secondary alcohols is known to be lower compared to that of primary alcohols. Such reactivity issue for different protic compounds has also been found for the initiation of ring opening polymerization.[26,27] Consequently, the presence of bis-hydroxy terminal groups on PDLLA influences the reactivity of the block copolymerization. Steric hindrance from methyl group of lactic acid unit might significantly impair the ring opening polymerization. In addition, it has been suggested from the literature that the activation of the hydroxyl end groups of poly(lactide) is lowered by the well-dispersing negative charges which reduces the nucleophilicity of the protic group and consequently weaken the ROP initiation from that site.[13,17] In this study, we demonstrated that B-A-B block copolymers with PDLLA central block can only be efficiently activated without any transesterification via an activated monomer mechanism (AMM) (Figure II-6). Hence, electrophilic activation with MSA catalyst generated proper B-A-B triblock copolymers without transesterification while activated chain-end mechanism (ACEM) caused by $Sn(Oct)_2$ and nucleophilic TBD (Figure II-6) leads to transesterification or no copolymerization and is therefore not appropriate for copolymerization *via* PLA first route.

Lastly, the study on step copolymerization allowed to determine that MSA activation was the only solution to generate block copolymers based on PLA macroinitiator. This catalytic approach would take a remarkable advantage if sequential one-pot copolymerization could also lead to a fitting block copolymer with PDLLA first route and without transesterification. Traditionally, sequential copolymerization is the classic approach for obtaining highly defined and well-controlled block copolymerization with low molar mass dispersity. Typically, sequential copolymerization consists of feeding the reaction by addition of a second monomer once the initial block polymer has been achieved. Hence, we tried to generate triblock copolymers PTMC-*b*-PDLLA-*b*-PTMC and PCL-*b*-PDLLA-*b*-PCL in one pot by sequential copolymerization, with a particular interest in the conversion rate and absence of transesterification (Figure II-S6, II-S7). As we mentioned in the introduction, block copolymerization by sequential polymerization using organocatalysis is not frequent in the literature especially due to the divergent reactivity between the monomers/catalysts couples.[10] In the traceless switching approach from Wang *et al.*, sequential one pot block copolymerization has been obtained by switching the catalysis from a Bronsted cationic acid to a nucleophilic base one. A similar approach was thus used in our block copolymerization, where the first PDLLA block was synthesized by nucleophilic activation and then switched to an electrophilic one for the synthesis of the second block.

Hence, a traceless switch organocatalysis strategy from Bronsted guanidine base to cationic sulfonic acid was employed for one pot PDLLA first-route block copolymerization. The conversion of the second block was similar to those obtained by step copolymerization, and no trace of transesterification was detected by NMR and SEC.

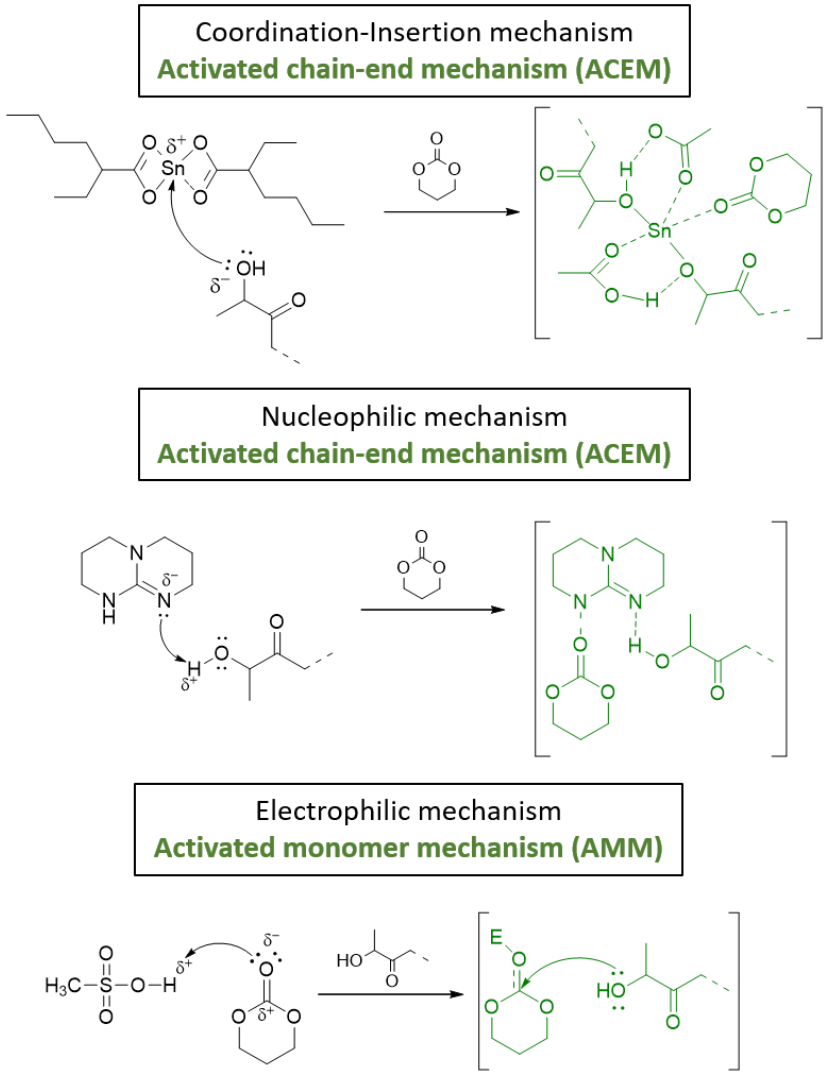

Figure II-6. Activation mechanisms of the different employed catalysts through ACEM or AMM approaches.

4. Conclusion

Owing to the deep investigation of the different ring opening polymerization mechanisms, we succeeded in the determination of the most appropriate catalytic pathway for the preparation of well-defined triblock copolymers starting from PDDLA as macroinitiator. In particular, cationic catalysis using electrophilic MSA was the single approach to synthesize PTMC-*b*-PDLLA-*b*-PTMC and PCL-*b*-PDLLA-*b*-PCL triblock copolymers without any secondary reactions such transesterification. Activated monomer mechanism was the most convenient approach leading to a controlled block copolymerization. In such a way, sequential copolymerization was achieved via traceless switching organocatalysis using sequentially TBD and MSA catalysts to successfully generate triblock copolymers according to the PDLLA first route.

Supporting Information

A simple and general approach for the synthesis of degradable triblock copolymers by organocatalytic ROP from poly(lactide) macroinitiators

Monomer conversion is followed by the disappearance of the characteristic monomer peaks and by appearance of new, shifted ones, polymer peaks. The monomer conversion is calculated by the following formula:

$$\%\ monomer\ conversion = \frac{peak\ area\ of\ polymer}{peak\ area\ monomer + peak\ area\ polymer}\ \text{x}\ 100$$

Homopolymerization of DL-LA.

In the case of DL-LA homopolymerization, the polymer peak area at 5.17 ppm and the monomer peak area at 5.02 ppm are taken into consideration for the calculation of monomer conversion percentage. In Figure II-S1A, we observe no presence of any monomer peaks after 2 minutes of reaction (catalyzed by TBD) and therefore we conclude that the reaction is complete (> 97 % conversion). TBD catalyst residues are present between 3.2 and 3.3 ppm, observable in the reaction mixture and later eliminated through precipitation. On the opposite, on the spectra in Figure II-S1B, we note weak DL-LA conversion of around 10 % after 17 hours of reaction (catalyzed by MSA). Figure II-S1C represents PDLLA homopolymer after precipitation in methanol. ^{1}H-NMR spectrum of PDLLA homopolymer obtained by stannous octanoate catalysis is similar to the spectra of Figure II-S1C and is therefore not represented. The degree of polymerization equals to the initially desired 100 units is calculated by comparing the ratio of the peak area at 4.14 ppm (belonging to 4 equivalent H of the hexane diol initiator) with the peak area at 5.17 ppm (belonging to the -CH- in the PDLLA repeating unit).

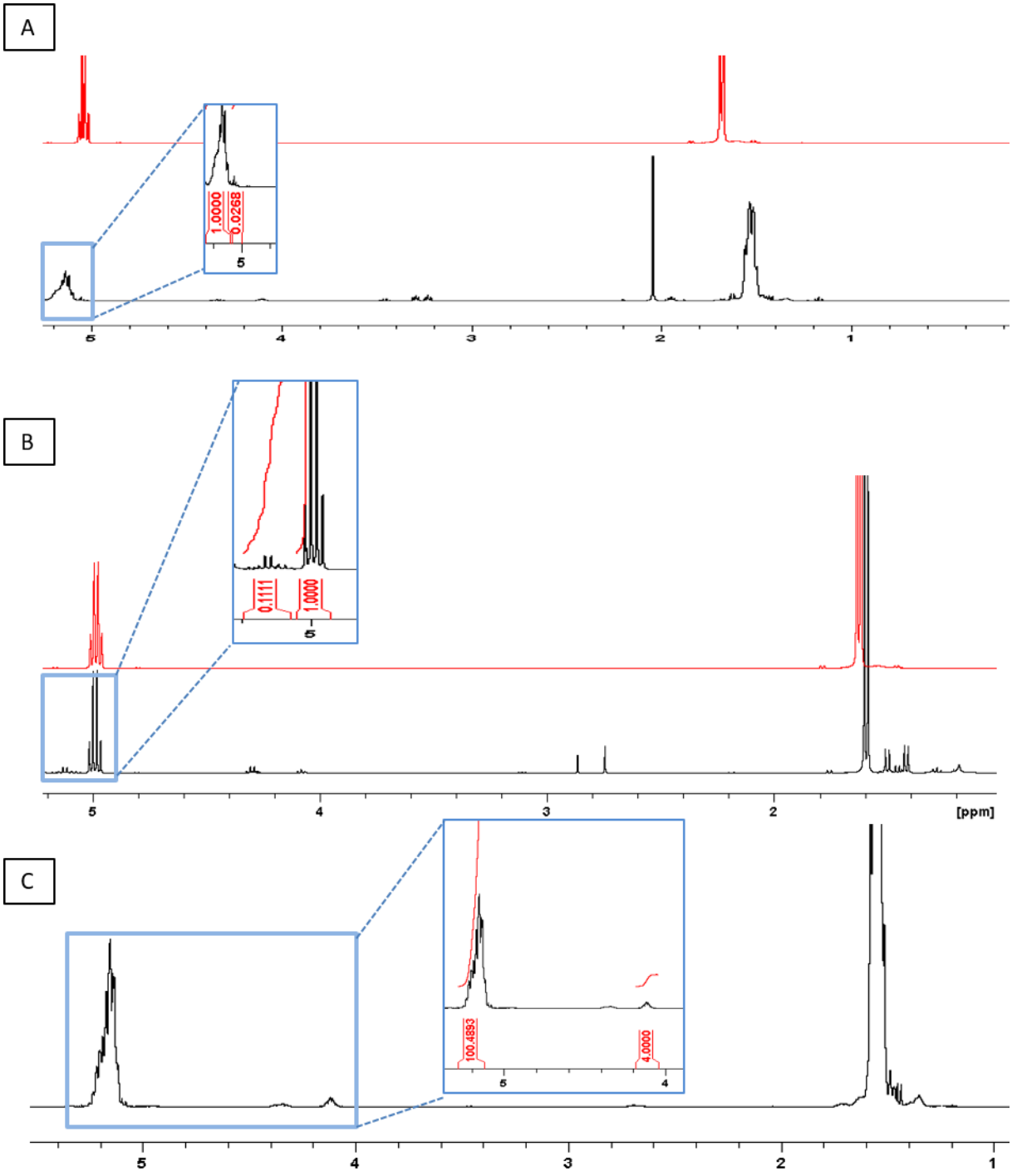

Figure II-S1. ^{1}H-NMR spectra of DL-LA homopolymerization. A/ Full conversion of DL-LA after 2 minutes of reaction, catalyzed by TBD (in red - DL-LA monomer, in black - PDLLA after full conversion, before precipitation: absence of all monomer peaks); B/ 10% of DL-LA conversion after 17 hours of reaction, catalyzed by MSA (in red - DL-LA monomer, in black - the reaction mixture); C/ Final spectrum of PDLLA homopolymer after precipitation with end-chain functionalities present at 4.2 ppm.

Homopolymerization of TMC.

In the case of TMC homopolymerization, the polymer peak area at 4.18 ppm and the monomer peak area at 4.35 ppm are taken into consideration for the calculation of monomer conversion percentage. On the spectrum represented in Figure II-S2A we note a conversion of 99% (by MSA catalysis) and therefore absence of all monomer peaks. The ^{1}H-NMR spectra of TMC homopolymer obtained by stannous octanoate and TBD catalysis are similar to Figure II-S2B and are not represented. The degree of polymerization equals to the initially desired 100 units and is calculated by comparing the ratio of the peak area at 3.67 ppm (belonging to 4 equivalent H of the hexane diol initiator) with the peak area at 4.18 ppm (belonging to the 2-CH_2- in the PTMC repeating unit).

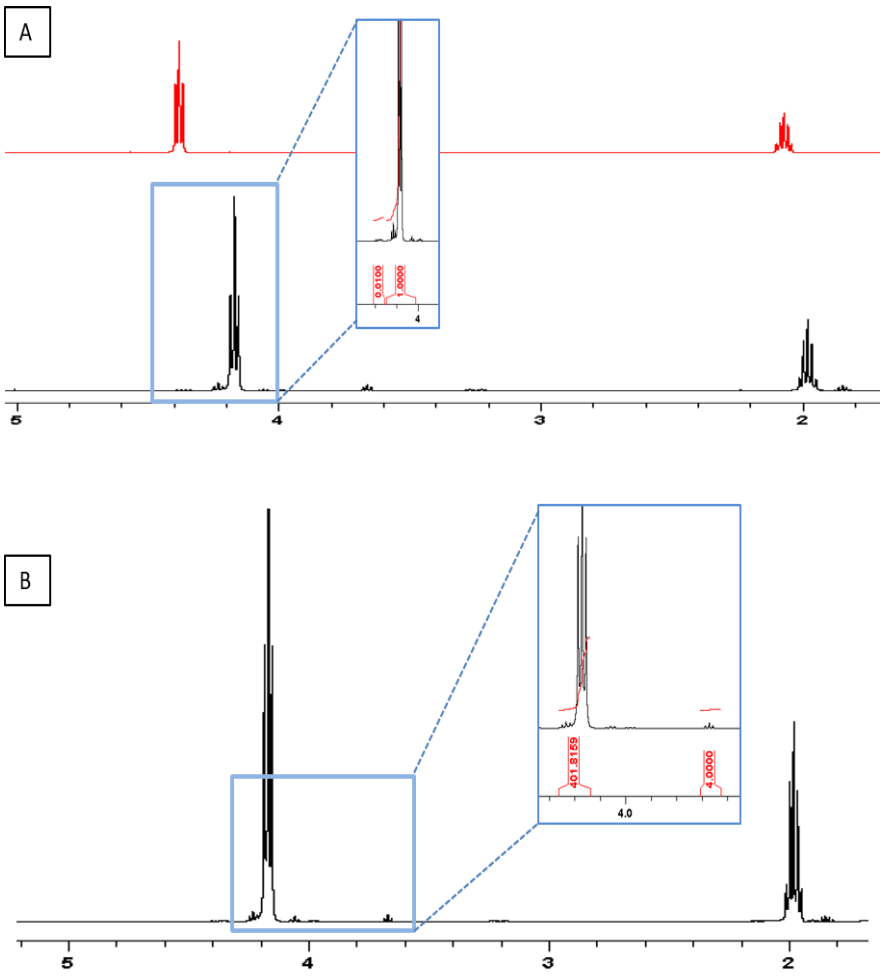

Figure II-S2. ^{1}H-NMR spectra of TMC homopolymerization. A/ Full conversion of TMC after 17h of reaction, catalyzed by MSA (in red - TMC monomer, in black - PTMC after full conversion, before precipitation: absence of all monomer peaks) B/ Final spectrum of PTMC homopolymer after precipitation with end-chain functionalities present at 3.67 ppm.

Homopolymerization of ε-CL.

In the case of ε-CL homopolymerization, the polymer peak area at 4.06 ppm and the monomer peak area at 4.15 ppm are taken into consideration for the calculation of monomer conversion percentage. On the spectra represented in Figure II-S3A, we observe no presence of any monomer peaks after 24 hours of reaction (catalyzed by stannous octanoate) and therefore we conclude that the reaction is complete (> 99 % conversion). On the opposite, on the spectra in Figure II-S3B, we note weak ε-CL conversion of around 17 % after 24 hours of reaction, catalyzed by TBD, with catalyst residues present between 3.2 and 3.3 ppm. The ^{1}H-NMR spectrum of ε-CL homopolymer obtained by MSA catalysis is not represented because it is similar to the spectrum of Figure II-S3C. The degree of polymerization equals to the initially desired 100 units and is calculated by comparing the ratio of the peak area at 3.67 ppm (belonging to 4 equivalent H of the hexane diol initiator) with the peak area at 4.06 ppm (belonging to the $–CH_2$- in the PCL repeating unit).

Table II-S1: Reactivity ratios of DL-LA, TMC and ε-CL monomers at 1, 3, 6 and 10 hours with $Sn(Oct)_2$ as catalyst.

Time (h)	**Conversion (%) DL-LA**	**Conversion (%) TMC**	**Conversion (%) ε-CL**
1	43	6	4
3	75	15	8
6	87	45	26
10	93	71	64

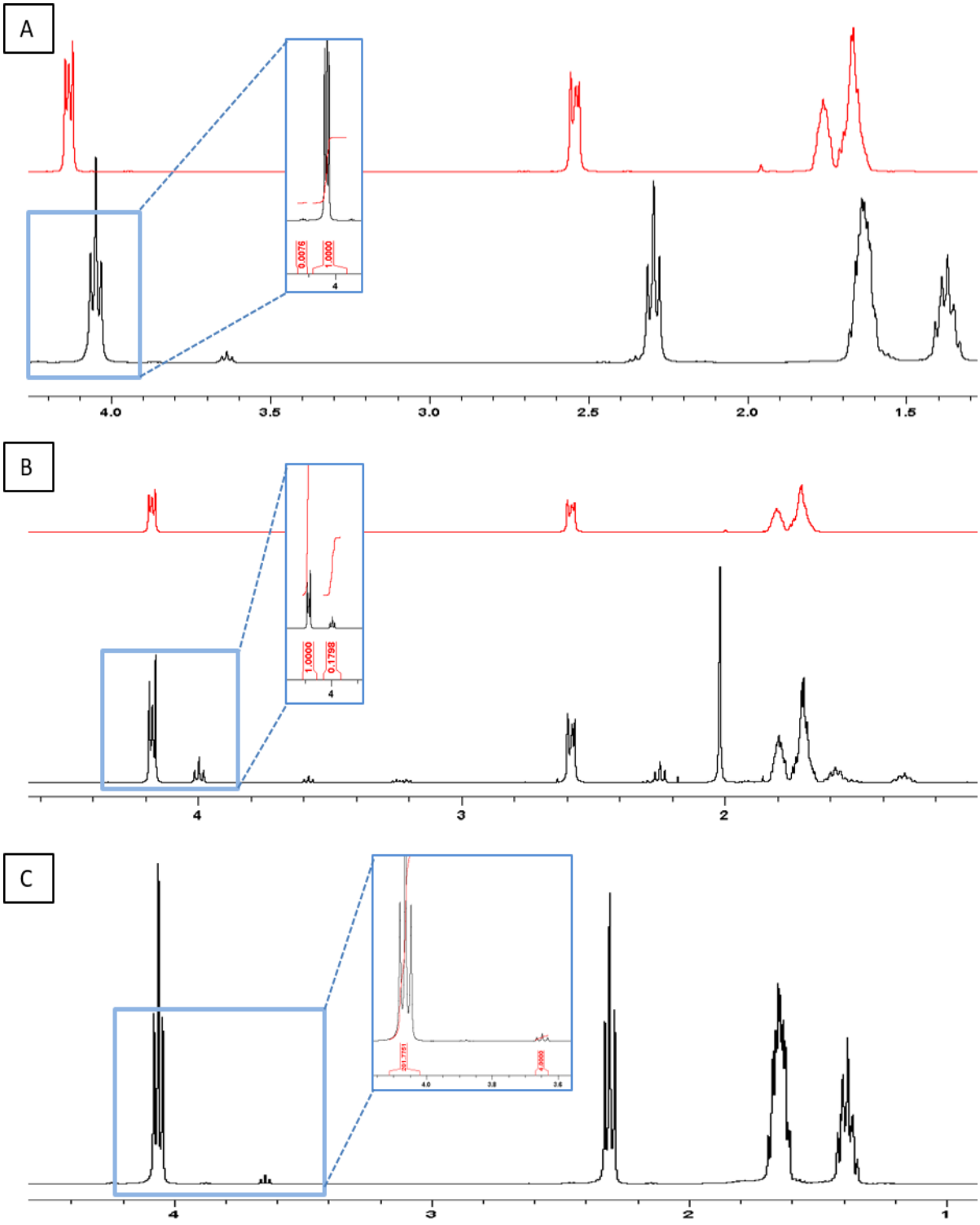

Figure II-S3. ^{1}H-NMR spectra of ε-CL homopolymerization. A/ Full conversion of ε-CL after 24 hours of reaction, catalyzed by stannous octanoate (in red - ε-CL monomer, in black - PCL homopolymer after full conversion, before precipitation); B/ 17% of ε-CL conversion after 24 hours of reaction, catalyzed by TBD (in red - ε-CL monomer, in black - the reaction mixture); C/ Final spectrum of PCL homopolymer after precipitation with end-chain functionalities present at 3.67 ppm.

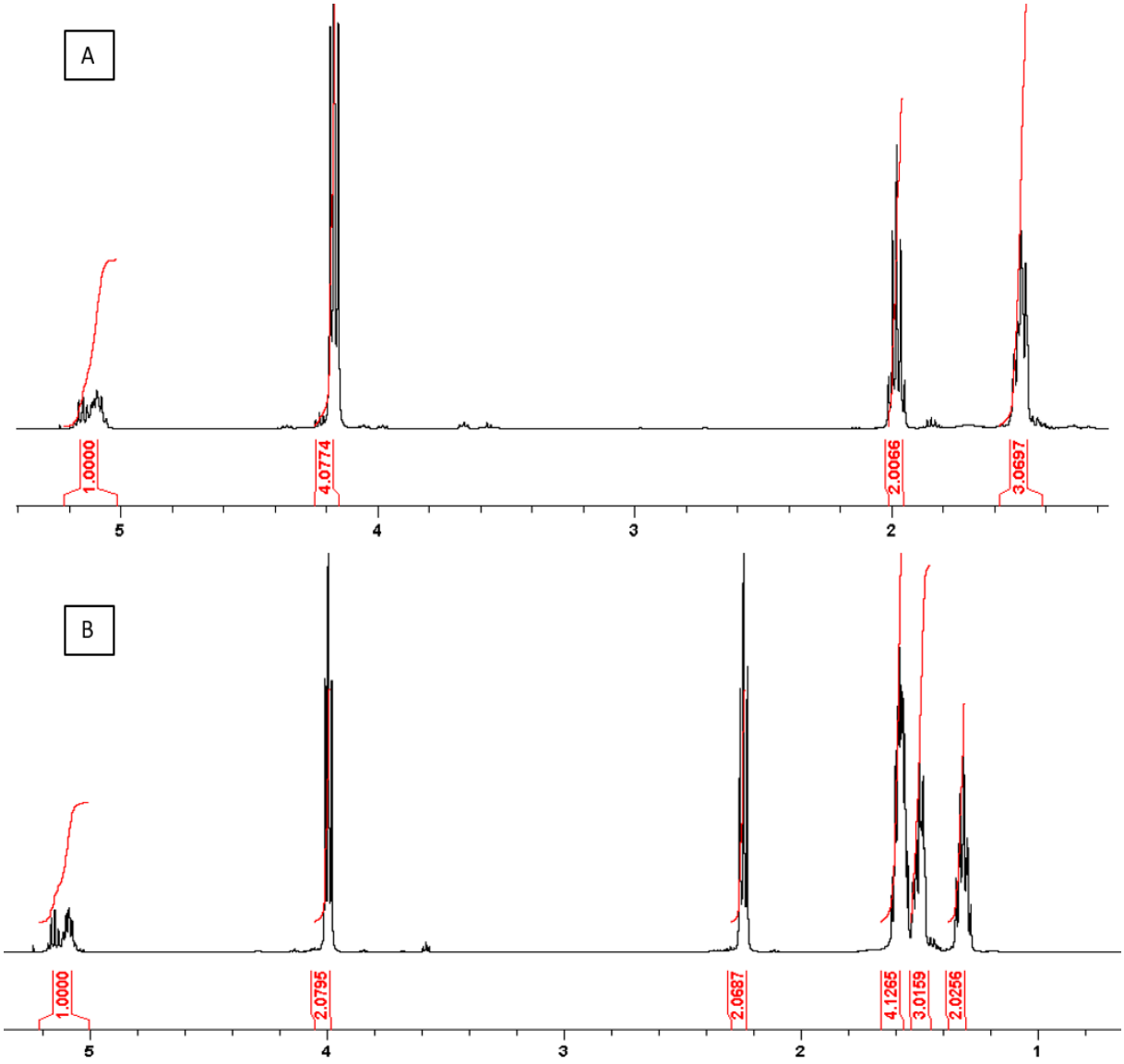

Figure II-S4. ^{1}H-NMR spectra of block copolymers with PDLLA first route. A/ ^{1}H-NMR spectra of $PTMC_{50}$-$PDLLA_{100}$-$PTMC_{50}$ triblock copolymer; B/ ^{1}H-NMR spectra of PCL_{50}-$PDLLA_{100}$-PCL_{50} triblock copolymer.

The molar ratios of (50/50) were determined by comparing the characteristic peak areas of the –CH- repeating unit of PDLLA situated at 5.17 ppm with the peak area of the 2-CH_2- repeating units of PTMC at 4.18 ppm for the $PTMC_{50}$-$PDLLA_{100}$-$PTMC_{50}$ triblock copolymer represented in Figure II-S4A.

For the PCL_{50}-$PDLLA_{100}$-PCL_{50} triblock copolymer represented in Figure II-S4B the molar ratios of 50/50 were determined by comparing the characteristic peak areas of the –CH- repeating unit of PDLLA situated at 5.17 ppm with the peak area of the –CH_2- repeating unit of PCL at 4.06 ppm.

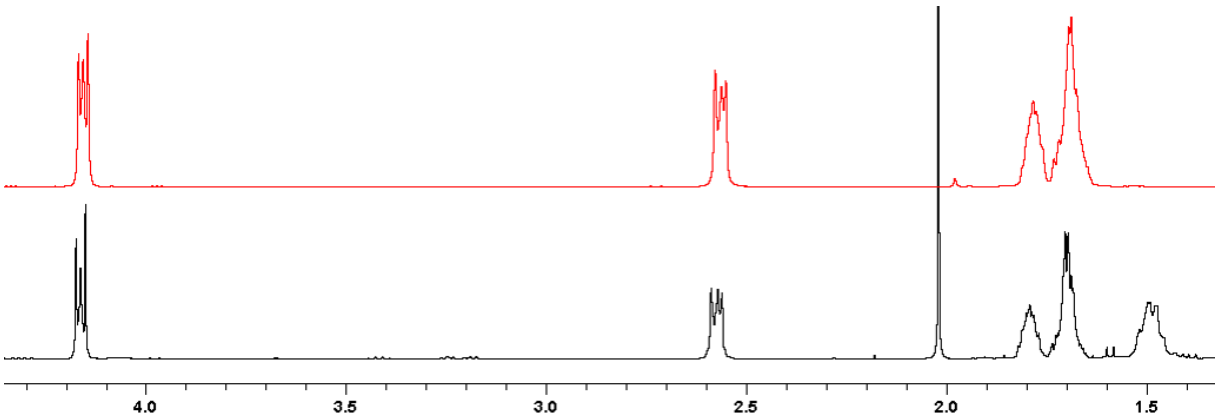

Figure II-S5. ^{1}H-NMR spectra of PCL-*b*-PDLLA-*b*-PCL triblock copolymer formation catalyzed by TBD after 72 hours of reaction (in black - the reaction medium; in red - ε-CL monomer).

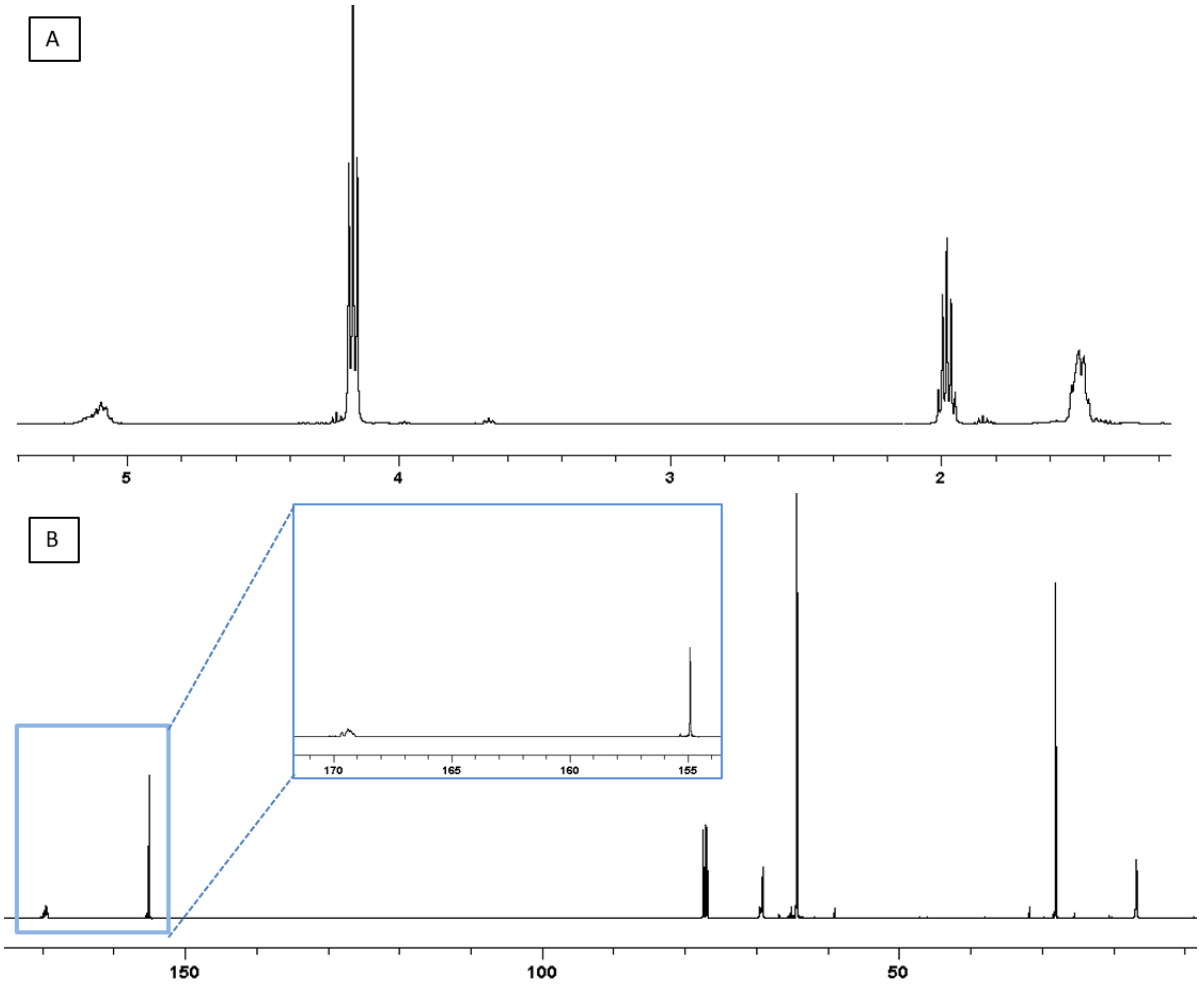

Figure II-S6. Characterization of PTMC-*b*-PDLLA-*b*-PTMC by sequential one-pot copolymerization A/ ^{1}H-NMR; B/ ^{13}C-NMR spectra.

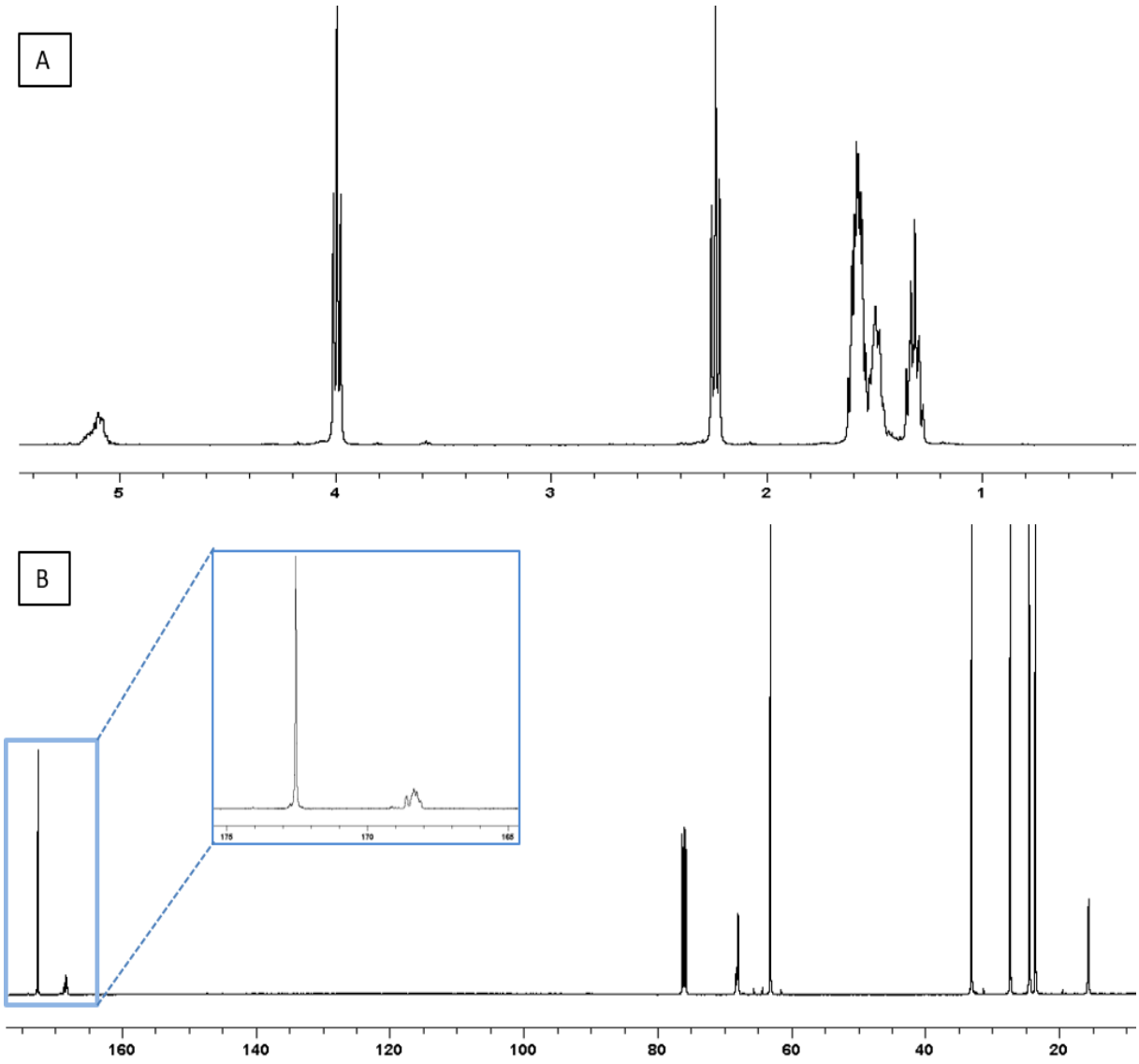

Figure II-S7. Characterization of PCL-*b*-PDLLA-*b*-PCL by sequential one-pot copolymerization A/ ^{1}H-NMR; B/ ^{13}C-NMR spectra.

References

[1] D.M. Cui, T. Tang, W.G. Bi, J.H. Cheng, W.Q. Chen, B.T. Huang, *J Polym Sci Pol Chem* 41(17) **(2003)** 2667-2675.

[2] D. Pospiech, H. Komber, D. Jehnichen, L. Haussler, K. Eckstein, H. Scheibner, A. Janke, H.R. Kricheldorf, O. Petermann, Biomacromolecules 6(1) **(2005)** 439-446.

[3] Z. Zhang, D.W. Grijpma, J. Feijen, Macromol Chem Phys 205(7) **(2004)** 867-875.

[4] H.R. Kricheldorf, S. Rost, Macromolecules 38(20) **(2005)** 8220-8226.

[5] S.M. Guillaume, Eur Polym J 49(4) **(2013)** 768-779.

[6] A.C. Albertsson, I.K. Varma, Biomacromolecules 4(6) **(2003)** 1466-1486.

[7] H.R. Kricheldorf, I. Kreiser-Saunders, A. Stricker, Macromolecules 33(3) **(2000)** 702-709.

[8] W. Guerin, M. Helou, J.F. Carpentier, M. Slawinski, J.M. Brusson, S.M. Guillaume, Polym Chem-Uk 4(4) **(2013)** 1095-1106.

[9] R.P. Brannigan, A. Walder, A.P. Dove, J Polym Sci Pol Chem 52(16) **(2014)** 2279-2286.

[10] X. Wang, J.Q. Liu, S.Q. Xu, J.X. Xu, X.F. Pan, J.J. Liu, S.D. Cui, Z.J. Li, K. Guo, Polym Chem-Uk 7(41) **(2016)** 6297-6308.

[11] A. Couffin, B. Martin-Vaca, D. Bourissou, C. Navarro, Polym Chem-Uk 5(1) **(2014)** 161-168.

[12] P. Schmidt, H. Keul, H. Hocker, Macromolecules 29(11) **(1996)** 3674-3680.

[13] X.M. Deng, Z.X. Zhu, C.D. Xiong, L.L. Zhang, J Polym Sci Pol Chem 35(4) **(1997)** 703-708.

[14] P. Dubois, C. Jacobs, R. Jerome, P. Teyssie, Macromolecules 24(9) **(1991)** 2266-2270.

[15] A. Duda, T. Biela, J. Libiszowski, S. Penczek, P. Dubois, D. Mecerreyes, R. Jerome, Polym Degrad Stabil 59(1-3) **(1998)** 215-222.

[16] Y. Lemmouchi, M.C. Perry, A.J. Amass, K. Chakraborty, E. Schacht, J Polym Sci Pol Chem 46(16) **(2008)** 5348-5362.

[17] P.J.A. In't Veld, E.M. Velner, P. VanDeWitte, J. Hamhuis, P.J. Dijkstra, J. Feijen, J Polym Sci Pol Chem 35(2) **(1997)** 219-226.

[18] M. Socka, A. Duda, A. Adamus, R.A. Wach, P. Ulanski, Polymer 87 **(2016)** 50-63.

[19] M. Florczak, J. Libiszowski, J. Mosnacek, A. Duda, S. Penczek, Macromol Rapid Comm 28(15) **(2007)** 1581-1581.

[20] V.T. Lipik, M.J.M. Abadie, Int J Biomater **(2012)**.

[21] D. Pappalardo, L. Annunziata, C. Pellecchia, Macromolecules 42(16) **(2009)** 6056-6062.

[22] D. Dakshinamoorthy, F. Peruch, J Polym Sci Pol Chem 50(11) **(2012)** 2161-2171.

[23] L.L. Han, Q. Xie, J.N. Bao, G.R. Shan, Y.Z. Bao, P.J. Pan, Polym Chem-Uk 8(6) **(2017)** 1006-1016.

[24] J. Kasperczyk, M. Bero, Makromol Chem 194(3) **(1993)** 913-925.

[25] J. Kasperczyk, M. Bero, Makromol Chem 192(8) **(1991)** 1777-1787.

[26] H. Alamri, J.P. Zhao, D. Pahovnik, N. Hadjichristidis, Polym Chem-Uk 5(18) **(2014)** 5471-5478.

[27] Y.Q. Zhu, C. Romain, V. Poirier, C.K. Williams, Macromolecules 48(8) **(2015)** 2407-2416.

CHAPTER III / CHAPITRE III

Introduction Chapitre III

La théorie de séparation de phases dans les copolymères à blocs

Alors que les homopolymères sont constitués d'un seul type de monomère, le terme copolymère correspond à un arrangement de chaines d'au minimum deux unités macromoléculaires chimiquement distinctes. Les structurations à blocs sont une sous-classe intéressante de la famille des copolymères dont les différentes unités de monomères (A, B ou plus) sont arrangées d'une façon linéaire. D'un autre côté, un mélange d'homopolymères fait référence à un *blend*, terme utilisé par la suite.

Les composants d'un mélange de polymères ont tendance à se séparer l'un de l'autre en raison de leurs interactions généralement défavorables. Dans le cas d'un *blend*, cette séparation survient à l'échelle macroscopique. A l'inverse, dans le cas de copolymères à blocs, la séparation se produit à l'échelle nanoscopique notamment à cause des liaisons covalentes qui joignent les différentes chaines de polymère. La capacité des copolymères à blocs à générer une microséparation de phases dans des structures nanoscopiques bien ordonnées est leur particularité majeure.

Dans tout mélange de polymères, la miscibilité est définie par l'enthalpie libre de mélange (ΔG_m), qui est une fonction de l'enthalpie de mélange (ΔH_m), la température (T) et l'entropie de mélange (ΔS_m). Cette relation est définie par l'équation (1) de la loi thermodynamique exprimant l'énergie libre de Gibbs, notée G, combinant l'enthalpie et l'entropie en l'expression suivante :

$$\Delta G_m = \Delta H_m - T\Delta S_m \qquad (1)$$

Le comportement des phases des copolymères linéaires à deux blocs dépend principalement de trois facteurs contrôlables expérimentalement : le paramètre d'interaction de Flory-Huggins χ, les fractions volumiques des blocs *f* et le degré de polymérisation N.
Les deux derniers termes influencent l'entropie de translation et de configuration et sont réglables par la stœchiométrie de polymérisation. De ce fait, la contribution entropique dans l'équation précédente est inversement proportionnelle aux nombres totaux d'unités répétitives N. Par ailleurs, le paramètre sans dimension de Flory-Huggins représente la contribution enthalpique dans l'équation (1) et fait référence au coût énergétique par monomère lors d'un contact entre deux unités monomères. Ce paramètre est défini par l'équation suivante :

$$\chi = \chi_{AB} = \frac{Z}{K_B T}\left(\varepsilon_{AB} - \frac{\varepsilon_{AA} + \varepsilon_{BB}}{2}\right) \quad (2)$$

dont ε_{AA}, ε_{AB} et ε_{BB} sont les énergies d'interaction des composantes A-A, A-B et B-B respectivement. k_B (la constante de Boltzmann) et T (la température) traduisent le terme d'énergie thermique (k_BT) et z définit le nombre de voisins monomères les plus proches (la coordinence du réseau). Expérimentalement, le paramètre χ peut être exprimé en fonction de la température selon l'équation (2):

$$\chi = a/T + b \quad (3)$$

Dans cette équation (3), le paramètre de Flory-Huggins est exprimé comme une somme des deux termes dont a et b sont des valeurs constantes expérimentalement établies pour une large gamme de polymères.[1]

Lorsque $\chi_{AB} > 0$, les deux espèces A et B interagissent d'une manière répulsive. Plus cette valeur est élevée, plus les contacts entre les différents blocs sont réduits, ce qui mène à la configuration énergétique la plus favorable en vue d'une séparation de phases efficace. Si le nombre d'unités répétitives N est suffisamment élevé, la perte de l'entropie configurationnelle est ainsi accompagnée par une ségrégation locale en microdomaines.

Par conséquent, comme la contribution enthalpique est définie par X et la contribution entropique est liée à N, c'est le produit χN qui définit le comportement et l'organisation d'un copolymère à blocs linéaires dans les différentes organisations. Plus la valeur de ce produit augmente, plus la composante enthalpique prédomine, ce qui conduit à des systèmes de plus en plus ordonnés. En revanche, plus cette valeur est petite, plus la composante entropique prévaut, donnant naissance à un état désordonné. Ainsi, le terme χN impacte directement les transitions ordre-désordre (ODT) dans un système de copolymères à blocs. Cette transition qui dépend directement de la température (T_{ODT}) dans laquelle se trouve le système, a lieu lorsque la valeur de χN dépasse la valeur critique de l'ordre-désordre. Donc, comme la valeur de χ est inversement proportionnelle à la température (Equation (3)), la grandeur du produit ségrégationnel χN doit être accompagnée par des températures décroissantes, afin de favoriser la séparation de phases.

Dans le but de précisément définir ce phénomène et déterminer les transitions ODT d'un système en fonction de leur χN, la théorie du champ moyen auto-cohérent (Self-consistent

Mean Field Theory, ou SCFT en anglais) a été développée. Ainsi, en fonction de la magnitude du produit χN, il existe trois régimes de ségrégation : faible (χN << 10), intermédiaire (χN ~ 10) et fort (χN >> 10), ce dernier conduisant à une séparation de phase optimale illustrée par des interfaces A-B précises et microdomaines de A et B purs.[1–4]

Selon la théorie SCFT, lorsque le degré d'incompatibilité de deux blocs (χN) est combiné avec la fraction volumique d'un bloc (f_A), un diagramme de phases peut être établi, représentant ainsi les arrangements possibles des blocs A et B dans des microdomaines tels que: sphères, cylindres, lamelles ou gyroides (Figure III-A). Dans cette figure établie par les travaux de Bates et Frendrickson,[5] l'augmentation de la fraction volumique du bloc A, à un χN fixe au-dessus de la transition ODT (χN > 10.5), produit l'évolution de cette transition à partir des sphères cubiques centrées jusqu'au lamelles, en passant par des cylindres et gyroïdes bicontinues comme microdomaines. Les sphéres cubiques centrées représentent le premier état ordonné dans ce cas. Lorsque la composition de blocs est inversée, une inversion morphologique a lieu. Ainsi, la Figure III-A-b décrit un diagramme de phase idéal d'un copolymère à blocs prédit par la théorie SCMF.[3]

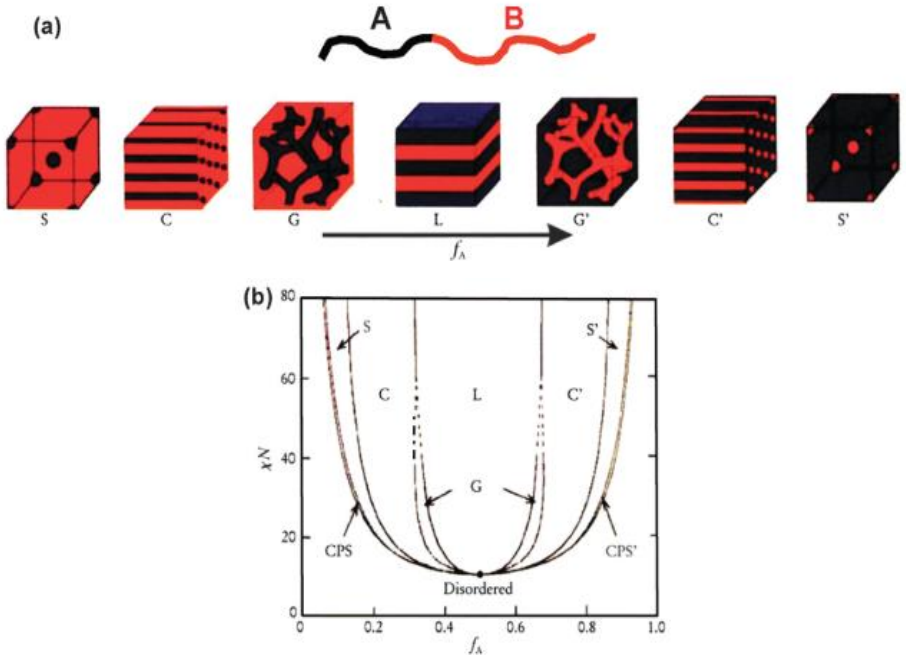

Figure III-A : (a) Morphologies d'équilibre des copolymères diblocs AB en masse : S et S'= sphères cubiques centrées, C et C'= cylindres hexagonaux, G et G' = gyroïdes bicontinues, et L = lamelles. (b) Diagramme de phase théorique des copolymères diblocs AB prédit par la théorie du champ moyen auto-cohérent (self-consistent mean-field (SCMF) theory en anglais, en fonction de la fraction volumique (*f*) des blocs et du paramètre de ségrégation χN.[5]

Comme nous pouvons l'observer, la maîtrise des paramètres χ, N, f et T est cruciale pour une séparation de phases efficace pour tout assemblage de copolymères à blocs. Des études abondantes ont été effectuées depuis les années 1980 afin de mieux comprendre le comportement en masse des copolymères à blocs.[6–12]

Le comportement des multiples associations de copolymères à blocs non-dégradables et leur auto-assemblage ont été présentés dans le Chapitre I. L'objectif de ce chapitre III est d'abord de définir et d'étudier une association de copolymères dont les deux blocs sont complètement dégradables. Jusqu'à présent des assemblages de copolymères de poly(styrène) ou poly(isoprène) avec le bloc dégradable de poly(acide lactique) (PLA) ont été étudiés.[13–16] La dégradation hydrolytique de ce dernier bloc conduit à des systèmes avec des porosités ordonnées comme nous l'avons détaillé dans l'étude bibliographique focalisée sur le cas des films minces. Récemment, le groupe de Borsali a rapporté des arrangements auto-assemblés de poly(styrène) avec un autre type de bloc dégradable – les poly(saccharides).[17–19] Il s'agit d'auto-assemblages en solution d'associations du type poly(styrène)-*bloc*-maltoheptoase ou poly(styrène)-*bloc*-dextrane qui représentent des candidats potentiels pour des applications dans les domaines de la nanolithographie. Néanmoins, le bloc non-dégradable de poly(styrène) est encore présent dans ces systèmes, ce qui mène au défi principal de notre projet de recherche présenté dans ce chapitre : utiliser l'auto-assemblage de copolymères à blocs entièrement dégradables et par la suite, lors d'une dégradation sélective d'un des blocs, arriver à une structuration ordonnée nanoporeuse et dégradable. De plus, au-delà de l'aspect dégradable des copolymères, les matériaux que nous avons étudiés sont reconnus comme biocompatibles, ce qui pourrait ouvrir la voie à des applications biomédicales. L'intégralité des résultats de ce Chapitre III doit être soumis à publication dans le journal *Applied Functional Materials* et est donc présenté sous la forme de manuscrit.

Références

[1] N. P. Balsara, In *Physical properties of polymers Handbook*, **1996**, Chap. 19.

[2] F. S. Bates, G. H. Fredrickson, *Annu. Rev. Phys. Chem.* **1990**, *41*, 525.

[3] Y. Mai, A. Eisenberg, *Chem. Soc. Rev.* **2012**, *41*, 5969.

[4] I. W. Hamley, *The physics of block copolymers*, Oxford Uni., **1998**.

[5] F. S. Bates, G. H. Fredrickson, *Phys. Today* **1999**, *52*, 32.

[6] C. A. Ross, K. K. Berggren, J. Y. Cheng, Y. S. Jung, J. B. Chang, *Adv. Mater.* **2014**, *26*, 4386.

[7] M. W. Matsen, M. Schick, *Curr. Opin. Colloid Interface Sci.* **1996**, *1*, 329.

[8] M. W. Matsen, F. S. Bates, *Macromolecules* **1996**, *29*, 1091.

[9] M. W. Matsen, F. S. Bates, *Macromolecules* **1996**, *29*, 7641.

[10] M. W. Matsen, *J. Chem. Phys.* **1997**, *106*, 7781.

[11] M. Stefik, S. Guldin, S. Vignolini, U. Wiesner, U. Steiner, *Chem. Soc. Rev.* **2015**, *44*, 5076.

[12] C. Cummins, R. Lundy, J. J. Walsh, V. Ponsinet, G. Fleury, M. A. Morris, *Nano Today* **2020**, *35*, 100936.

[13] B. Gorzolnik, P. Davidson, I. Beurroies, R. Denoyel, D.Grande, *Macromol. Symp.* **2010**, *287*, 127.

[14] T. S. Bailey, J. Rzayev, M. A. Hillmyer, *Macromolecules* **2006**, *39*, 8772.

[15] C. Sinturel, D. Grosso, M. Boudot, H. Amenitsch, M. A. Hillmyer, A. Pineau, M. Vayer, *ACS Appl. Mater. Interfaces* **2014**, *6*, 12146.

[16] K. A. Cavicchi, T. P. Russell, *Macromolecules* **2007**, *40*, 1181.

[17] C. Houga, J. Giermanska, S. Lecommandoux, R. Borsali, D. Taton, Y. Gnanou, J. F. Le Meins, *Biomacromolecules* **2009**, *10*, 32.

[18] I. Otsuka, N. Nilsson, D. B. Suyatin, I. Maximov, R. Borsali, *Soft Matter* **2017**, *13*, 7406.

[19] I. Otsuka, M. Osaka, Y. Sakai, C. Travelet, J. L. Putaux, R. Borsali, *Langmuir* **2013**, *29*, 15224.

Chapter III

Self-assembled degradable block copolymer precursors for nanoporous PTMC thin films

Keywords

degradable polymers, block-copolymer phase separation, nanoporous thin films, poly (trimethylene carbonate), poly (lactide), photo-crosslinking, solvent vapor annealing

Abstract

Even though the domain of nanoporous templates manufacturing from self-assembled block copolymers is in full expansion, challenging studies addressing innovative degradable block copolymer assemblies are still not reported. Consequently, PTMC-*b*-PDLLA-*b*-PTMC triblock copolymers, demonstrating a favorable interaction parameter for phase-separation, are employed as original degradable precursors for nanoporous thin films. Differential scanning calorimetry indicates a phase-separated system by the appearance of two distinctive glass transition temperatures, corresponding to each of the blocks. Thin films are firstly produced by spin-coating onto Si-substrate and three methods are investigated for achieving ordered self-assembly of the system: solvent evaporation, solvent vapor annealing and thermal annealing. Well-organized bicontinuous nanoscopic phase-separated morphologies consisting of PTMC and PDLLA domains are achieved under precise solvent vapor annealing conditions for a particular composition of the triblock copolymer. Triblock copolymer self-assembly is compared to the one occurring in PTMC/PDLLA blends where no ordered phase-separation is observed. Moreover, thin films photo-crosslinking of previously methacrylated PTMC end-blocks, beneficial to the stability of a porous matrix, does not alter the phase separation. From the optimal oriented block copolymer thin films, selective etching *via* PDLLA mild hydrolysis results in nanoporous PTMC with maintained long-range order and stability.

1. Introduction

In recent times, the employment of organic porous materials has greatly increased for energy (heterogeneous catalysis and storage), environmental (adsorption/separation processes) and medical (drug delivery and regenerative medicine) applications.[1] Among varied precursors, the branch of materials demonstrating versatility in manufacturing functional nanoporous structures are the block copolymers (BCPs).[2–4] BCPs consist of two or more chemically dissimilar and generally immiscible polymer chains joined together in covalent manner. Their ability to phase-separate in ordered morphologies within 10-200 nm range derives from the thermodynamic incompatibility between the blocks and is governed by the BCP composition and its molar mass.[5,6] Hence, three parameters directly influence the microphase separation: the Flory-Huggins interaction parameter (χ), the volume fraction of the minority block (f), as well as the degree of polymerization (N).[7] The dimensionless χ-value designates the incompatibility between the differing blocks, whereas the segregation product χN shapes out the degree of microphase separation. Thus, particular attention was accorded to these parameters in the area of BCP phase-separation since the 1960s.[8,9]

In the frame of the generation of porous nanostructures, BCP assemblies where the minority block organizes into porogenic nanophases while the majority component acts as mechanically robust framework supporting the voids, have widely expanded.[10] Therefore, dating from 1988, the selective removal of an etchable component from a self-assembled system has been throughout examined toward the “bottom-up” generation of nanoporous monoliths and thin films.[11] The so far reported methods for selective minor block removal include ozonolysis,[12] UV degradation,[13] reactive ion etching[14] or chemical etching.[15] Each approach is closely related and dependent on the chemistry of the BCP association. In most cases, poly(styrene) (PS) is imposed as the porous matrix due to its mechanical properties and the mastered synthesis of PS based BCPs is favorable to effective phase-separation. Even though various di-, tri- or multiblock copolymer precursors result commonly in nanoporous PS, the first introduction of a degradable block in the research area of nanoporous thin films was reached *via* poly(styrene)-poly(lactide) copolymers.[16–18] Hence, several precursors containing semi-crystalline or amorphous poly(lactic acid) as etchable component have been reported until now.[19–21]

However, two major obstacles persist when aiming for defect-free nanoporous structures: achieving long-range order upon BCP self-assembly accompanied by etching conditions that do not disturb the matrix integrity nor its mechanical properties.[22–24] Therefore, the most used methods for enhancing long-range order in BCPs systems are either thermal or solvent vapor annealing, known to induce additional mobility to the polymer chains to achieve the least energetically demanding morphology.[25–27] On the other side, matrix crosslinking has been often used as a beneficial method to strengthened both mechanical properties and robustness of the porous component.[28]

Consequently, motivated by the necessity to explore contemporary self-assembled BCP associations and above all oriented towards the degradable BCPs as the future of polymer materials,[29] we decided to examine the likely phase-separation leading to nanoporous thin films from such system. Two important factors influenced our selection of degradable BCP: the Flory-Huggins interaction parameter (calculated by the Hoftyzer – Van Krevelen method) together with the necessity of a differing biodegradability of the blocks in regard to selective etching. Therefore, taking into account the previously mentioned criteria, we choose to focus on amorphous polymers and the poly (trimethylene carbonate)/poly (D,L-lactic acid) (PTMC/PDLLA) system attracted our attention.

High-molar mass PTMC is a degradable and biocompatible amorphous elastomer presenting high flexibility at room temperature.[30] PTMC photo-crosslinking leads to mechanical stable network, opening the pathway toward additive manufacturing techniques.[31,32] Moreover, PTMC is prone to surface degradation in enzymatic *in vivo* conditions, thus inducing high interest for soft-tissue regeneration applications.[33–35] On the other hand, amorphous PDLLA is known to display a rapid degradation rate undertaking a hydrolytic bulk erosion mechanism, promoting it as fitting candidate for an etchable block.[36]

To summarize, in the aim to investigate the phase-separation in the PTMC/PDLLA system, we focused onto PTMC-*b*-PDLLA-*b*-PTMC triblock copolymers. Moreover, triblock copolymer system was preferred over diblock copolymer in order to anticipate the nanoporous matrix stabilization by further crosslinking of PTMC moieties after their functionalization by methacrylate groups. In addition, the phase-separation of triblock copolymer system was compared to the one occurring in PTMC/PDLLA blend. In the beginning of the study, the differential scanning calorimetry (DSC) technique was used to confirm the first manifestation of a phase-separated system, by evidencing two distinct glass transition temperatures corresponding to each block. The impact of the copolymer processing, that is to say, the solvent evaporation, the solvent vapor annealing, and the thermal effect was investigated on previously

spin-coated thin films of PTMC/PDLLA blends, PTMC-*b*-PDLLA-*b*-PTMC triblock copolymers and photocrosslinked PTMC-*b*-PDLLA-*b*-PTMC. Hence, Atomic Force Microscopy (AFM) was employed to visualize the phase-separation phenomena occurring in these samples. In the second part of the study, selective PDLLA etching was employed as a method for achieving nanoporous PTMC thin films as represented in Figure III-1. The porosity of the structure was investigated by Scanning Electron Microscopy (SEM) and efficient PDLLA removal was confirmed by DSC.

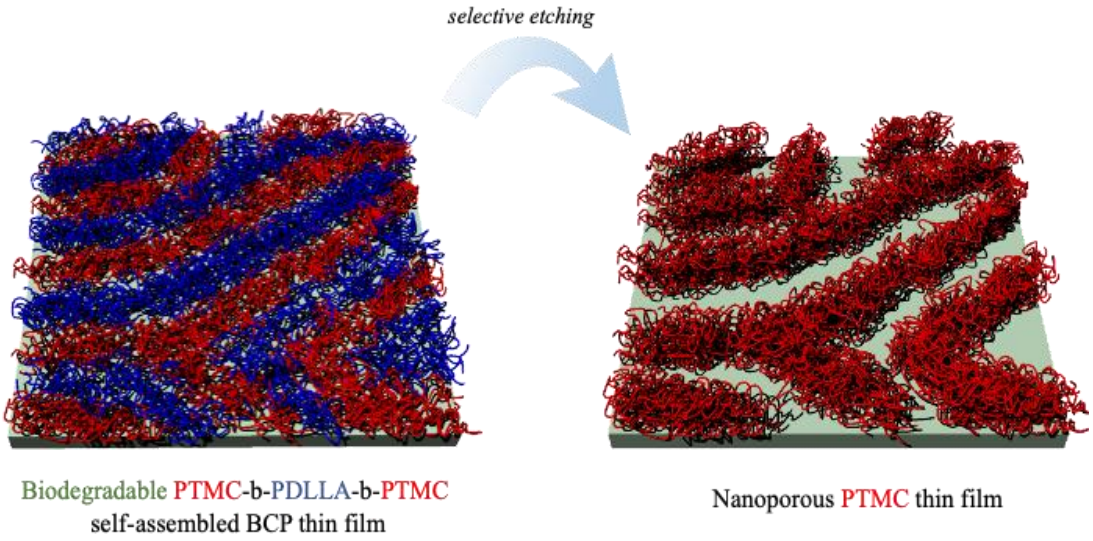

Figure III-1: Graphical representation of the investigated PTMC-*b*-PDLLA-*b*-PTMC BCP thin films leading to nanoporous PTMC templates.

2. Experimental Section/Methods

Materials and chemicals

The DL-LA monomer was purchased from Corbion (The Netherlands), while TMC monomer was obtained from Foryou Medical (China). The initiator (1,6-hexane diol), catalyst (methanesulfonic acid (MSA)) and other chemicals such as methacrylic anhydride (MMA) and triethyl amine (TEA), as well as the solvents (chloroform, dichloromethane and propylene carbonate) were purchased from Sigma Aldrich (France) and used as received. Anhydrous dichloromethane, retrieved from solvent purificator Inert PureSolv™ (France), was employed as diluting medium for the synthesis of triblock copolymer and end-methacrylate functionalization. 2-hydroxy-2-methylpropiophenone (Darocur 1173) was obtained by BASF Chemicals (Germany). Si-wafer substrates ((100)-oriented, p-type/boron doped) were obtained from STMicroelectronics Co. (Switzerland).

Synthesis of PTMC-*b*-PDLLA-*b*-PTMC triblock copolymer

Two PTMC-*b*-PDLLA-*b*-PTMC triblock copolymers were employed in this study. The first one had a total molar mass of 17.4 kg.mol^{-1} with Mn (PDLLA) = 7.2 kg.mol^{-1} and M_n (PTMC) = 10.2 kg.mol^{-1}. For the second one, the molar mass was 27.8 kg.mol^{-1} with M_n (PTMC) = 20.6 kg.mol^{-1} and M_n (PDLLA) = 7.2 kg.mol^{-1}. The dispersities (*Đ)* were 1.23 and 1.27, respectively. Their synthesis was previously reported.[37] Typically, in the case of the synthesis of PTMC-*b*-PDLLA-*b*-PTMC block copolymers with defined molar ratios of PTMC/PDLLA = 50/50, the macroinitiator (1,05 g, 0,138 mmol, 1 equiv.) was introduced in a round bottom flask with the TMC monomer (1,43 g, 13,8 mmol, 100 equiv.). Some vacuum-dry argon cycles were performed before the injection of the anhydrous dichloromethane solvent ($[TMC/\varepsilon\text{-}CL]_0$ = 1 mol/L). Finally, the MSA catalyst (0,026g, 0,276 mmol, 2 equiv.) was added to the reaction mixture. The reaction was performed at 30°C. After full TMC conversion as evidenced by NMR, an excess amount of triethylamine (3 equiv. in respect to catalyst) was added when using MSA, to neutralize this one. Finally, the polymers were slowly poured in cold methanol, then filtered and washed several times in the same solvent and dried in vacuum oven for 24 h.

Synthesis of PTMC-*b*-PDLLA-*b*-PTMC dimethacrylates

Both $PTMC_{50}$-*b*-$PDLLA_{100}$-*b*-$PTMC_{50}$ and $PTMC_{100}$-*b*-$PDLLA_{100}$-*b*-$PTMC_{100}$ triblock copolymers (1,5 g, 1 equiv.) were methacrylated employing methacrylic anhydride (MMA) (0,053 g, 4 equiv.) with triethyl amine (TEA) (0,035 g, 4 equiv.) in anhydrous dichloromethane solution ($[\text{triblock copolymer}]_0$ = 0,2 g.ml^{-1}). The reaction was left stirring at room temperature in the dark for one week. Afterwards, the dimethacrylated copolymers were purified by precipitation in cold methanol, dried in vacuum oven at room temperature for 24 h and stored at -18°C until further use.

Polymer characterizations

^{1}H NMR spectra were recorded on 400 MHz Bruker Aspect Spectrometer with $CDCl_3$ was as deuterated solvent. Chemical shifts were defined in parts per million (ppm), whereas the reference peak was residual $CDCl_3$ at 7.26 ppm.

DSC analysis and measurements of the thermal properties of the materials were carried out on Mettler Toledo (Mettler Toledo, France) DSC1 calorimeter, where calibrations were achieved using biphenyl, indium, bismium, zinc and cesium chloride standards. 12 to 15 mg of the samples (homopolymers, blends and triblock copolymers) were subjected to thermal

analysis after purification and drying. The samples were heated from -150°C and 100°C with a heating of rate of 20°C/min and two cycles were recorded. Glass transition temperature (T_g) points were evaluated in the second scan of DSC thermograms, as the transition midpoint.

Blend preparation

The homopolymer blends of PTMC and PDLLA (with 60/40 and 75/25 v/v ratios, respectively) were prepared by dissolving them in a small excess of dichloromethane (2 ml for 1g of polymer), followed by 24 h stirring. The blend was firstly separated by evaporation of the solvent, then dried in vacuum oven at room temperature for 24 h.

Thin-film preparation and spin-coating

Si-wafers were used as substrates for the spin-coating of thin films. The latter were prepared by spin-coating 10 wt % of blend or triblock copolymer solutions (in dichloromethane or propylene carbonate) at 4000 rpm during 90 s at room temperature. In the case of photo-crosslinked films, prior to spin-coating, 5 wt % of photoinitiator (Darocur 1173) in respect to the polymer was added to the solution formulation for thin films. The photo-crosslinking (induced after solvent evaporation or solvent vapor annealing processes) was performed in a UV Crosslinker Biolink chamber (Thermo Fischer, France). The irradiation time was 10 min at 3 $mW.cm^{-2}$ using a 365 nm wavelength at 10 cm from the surface of the specimens.

Solvent evaporation

Once spin-coated, the thin films were placed in a chamber with controlled room temperature of 20°C for six hours under open air atmosphere. Afterwards, they were dried under vacuum at room temperature for 12 h.

Solvent-vapor annealing (SVA) of thin films

During the SVA process, the thin films from propylene carbonate solutions were exposed to vapors of the selected solvent (chloroform). The polymer solvent incompatibility ($\chi_{P\text{-}S}$) was calculated by Equation (0), where $V_{M,S}$ is the molar volume of the solvent, while δ_d is the dispersive and δ_p is the polar component of the polymer and the solvent.

$$\chi_{P-S} = \frac{v_{M,S}}{RT}\left((\delta_{P,d} - \delta_{S,d})^2 x (\delta_{P,p} - \delta_{S,p})^2\right) \quad (0)$$

Afterwards, the samples were placed in a closed desiccator of 4 L at 20°C. A constant solvent vapor pressure in the closed chamber was maintained thanks to 40 mL of solvent in a beaker. The samples were placed on a support near the upper part of the desiccator while the solvent beaker was located on the bottom of the desiccator, to achieve the saturated solvent pressure. At the end of the SVA process (1 h or more), the thin films were removed from the desiccator and dried in vacuum oven at room temperature for 12 h.

Thermal treatment of thin films

In the case where the samples were thermally inspected after spin-coating and SVA, the thin-films were stored in a vacuum oven at 65°C for a specific time duration.

PDLLA-hydrolysis

Selective PDLLA etching from the self-assembled thin films was performed by covering the film surface with 0.5 M sodium hydroxide 40/60 (v/v) methanol/water solution for 30 min. After removal of the 0.5 M NaOH solution, the sample was washed with 40/60 (v/v) methanol/water solution for 10 min, before being dried under vacuum at room temperature for 24 h.

Thin film analysis

Atomic Force Microscopy **–** The AFM mechanical characterization performed in HarmoniX mode from Bruker AFM is presented herein. Harmonix™ mode provides simultaneous topography and (semi)-quantitative mechanical property mapping at typical tapping mode imaging speed.[38,39] The relatively high bandwidth and force sensitivity of the so-called Torsional harmonic cantilever (THC) probes offers a good mechanical property in the mapping capability, especially for complex systems composed of different phases with contrasting properties.

THC soft probers (HMSX from bruker) with spring constant of 0.5 to 1.5 N/m were used on a Nanoman V AFM from Bruker Instruments to record images at different magnifications

(20x20µm², 10x10µm², 5x5µm², 2x2µm²) on different areas of the surface of each sample. The image resolution was 512 x 512 pixels with a scan rate of 0.5Hz. The tapping ratio (the ratio of the setpoint amplitude to the free vibration amplitude, $r_{sp} = A_{sp}/A_0$) was set to 0.6 in order to maintain « hard tapping » conditions and to enhance the mechanical contrast on different materials while keeping a good spatial resolution. Several images at several magnifications were captured with the aim of improving the confidence in the statistical analysis. The DMT modulus sensitivity was calibrated by using a reference sample from Bruker Instruments (PS/LDPE) with known modulus value (2.3GPa/70MPa). Our relative DMT modulus calibration gives 2.37 GPa ± 0.24 GPa and 73 MPa ± 9 MPa for PS and LDPE respectively.

Scanning electron microscopy - The samples were firstly coated with an ultrathin layer of electrically conducting platinum that was deposited by high-vacuum evaporation. Afterwards, prior to analysis, they were folded on a 45° SEM mount. SEM experimentations were performed on Hitachi S-4800 instrument operating at a spatial resolution of 1.5 nm at 2 kV energy.

3. Results and discussion

3.1 Theoretical considerations on the phase-separation in PTMC-b-PDLLA-b-PTMC triblock copolymers

In order to anticipate the possible phase-separation in a PTMC-PDLLA system, the Flory-Huggins PTMC-PDLLA ($\chi_{PTMC\text{-}PDLLA}$) interaction component was calculated. This parameter measures the total interaction energy between a pair of PTMC and PDLLA polymer chains and is defined by the following equation (1):

$$\chi_{AB} = \frac{\nu_{M,AB}}{RT}(\delta_A - \delta_B)^2 \quad (1)$$

$$\nu_M = \frac{M}{\rho_A} \quad (2)$$

where $\nu_{M,AB}$ is the geometric mean of the molar volumes of both polymers (calculated by equation (2) where ρ and M are the amorphous material density and molar mass of the repeating unit), R and T are the universal gas constant and the absolute temperature, while $(\delta_A - \delta_B)^2$ is the cohesive energy density from the solubility parameters of both polymers (δ_{PTMC} and δ_{PDLLA}).

The Hoftyzer-van Krevelen method was used to calculate the solubility parameters for both PTMC and PDLLA, leading to the Flory-Huggins interaction parameter (equations (3) to (6)):

$$\delta_T = \sqrt{\delta_d^2 + \delta_p^2 + \delta_h^2} \quad (3)$$

$$\delta_d = \frac{\Sigma F_{di}}{V_m} \quad (4)$$

$$\delta_p = \frac{\sqrt{\Sigma F_{pi}^2}}{V_m} \quad (5)$$

$$\delta_h = \frac{\sqrt{\Sigma E_{hi}}}{V_m} \quad (6)$$

This method is based on the determination of the solubility parameters by the group-contribution approach.[40] The latter is an approximation applying the additivity rule of contributions of the structural and functional groups of the repeating unit in a polymer chain. In fact, the Hoftyzer-van Krevelen method, among others such as Hansen's or Hoy's ones, is the most suitable for amorphous polymers, since they particularly optimized the group contributions from experimental data for numerous non-crystalline polymers.[41] Therefore, the solubility parameter ($\delta_{T,polymer}$) is calculated as represented in equation (3), and is in direct dependence on the dispersion (δ_d), the polarity (δ_p) and the hydrogen bonding (δ_h) components. Therein, F_{di}, F_{pi} are group contributions while E_{hi}, also calculated by the group-contribution

approach stands for the hydrogen bonding energy. On the other side, V_m means the molar volume of the polymer repeating unit.

Accordingly, by using the contributions of each group present in the repeating unit of a respective polymer, as reported in the literature,[40] the values of the group-contribution segments (F_{di}, F_{pi} and E_{hi}) for both PTMC and PDLLA were firstly calculated. The results are depicted in Table III-1 and Table III-2, respectively.

Table III-1: Determination of the solubility parameter component group contributions of PTMC with a repeating unit [-O-CH_2-CH_2-CH_2-O-CO-].

	$\mathbf{F}_{di}$	$\mathbf{F}_{pi}^2$	$\mathbf{E}_{hi}$
-O-	100	160 000	3000
3 -CH_2-	810	0	0
-O-CO-	390	240100	7000
Σ	1300	400100	10 000

Table III-2: Determination of the solubility parameter component group contributions of PDLLA with a repeating unit [-O-CH(CH_3)-CO-].

	$\mathbf{F}_{di}$	$\mathbf{F}_{pi}^2$	$\mathbf{E}_{hi}$
-CH-	80	0	0
-CH_3-	420	0	0
-O-CO-	390	240100	7000
Σ	890	240100	7000

By applying these values in the equations (4) to (6), and consequently by using the equation (3), the overall values of PTMC and PDLLA solubility parameters were determined, as presented in Table III-3.

Table III-3: PTMC and PDLLA solubility parameters (δ_T) and their dispersion, polar and hydrogen bonding component.

Polymer	$\boldsymbol{\delta_T}$ $(MPa)^{0.5}$	$\boldsymbol{\delta_d}$ $(MPa)^{0.5}$	$\boldsymbol{\delta_p}$ $(MPa)^{0.5}$	$\boldsymbol{\delta_h}$ $(MPa)^{0.5}$	$\mathbf{V_m}$ $(ml.mol^{-1})$
Poly (D,L-lactic acid)	**18.2**	13.2	7.3	10.2	67.2
Poly (trimethylenecarbonate)	**21.7**	16.7	8.1	11.3	78

Therefore, by implementing the equation (1) when using δ_A and δ_B as solubility parameters for PTMC and PDLLA, respectively, the PTMC-PDLLA interaction parameter gives a value of 0.36 (Table III-4). The segregation trend of the system can be foreseen since it can be measured by the $\chi_{AB}N$ product term. The coefficient N stands for the number of repeating units of both blocks. In our study, the number of repeating units of the PDLLA middle-block was settled to 100, while the PTMC end-blocks had 100 and 200 repeating units (Table III-4). The volume fraction of the blocks was determined by Equation (7), taking into consideration that $f_{PTMC} + f_{PDLLA} = 1$.

$$f_{PTMC} = \frac{(M_{w,PTMC} \times d_{PTMC})}{(M_{w,PTMC} \times d_{PTMC}) + (M_{w,PDLLA} \times d_{PDLLA})} \quad (7)$$

where d_{PTMC} = 1.316 g.cm^{-3} and d_{PLA} = 1.161 g.cm^{-3} are the density values of the respective PTMC and PDLLA amorphous polymers.

The defined block lengths of PTMC and PDLLA were set on purpose for the synthesis of the *t*BCPs employed in this study, so that the system could belong to the strong segregational limit ($\chi N > 10.5$).[42] This parameter is crucial in the aim of satisfying the theoretical requirements for phase-separation in a blend or in a copolymer system.

Table III-4: $\chi_{AB}N$ values for PTMC/PDLLA block copolymers as a function of their respective volume fractions and Flory-Huggins interaction parameter.

Block copolymer	**block molar ratio**	**block volume fractions**	**Calculated $\chi_{PTMC-PDLLA}$**	**$\chi_{AB}N$ value**
$PTMC_{50}$-*b*-$PDLLA_{100}$-*b*-$PTMC_{50}$	50/50	60/40	0.36	72
$PTMC_{100}$-*b*-$PDLLA_{100}$-*b*-$PTMC_{100}$	67/33	75/25	0.36	108

3.2 End-functionalization of PTMC-b-PDLLA-b-PTMC dimethacrylate (dMA) triblock copolymers

Formerly reported literature data pointed out towards a challenging synthesis of block copolymers employing PDLLA macroinitiators (later used as the middle block) due to the partial reactivity of secondary hydroxyl chain ends.[43] Nevertheless, we managed to outpace this problem by the employment of a special organocatalytic system (methanesulfonic acid) for the ring-opening polymerization of TMC from PDLLA macroinitiators, as reported in our previous study.[37] Therein, we demonstrated the controlled synthesis of the PTMC-*b*-PDLLA-*b*-PTMC triblock copolymers without side reactions such as transesterification and the desired pure triblock architecture was confirmed by NMR (^{1}H, ^{13}C and DOSY techniques) and SEC.

An ultimate modification of the block copolymers was performed before proceeding to the investigation of the self-assembly in a PTMC/PDLLA system. Therefore, in the goal of the (porous) matrix stabilization, end-functionalization of the BCPs with methacrylate groups was performed (Scheme III-1), the latter having the ability to lead to photo-crosslinked thin films under UV light and in the presence of photoinitiator. Hence, the elevated functionalization percentage (> 80 %) can be calculated *via* the ^{1}H NMR spectrum (Figure III-S1) of the methacrylated polymers (PTMC-*b*-PDLLA-*b*-PTMC-dMa) by integration of the *Ha* and *Hb* protons (5.5 and 6.1 ppm) of the characteristic peak of the double bond of the methacrylate units and comparing them with the peaks of the PTMC or PDLLA blocks.

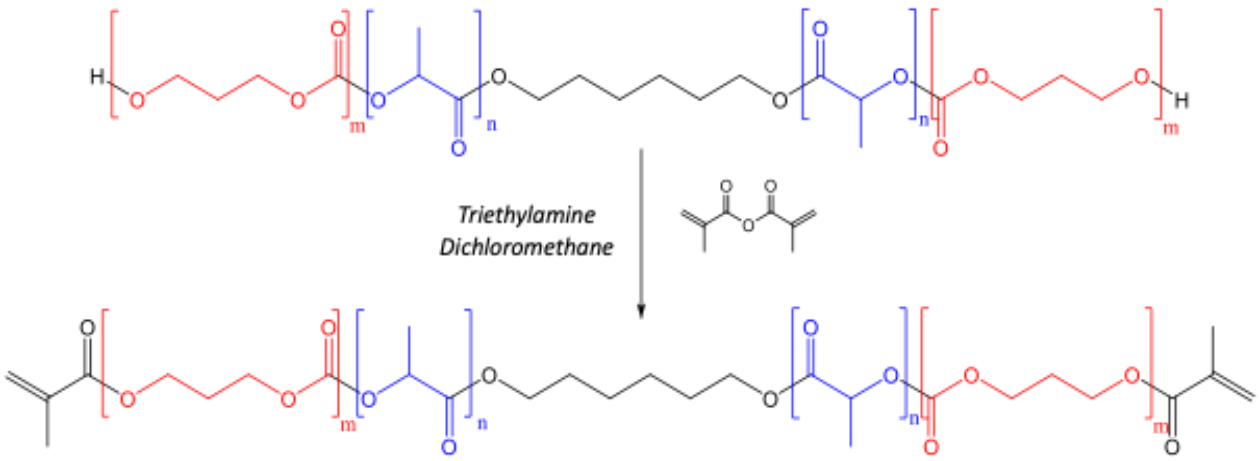

Scheme III-1: *dMa*-PTMC-*b*-PDLLA-*b*-PTMC-*dMa* triblock copolymers with photo-sensitive methacrylate end-groups.

3.3 Phase-separation and self-assembly phenomena in PTMC/PDLLA blends, triblock copolymers, and photo-crosslinked triblock copolymers

3.3.1 Differential scanning calorimetry (DSC) as a tool for studying phase-separation

DSC technique has been widely used to access the thermal properties of composites, polymer blends and self-organized systems.[44–46] Moreover, the observable glass transition temperature is directly related to the phase equilibrium and the miscibility character of a polymer system. Hence, if a single broad glass transition scope is observed, a polymer blend can be considered as miscible. On the contrary, immiscible structures precisely demonstrate two distinct Tg points.

Therefore, DSC scans of PTMC-PDLLA triblock copolymers were performed, and their respective glass transitions were compared to the ones of PTMC and PDLLA homopolymers. The thermograms of the *t*BCPs can be visualized in Figure III-2.

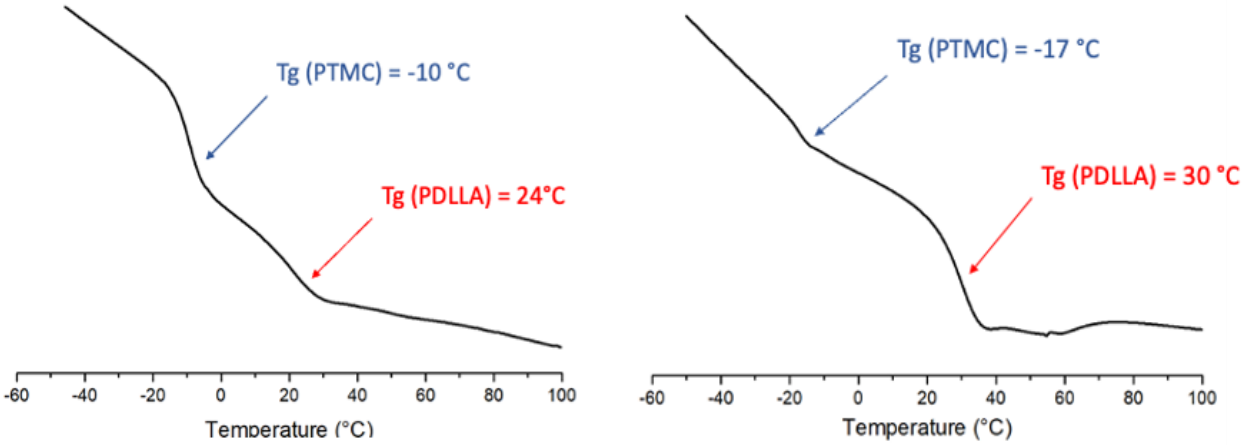

Figure III-2: DSC scans of $PTMC_{50}$-*b*-$PDLLA_{100}$-*b*-$PTMC_{50}$ (left) and $PTMC_{100}$-*b*-$PDLLA_{100}$-*b*-$PTMC_{100}$ (right).

As expected by the theoretical studies, the phase-separation in PTMC-*b*-PDLLA-*b*-PTMC triblock copolymers (with differing molar ratios) was confirmed with the appearance of two glass transition temperatures, close to that of the corresponding homopolymers (Table III-5). This behavior confirms that phase segregation occurs as predicted by the thermodynamic data of Table III-4.

Table III-5: Values of glass transition temperatures of the homopolymers and triblock copolymers.

Sample	Tg (PTMC) (°C)	Tg (PDLLA) (°C)
$PTMC_{100}$	-17	/
$PDLLA_{100}$	/	27
$PTMC_{50}$-*b*-$PDLLA_{100}$-*b*-$PTMC_{50}$ *t*BCP	-10	24
$PTMC_{100}$-*b*-$PDLLA_{100}$-*b*-$PTMC_{100}$ *t*BCP	-17	30

Since the thermal analysis of the triblock copolymers point out a phase-separated system, we continued the investigation of their self-assembly by the means of Atomic Force Microscopy (AFM).

3.3.2. Study of the PTMC-PDLLA phase-separation by means of Atomic Force Microscopy (AFM)

The phase separation phenomena taking place in solid state thin films of blends or block copolymers have been more and more investigated by this method since it leads to the characterization of differing nanoscale processes occurring at the top-surface of materials.[27,47,48] By measuring the pressure variations between the sample surface and the AFM tip, a cartography of the microdomains together with their properties such as size, shape, organization into various morphologies but also an insight in their elasticity is provided.[49] Among the three AFM operation modes, the tapping mode grants an optimal imaging resolution.[50] Meanwhile, due to the remarkably short interval of tip-surface contact, the distortion of surface topography, occasionally occurring when analyzing elastomers in contact mode, is avoided. Moreover, the elastic moduli of PTMC and PDLLA being significantly contrastive, favors the AFM characterization.[51] By these means, tapping-mode AFM was selected to study the phase-separation morphologies in both PTMC/PDLLA blends and triblock copolymers.

Multiple parameters such as the type of material (blend or block copolymer), the influence of the copolymer composition together with photo-crosslinking, the annealing techniques such as solvent vapor annealing (SVA) the choice of the SVA solvent have been investigated to optimize the conditions for self-assembly of the PTMC/PDLLA system.

Solvent evaporation method

In the first place, simple solvent evaporation from thin films of blends, triblock copolymers and photo-crosslinked *t*BCPs has been investigated. Thus, the samples were primarily processed as a thin film geometry *via* spin-coating and the latter was quenched by the (fast) solvent evaporation at room temperature. This straightforward process is known to produce ordered microdomain morphologies in BCP thin films.[52] The latter is the result of an ordering front in the thin film propagating from the surface to the interior of the film as the solvent evaporates.[53]

For that purpose, good solvent (dichloromethane) for both PTMC and PDLLA components was chosen as the diluting medium for spin-coating. Once the solvent was evaporated and the films were dried, they were analyzed by AFM.

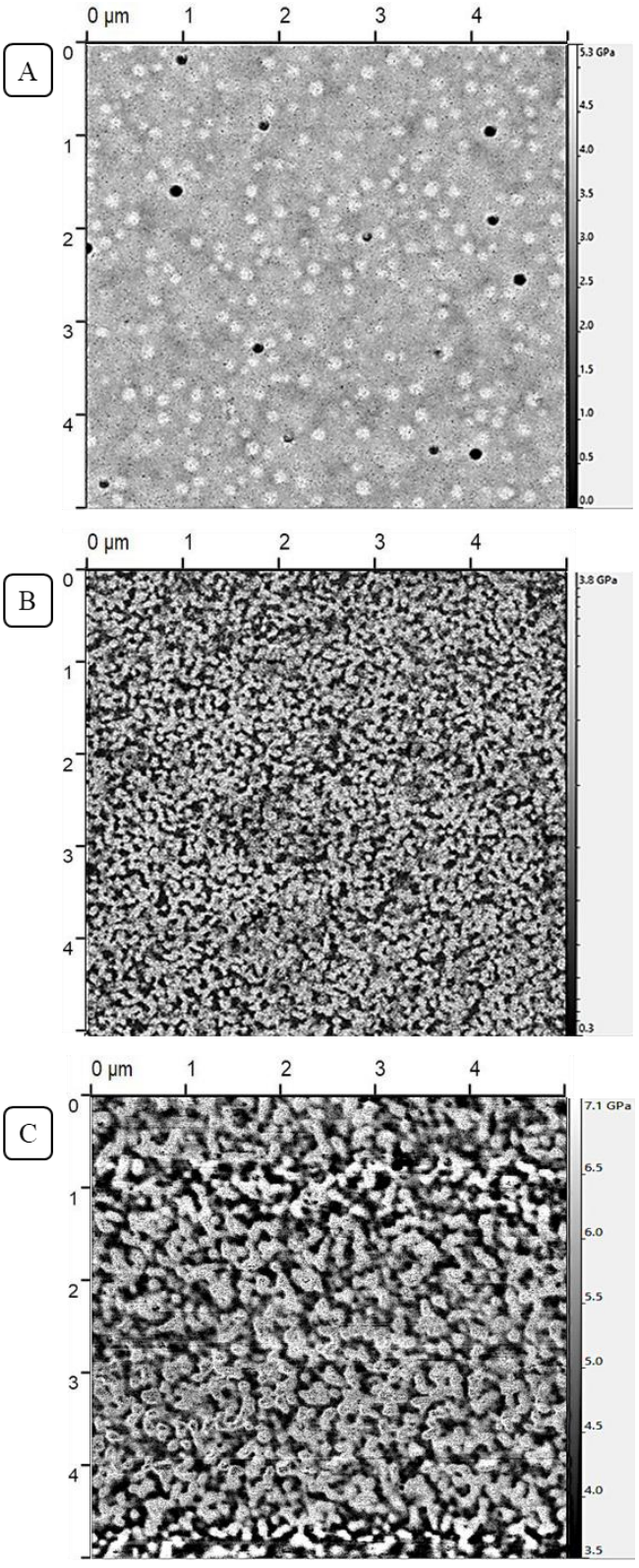

Figure III-3: AFM stiffness images of A) $PTMC_{100}/PDLLA_{100}$ blend; B) $PTMC_{50}$-*b*-$PDLLA_{100}$-*b*-$PTMC_{50}$ *t*BCP and C) photo-crosslinked $PTMC_{50}$-b-$PDLLA_{100}$-b-$PTMC_{50}$ *t*BCP on 5 x 5µm length scale.

An evident difference between $PTMC_{100}$/$PDLLA_{100}$ blend (Figure III-3A) and $PTMC_{50}$-*b*-$PDLLA_{100}$-*b*-$PTMC_{50}$ *t*BCP thin film (Figure III-3B) is observable on the AFM stiffness images. On one side, the blend demonstrates a smooth surface of almost homogeneous polymer layer with islands consisting of the PDLLA phase. On the other side, in the case of triblock copolymer architecture, even though highly ordered morphologies were not discernible, phase-separation on the nanometer range scale is clearly present. In this kinetically trapped self-assembly, the PDLLA phase appears bright due to its rigidity with Young modulus magnitude of around 4 GPa, while the rubber-like PTMC phase occurs darker with magnitudes of around 0.3 GPa (as suggested by the AFM approximation for lower values of Young modulus). A beginning of bicontinuous morphology consisting of PDLLA and PTMC phase can be also observed in the case of a photo-crosslinked thin film (Figure III-3C). Therefore, despite the slight widening of the microdomains when creating a dense crosslinked network, it can be concluded that photo-crosslinking of methacrylated PTMC does not disrupt the self-assembly of the BCP system. In the Figure III-S2, AFM thin film analysis of $PTMC_{200}$/$PDLLA_{100}$ blend (A), $PTMC_{100}$-*b*-$PDLLA_{100}$-*b*-$PTMC_{50}$ *t*BCP (B) and the photo-crosslinked *t*BCP (C) are represented. Likewise, significantly more pronounced phase-separation is observed in the case of the copolymers (*t*BCP) in comparison with the blend. However, the self-assembly of these BCPs with PTMC/PDLLA 75/25 volume ratios is less developed compared to the block copolymers with 60/40 volume ratios in the case of rapid solvent evaporation from spin-coated thin films.

Nevertheless, even though phase-separated structures were observable in the *t*BCP architectures herein, these images show the debuting point of self-assembly since the fast solvent evaporation kinetically traps the as-spun thin films in a disordered state. Hence, additional mobility of the polymer chains should be induced to achieve more organized morphologies. Therefore, solvent vapor annealing as a method for optimizing the self-assembly in PTMC-PDLLA triblock copolymers was proceeded.

Solvent vapor annealing (SVA)

Solvent vapor annealing is an advantageous technique allowing achievement of ordered morphologies and domains even in BCPs of high molar mass and elevated Flory-Huggins interaction parameters like in this study. This method favors a faster self-assembly reorganization compared to thermal annealing, attainable even in lower temperatures (room temperature in some cases) due to favorable thermodynamic forces in the swollen state leading

to an optimized control of the phenomena occurring at the BCP interface.[25,54,55] More precisely, the SVA approach consists in exposing the thin films to vapors of precisely selected solvent. By absorbing this solvent the polymer swells, thus allowing bigger mobility of the polymer chains leading to metastable morphologies, unachievable by other approaches.[56–58] Moreover, SVA is beneficial to PDLLA containing block copolymers due to its thermal sensitivity, possibly leading to degradation.[59]

In our study, two different block copolymer compositions were tested for the SVA approach, with a precisely selected solvent, given the fact that the solvent choice for the swollen state is being highly important for well-controlled ordered morphologies.[60] Previously, the thin films were spin-coated from propylene carbonate solutions, a good solvent for both blocks with elevated evaporation point allowing a convenient reorganization in the SVA state.

Despite the promoting annealing conditions, once again, the blend sample did not undertake clear phase-separation (Figure III-4A). On the other side, well-ordered morphologies for the photo-crosslinked $PTMC_{100}$-*b*-$PDLLA_{100}$-*b*-$PTMC_{100}$ *t*BCP are clearly observable in Figure III-4B. Moreover, the uniformity, achieved under short annealing times of 1 h, was kept on a long-length scale of 20 x 20 µm, whereas numerous literature examples reported self-assemblies on noticeably smaller scales.[53,61,62] This result could be expected taking into account that the optimal SVA assemblies come from good solvents for both blocks or preferential to one of the blocks.[25] In this case, chloroform is slightly more PTMC selective compared to PDLLA ($\chi_{PTMC\text{-}chloroform}$=0.92, $\chi_{PDLLA\text{-}chloroform}$=1.26 , as calculated by the equation (0) represented in the experimental part). As presented in Figure III-5, by comparing the photo-crosslinked with the non-cured $PTMC_{100}$-*b*-$PDLLA_{100}$-*b*-$PTMC_{100}$ *t*BCP thin-film, a slight increase of the microdomains is noticeable. However, the bicontinuous nanoscopic phase-separation of PTMC (dark) and PDLLA (bright) domains is still conserved.

Hence, AFM calculations demonstrate average domain size of 160 nm for the non-cured film and 230 nm for the photo-crosslinked thin film. Moreover, for the image presented in Figure III-5A, for analyzed surface of 9.808 µm², the AFM calculations reveal occupancy of the rigid PDLLA phase of 5.537 µm² and average modulus of 3.76 GPa (±0.6 GPa) while the soft PTMC phase covers 4.271µm² with an average modulus of 0.845 GPa (± 0.41 GPa). On the other side, in the crosslinked sample presented in Figure III-5B, the PTMC and PDLLA phases cover 6.708µm² and 2.952µm², respectively, on 9.76 µm² analyzed surface.

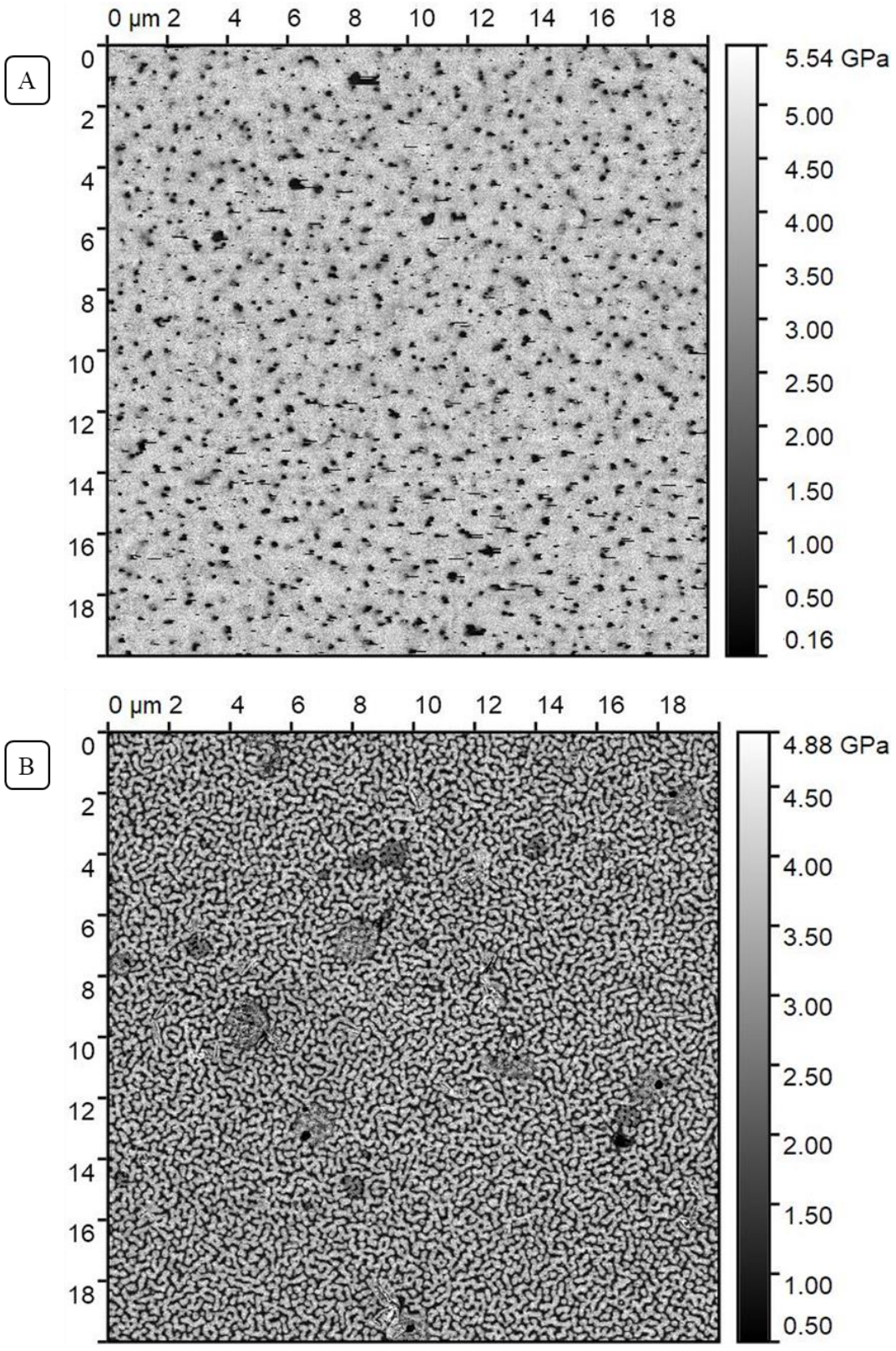

Figure III-4: AFM stiffness images of solvent vapor annealed A) $PTMC_{200}/PDLLA_{100}$ blend; B) photo-crosslinked $PTMC_{100}$-*b*-$PDLLA_{100}$-*b*-$PTMC_{100}$ *t*BCP on 20 x 20 µm length scale.

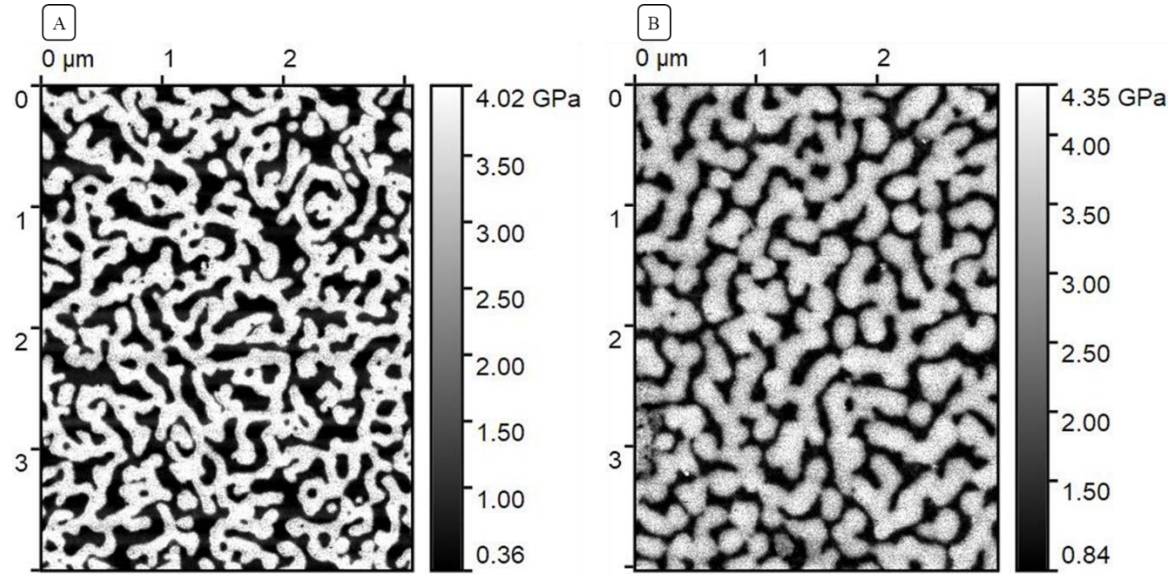

Figure III-5: AFM stiffness images of solvent-vapor annealed: A) $PTMC_{100}$-*b*-$PDLLA_{100}$-*b*-$PTMC_{100}$ *t*BCP thin film and B) photo-crosslinked $PTMC_{100}$-*b*-$PDLLA_{100}$-*b*-$PTMC_{100}$ *t*BCP thin film on 4 x 3 µm length scale.

Hence, it can be concluded that the SVA process further promoted the phase-organization when compared to simple solvent evaporation. The Young Modulus of both phases remained consistent as in the previous case. Also, it is important to mention that the photo-crosslinking was performed after the SVA process and film drying, so that no restriction of the chain mobility could occur.

In the following part, we studied samples from $PTMC_{50}$-*b*-$PDLLA_{100}$-*b*-$PTMC_{50}$ *t*BCP with a different molar ratio (PTMC/PDLLA = 60/40 v/v) than the previous one and processed in identical SVA conditions. Thus, the AFM image of *t*BCP thin film, is presented in Figure III-S3. Interestingly, more organized morphologies were observed for *t*BCPs with higher PTMC ratios. The latter, in some way, could occur due to the bigger content of the majority PTMC component, favoring a more organized morphology resulting from the bigger mobility of this phase in chloroform which is slightly more PTMC selective.

Study of the thermal stability of PTMC-PDLLA self-assemblies

Optimized polymer diffusivity and increased mobility of the chains by thermal treatment has been also employed for achieving well phase-separated structures in differing block copolymer associations.[63,64] While inspecting the thermal influence on our amorphous systems, we set a precise temperature value of 65°C above the glass transitions of both blocks.

The thermal process was performed in a vacuum oven, to avoid any possible decomposition or oxidation of the organic polymer. Nevertheless, as presented in Figure III-6B, the crosslinked *t*BCP thin film started demonstrating a disorganized morphology after 1 h.

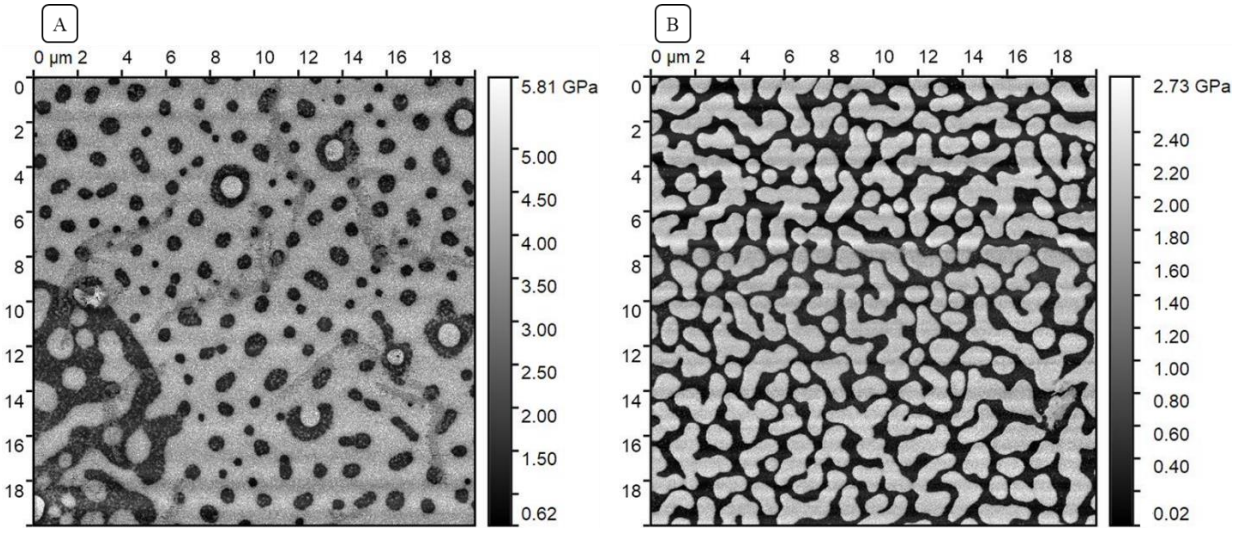

Figure III-6: AFM thin film stiffness images of A) thermally annealed $PTMC_{100}/PDLLA_{100}$ blend; B) thermally annealed $PTMC_{50}$-*b*-$PDLLA_{100}$-*b*-$PTMC_{50}$ cured *t*BCP on 20 x 20 µm length scale.

We propose two possible hypotheses for this phenomenon: either the material is possibly starting to degrade or the more rigid PDLLA phase starts reorganizing, thus forming a wetting surface on top of the film.[54] On the other side, the blend sample collapses completely in the same thermal conditions (Figure III-6A), thus demonstrating that the block copolymer architecture presents once again bigger stability of the self-assembly.

The thermal behaviour of the self-assembly of solvent vapor annealed *t*BCP was also examined *via* SEM microscopy (Figure III-S4). The destructuration of the phase organization is represented on different scale bars as the SEM imaging progressed. In fact, since the electron beam induces local heating while analyzing the sample, the PDLLA phase expands in size meanwhile organizing itself as a surface wetting layer. This phenomenon prevents the microscope to drop further than the scale (of 3 µm) indicated on the image in Figure III-S4C.

To conclude, this study of thermal behavior demonstrates that the assemblies are stable up to temperatures neighboring the glass transition points of the system. Heating above room temperature provokes the reorganization of the self-assemblies and alters the phase-separated morphologies. Ideally this system should be handled at temperatures no higher than 30°C, with the appropriate annealing technique (SVA) as previously demonstrated.

3.4 Nanoporous PTMC thin films

In the aim to produce nanoporous templates, the highly ordered photo-crosslinked $PTMC_{100}$-*b*-$PDLLA_{100}$-*b*-$PTMC_{100}$ thin films resulting from solvent vapor annealing are the most suitable candidate for selective PDLLA etching due to their attractive bicontinuous morphology on a long-range (20 x 20 μm) scale. The films were previously cured under UV to induce additional stability of the PTMC phase, presumed to support the cavities after PDLLA removal. In fact, matrix crosslinking as a method for porous structure stabilization has been reported for various porous monoliths and thin films.[10] Moreover, the fact that PTMC constitutes the majority of the structure (75/25 PTMC/PDLLA v/v) herein, should be beneficial to the stability of the porous network as well.
Hence, after UV crosslinking, hydrolysis of PDLLA and washing, the thin films were initially analyzed by DSC to confirm the selective PDLLA etching. Consequently, the DSC scan of this sample (Figure III-7A) demonstrated a single glass transition temperature corresponding to the PTMC block (-16°C), justifying the successful PDLLA degradation and extraction of the by-products. Moreover, the glass transition point remained undeniably close to the one of PTMC in the triblock copolymer, demonstrating a resistance of the PTMC phase in the employed hydrolysis conditions.

Subsequently, the porosity of the sample was investigated by the means of SEM imaging. The SEM image presented in Figure III-7B confirms that a 30 min basic hydrolysis solution treatment is efficient for effective PDLLA removal and pore generation from the crosslinked thin film. In addition, and quite importantly, the high degree of long-range order remained resistant upon hydrolysis. The staining contrast of the SEM imaging makes the PTMC phase appear in bright, whereas instead of the PDLLA phase, interconnected cavities in the nanometer range scale are observable. Moreover, this analysis was performed on the same support for spin-coating and hydrolysis, implicating that the films stayed strongly immobilized to the surface and their delamination was avoided thanks to UV photo-crosslinking. In the likewise context, it is important to mention that non-crosslinked thin films did not remain adhered to the substrate upon hydrolysis, once again pointing towards the necessity of crosslinking.

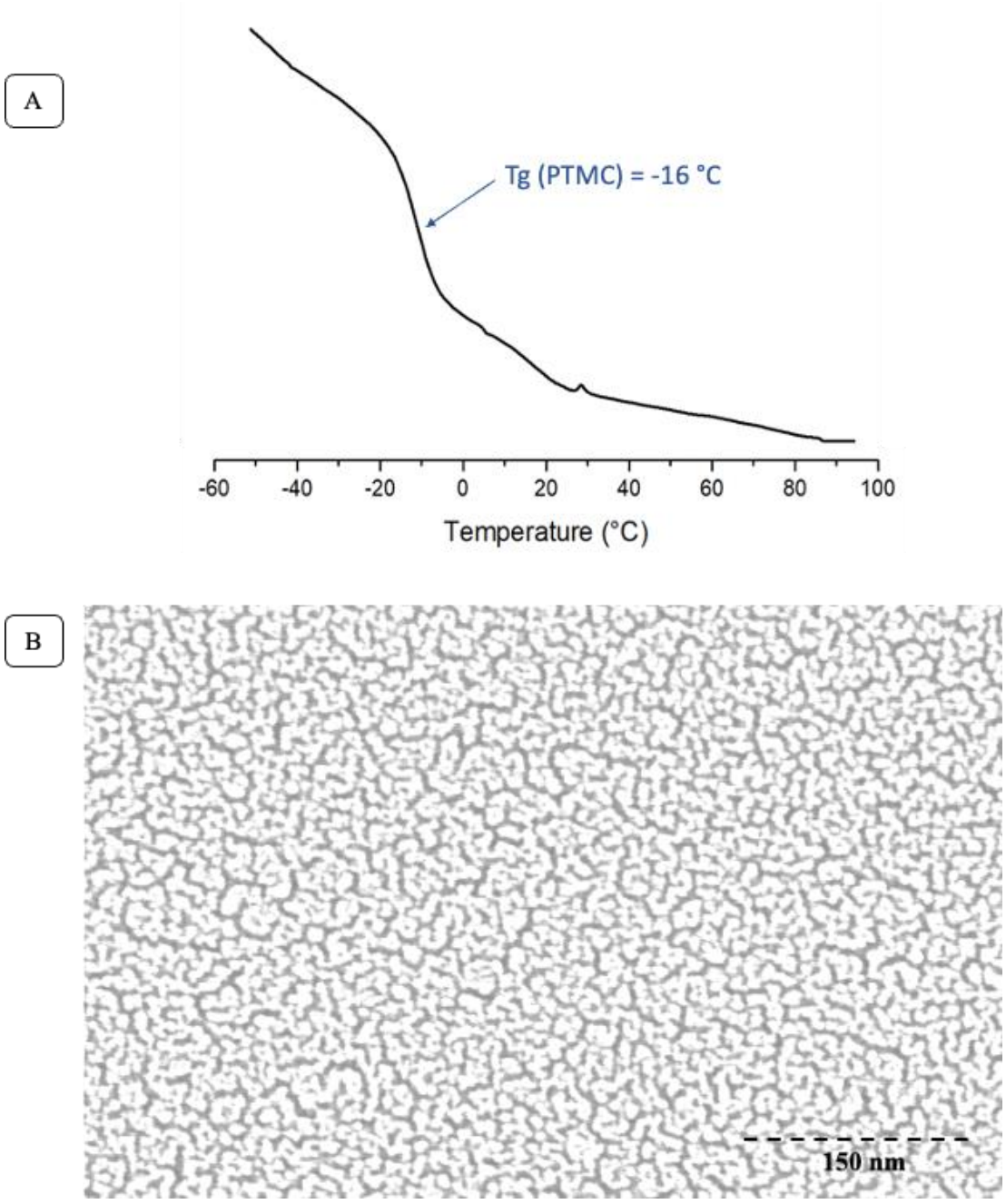

Figure III-7: (A) DSC cooling scan of photo-crosslinked $PTMC_{100}$-*b*-$PDLLA_{100}$-*b*-$PTMC_{100}$ thin film after hydrolysis and (B) Scanning electron micrograph of nanoporous PTMC thin film. The scale bar in the lower right corner is 150 nm.

4. Conclusion

The phase separation in degradable block copolymers has been slightly studied up to day. Therefore, we decided to investigate such phenomena in a carefully selected block copolymer association. Theoretical studies on the PTMC-PDLLA interaction parameter let us expect a possible phase-separation in such system, which was further confirmed by DSC analysis. Their self-assembly was investigated in a thin-film geometry produced by the spin-coating technique. Solvent vapor annealing resulted as the optimal annealing technique, leading to bicontinuous microdomains of nanoscopic PTMC and PDLLA phases on a long-length scale while employing triblock copolymer thin films. In contrast, the same annealing conditions did not result in ordered morphologies in the case of PTMC/PDLLA blends. The thin film presenting the most homogenized organization herein, once subjected to selective PDLLA etching upon hydrolysis, resulted in nanoporous PTMC. Moreover, thin films photo-crosslinking, initially employed towards porous matrix stabilization, did not influence the phase-separation of the system.

These advances represent an important contribution to the large area of block copolymer phase-separation and the production of nanoporous templates from degradable amorphous self-assembled associations. All at once, this study could represent the starting point to any future optimization of the PTMC-PDLLA self-assembly in terms of solvent vapor annealing, the choice of solvents, impact of block copolymer lengths, etc. Moreover, potential biomedical applications of these obtained nanoporous systems could be foreseen taking in account the well-known PTMC biocompatibility.

Supporting Information

Self-assembled degradable block copolymer precursors for nanoporous PTMC thin films

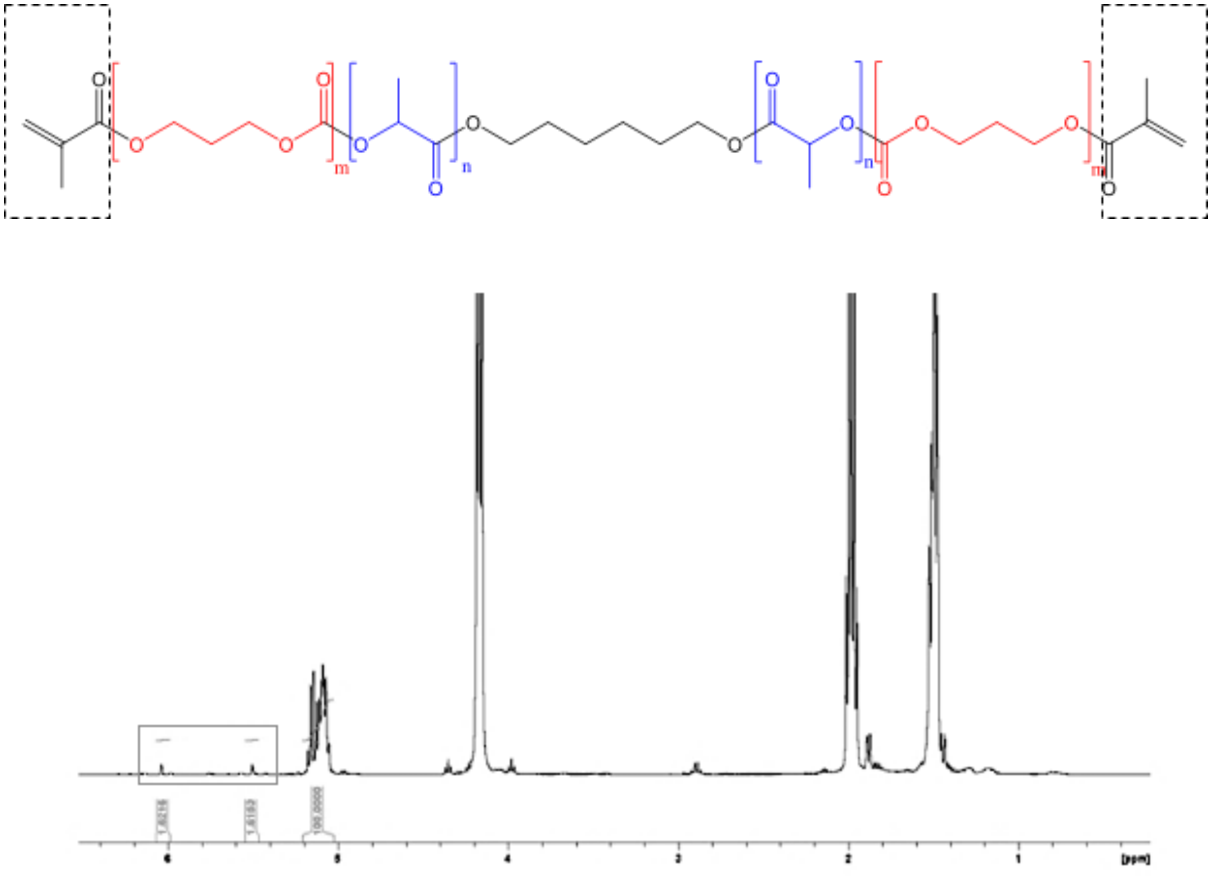

Figure III-S1: ^{1}H-NMR of methacrylated $PTMC_{100}$-*b*-$PDLLA_{100}$-*b*-$PTMC_{100}$ BCP.

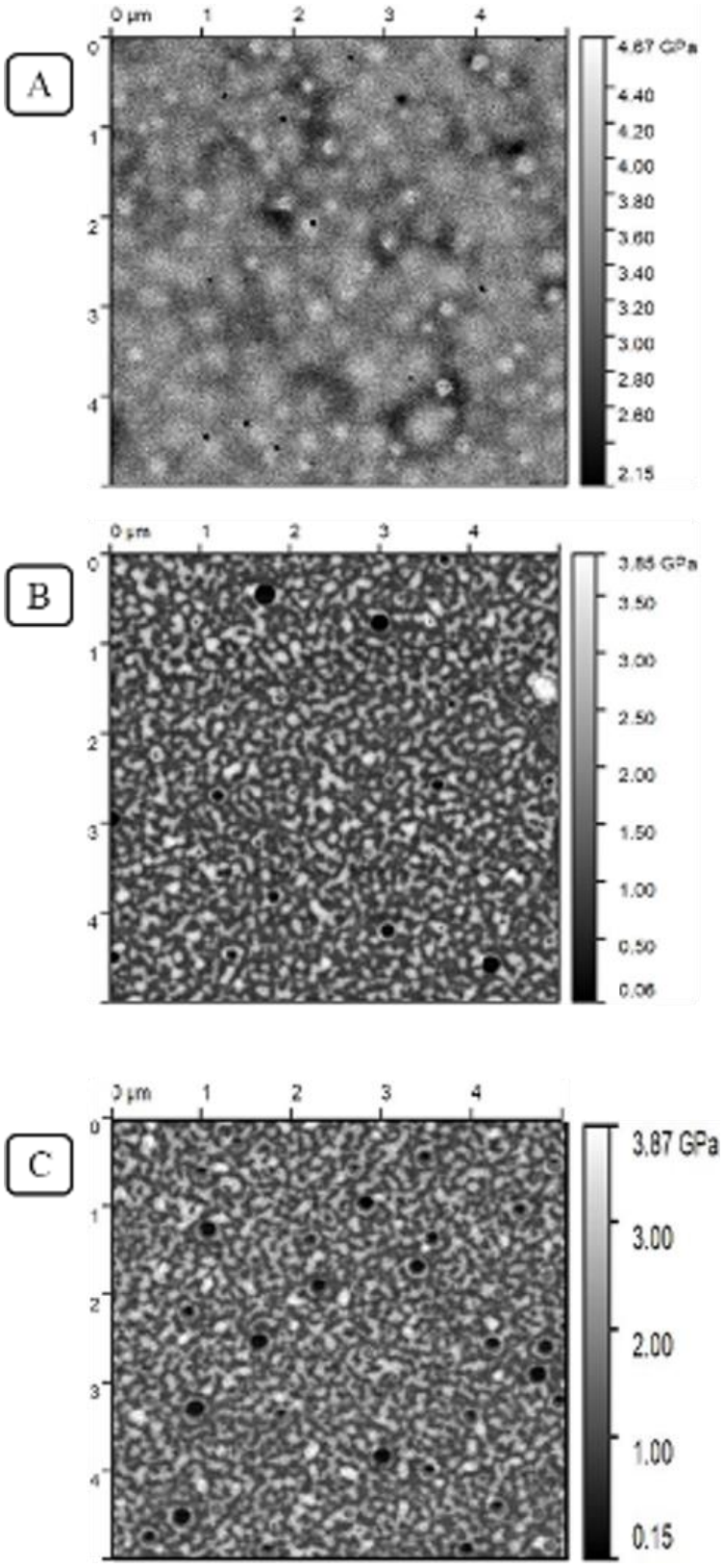

Figure III-S2: AFM stiffness images of thin films of A) $PTMC_{200}/PDLLA_{100}$ blend; B) $PTMC_{100}$-*b*-$PDLLA_{100}$-*b*-$PTMC_{100}$ *t*BCP and C) photo-crosslinked $PTMC_{50}$-*b*-$PDLLA_{100}$-*b*-$PTMC_{50}$ *t*BCP on 5 x 5 µm length scale.

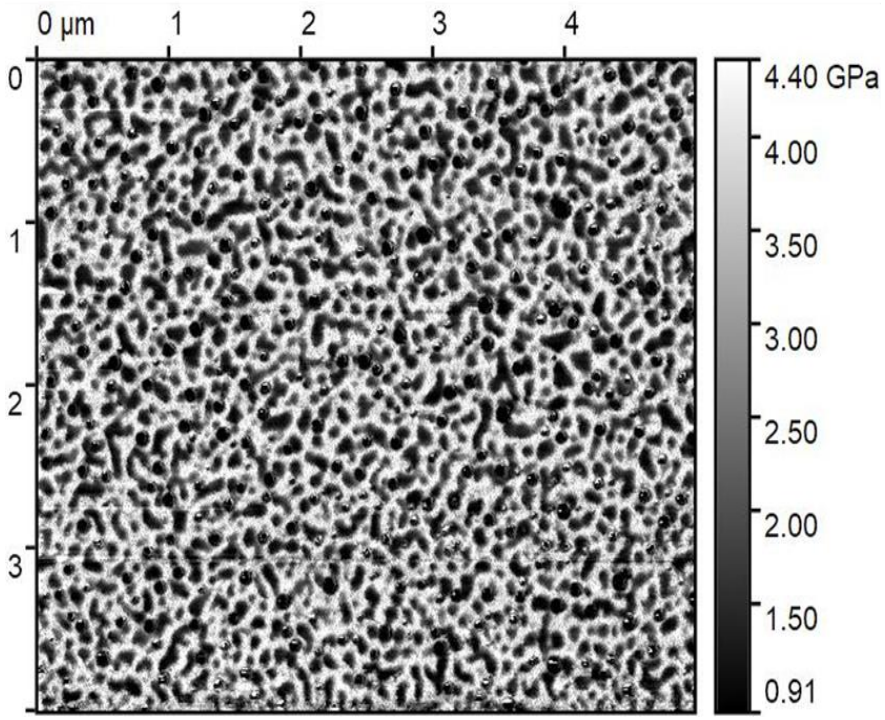

Figure III-S3: AFM stiffness images (4 x 5 µm) of $PTMC_{50}$-*b*-$PDLLA_{100}$-*b*-$PTMC_{50}$ *t*BCP thin films annealed in chloroform vapors for 1h.

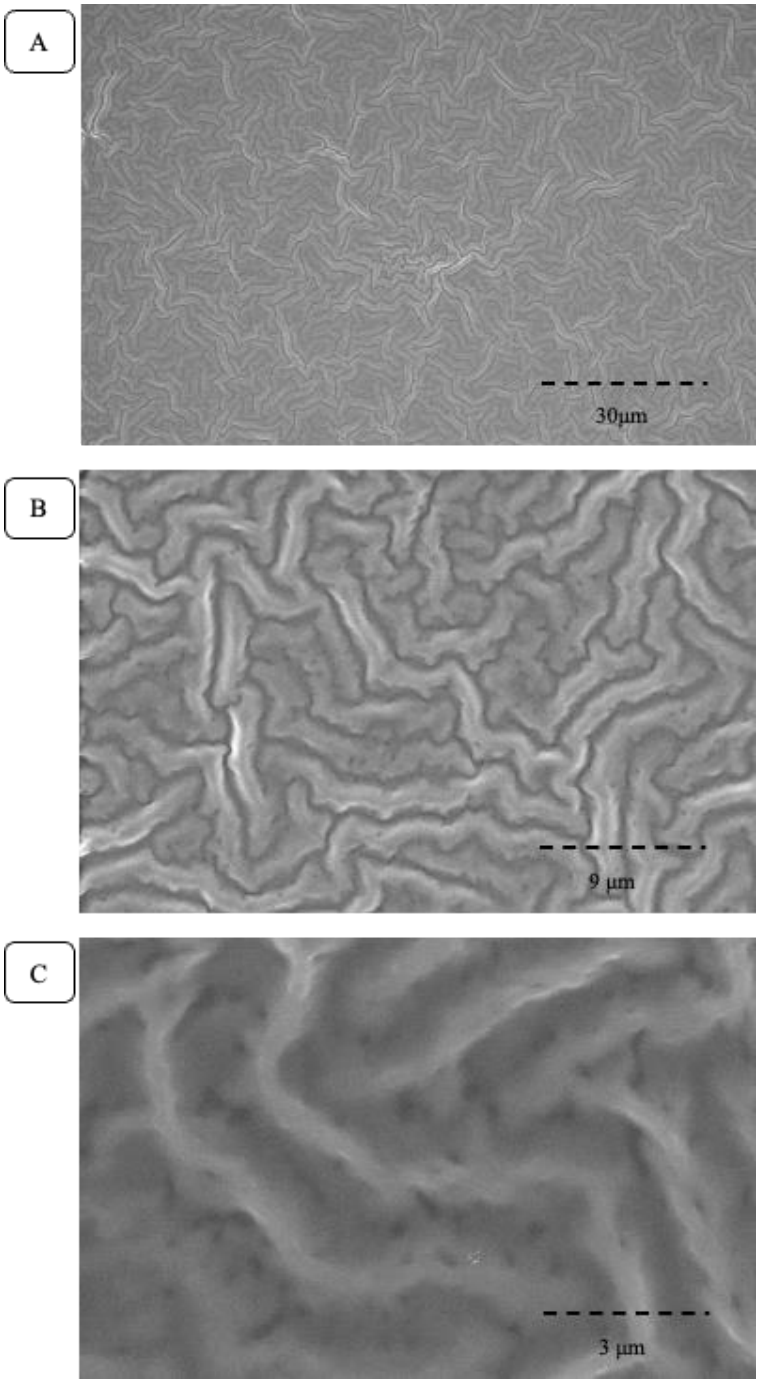

Figure III-S4: Scanning electron micrograph of solvent vapor annealed and cured $PTMC_{100}$-*b*-$PDLLA_{100}$-*b*-$PTMC_{100}$ thin film. The scale bar in the lower right corner is 30 µm for image (A), 9 µm for image (B) and 3 µm for image (C).

References

[1] T. Liu, G. Liu, *Nat. Commun.* **2020**, *11*, 10.

[2] D. A. Olson, L. Chen, M. A. Hillmyer, *Chem. Mater.* **2008**, *20*, 869.

[3] B. Le Droumaguet, R. Poupart, D. Grande, *Polym. Chem.* **2015**, *6*, 8105.

[4] C. G. Gamys, J. M. Schumers, C. Mugemana, C. A. Fustin, J. F. Gohy, *Macromol. Rapid Commun.* **2013**, *34*, 962.

[5] F. S. Bates, G. H. Fredrickson, *Annu. Rev. Phys. Chem.* **1990**, *41*, 525.

[6] Y. Mai, A. Eisenberg, *Chem. Soc. Rev.* **2012**, *41*, 5969.

[7] W. Li, M. Liu, F. Qiu, A. C. Shi, *J. Phys. Chem. B* **2013**, *117*, 5280.

[8] F. S. Bates, G. H. Fredrickson, *Phys. Today* **1999**, *52*, 32.

[9] J. K. Kim, S. Y. Yang, Y. Lee, Y. Kim, *Prog. Polym. Sci.* **2010**, *35*, 1325.

[10] M. A. Hillmyer, *Adv. Polym. Sci.* **2005**, *190*, 137.

[11] J. S. Lee, A. Hirao, S. Nakahama, *Macromolecules* **1988**, *21*, 274.

[12] S. Matsumura, A. R. Hlil, C. Lepiller, J. Gaudet, D. Guay, Z. Shi, S. Holdcroft, A. S. Hay, *J. Polym. Sci. Part A Polym. Chem.* **2008**, *46*, 7207.

[13] T. Thurn-Albrecht, R. Steiner, J. DeRouchey, C. M. Stafford, E. Huang, M. Bal, M. Tuominen, C. J. Hawker, T. P. Russell, *Adv. Mater.* **2000**, *12*, 787.

[14] K. Asakawa, T. Hiraoka, *Japanese J. Appl. Physics, Part 1 Regul. Pap. Short Notes Rev. Pap.* **2002**, *41*, 6112.

[15] A. Malafronte, F. Auriemma, C. Santillo, R. Di Girolamo, R. Barker, Y. Gerelli, C. De Rosa, *Adv. Mater. Interfaces* **2020**, *7*, 1.

[16] C. Wochnowski, M. A. S. Eldin, S. Metev, *Polym. Degrad. Stab.* **2005**, *89*, 252.

[17] S. Rakovsky, G. Zaikov, *J. Appl. Polym. Sci.* **2004**, *91*, 2048.

[18] M. S. She, T. Y. Lo, H. Y. Hsueh, R. M. Ho, *NPG Asia Mater.* **2013**, *5*, e42.

[19] E. A. Jackson, Y. Lee, M. R. Radlauer, M. A. Hillmyer, *ACS Appl. Mater. Interfaces* **2015**, *7*, 27331.

[20] J. Arredondo, L. E. Elizalde, B. Le Droumaguet, D. Grande, *React. Funct. Polym.* **2016**, *104*, 62.

[21] D. Grande, J. Penelle, P. Davidson, I. Beurroies, R. Denoyel, *Microporous Mesoporous Mater.* **2011**, *140*, 34.

[22] J. Zhang, X. Yu, P. Yang, J. Peng, C. Luo, W. Huang, Y. Han, *Macromol. Rapid Commun.* **2010**, *31*, 591.

[23] M. Vayer, M. A. Hillmyer, M. Dirany, G. Thevenin, R. Erre, C. Sinturel, *Thin Solid Films* **2010**, *518*, 3710.

[24] J. Bang, S. H. Kim, E. Drockenmuller, M. J. Misner, T. P. Russell, C. J. Hawker, *J. Am. Chem. Soc.* **2006**, *128*, 7622.

[25] C. Sinturel, M. Vayer, M. Morris, M. A. Hillmyer, *Macromolecules* **2013**, *46*, 5399.

[26] E. Han, K. O. Stuen, M. Leolukman, C. C. Liu, P. F. Nealey, P. Gopalan, *Macromolecules* **2009**, *42*, 4896.

[27] C. Cummins, P. Mokarian-Tabari, P. Andreazza, C. Sinturel, M. A. Morris, *ACS Appl. Mater. Interfaces* **2016**, *8*, 8295.

[28] J. M. Leiston-Belanger, T. P. Russell, E. Drockenmuller, C. J. Hawker, *Macromolecules* **2005**, *38*, 7676.

[29] S. RameshKumar, P. Shaiju, K. E. O'Connor, R. B. P, *Curr. Opin. Green Sustain. Chem.* **2020**, *21*, 75.

[30] B. van Bochove, D. W. Grijpma, *Eur. Polym. J.* **2021**, *143*.

[31] M. A. Przeradzka, B. van Bochove, T. C. Bor, D. W. Grijpma, *Polym. Adv. Technol.* **2017**, *28*, 1212.

[32] S. B. G. Blanquer, S. P. Haimi, A. A. Poot, D. W. Grijpma, *Macromol. Symp.* **2013**, *334*, 75.

[33] Z. Zhang, R. Kuijer, S. K. Bulstra, D. W. Grijpma, J. Feijen, *Biomaterials* **2006**, *27*, 1741.

[34] S. B. G. Blanquer, S. Sharifi, D. W. Grijpma, *J. Appl. Biomater. Funct. Mater.* **2012**, *10*, 177.

[35] K. Fukushima, *Biomater. Sci.* **2016**, *4*, 9.

[36] M. A. Elsawy, K. H. Kim, J. W. Park, A. Deep, *Renew. Sustain. Energy Rev.* **2017**, *79*, 1346.

[37] N. Toshikj, J. J. Robin, S. Blanquer, *Eur. Polym. J.* **2020**, *127*, 109599.

[38] O. Sahin, *Phys. Rev. B - Condens. Matter Mater. Phys.* **2008**, *77*, 1.

[39] O. Sahin, S. Magonov, C. Su, C. F. Quate, O. Solgaard, *Nat. Nanotechnol.* **2007**, *2*, 507.

[40] G. Scott, *Properties of polymers. Their correlation with chemical structure; their numerical estimation and prediction from additive group contributions*, Vol. 16, **1992**.

[41] H. S. Elbro, A. Fredenslund, P. Rasmussen, *Ind. Eng. Chem. Res.* **1991**, *30*, 2576.

[42] M. W. Matsen, F. S. Bates, *Macromolecules* **1996**, *29*, 1091.

[43] X. Deng, Z. Zhu, C. Xiong, L. Zhang, *J. Polym. Sci. Part A Polym. Chem.* **1997**, *35*,

703.

[44] T. O. Ahn, J. H. Kim, H. M. Jeong, S. W. Lee, L. S. Park, *J. Polym. Sci. Part B Polym. Phys.* **1994**, *32*, 21.

[45] I. M. Kalogeras, W. Brostow, *J. Polym. Sci. Part B Polym. Phys.* **2009**, *47*, 80.

[46] L. M. Pitet, A. H. M. Van Loon, E. J. Kramer, C. J. Hawker, E. W. Meijer, *ACS Macro Lett.* **2013**, *2*, 1006.

[47] T. H. Nguyen, M. Vayer, C. Sinturel, *Appl. Surf. Sci.* **2018**, *427*, 464.

[48] U. Maver, T. Velnar, M. Gaberšček, O. Planinšek, M. Finšgar, *TrAC - Trends Anal. Chem.* **2016**, *80*, 96.

[49] H. J. Butt, B. Cappella, M. Kappl, *Surf. Sci. Rep.* **2005**, *59*, 1.

[50] P. Nguyen-Tri, P. Ghassemi, P. Carriere, S. Nanda, A. A. Assadi, D. D. Nguyen, *Polymers (Basel).* **2020**, *12*, 1.

[51] E. Zant, D. W. Grijpma, *Acta Biomater.* **2016**, *31*, 80.

[52] W. A. Phillip, M. A. Hillmyer, E. L. Cussler, *Macromolecules* **2010**, *43*, 7763.

[53] S. H. Kim, M. J. Misner, T. Xu, M. Kimura, T. P. Russell, *Adv. Mater.* **2004**, *16*, 226.

[54] K. A. Cavicchi, T. P. Russell, *Macromolecules* **2007**, *40*, 1181.

[55] A. Baruth, M. Seo, C. H. Lin, K. Walster, A. Shankar, M. A. Hillmyer, C. Leighton, *ACS Appl. Mater. Interfaces* **2014**, *6*, 13770.

[56] J. Kao, J. Tingsanchali, T. Xu, *Macromolecules* **2011**, *44*, 4392.

[57] C. Jin, B. C. Olsen, E. J. Luber, J. M. Buriak, *Chem. Mater.* **2017**, *29*, 176.

[58] M. A. Chavis, D. M. Smilgies, U. B. Wiesner, C. K. Ober, *Adv. Funct. Mater.* **2015**, *25*, 3057.

[59] D. Garlotta, *J. Polym. Environ.* **2019**, *9*, 63.

[60] X. Yu, J. Peng, L. Cui, H. Wang, B. Li, Y. Han, *Macromolecules* **2004**, *37*, 7301.

[61] C. G. Gamys, J. M. Schumers, A. Vlad, C. A. Fustin, J. F. Gohy, *Soft Matter* **2012**, *8*, 4486.

[62] T. Ito, H. Coceancigh, Y. Yi, J. N. Sharma, F. C. Parks, A. H. Flood, *Langmuir* **2020**, *36*, 9259.

[63] R. Olayo-Valles, S. Guo, M. S. Lund, C. Leighton, M. A. Hillmyer, *Macromolecules* **2005**, *38*, 10101.

[64] K. W. Guarini, C. T. Black, S. H. I. Yeung, *Adv. Mater.* **2002**, *14*, 1290.

Annexe Chapitre III

Au cours de ce chapitre, nous avons tenté de figer les structures obtenues à partir de nos copolymères à blocs en fonctionnalisant leurs bouts de chaines par des doubles liaisons méthacrylates avant leur photopolymérisation ultérieure. Cela rajoute une étape supplémentaire qu'il serait idéal de supprimer en utilisant un monomère capable lui-même de photopolymériser (Figure III-B). Notre choix s'est porté vers un monomère cyclique, l'α-angelica lactone (α-AL). Cette lactone conduit à un polyester très peu étudié dans la littérature, mais pour autant présentant des propriétés diverses et remarquables, la poly(α-angelica lactone) (PAL). Il s'agit d'un polyester amorphe et dégradable obtenu par ROP à partir du monomère cyclique α-angelica lactone (α-AL) (Figure III-B).

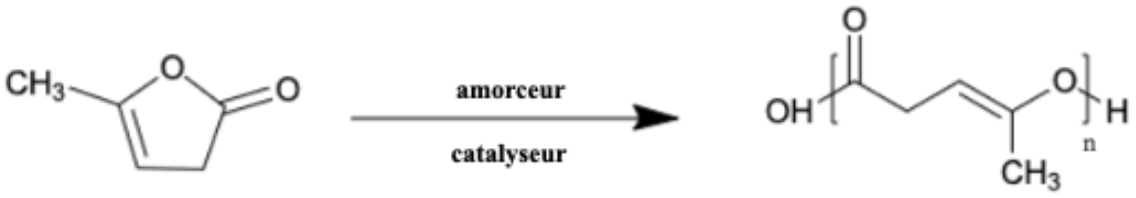

Figure III-B: Les structures chimiques du monomère α-AL et du polymère PAL.

De plus, ce polymère est issu d'une lactone insaturée et biosourcée, possédant une double liaison entre deux atomes de carbone (C=C), ce qui le rend dégradable et/ou adaptée à une modification chimique. Ce polymère PAL devrait être potentiellement photosensible. Il serait intéressant d'étudier sa photoréactivité qui permettrait d'éviter la fonctionnalisation des bouts de chaines des copolymères comme nous l'avons fait jusqu'à maintenant dans ce manuscrit.[1] On photopolymériserait alors le bloc de PAL lui-même et non pas seulement les bouts de chaines des copolymères. Le spectre ^{1}H-NMR du monomère α-AL est présenté en Figure III-C.

Même si les lactones à 5 membres telles que les γ - butyrolactone et γ - valérolactone révèlent des difficultés pour atteindre des polymères de hautes masses molaires par ouverture de cycle (ROP) (dues à leur énergie libre (de Gibbs) de polymérisation positive et leur énergie de contrainte de cycle très faible),[2–4] des études théoriques ont déterminé des conditions thermodynamiques favorables pour la synthèse des PALs.[5]

Il faut noter que de façon très surprenante, la synthèse de ces polymères a été rapportée seulement par deux équipes de recherche jusqu'à maintenant, une utilisant un mélange de butyrate de sodium et hydroxyde de sodium comme système catalytique et l'autre employant un système organométallique ($Sn(Oct)_2$).[2,6]

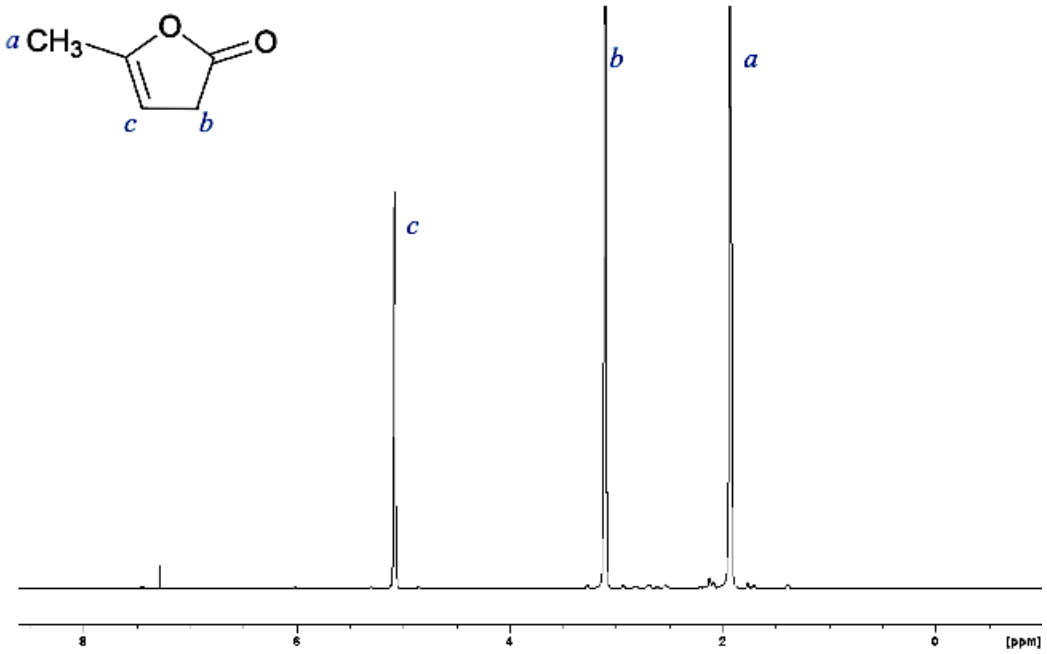

Figure III-C: Spectre ^{1}H-NMR du monomère α-angelica lactone.

Néanmoins, malgré les résultats rapportés par Chen *et al.*, les différents protocoles expérimentaux présentés en Tableau III-A (avec des équivalents identiques de monomère (α-AL) et amorceur (1,6 hexane diol) que ceux décrits en partie 2.2.1 du Chapitre II), n'ont pas abouti à une polymérisation efficace et contrôlée. Parmi les différents systèmes catalytiques testés dans notre étude, le meilleur résultat a été atteint avec l'octanoate d'étain comme catalyseur pour une synthèse en masse pendant 24 h à 130 °C. Ainsi, un polymère précipitable dans l'éther diéthylique a été obtenu mais avec une reproductibilité faible et un rendement limité.

Tableau III-A: Conditions opératoires employées pour la synthèse du PAL.

Système catalytique	**Conditions opératoires et milieu réactionnel**	**Observations**
Sn (Oct)$_2$ (0.05 wt. % / amorceur)	En masse, 130 °C, 24h	Rendement 10 %
	En masse, 130 °C, 48h	*Pas de polymérisation*
	En masse, 130°C, 72h	*Pas de polymérisation*
	En solution (Toluène), 130°C, 24 h	*Pas de polymérisation*
TBD (1.4 equiv.)	*En solution (DCM), RT, 24 h*	*Pas de polymérisation*
	En masse, 130 °C, 24h	*Pas de polymérisation*
MSA (2.5 equiv.)	*En solution (DCM), RT, 24 h*	*Pas de polymérisation*

Le spectre ^{1}H-RMN du polymère PAL obtenu est représenté en Figure III-D. Il parait évident que l'interprétation du spectre est très complexe et traduit la présence d'un polymère de faible masse molaire. L'analyse par la chromatographie d'exclusion stérique présentée en Figure III-E, montre que nous avons obtenu un polymère ayant une masse molaire de 1000 g.mol^{-1} et une dispersité élevée ($Đ$ = 2.4). Il est à noter que dans les études publiées Tarabanko *et al*., des polymères de masses molaires très faibles de l'ordre de 1000 à 2000 g.mol^{-1} ont été également atteintes, ce qui confirme la difficulté de la polymérisation de l'α-AL.[6]

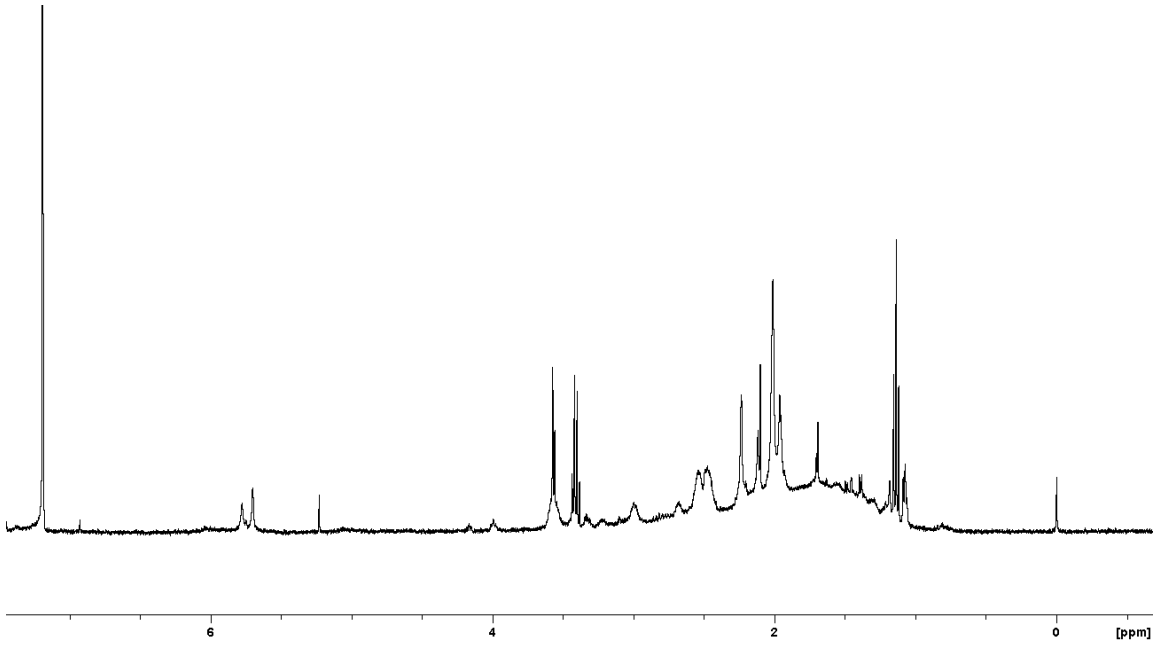

Figure III-D: Spectre ^{1}H-NMR ($CDCl_3$) du PAL obtenu dans le cas de notre étude.

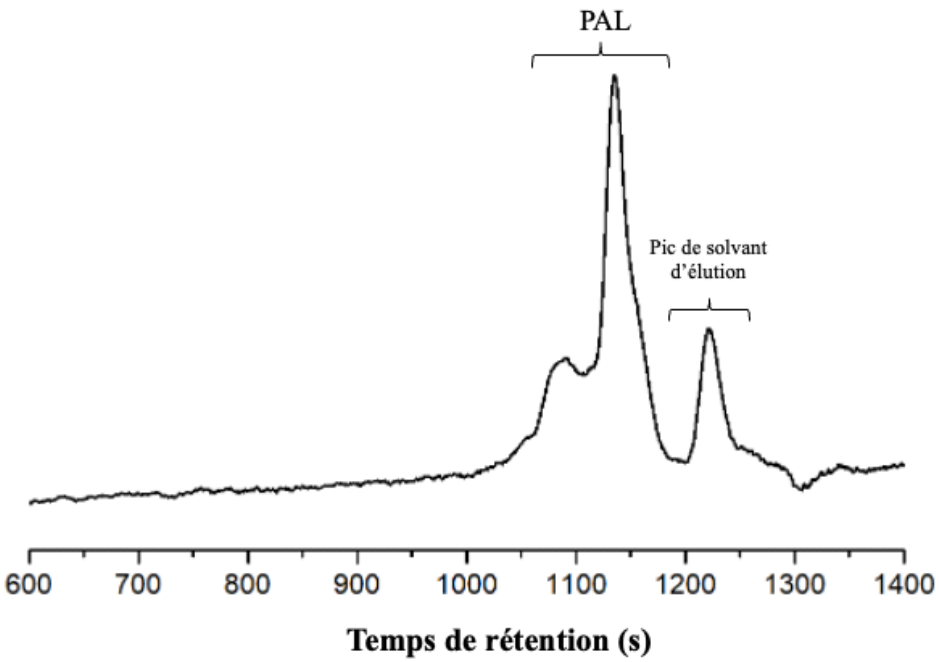

Figure III-E: Chromatogramme d'exclusion stérique du PAL obtenu dans le cas de notre étude.

Pour conclure, cette étude ne nous a pas permis, (faute de temps), d'envisager l'usage de PAL dans nos systèmes copolymères triblocs. Des investigations plus poussées seraient nécessaires de polymériser ce monomère. L'élaboration de polymères PAL de hautes masses molaires et à structure contrôlée reste un défi illustré par les rares rapports scientifiques rapportés sur ce sujet jusqu'à présent.

Références

[1] A. Dell'Acqua, B. M. Stadler, S. Kirchhecker, S. Tin, J. G. De Vries, *Green Chem.* **2020**, *22*, 5267.

[2] T. Chen, Z. Qin, Y. Qi, T. Deng, X. Ge, J. Wang, X. Hou, *Polym. Chem.* **2011**, *2*, 1190.

[3] K. N. Houk, A. Jabbari, H. K. Hall, C. Alemán, *J. Org. Chem.* **2008**, *73*, 2674.

[4] W. Saiyasombat, R. Molloy, T. M. Nicholson, A. F. Johnson, I. M. Ward, S. Poshyachinda, *Polymer (Guildf).* **1998**, *39*, 5581.

[5] K. L. Kaygorodov, V. E. Tarabanko, N. Tarabanko, *Cogent Chem.* **2018**, *4*, 1443689.

[6] V. E. Tarabanko, N. K. L. Kaygorodov, **2010**, *18*, 321.

CHAPTER IV / CHAPITRE IV

Introduction Chapitre IV

Les états solides d'un matériau sont classifiables en fonction de leur organisation à l'échelle atomique et moléculaire. Dans le domaine de la chimie des polymères, la morphologie est un facteur clé pour faire la distinction entre les solides amorphes et cristallins. Ainsi, les premiers démontrent une morphologie des macromolécules avec des enchevêtrements formant des boucles et nœuds, ne présentant pas une organisation particulière ni prévisible. De l'autre côté, les matériaux cristallins possèdent des arrangements moléculaires structurés en motifs répétés dans l'espace et qui adoptent des morphologies particulières aisément caractérisables par les techniques de la cristallographie contemporaine.

La cristallisation des microdomaines de polymères est un phénomène de transition de phase du premier ordre pouvant avoir une implication remarquable sur les propriétés finales et les applications de ces matériaux. En effet, les propriétés mécaniques, optiques, thermiques et chimiques d'un (co)polymère dépendent directement de la présence de cristaux dans leur structure. Ce phénomène se produit lorsque les chaines flexibles d'un polymère se réorganisent et se replient sur elles-mêmes formant ainsi un réseau cristallin. Ce réseau est donc composé par des régions lamellaires ordonnées qui assemblées, forment des structures sphéroïdales à plus large échelle, connues sous le nom de sphérulites (ou sphérolites). Si un polymère cristallise, son degré de cristallinité est toujours inférieur à 100 %. En effet, ce degré de cristallinité qui correspond à la proportion relative de la phase cristalline, est dépendant de l'alignement partiel des chaînes macromoléculaires. En raison de la présence de longues chaînes macromoléculaires, le concept de cristallinité dans les polymères est différent de celui des substances de faible masse molaire. Un alignement parallèle complet n'est pas possible dans le cas des polymères et c'est donc pourquoi les polymères cristallins sont plutôt connus comme étant ''semi-cristallins''. Ainsi, les polymères semi-cristallins, tels que la poly(caprolactone) (PCL) par exemple, sont composés d'un empilement des zones cristallines et des zones amorphes, de l'ordre d'une dizaine de µm (Figure IV-A).

L'épaisseur des lamelles peut varier de quelques nanomètres à quelques dizaines de nanomètres et est directement reliée à la température de fusion du matériau suivant l'équation de Gibbs-Thomson ($\Delta G = \Delta H - T_f \Delta S$). Néanmoins, les différentes possibilités conformationnelles de la phase amorphe présente au sein de cette phase cristalline ont une incidence significative sur la température de fusion de ces matériaux semi-cristallins.

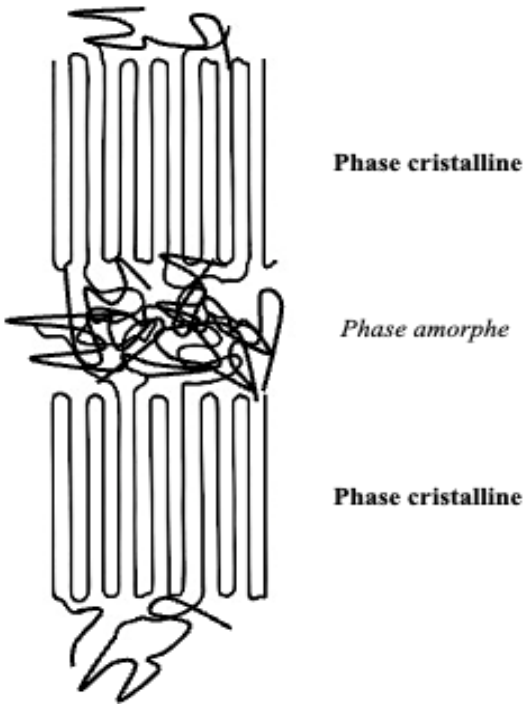

Figure IV-A: Organisation schématique d'un polymère semi-cristallin.

Nous pouvons en conclure que la présence de la phase amorphe a un impact direct sur la cristallinité d'un polymère. Les copolymères à blocs semi-cristallins, où un des blocs est semi-cristallin (A) et l'autre complètement amorphe (B), sont parmi les plus rapportés dans la littérature. Leur morphologie provient donc de la cristallisation du bloc (A) mais aussi de la séparation des phases entre les blocs différents (A et B) à l'état fondu, sous réserve qu'ils présentent un produit de ségrégation χN suffisamment élevé.[1–8]

Contrairement aux homopolymères où la cristallisation a lieu lors d'une conformation étendue ou d'un repliement de chaînes contrôlé cinétiquement, dans le cas des copolymères à blocs, un repliement de chaînes se produit lorsque la structure se trouve dans un état d'équilibre et le nombre de repliements est contrôlé par le bloc amorphe. C'est la raison pour laquelle la morphologie finale après cristallisation dépend du mode de cristallisation : soit à partir de l'état fondu où une séparation de phases est présente, ou bien à partir d'un état fondu homogène ou encore à partir d'une solution. Par conséquent, le comportement des microstructures dans un copolymère à bloc linéaire semi-cristallin dépend de deux mécanismes d'auto-organisation concurrents : la cristallisation et la séparation de phase.

Il existe trois températures de transition distinctes qui simultanément impactent ces deux mécanismes d'auto-organisation : la température de transition de phase du bloc amorphe (Tg), la température de cristallisation du bloc semi-cristallin (Tc) et la température de transition d'ordre-désordre du système (T_{ODT}). Cette dernière correspond à la transformation des blocs fondus homogènes en microphases hétérogènes.

En fonction de ces trois températures, cinq différents scénarii morphologiques sont envisageables pour les copolymères à blocs linéaires semi-cristallins : i) lorsque T_{ODT}>Tc<Tg une cristallisation strictement confinée est présente dans un système fortement ségrégé avec un confinement dur ; ii) pour une condition T_{ODT}>Tc>Tg et un système fortement ségrégé avec un confinement doux, la cristallisation peut être confinée dans des domaines sphériques, cylindriques ou lamellaires ; iii) en cas d'un état fondu homogène (T_{ODT}<Tc>Tg), la séparation de phases est gouvernée par la cristallisation si le point de transition vitreuse du bloc amorphe est inférieur au point de cristallisation du bloc cristallin, conduisant à la coexistence des morphologies lamellaires et des sphérulites selon la composition des blocs; iv) lorsqu'il s'agit d'un système faiblement ségrégé avec un confinement doux (T_{ODT}>Tc>Tg), la cristallisation (sous la forme de sphérullites et lamelles) résulte de l'arrangement morphologique prédominant sur la séparation de phases thermodynamique lors du refroidissement de l'état fondu; et v) dans le cas d'un système faiblement ségrégé avec un confinement dur (T_{ODT}>Tc<Tg), la cristallisation prédomine sur la séparation de phase thermodynamique en raison de la faible ségrégation des blocs.[9,10] Par conséquent, la composition de copolymères à blocs semi-cristallins gouverne les différents phénomènes morphologiques qui l'on peut observer.

Des associations de copolymères à blocs semi-cristallins dégradables sont de plus en plus étudiées ces derniers temps, pouvant ainsi conduire i) aux systèmes avancées pour la délivrance de médicaments (par exemple un système copolymère pentabloc poly(acide lactique)-*b*-poly(caprolactone)-*b*-poly(éthylène glycol)-poly(caprolactone)-*b*-poly(acide lactique)),[11] ii) aux hydrogels thermoréversibles à base de copolymères à blocs en étoile de poly(éthylène glycol)-*b*-poly(acide lactique) liés par une liaison amide (il s'agit d'un stéreocomplexe de (PEG)-NHCO-(PLA) où les liaisons amide utilisées dans ce cas confèrent les propriétés thermoréversibles à l'hydrogél en remplacant les liaisons ester traditionnellement utilisées entre ces deux blocs),[12] ou simplement iii) aux matériaux biosourcés présentant des propriétés mécaniques avancées à base de copolymères multiblocs de poly(butylène succinate)-*b*-poly (butylène sebacate).[13]

Castillo *et al*. ont étudié dans le détail l'architecture des copolymères di- et triblocs de PTMC-PCL et en ont conclu que l'abaissement de la cristallinité globale de ce système est dû à la présence du bloc amorphe de PTMC.[14]

L'association du couple PTMC-PCL est intéressante à étudier en raison de leur paramètre de Flory-Huggins élevé ($\chi_{PTMC\text{-}PCL}$= 0.1)[15] qui est avantageux pour une séparation de phase thermodynamique. Nous avons souhaité étudier dans ce chapitre l'interrelation et l'interdépendance de la cristallinité et de la séparation de phases dans un système de copolymères triblocs de PTMC-PCL par deux moyens. Premièrement, nous avons employé la photoréticulation comme un processus chimique pouvant influencer la cristallinité du système. Par la suite, la cinétique ayant un impact essentiel dans la cristallisation, nous avons exploré une approche de refroidissement rapide de l'état fondu dans le but d'accéder uniquement à une séparation de phases thermodynamique dans ce système.[16]

Dans l'ensemble, cette étude nous a permis d'établir des propriétés originales dans ce copolymère à blocs, ouvrant ainsi son champ d'applications. Les travaux présentés dans ce chapitre IV ont été publiés sous forme d'un article scientifique dans le journal *ACS Applied Polymer Materials* (accepté le 17 septembre 2021).[17]

Références

[1] G. C. Alfonso, T. P. Russell, *Macromolecules* **1986**, *19*, 1143.

[2] T. Shiomi, H. Tsukada, H. Takeshita, K. Takenaka, Y. Tezuka, *Polymer (Guildf).* **2001**, *42*, 4997.

[3] W. N. He, J. T. Xu, *Prog. Polym. Sci.* **2012**, *37*, 1350.

[4] M. Salmerón Sánchez, B. . M. Vincent, G. Vanden Poel, J. L. Gómez-Ribelles, *Macromolecules* **2007**, *40*, 7989.

[5] R. V. Castillo, A. J. Müller, *Prog. Polym. Sci.* **2009**, *34*, 516.

[6] S. Huang, S. Jiang, *RSC Adv.* **2014**, *4*, 24566.

[7] A. Wurm, E. Zhuravlev, K. Eckstein, D. Jehnichen, D. Pospiech, R. Androsch, B. Wunderlich, C. Schick, *Macromolecules* **2012**, *45*, 3816.

[8] E. Zhuravlev, J. W. P. Schmelzer, B. Wunderlich, C. Schick, *Polymer (Guildf).* **2011**, *52*, 1983.

[9] B. Nandan, J. Y. Hsu, H. L. Chen, *Polym. Rev.* **2006**, *46*, 143.

[10] A. J. Müller, V. Balsamo, M. L. Arnal, In *Block Copolymers II* (Ed.: Abetz, V.), Springer Berlin Heidelberg, Berlin, Heidelberg, **2005**, pp. 1–63.

[11] V. Tamboli, G. P. Mishra, A. K. Mitra, *Colloid Polym. Sci.* **2013**, *291*, 1235.

[12] S. J. Buwalda, L. Calucci, C. Forte, P. J. Dijkstra, J. Feijen, *Polymer (Guildf).* **2012**, *53*, 2809.

[13] Y. Shang, Z. Jiang, Z. Qiu, *Polymer (Guildf).* **2021**, *214*, 123248.

[14] R. V. Castillo, G. Fleury, C. Navarro, A. Couffin, D. Bourissou, B. Martín-Vaca, *Eur. Polym. J.* **2017**, *95*, 711.

[15] X. Zhang, X. Peng, S. W. Zhang, In *Science and Principles of Degradable and Bioresorbable Medical Polymers: Materials and Properties*, Elsevier Inc., **2017**, pp. 217–254.

[16] C. E. Carraher Jr., *Introduction to Polymers*, **2020**.

[17] N. Toshikj, J.-J. Robin, M. Ramonda, S. Catrouillet, S. Blanquer, *ACS Appl. Polym. Mater.* **2021**.

Chapter IV

Photocrosslinked poly(trimethylene carbonate)/poly(ε-caprolactone) triblock copolymers with controlled architectures: from phase-separated structures to shape-memory materials

Keywords

Degradable block copolymers, organocatalytic ROP, poly(ε-caprolactone), poly(trimethylene carbonate), self-assembly, crystallization, shape-memory

Abstract

Efficient and rapid organocatalyzed ring opening polymerization (ROP) of trimethylene carbonate (TMC) and epsilon caprolactone (ε-CL) was reported for the synthesis of PTMC-*b*-PCL-*b*-PTMC block copolymers with controlled architectures and desired block proportions. These block copolymers were processed as thin films and the improvement of their stability and mechanical properties was achieved *via* an additional reticulation step of previously chain ends methacrylation. Subsequently, the morphology (phase separation and crystallinity) of these semi-crystalline block copolymers was investigated by differential scanning calorimetry (DSC) and atomic force microscopy (AFM). DSC measurements of such block copolymers with $\chi_{AB}N$ values superior to 20 showed two distinct glass transition temperatures, thus indicating a phase-separated system. As expected, the crystallinity-driven phase-separated morphology predominated as revealed by AFM analysis of the block copolymers. The crosslinking step at the melt state, hence creating a dense polymer network, revealed to not disturb the crystallinity phenomenon. However, melt state crosslinked block copolymer thin films manifested to be sensitive to rapid liquid nitrogen quenching.

Thereby, as evidenced by AFM, under these circumstances, thermodynamically driven phase-separation clearly predominates over the originally crystalline one. The crosslinked thin films remained stable even after 4 months with access to thermodynamical phase-separated morphologies at temperatures below the poly(ε-caprolactone) melting point. Precisely this coexistence of dual crosslinked/crystalline networks in the same copolymer structure allowed to establish, for the first time, the shape-memory properties in such block copolymers, as verified by thermomechanical analysis.

1.Introduction

Degradable and biocompatible polymers are considered as arising materials for potential applications in both industrial and medical eco-friendly fields.[1] Among them, aliphatic polyesters such as poly(ε-caprolactone) (PCL) are particularly studied for drug delivery, tissue engineering or even as packaging alternatives due to their easy processability and overall versatility.[2-4] The widely affordable PCL offer interesting physical properties with low glass transition and melting temperatures (Tg ≈ -60 °C; Tm ≈ 60°C). Nevertheless, the high crystallinity and the moderate mechanical characteristics of PCL homopolymer represent a limiting factor to a broader scope of applications**.** However, the properties of the homopolymer can be modified *via* copolymerization techniques. Accordingly, as a result of the recent advances in ring-opening polymerization (ROP), random, gradient or block copolymers containing PCL blocks have been reported in the literature.[5-7] Thus, various copolymers of PCL with poly(lactide), poly(glycolide) or poly(ethylene glycol) have been developed mainly as systems with lower-tuned degradation rates.[8,9] Furthermore, amorphous poly(trimethylene carbonate) (PTMC) is well-known in both tissue engineering and drug delivery domains due to its soft and elastic properties and harmless degradation products during metabolic processes.[10,11] Therefore, copolymerization of TMC with ε-CL can lead to materials combining both elasticity, softness and bioresorption with a great potential in nerve guide reconstruction and as antithrombotic stents.[12,13]

A commonly used method for the synthesis of triblock copolymers with controlled architectures is based on the preliminary creation of a middle “pre-polymer” block. The latter carries reactive terminal groups being able to initiate the synthesis of the terminal blocks, achievable by either “one-pot” or “two-step” block copolymerizations.

Nevertheless, particular attention needs to be devoted in the choice of appropriate catalytic systems. In practical terms, the ROP of cyclic esters but also cyclic carbonates can be generally ensured *via* cationic, anionic, or coordination-insertion mechanisms. Historically, syntheses of copolymers based on ε-CL with TMC were catalyzed by zinc, tin, bismuth or aluminum *d*-transition metal complexes, as well as rare-earth metals,[14,15] generally leading to high molar mass copolymers. However, such organometallic catalysts show satisfactory reactivity rates only after long periods (≈3 days) while demanding overly elevated reaction temperatures causing potential transesterification reactions.[16] Additionally, good control of the block composition and especially the absence of residual metals in the final polymer is nowadays more and more required, especially when targeting biomedical applications.[17] Hence, the alternative organocatalysis appears as a promising way and shows successful polymerizations.

TMC/ε-CL copolymers are also attractive to be studied in terms of the crystallinity-phase separation interrelationship in consideration of the dissimilar amorphous and semi-crystalline nature of both blocks. In general, the crystallization behavior in single crystalline block copolymers is simpler than the one occurring in double crystalline block copolymers.[18,19] Nevertheless, in both cases, the competition between phase-separation and crystallization phenomena has a direct impact on the microstructure morphology. Phase-separation, due to the thermodynamic incompatibility of both blocks, favors the formation of self-assembled nanodomains. On the other side, a succession of amorphous and crystalline layers is expected upon the predomination of crystallinity. Consequently, the crystallization (T_c) and melting (T_m) temperatures of the crystalline block, as well as the glass transition temperatures (T_g) have a direct impact on the resulting polymer properties. The crystallization phenomenon in PCL homopolymers and in some of the PCL block copolymer systems such as PCL-PEO, PCL-PLLA, PCL-PPDX or PCL-PS-PB has been extensively studied.[20-22] In spite of that, phase-separation and crystallization developments occurring in degradable PTMC-*b*-PCL block copolymers have been poorly investigated. The crystallization can be possibly influenced by the presence, the position and the amount of amorphous PTMC blocks, hence pointing out towards differing organized morphologies.[23] To our knowledge, solely Castillo *et al.* studied the impact of the architecture on the crystallization kinetics in such di- and triblock copolymer systems, thus establishing the deceleration in the spherulitic growth rate induced by the covalently linked amorphous block.[24]

Anteriorly, in a reported study by Nojima *et al*., it was demonstrated that PCL-*b*-PB block copolymers photoscrosslinking permitted the conservation of microphase separated

morphologies.[25] On the contrary, uncrosslinked samples of the same block copolymer undertook morphological changes upon crystallization, leading to alternating structures of amorphous layers and crystalline lamellae. As a matter of fact, this study designates the crosslinking reactions as a method for governing morphological phenomena in block copolymers with crystalline chains. Additionally, it has to be noticed that the combination of double organized systems, displaying crystalline and crosslinked networks, can lead to materials with remarkable properties. Thereby, radiation cured PCL have been reported as one of the first shape-memory materials presenting low recovery temperatures and large recovery deformations.[26-27] Nonetheless, smart materials with shape-memory properties based on PTMC-PCL block copolymers have not been reported till date.

In this work, we report a different organocatalytic pathway for controlled, rapid and metal-free synthesis of PTMC-*b*-PCL-*b*-PTMC. Block copolymers with different molar ratios were chemically characterized *via* NMR spectroscopy, size-exclusion chromatography (SEC) and differential scanning chromatography (DSC) while the phase organization was observed *via* Atomic Force Microscopy (AFM). The chain ends methacrylation was achieved so that the polymers could crosslink under UV-irradiation. Thereupon, the effect of crosslinking as well as the copolymer composition on the crystallinity and phase separation were discussed. Finally, the simultaneous existence of both crosslinked and crystalline networks allowed the conception of a shape-memory polymer (Figure IV-1).

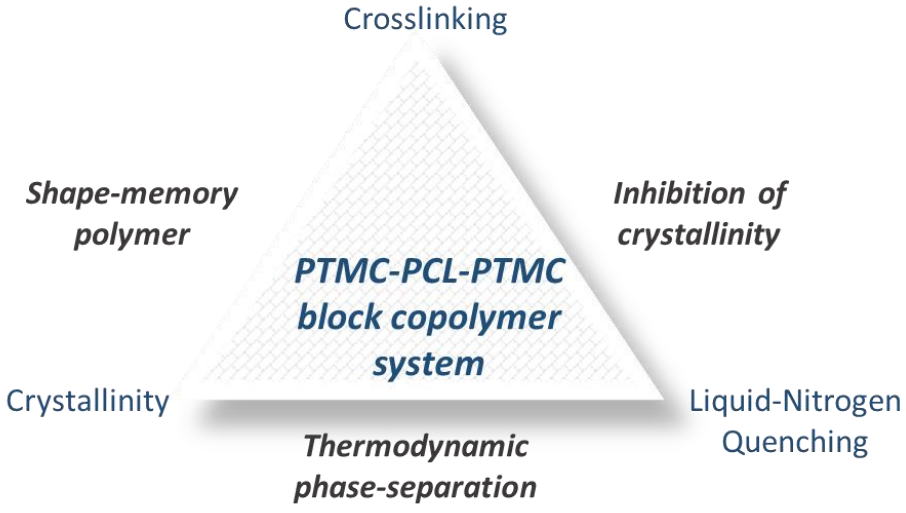

Figure IV-1: Overview of the PTMC-*b*-PCL-*b*-PTMC block copolymer phase-separation and the generated properties.

2. Experimental Section/Methods

Materials and chemicals

ε-caprolactone (ε-CL) was obtained from Santa Cruz Biotechnologies (Germany) and trimethylene carbonate (TMC) monomer was purchased from Foryou Medical (China). The monomers were used as received. The catalysts (1,5,7- triazabicyclo [4.4.0]dec-5-ene (TBD), methanesulfonic acid (MSA), tin(II) 2-ethyl hexanoate ($Sn(oct)_2$), initiator (1,6 hexane diol, 99%), methacrylic anhydride (MMA), triethyl amine (TEA)) were purchased from Sigma Aldrich (France) and used as received. 2-hydroxy-2-methylpropiophenone (Darocur 1173) was provided by BASF Chemicals (Germany). Anhydrous Toluene (99.8%) purchased from Sigma Aldrich (France) and anhydrous dichloromethane retrieved from solvent purificator Inert PureSolv™ (France) were used as polymerization solvents.

General synthetic procedures

All the following syntheses were carried out in two-necked round bottom flasks (250 ml), equipped with a magnetic stirrer and thermometer and previously dried in oven at 130°C for at least 24h. Multiple vacuum and dry argon cycles were performed prior to anhydrous solvent injection and the beginning of the reaction.

PCL homopolymer synthesis by ROP of ε-CL monomer **-** PCL block was synthesized either with $Sn(Oct)_2$ or MSA as catalyst using 1,6 hexanediol as initiator. In case of the first catalytic system, ε-CL monomer (10 g, 87,7 mmol, 100 eq), $Sn(Oct)_2$ (0,01g, 0,0247 mmol, 0.028 eq) and 1,6 hexane diol (0,104 g, 0,877 mmol, 1 eq) were reacted in the bulk at 100°C for 24 h. Otherwise, while using MSA (0,118 g, 1,23 mmol, 1,4 eq) as catalyst and anhydrous toluene (20ml, $[\varepsilon\text{-CL}]_0 = 4{,}4\ mol.l^{-1}$) as solvent, the reaction mixture was stirred at 60 °C for 2h. For the same synthesis at room temperature, anhydrous dichloromethane was used as solvent (70 ml, $[\varepsilon\text{-CL}]_0 = 1{,}25\ mol.l^{-1}$) with a reaction time of 6h. Monomer conversion was evidenced *via* ^{1}H-NMR, and in the case of MSA catalysis, the reaction media was neutralized with 3 times molar excess of triethylamine (TEA). Finally, the polymer was precipitated in cold methanol and dried in vacuum oven for 24 h (97 % yield).

PTMC homopolymer synthesis by ROP of TMC monomer - TMC monomer (10g, 97,2 mmol, 100 eq) was solubilized in anhydrous dichloromethane (70ml, $[TMC]_0$ = 1,4 $mol.l^{-1}$) with the initiator 1,6 hexanediol (0,115 g, 0,972 mmol, 1 eq) and the catalyst TBD (0,189 g, 1,36 mmol, 1,4 eq) afterwards being added to the solution. The reaction mixture was stirred for 1 h at room temperature. After evidencing almost complete monomer conversion, the catalyst was neutralized by three times molar excess of acetic acid. Lastly, the polymer was precipitated in cold methanol and dried in vacuum oven for 24 h (96 % yield).

Standard procedure for one-pot synthesis of PTMC-b-PCL-b-PTMC triblock copolymer - Monitoring the procedure for the MSA-catalysed PCL homopolymer synthesis at room temperature stated above, once the conversion of the previous reaches > 99 %, TBD (2.5 eq to MSA) is added to the reaction media, in order to neutralize the acidic catalyst, thus instantly permitting the TMC polymerization step to carry on. After complete conversion of the TMC monomer under 1.5 hours, the TBD was quenched with a three times molar excess of acetic acid. In the final step, the polymer was slowly precipitated in cold methanol, washed several times with the same solvent and lastly, dried in vacuum oven for 24 h. TMC conversion rate was > 97% and final yield reaction rounding 96%.

Standard procedure for one-pot synthesis of PCL-b-PTMC-b-PCL triblock copolymer - Following the previously reported procedure for PTMC synthesis with rapid TBD catalysis, once the conversion of the latest reaches its maximum, MSA (2.5 eq to TBD) was added to the reaction media in order to quench the basic catalyst. In the round bottom flask additional volume of anhydrous DCM (($[\varepsilon\text{-CL}]_0$ = 1 $mol.l^{-1}$) was added. Lastly, ε-CL monomer (11,08 g, 97,2 mmol, 100 eq) was introduced and the reaction was allowed to continue for 2 h. Finally, MSA was neutralized with 3 times molar excess of TEA, the polymer was concentrated under vacuum, then slowly precipitated and numerous times washed in cold methanol before being dried in vacuum oven for 24 h. ε-CL conversion rate was 95 % with a final reaction yield of 93 %.

Synthesis of PTMC-b-PCL-b-PTMC and PCL-b-PTMC-b-PCL dimethacrylates - Both classes of PTMC-PCL hydroxyl-terminated block copolymers were methacrylated using methacrylic anhydride (MMA) in the presence of triethyl amine (TEA). Firstly, the block copolymers were dissolved in anhydrous dichloromethane ($[triblock\ copolymer]_0$ = 0,2 $g.ml^{-1}$)

in a round bottom flask, then MMA and TEA (with 6 molar equivalents in respect to the polymer) were introduced. The reaction proceeded for 7 days at room temperature in the dark. The dimethacrylated block copolymers were later purified by precipitation in cold methanol, dried in vacuum oven at room temperature for 24h and stored at -18°C until further use.

Blending PTMC and PCL homopolymers

A blend (50/50 wt. %) of the homopolymers was dissolved in small excess of the dichloromethane (good solvent for both polymers) and stirred for 24h. The blend was separated by first evaporation of the solvent, then drying in vacuum oven for 24 h.

Preparation of polymer thin films

Thin polymer films for AFM-analysis were prepared by spin-coating (4000 rpm during 90s) of 10 wt. % polymer solutions in dichloromethane on clean Si-wafer substrates. In the case of photocrosslinked films, prior to spin-coating and UV irradiation, 5 wt. % of Darocur 1173 photoinitiator in respect to the polymer was added to the solution formulation for thin films. Afterwards, the irradiation was performed in a UV Crosslinker Bio-Link chamber (Thermo Fischer, France). The irradiation time was 10 min at 100 $J.cm^{-2}$ using 365 nm wavelength at 10 cm from the surface of the specimens.

Weight fraction degree of crystallinity (Xc)

Degree of crystallinity was deduced from the usual following equation (1).

$$Xc = \frac{\Delta Hf\ (Tm)}{\Delta Hf_m^0(T_m^0)} \quad (1)$$

where $\Delta H_f\,(Tm)$ represents the enthalpy of fusion measured by DSC at the PCL melting point while $\Delta H_f{}^0(Tm^0)$ is the enthalpy of fusion of completely crystalline PCL, with reference value of 135.31 $J.g^{-1}$.[28]

Flory-Huggins interaction parameter

The χ_{AB} value for PTMC/PCL system of 0.1[29] measures the total interaction energy between a pair of PTMC and PCL polymer chains and was defined from the following equation (2):

$$\chi_{AB} = \frac{\nu_{AB}}{RT}(\delta_A - \delta_B)^2 \quad (2)$$

with

- R as the universal gas constant (8.314 $J.mol^{-1}.K^{-1}$),
- T as the absolute temperature
- ν_{AB} is the geometric mean of molar volumes of PTMC and PCL polymers, and
- $(\delta_A - \delta_B)^2$ is the cohesive energy density in $J.cm^{-3}$ from Hildebrand solubility parameters of both polymers (δ_{PTMC} and δ_{PCL}).

The product $\chi_{AB}N$ term values representing the segregation strength of our systems are gathered in the Table IV-S1. The coefficient N represents the number of repeating units of both blocks, whereas in our studies the number of repeating units of the middle block (PTMC or PCL) was fixed to 100.

The volume fraction of PTMC block was deduced from the following equation (3):

$$f_{PTMC} = \frac{(M_{w,PTMC} \times d_{PTMC})}{(M_{w,PTMC} \times d_{PTMC}) + (M_{w,PCL} \times d_{PCL})} \quad (3)$$

where d_{PTMC} = 1.31 $g.cm^{-3}$ and d_{PCL} = 1.14 $g.cm^{-3}$ are the respective densities of PTMC and PCL polymers.

Polymer characterizations

Nuclear Magnetic Resonance Spectrometry (NMR) and Size Exclusion Chromatography (SEC) Analysis were performed as previously described in our previous works and the respective measurements were performed using the apparatus described in the same publication.[34]

DSC analysis and measurements of the thermal conduct of the materials were performed on a Mettler Toledo (Mettler Toledo, France) DSC1 calorimeter where constant calibrations were implemented *via* biphenyl, indium, bismium, zinc and cesium chloride standards. To erase the thermal history of the samples, they were heated between -150 °C and 100 °C on rate of 20 °C/min while using nitrogen as a purge gas. Samples within 10 to 15 mg range of PTMC and PCL homopolymers as well as their corresponding blend and triblock copolymers were subjected to thermal analysis after purification, drying and in some cases crosslinking and speed cooling. All the samples were analyzed in the second scan of DSC thermograms, as the midpoint of transition for the glass transition temperature and at the maximum peak for the fusion and crystalline temperature.

Atomic Force Microscopy (Peak Force Quantitative Nano-Mechanical property mapping (PF-QNM)) - Mechanical characterization was performed with a Multimode AFM instrument (from Bruker Corporation, USA) upgraded with Nanoscope V using PF-QNM imaging mode. Firstly, a Bruker-RTESPA-300-30 probe with a spring constant of the lever of 38.5 N/m and a tip radius of 50 nm was used for samples at Image 1, 2 and 3 and secondly, Bruker-RTESPA-150-30 probe with a spring constant of the lever of 2.18 N/m and a tip radius of 50 nm was used for all the other samples. After an initial step to calibrate sensitivity deflection and sync distance QNM on a sapphire sample from Bruker Instruments, these values were confirmed during measurement on a blend of polymers (PS-LDPE) from Bruker, providing an indentation modulus of around 100 MPa for LDPE phase. The applied maximum load was set at 60 nN for all the measurements with RTESPA-150 tip and the peak force amplitude was set at 60 nm. For measurements with RTESPA-300, the maximum load was set at 25nN, and the peak force amplitude was set at 20 nm. The obtained force versus separation curves were analyzed in real time to obtain different mechanical properties: adhesion force, elastic modulus, deformation, and energy dissipation. The well-known DMT model was used to fit retract curve to calculate indentation modulus (Poisson's coefficient set at 0).[30] These values were then sent to different data channels that are shown as a set of different images simultaneously with the topography image.

Dynamic mechanical analysis (DMA) was carried out using a Metravib DMA 25 with Dynatest 6.8. The cyclic thermo-mechanical tensile tests were performed using 11 × 11 × 1 mm films as follows: the sample was stretched at a temperature of 70 °C to an elongation of 10% (step 1). The stretched sample was kept at this elongation for 10 min, then cooled to 30°C at a cooling rate of 0.3 °C min^{-1} (step 2) and equilibrated at this temperature for 30 min. The sample being in its temporary fixed state, was unloaded to σ = 0 MPa (step 3) and the temperature was raised to 70 °C at a heating rate of 10 °C min-1 (step 4) and held there for 10 min. This program was repeated three times with the same sample (N = 3).

The strain fixity ratio Rf and the strain recovery ratio Rr were calculated from Eqs. (4) and (5), respectively.

$$Rf(N) = \frac{\varepsilon_u(N)}{\varepsilon_m(N)} \tag{4}$$

$$Rr(N) = \frac{\varepsilon_m(N) - \varepsilon_p(N)}{\varepsilon_m(N) - \varepsilon_p(N-1)} \tag{5}$$

where $\varepsilon_m(N)$ is the total deformation in a cyclic thermomechanical experiment in the Nth cycle, $\varepsilon_u(N)$ is the strain in the stress-free state after the retraction of the tensile stress in the Nth cycle, $\varepsilon_p(N-1)$ and $\varepsilon_p(N)$ are the strain of the sample once the sample has fully recovered in two successively passed cycles.

3. Results and discussion

3.1 Block copolymer synthesis and characterization

With regard to advanced organocatalysis, eco-friendly MSA has been notably used for mild and controlled polymerizations of ε-CL, initiated by both primary and secondary alcohols.[31] On the other side, organocatalysis for the ROP of cyclic carbonates has been less explored. In fact, the previously reported sulfonic Brönsted acid catalyst for the ROP of TMC is known to potentially produce troublesome secondary decarboxylation reactions due to the coexistence of activated monomer (AM) and activated chain-end (ACE) mechanisms.[32] However, Couffin *et al.*, while employing MSA organocatalysis, succeeded in achieving PCL-*b*-PTMC-*b*-PCL and PTMC-*b*-PCL-*b*-PTMC triblock copolymers with low polydispersities by a sequential addition of the monomers and catalytic cross-propagation.[33] Interestingly, in our case the optimal copolymerization conditions were obtained by altering the catalytic pathway for the synthesis of the second PTMC block. Accordingly, we investigated a nucleophilic activation of TMC *via* guanidine molecules such as TBD in favor of the synthesis of PTMC-*b*-PCL-*b*-PTMC block copolymers *via* dihydroxylated PCL first route (Figure IV-2).

A successful copolymerization in this case could be carried out by either “two-step” or “one-pot switch catalysis” polymerization. Therefore, in regard to less time-consuming synthetic procedures, we proceeded with the “one-pot switch catalysis” copolymerization. For that purpose, at first, the PCL pre-polymer was synthesized in 6 hours at room temperature by MSA catalysis. The kinetics could be accelerated if needed and the polymerization time reduced to 2 h when polymerizing at 60 °C. Subsequently, TMC copolymerization was initiated by switching to guanidine base TBD catalysis at room temperature. Full conversion was evidenced after 90 minutes by NMR spectroscopy, which is more rapid compared to previously reported MSA copolymerization (PTMC/PCL triblock copolymers of 30 000 $g.mol^{-1}$ required 24 h of synthesis).[33]

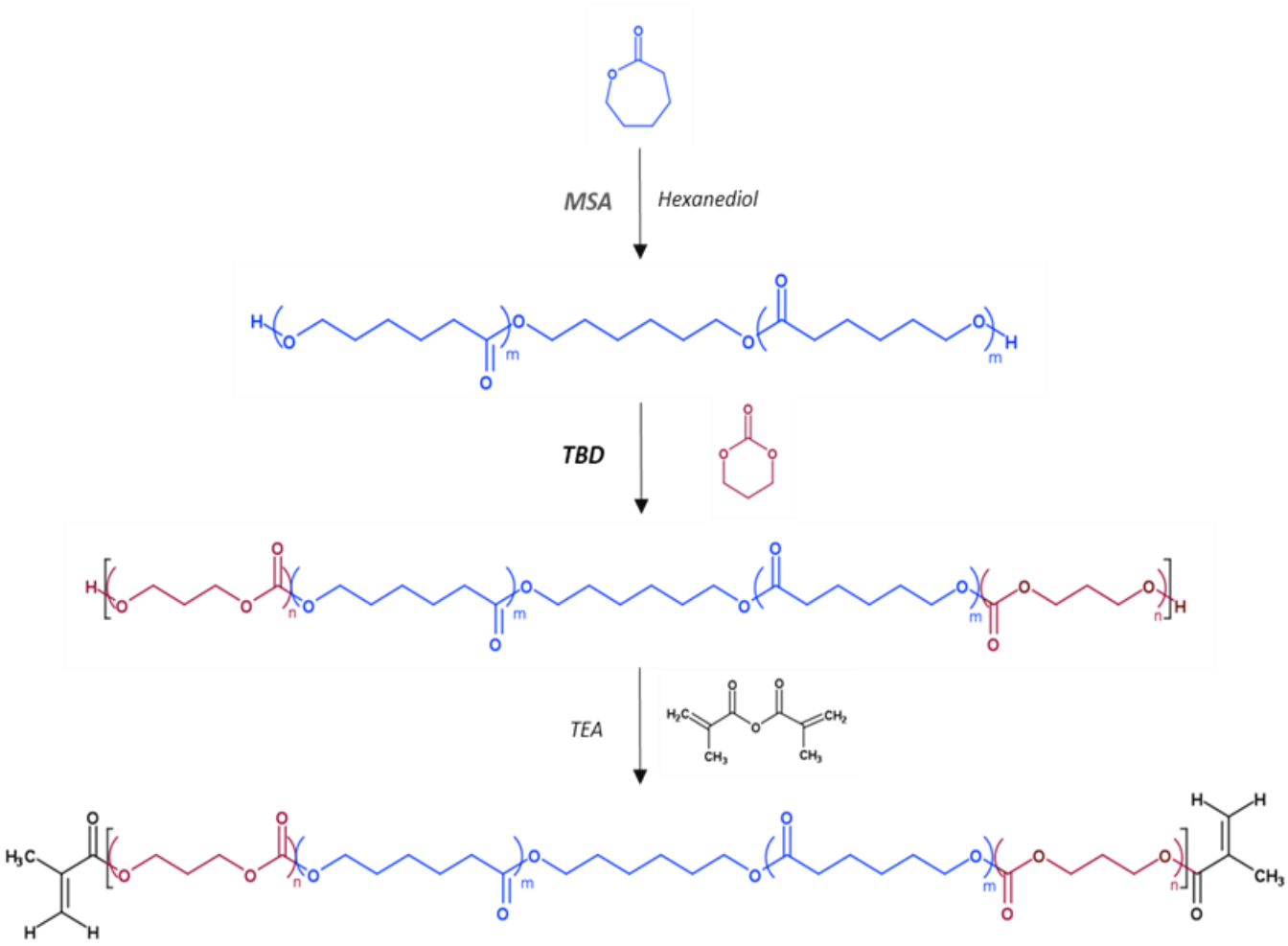

Figure IV-2: Synthesis of PTMC-*b*-PCL-*b*-PTMC block copolymers with PCL first route by nucleophilic TBD activation, and functionalization by methacrylate groups.

The synthesis of block copolymers with different molar ratios was consistent with the established protocols and reaction mechanisms. The efficient formation of pure PTMC-*b*-PCL-*b*-PTMC triblock copolymers with controlled architectures was confirmed by ^{1}H-NMR, 2D DOSY-^{1}H NMR spectroscopy and SEC analyses, as presented in Figure IV-3.

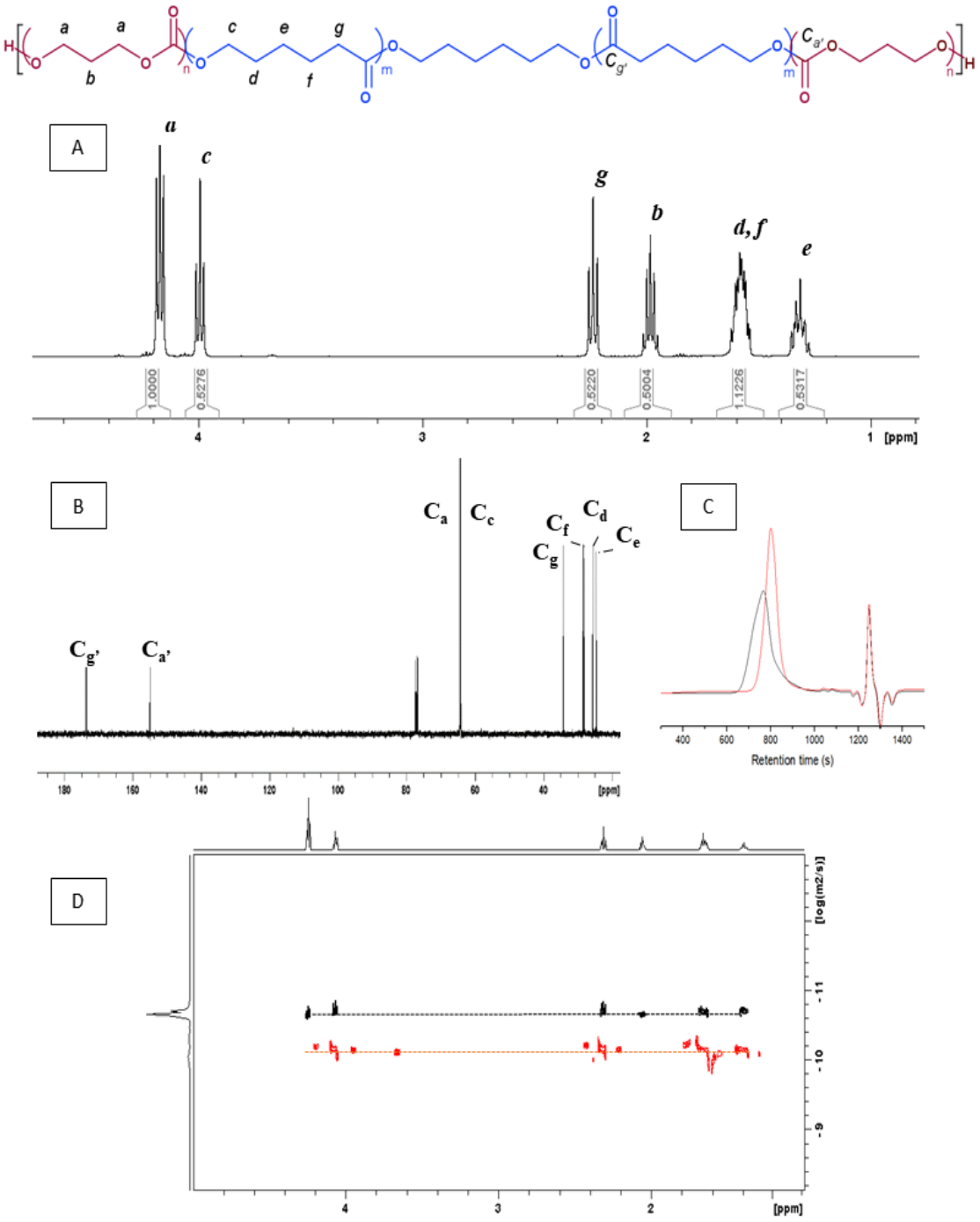

Figure IV-3: Spectroscopy analyses of PTMC-*b*-PCL-*b*-PTMC triblock copolymer synthesized via anionic organocatalysis (TBD).

(A) ^{1}H NMR spectrum in $CDCl_3$ of the copolymer with the assigned signals;

(B) ^{13}C NMR spectrum of the copolymer in $CDCl_3$ with the assigned signals;

(C) SEC chromatograms of PCL macroiniator (in red) and final triblock copolymer (in black);

(D) 2D DOSY-^{1}H NMR spectrum with distinct diffusion coefficients, the peaks of initial PCL homopolymer in red and the peaks of the triblock copolymer after reaction in black.

In the ^{1}H NMR spectrum, the main signals of the PTMC and PCL blocks exhibit relative intensities in close concordance with the targeted molar ratios between the different blocks (PTMC/PCL = 50/50 in Figure IV-3A; PTMC/PCL = 75/25 in Figure IV-S1A and PTMC/PCL = 25/75 for Figure IV-S2A). The composition of the resulting copolymers can be determined by comparing the values of the characteristic signal ratios at 4.24 ppm from PTMC and 4.06 ppm from PCL. Moreover, the unique triplet signal corresponding to the CH_2OH PTMC chain-end was clearly visible at 3.72 ppm. The multiplet signal at 4.15 ppm assigned to CL-TMC and TMC-CL (CH_2O-CO) linkages demonstrated negligible integrations, thus indicating the absence of any secondary transesterification reactions. The latter can be equally evidenced in the ^{13}C NMR spectrum (Figure IV-3B), where the carbonyl signals of the PTMC block (155 ppm) and PCL block (174.5 ppm) remained joined so that no additional peaks implicating transesterification process were present in between**.**

Moreover, SEC analysis demonstrated low dispersities with a monomodal population and an increase of molar mass compared to the initial PCL macroinitiator (Figure IV-3C and Table IV-1). At last, to further assist the previous characterizations, the DOSY-NMR diffusion spectrum (Figure IV-3D) revealed two separate diffusion coefficients between the PCL macroinitiator and the PTMC-*b*-PCL-*b*-PTMC block copolymer, hence confirming the successful copolymerization and TMC block initiation by the PCL unit. The diffusion coefficient of the block copolymer was uniform, thus implicating a precisely controlled triblock copolymer architecture.

Table IV-1: Molar mass and dispersities of the synthesized BCPs measured by SEC.

Block copolymer	**PTMC/PCL molar ratio**	**Mn th. (g.mol^{-1})**	**Mn SEC (g.mol^{-1})**	**Mw SEC (g.mol^{-1})**	***Đ***
$PTMC_{50}$-*b*-PCL_{100}-*b*-$PTMC_{50}$	50/50	21700	31400	37100	1.18
$PTMC_{150}$-*b*-PCL_{100}-*b*-$PTMC_{150}$	75/25	42300	47100	55000	1.17
$PTMC_{17}$-*b*-PCL_{100}-*b*-$PTMC_{17}$	25/75	14500	21000	25600	1.22
PCL_{50}-*b*-$PTMC_{100}$-*b*-PCL_{50}	50/50	21700	26700	35900	1.35

On the other side, PCL-*b*-PTMC-*b*-PCL triblock copolymer starting from dihydroxylated PTMC, could not be synthesized *via* TBD organocatalysis due to the insufficient activity of the ε-CL towards guanidine base (TBD).[34] Thus, the PCL-*b*-PTMC-*b*-PCL block copolymers employed in this study were synthesized *via* "one-pot" MSA organocatalysis.

Ultimately, the triblock copolymers were photocrosslinked for the purpose of investigating the influence of such occurence on the phase organization. In this regard, the block copolymers reported herein were end-functionalized with methacrylate groups, that are able to produce photocrosslinked networks in the presence of photoinitiator and UV light. The high percentage of functionalization (> 85 %) can be verified through the ^{1}H NMR spectrum (Figure IV-S3) of the methacrylated polymers by integration of the *Ha* and *Hb* protons (5.5 and 6.1 ppm) of the characteristic peak of the double bond of the methacrylate units and comparing them with the peaks of the PTMC or PCL blocks.

3.2 Crystallization and phase-separation behavior in PTMC/PCL triblock copolymers, established via DSC and AFM techniques

The thermal properties of the different copolymers were evaluated by DSC and are presented in Table IV-2 and Figure IV-S4.

In the first place, it is widely reported that the melting temperature of the PCL homopolymer increases consistently with its length.[35] In our case, PCL_{100} homopolymer demonstrated proper crystallinity with a melting temperature of 63 °C, a value consistent with those reported in the literature.[36] However, when PCL is blended or copolymerized with PTMC, the melting temperatures decreased between 52 and 57 °C, independently of their molar proportions and block positioning in the copolymer. Such decrease of Tm demonstrates the impact of rubbery PTMC chains on the crystallinity of PCL.[37]

Table IV-2: Thermal properties of the polymers obtained by DSC analyses.

Copolymers	**PTMC/PCL molar ratio**	**Tg (PCL) (°C)**	**Tg (PTMC) (°C)**	**Tc (PCL) (°C)**	**Tm (PCL) (°C)**	**$\|\Delta H_f$ (Tm)$\|$ ($J.g^{-1}$)**	**X_c (%)**
$PTMC_{150}$-*b*-PCL_{100}-*b*-$PTMC_{150}$	75/25	-56	-15	-6	56	21	15
$PTMC_{50}$-*b*-PCL_{100}-*b*-$PTMC_{50}$	50/50	-57	-16	17	57	42	31
$PTMC_{17}$-*b*-PCL_{100}-*b*-$PTMC_{17}$	25/75	-46		21	54	60	45
PCL_{50}-*b*-$PTMC_{100}$-*b*-PCL_{50}	50/50	-57	-11	14	52	31	23
PCL/PTMC Blend	50/50	-58	-15	18	57	46	34
PCL_{50}	-	-57	/	29	63	86	64
$PTMC_{50}$	-	/	-17	/	/	/	/

In the meantime, the degree of crystallinity X_c of the PTMC-*b*-PCL-*b*-PTMC block copolymer was deduced by taking in account the PCL molar ratio therein and found to proportionally increase with the PCL ratio (Table IV-2). As expected, the partial crystallinity rate of the samples increased simultaneously with the crystallization temperature of the triblock copolymers. Interestingly, the partial crystallinity in PCL-*b*-PTMC-*b*-PCL block copolymers was noticeably lower than that in PTMC-*b*-PCL-*b*-PTMC copolymer with the same molar ratio. Such statement can be possibly explained by the confined crystallization of the PCL chains and their hindrance by the bulky $PTMC_{100}$ middle block. In the case of $PTMC_{50}$/PCL_{50} blend sample, we observe that for this well phase separated system, the presence of PTMC hinders the crystallization of the PCL, thus confirming the previous comment.

In regard to the phase-separation properties of the block copolymers, two precisely distinct glass transition temperatures (T_g) corresponding to each block could be observed in the $PTMC_{50}$-*b*-PCL_{100}-*b*-$PTMC_{50}$, PCL_{50}-*b*-$PTMC_{100}$-*b*-PCL_{50} and $PTMC_{150}$-*b*-PCL_{100}-*b*-$PTMC_{150}$ block copolymers. Moreover, in all three cases, both the T_g from the PTMC block and the T_g from the PCL block were narrowly close to the glass transition temperatures of the corresponding homopolymers, signifying a strongly segregated system. As a matter of fact, this argument is in accordance with the Flory-Huggins phase-separation theory, where the $\chi_{AB}N$ value (eq. (2), Table IV-S1) for the block copolymers reported above is largely superior to the outlined limit for phase-segregation of 10.5.[38] However, the $PTMC_{17}$-*b*-PCL_{100}-*b*-$PTMC_{17}$,

having its $\chi_{AB}N$ value close to 10, demonstrated a single glass transition temperature of -45.7 °C, situated between those of the two homopolymers and undeniably close to the predicted value of -47°C by the Fox equation for miscible systems.[24] This single T_g signifies that partial miscibility is observed in the case of short PTMC blocks.

Therefore, we firstly validated mean-field theory requirements for thermodynamical phase-separation in symmetric block copolymers systems (eq. (3)). In a second step, we were interested in exploring such phase-separated morphologies, where crystalline phase-separation is conventionally known to predominate. Morphology studies on phase organization of PTMC-PCL copolymers have been poorly reported in the literature thus far.[24] As a matter of fact, phase-separated structures of this block copolymer have never been thoroughly investigated by AFM studies. Thus, thin films obtained by the spin-coating technique with different conditions of assembly were analyzed with the assumption of visualizing a thermodynamically driven phase-separation morphology, as suggested by DSC.

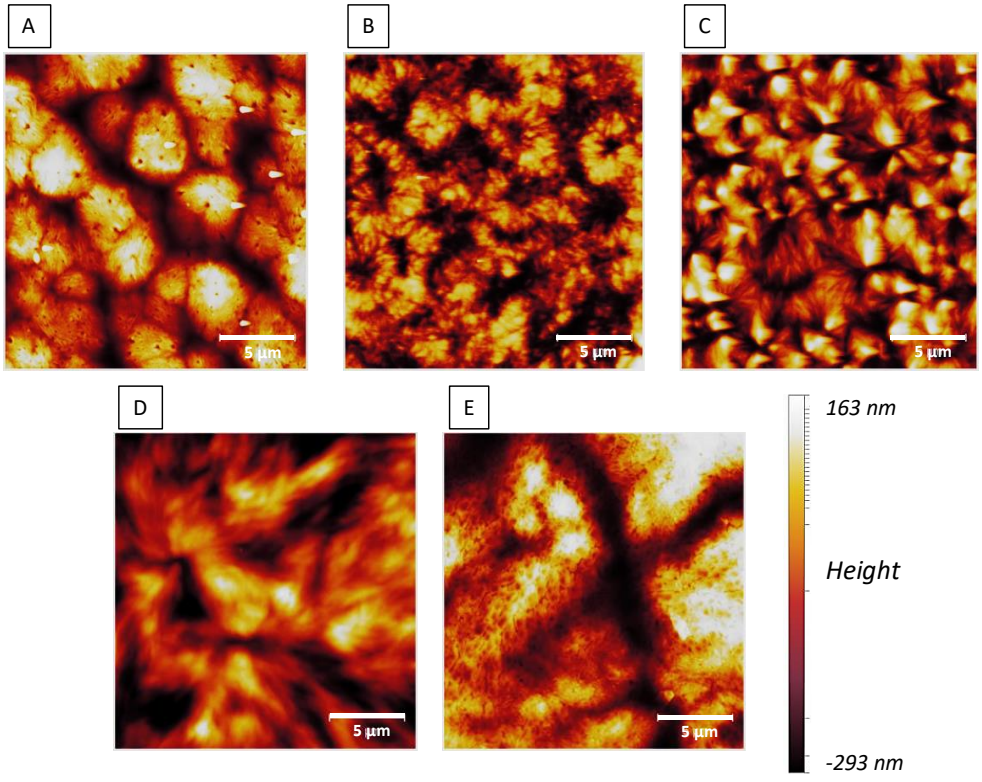

Figure IV-4: AFM height images (20x20 µm) from spin-coated DCM solution thin films. PTMC/PCL blend (A), $PTMC_{50}$-*b*-PCL_{100}-*b*-$PTMC_{50}$ block copolymer (B), UV-crosslinked $PTMC_{50}$-*b*-PCL_{100}-*b*-$PTMC_{50}$ block copolymer (C), thermally annealed and crosslinked $PTMC_{50}$-*b*-PCL_{100}-*b*-$PTMC_{50}$ block copolymer thin-film (D) and thermally annealed and crosslinked PCL_{50}-*b*-$PTMC_{100}$-*b*-PCL_{50} block copolymer thin film (E).

AFM images of $PTMC_{50}$-*b*-PCL_{100}-*b*-$PTMC_{50}$ block copolymer thin films compared with thin films of a blend of same molar proportions are presented in Figure IV-4A and IV-4B. Herein, even though differences in size of spherulites are visible between the two images, spherulitic morphologies characteristic to crystalline PCL systems are present in both cases. Subsequently, we attempted room temperature photocrosslinking of the chain end modified copolymers, thus creating a physically linked polymeric network as a way to disturb the crystallinity of the system (Figure IV-4C). If eventually photocrosslinking enabled to quench the system, thus inhibit the crystallization, we could expect to observe a thermodynamical phase-separated system. Nevertheless, same result with predominant spherulitic crystalline networks was obtained as in uncrosslinked block copolymer thin films. The spherulitic domains were noticeably more discernible in the blend compared to the photocrosslinked copolymer, signifying a stronger and more liberate crystallization in thin films of such system.

SAXS literature data reported crystalline lamellar phase-separated structures upon melt state quenching of PTMC-PCL copolymers.[24] Subsequently, we attempted photocrosslinking of the thin films directly in their melted state, in order to investigate if the dense polymer network could prevent the reappearing of a crystallization driven phase-separation once the sample is cooled down. For that purpose, methacrylated $PTMC_{50}$-*b*-PCL_{100}-*b*-$PTMC_{50}$ block copolymer thin films were previously thermally annealed at 80 °C (T > Tm (PCL)) and photocrosslinked at the same temperature. In fact, crosslinking is usually known to alter the semi-crystalline nature of a polymer towards an amorphous one.[39,40] Unexpectedly, despite thermal annealing and photocrosslinking at the melted state, the material retrieved its crystalline state upon cooling down, as it can be visualized in Figure IV-4D.

Undeniably, the crosslinked PTMC network in $PTMC_{50}$-*b*-PCL_{100}-*b*-$PTMC_{50}$ system was insufficient to disrupt the crystallinity state of the PCL blocks. Thereafter, we attempted photocrosslinking of the PCL phase in PCL_{50}-*b*-$PTMC_{100}$-*b*-PCL_{50} block copolymers to observe if in such case, where PCL is the side block, an impact on the crystallinity could be noticed. Nevertheless, as it can be evidenced on the image in Figure IV-4E, even though the spherulitic behavior was much less apparent on the photocrosslinked PCL terminal blocks, thermodynamical phase separation did not occur. Identical observations could be noted down for $PTMC_{150}$-*b*-PCL_{100}-*b*-$PTMC_{150,}$ a copolymer with lower molar ratio of the crystalline block (Figure IV-S5). Thus, even within lower volume fractions, the crystallization driven self-assembly persisted.

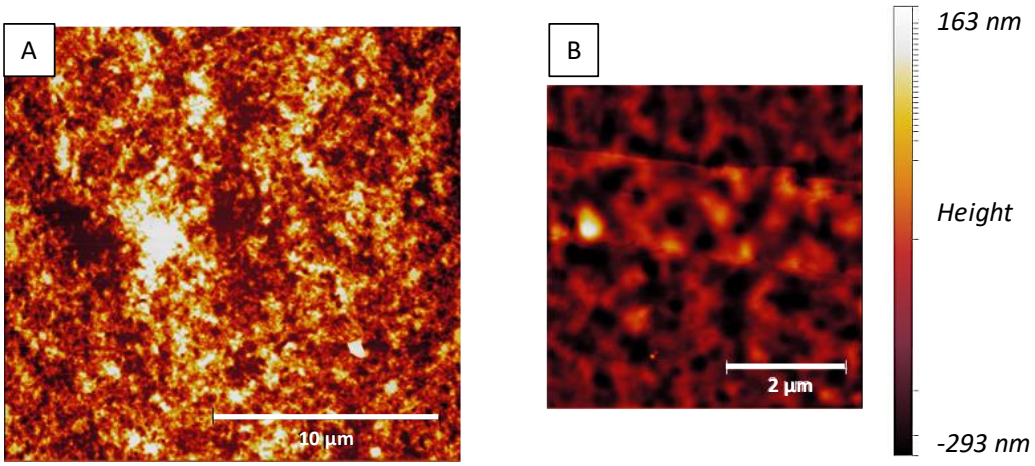

Figure IV-5: AFM height images of liquid nitrogen (LN2) quenched, uncrosslinked $PTMC_{50}$-*b*-PCL_{100}-*b*-$PTMC_{50}$ BCP thin film (20x20 µm) (A); and crosslinked $PTMC_{50}$-*b*-PCL_{100}-*b*-$PTMC_{50}$ BCP thin film (5x5 µm) (B).

Following the objective to investigate the effect of the semi-crystalline blocks on the final organization in respect to processing, we attempted freezing of the morphology directly from the melted state by rapid liquid nitrogen quenching. Once immersed therein for a couple of seconds, the melted photocrosslinked $PTMC_{50}$-*b*-PCL_{100}-*b*-$PTMC_{50}$ block copolymer structure loosens its crystalline behavior. Hence in Figure IV-5B, we can assist to a thermodynamically driven phase-separation, with the complete absence of spherulitic crystallites. However, the same result was obtained for uncrosslinked quenched block copolymer, with slightly less defined thermodynamical phase-separation (Figure IV-5A). Likewise, liquid nitrogen quenching enabled access to thermodynamically driven phase separation in the other crosslinked block copolymer system $PTMC_{150}$-*b*-PCL_{100}-*b*-$PTMC_{150}$ (Figure IV-S6). However, in the case of $PTMC_{17}$-*b*-PCL_{100}-*b*-$PTMC_{17}$, with a limiting value of $\chi_{AB}N$, no phase separation is expected as also evidenced in the DSC with a single glass transition temperature.

Interestingly, random "worm-like" morphologies could be observed in each case of a thermodynamically phase-separated system, independently on the block emplacement or their volume fractions. Therefore, this study could possibly represent the starting point for further investigations in thermodynamically phase-separated PTMC-PCL block copolymer associations. In addition, the crosslinked and quenched block copolymer thin films retained their thermodynamical phase-separated structures even after 16 weeks storage at room temperature (Figure IV-S7). Analogous image as that in the initial state could be observed,

thus indicating a stability in time of such systems. On the contrary, uncrosslinked LN_2 quenched thin films started recovering their crystalline state after 4 weeks (Figure IV-S8). However, once the crosslinked and quenched system was submitted to temperatures higher than the PCL melting point, the crystallization took over once again (Figure IV-S9). Therefore, to preserve a phase-separated system due to the thermodynamical incompatibility between the blocks, the block copolymer melt state needs to be quenched in liquid nitrogen, further photocrosslinked and preserved under 45 °C, which represents the beginning of the melting of the PCL blocks according to the DSC thermogram.

The thermal properties of the photocrosslinked and liquid nitrogen quenched thin-films of PCL_{50}-*b*-$PTMC_{100}$-*b*-PCL_{50} and $PTMC_{50}$-*b*-PCL_{100}-*b*-$PTMC_{50}$ block copolymers were measured by DSC in order to analyze if these thermal treatments disrupted the physical properties of the materials (Table IV-3).
The DSC measurements in Table IV-3 allow to conclude that neither the crosslinking nor the liquid-nitrogen quenching disturbs the crystalline network. Actually, both crosslinked and crystalline networks were maintained in the block copolymers independently on the emplacement of each block in the chains. The preservation of a crystalline network within a crosslinked system led us to the investigation of the shape-memory properties in these PTMC-PCL triblock copolymers.

Table IV-3: Thermal properties of crosslinked copolymer thin films measured by DSC with a cooling rate of 20 °C/min (* after crosslinking; ** after crosslinking and LN_2 quenching).

Block copolymer thin film	**Tg (PCL) (°C)**	**Tg (PTMC) (°C)**	**Tc (PCL) (°C)**	**Tm (PCL) (°C)**	**$\lvert\Delta H_f\,(Tm)\rvert$ ($J.g^{-1}$)**	**X_c (%)**
$PTMC_{50}$-*b*-PCL_{100}-*b*-$PTMC_{50}$ *	-55.4	-13.2	10	59	40	30
$PTMC_{50}$-*b*-PCL_{100}-*b*-$PTMC_{50}$ **	-55.4	-13.2	6	63	42	31
PCL_{50}-*b*-$PTMC_{100}$-*b*-PCL_{50} *	-55	-13.6	12.9	51	30	22
PCL_{50}-*b*-$PTMC_{100}$-*b*-PCL_{50} **	-56	-17	13.5	51	30	22

3.3 Shape Memory Material and Mechanical Properties

Polymers with shape memory properties feature the ability to return from a deformed state (temporary shape) to their original (permanent) shape through an external stimulation.[41] In the case of thermoresponsive polymers, the shape recovery is triggered by an external temperature stimulus. Shape memory polymer (SMP) is traditionally constituted of both i/ crosslinked networks that stabilize the permanent shape and ii/ semi-crosslinked phases, which are sensitive to temperature and represent the so-called switching segments.

It is recognized that photo-crosslinking has been more and more implemented as a tool for designing SMP.[42,43] On the other hand, PTMC photo-crosslinking can result in flexible and tough form-stable networks with superior elastomeric properties.[44] In addition, degradable SMP responding to temperatures as external stimuli are of great interest, particularly when the response temperature is low enough to be used in daily life applications such as biological or medical domains.[45] Therefore, to this extent segmented copolymers such as PTMC-PLLA or PCL-PLLA have been studied as shape memory materials.[46-49] However, smart SMPs based on degradable block copolymer are not common, and SMP based on specifically photo-crosslinked PTMC-PCL triblock copolymers have never been formerly reported. Therefore, in this study, as a result of the control on the crystallization that we previously demonstrated, we examined the shape-memory behavior in both PCL-*b*-PTMC-*b*-PCL and PTMC-*b*-PCL-*b*-PTMC block copolymers. As presented in Figure IV-6D, the shape memory effect was successfully evidenced on a cured PTMC-*b*-PCL-*b*-PTMC film. The temporary shape was achieved by cooling the polymer which has been initially deformed above the transition temperature. Shape recovery occurred within 5 seconds once the film was placed above the transition temperature which corresponds to the melting point of the sample (60 °C).

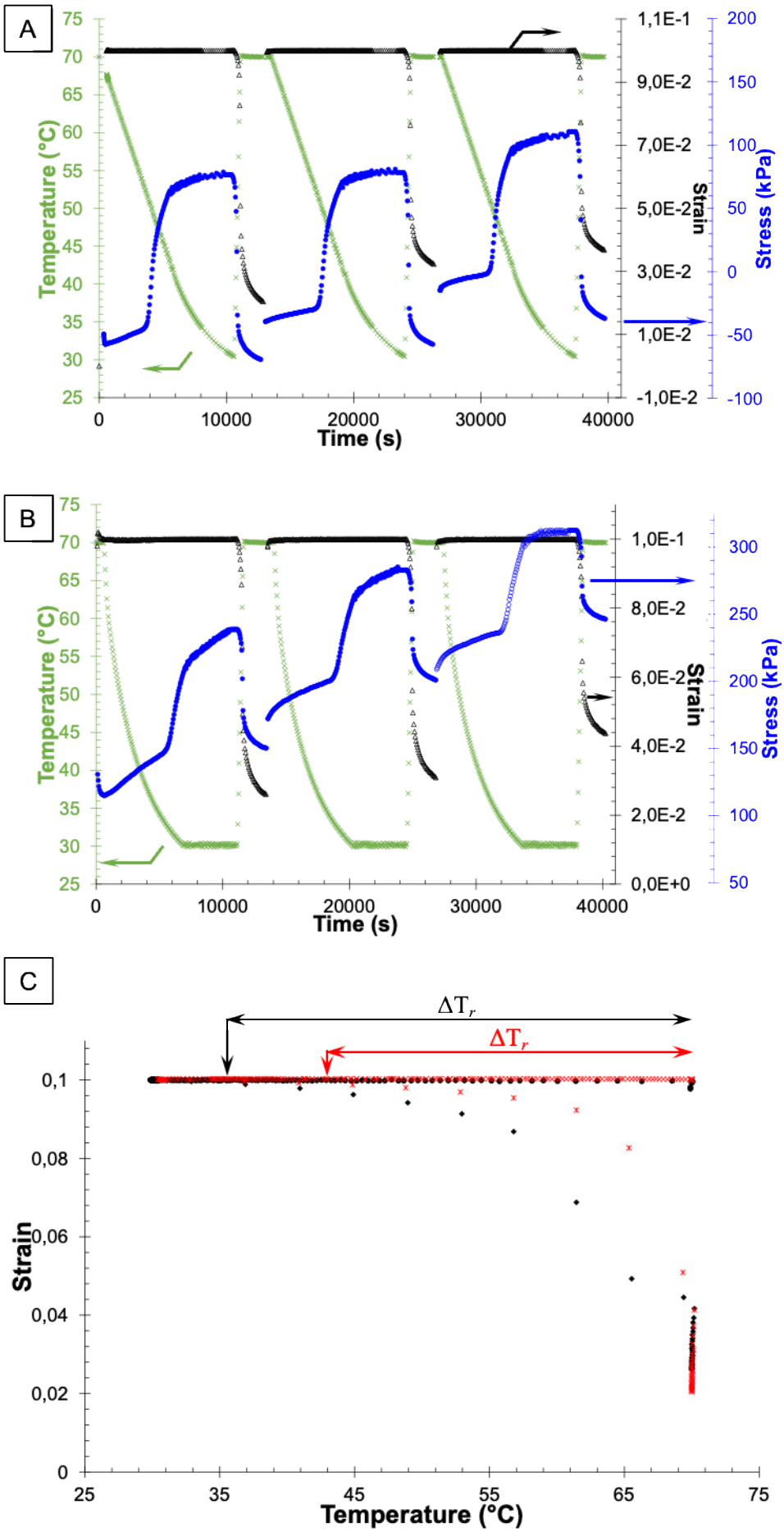
A
Temperature (°C)
Strain
Stress (kPa)
Time (s)
B
Temperature (°C)
Strain
Stress (kPa)
Time (s)
C
ΔT_r
ΔT_r
Strain
Temperature (°C)

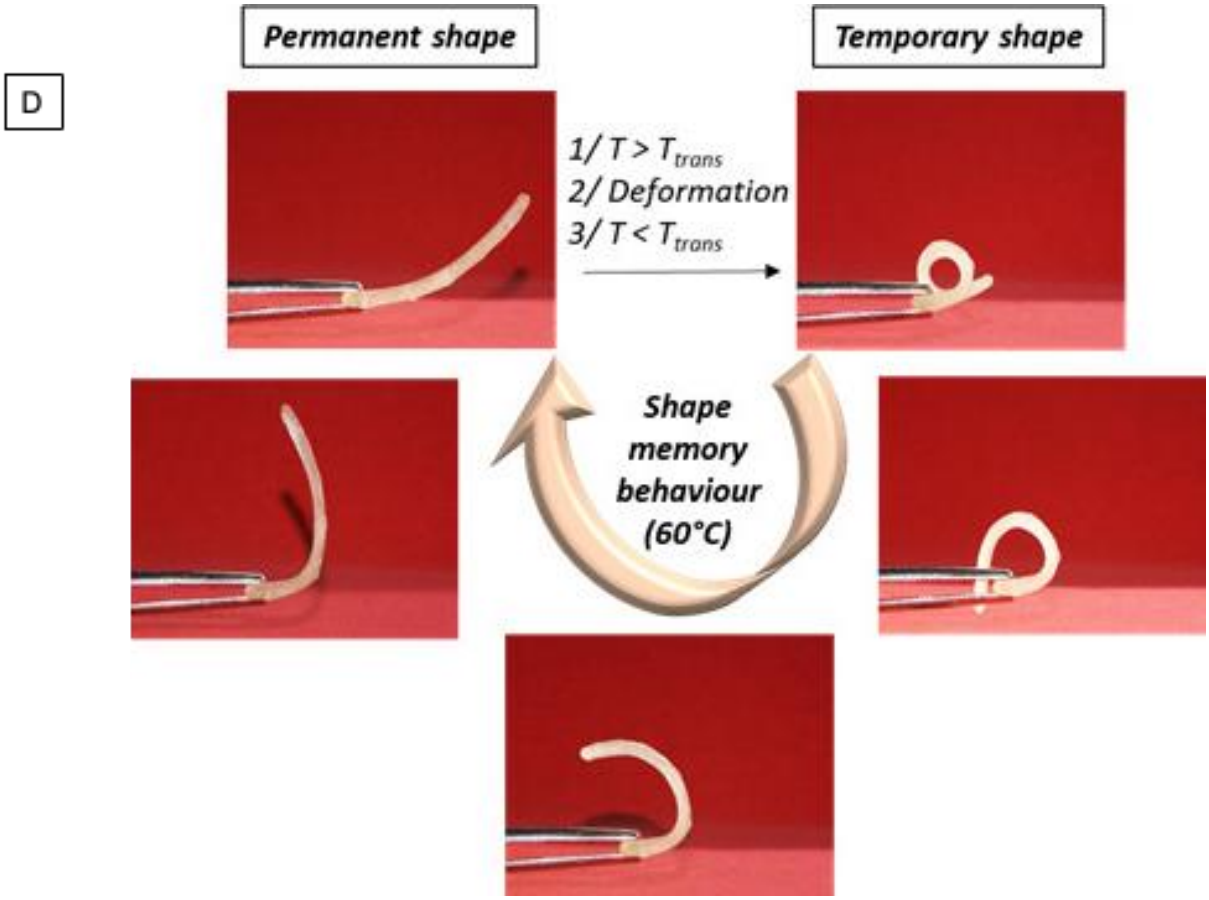

Figure IV-6: Thermo-mechanical shape-memory cycle of PCL_{50}-*b*-$PTMC_{100}$-*b*-PCL_{50} (A) and $PTMC_{50}$-*b*-PCL_{100}-*b*-$PTMC_{50}$ (B) polymer network. It is represented that in both cases, upon elongating the network to 10% at 70 °C, followed by cooling down to 30 °C at constant strain, succeeded by a release of the applied stress, the specimen can recover to its original dimensions by heating up to 70 °C. In (C) the specimen elongation is plotted as a function of temperature. Herein, the onset temperature of recovery (T_s, vertical arrows (C), the temperature at which the network segments start to relax and a contraction of the sample can be observed) and the shape transition temperature range (ΔT_r) are indicated. Shape memory effect on $PTMC_{50}$-*b*-PCL_{100}-*b*-$PTMC_{50}$ film (D), with shape recovery in 5 seconds at 60°C (just above the beginning of the melting state).

The shape-memory properties of the polymer networks were quantified by cyclic, thermomechanical tensile experiments (Figure IV-6A, IV-6B, IV-6C).[50] The strain recovery rate R_f and the strain recovery rate R_r were calculated. R_f describes the ability to fix the mechanical deformation, which has been applied during the programming process, and can be calculated by the amplitude ratio of the fixed deformation ε_u to the total deformation ε_m. The shape-recovery ratio R_r quantifies at what extent the shape recovers in the N_{th} cycle (for N > 1) with respect to the recovered shape of the previous $(N-1)_{th}$ cycle. R_f of all prepared samples were higher than 99% for all cycles whereas R_r were higher than 70% (Table IV-5). The shape-memory T_r (°C) properties varied slightly between the first and the second cycle because of the long holding time due to the slow cooling of the apparatus which generate segment-chain orientation and relaxation effects.[50] After the second cycle, R_f and R_r reached almost constant values. Zhu *et al.* proved a strong influence of the crosslink density on the recovery of γ-radiation crosslinked PCL.[51] Our systems are limited to two netpoints per polymer chains, which explains the limited R_r.

It was found that the transition temperature of the specimens was around 41 °C for PCL-*b*-PTMC-*b*-PCL and 49 °C for PTMC-*b*-PCL-*b*-PTMC. It closely related to the starting point of the melting temperature and agreed with the DSC scanning results.

Table IV-5: Shape-memory properties of PCL_{50}-*b*-$PTMC_{100}$-*b*-PCL_{50} and $PTMC_{50}$-*b*-PCL_{100}-*b*-$PTMC_{50}$ networks measured by cyclic thermo-mechanical analyses. The polymer networks were deformed at 70°C and the shape was fixed at 30°C. The shape-fixity ratio (R_f) and the shape recovery ratio (R_r) were assessed at 30°C and 70°C respectively. The onset temperature of recovery (T_s) and the temperature range of the shape-recovery transition (ΔT_r) are indicated in Figure IV-6.

Networks	**R_f (%)**	**R_r (%)**	**T_s (°C)**	**ΔT_r (°C)**
PCL_{50}-*b*-$PTMC_{100}$-*b*-PCL_{50}	99.97	85.5 ± 7	41	29
$PTMC_{50}$-*b*-PCL_{100}-*b*-$PTMC_{50}$	99.96	82.65 ± 10	49	21

4.Conclusion

To begin with, effective synthesis of PTMC-*b*-PCL-*b*-PTMC block copolymers was achieved *via* guanidine base (TBD) organocatalysis. Controlled copolymer architecture and desired block proportions were verified through NMR and SEC characterizations. Besides, end-functionalization with photosensitive methacrylate groups of the block copolymers enabled ameliorated properties when crosslinking the thin-films. Pioneering AFM investigations on thin films of PTMC-PCL block copolymers allowed access to the visualization of thermodynamical phase-separation in the semi-crystalline system. Liquid nitrogen quenching directly from melted state enabled suppression of the crystallinity while photo-crosslinking lead to preservation of the phase-separated morphology and stability in long term. Hence, on the account of deeper investigations in the morphology phenomena present in PTMC-PCL photocrosslinked block copolymers, we were able to establish the simultaneous existence of dual crosslinked/crystalline network. Accordingly, for the first time, a PTMC-PCL block copolymer shape-memory material was affirmed and characterized with mechanical properties by using the DMA technique. Furthermore, the transition temperature to the permanent shape being the PCL melting point, the shape memory properties can be customized by varying the PTMC and PCL block emplacement, as the latter proved to have direct impact on the melting transition temperature (T_m). To conclude, these shape-memory materials can potentially be contributing to advanced medical applications, such as a degradable cardiovascular stent, taking into account their opportune physical and reported biocompatible properties.

Supporting Information

Photocrosslinked poly(trimethylene carbonate)/poly(ε-caprolactone) triblock copolymers with controlled architectures: from phase-separated structures to shape-memory materials

Table IV-S1: $\chi_{AB}N$ values for PTMC/PCL block copolymers as a function of the respective molar ratio and volume fractions.

Block copolymer	**PTMC/PCL molar ratio**	**PTMC/PCL volume fractions**	**$\chi_{AB}N$ value**
$PTMC_{50}$-*b*-PCL_{100}-*b*-$PTMC_{50}$	50/50	0.51/0.49	20
PCL_{50}-*b*-$PTMC_{100}$-*b*-PCL_{50}	50/50	0.51/0.49	20
$PTMC_{17}$-*b*-PCL_{100}-*b*-$PTMC_{17}$	25/75	0.26/0.74	13.4
$PTMC_{150}$-*b*-PCL_{100}-*b*-$PTMC_{150}$	75/25	0.76/0.24	40

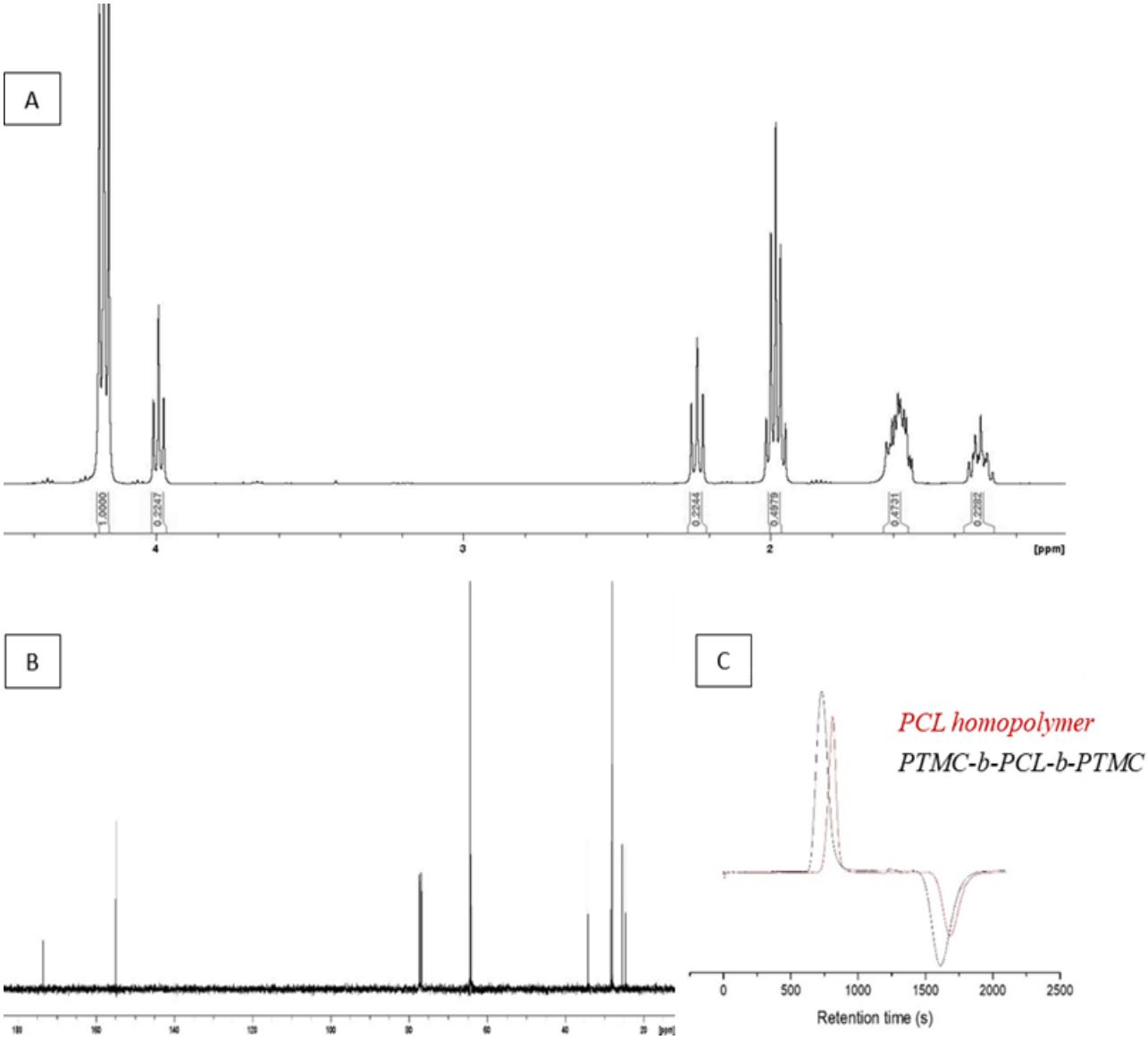

Figure IV-S1: (A) NMR ^{1}H, (B) NMR ^{13}C spectra and (C) SEC chromatogram of PTMC-*b*-PCL-*b*-PTMC triblock copolymer with PTMC/PCL (75/25) molar proportions.

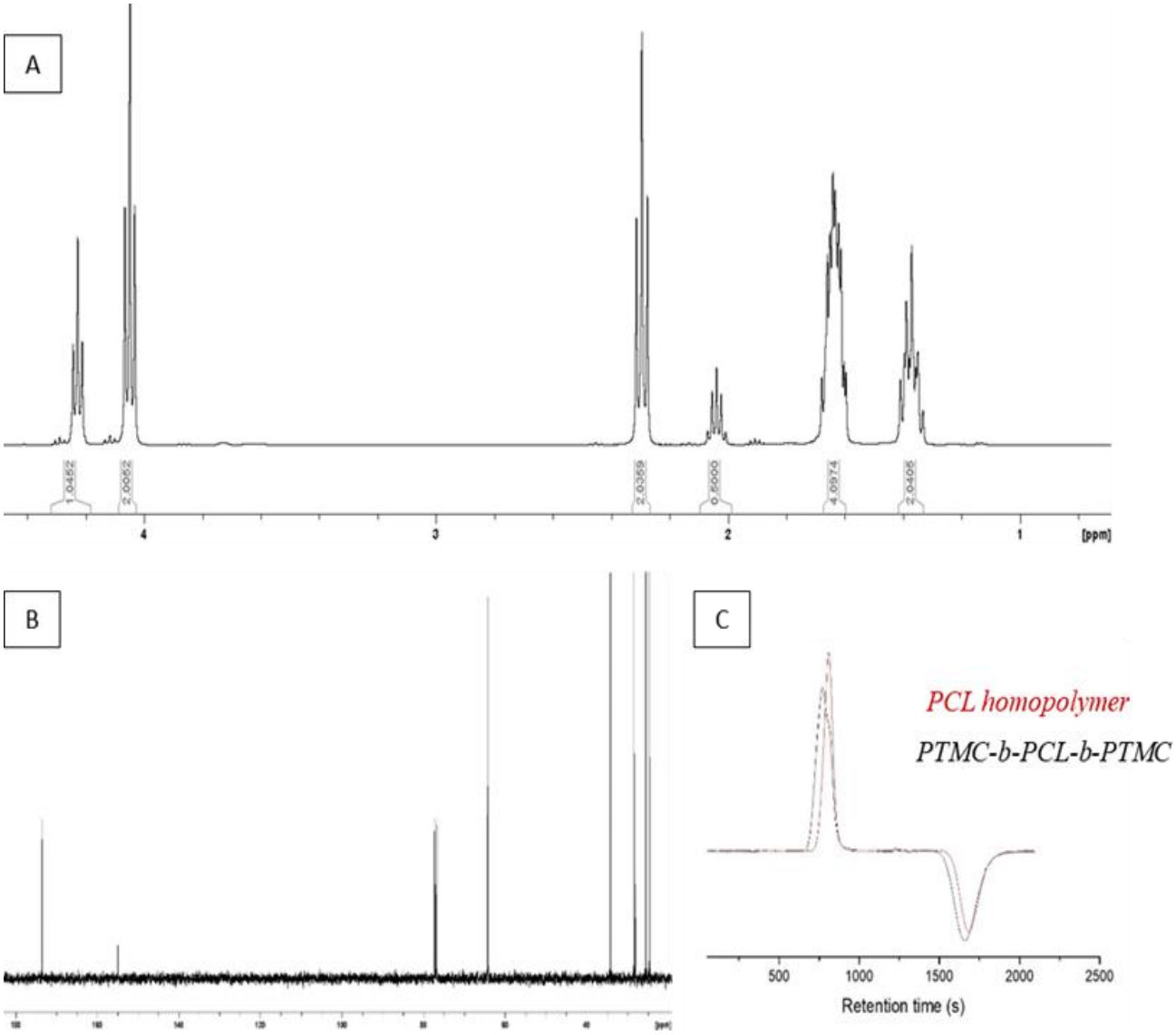

Figure IV-S2: (A) NMR ^{1}H, (B) NMR ^{13}C spectra and (C) SEC chromatogram of PTMC-*b*-PCL-*b*-PTMC triblock copolymer with PTMC/PCL (25/75) molar proportions.

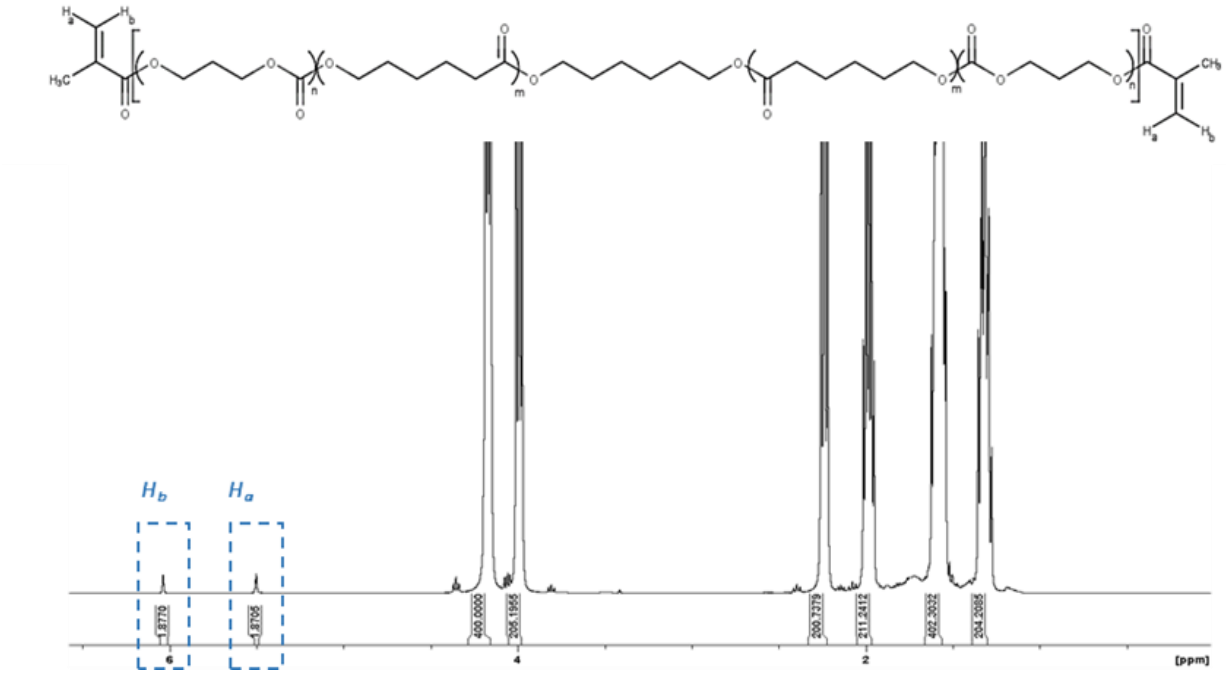

Figure IV-S3: NMR ^{1}H spectra of methacrylated PTMC-*b*-PCL-*b*-PTMC triblock copolymer

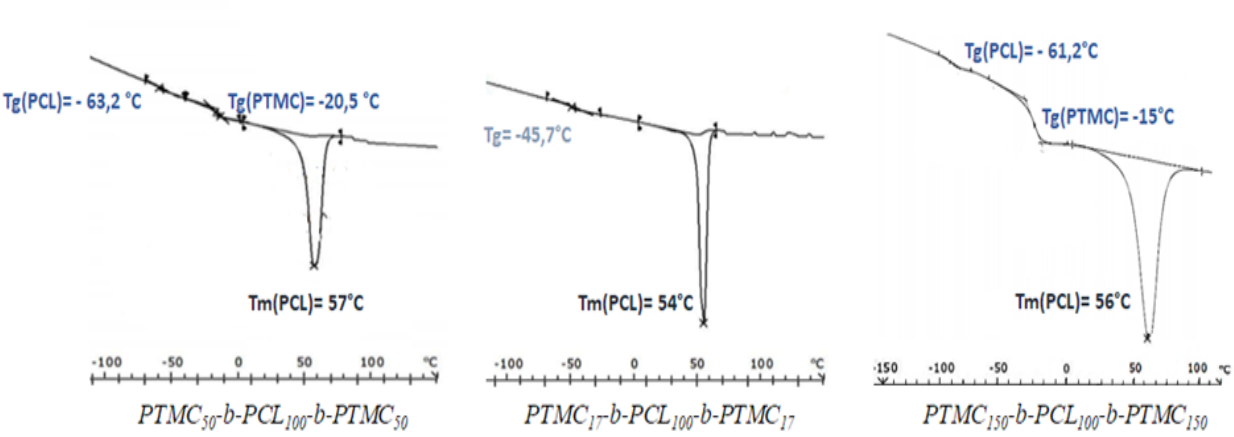

Figure IV-S4: DSC scans of PTMC-*b*-PCL-*b*-PTMC block copolymers with different molar ratios, performed at 20 °C/min.

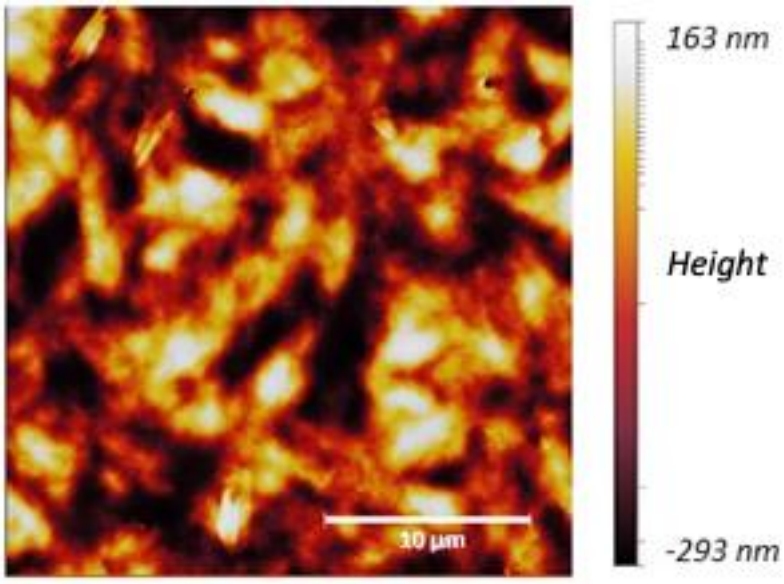

Figure IV-S5: AFM height image of melt crosslinked $PTMC_{150}$-*b*-PCL_{100}-*b*-$PTMC_{150}$ block copolymer thin film.

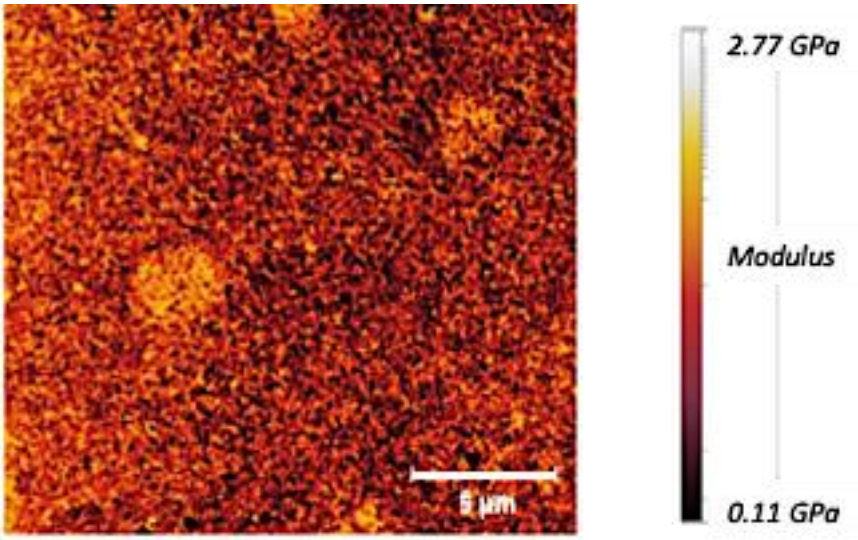

Figure IV-S6: AFM DMT image of liquid nitrogen (LN_2) quenched, crosslinked $PTMC_{150}$-*b*-PCL_{100}-*b*-$PTMC_{150}$ BCP thin film on (20x20 µm) length scale.

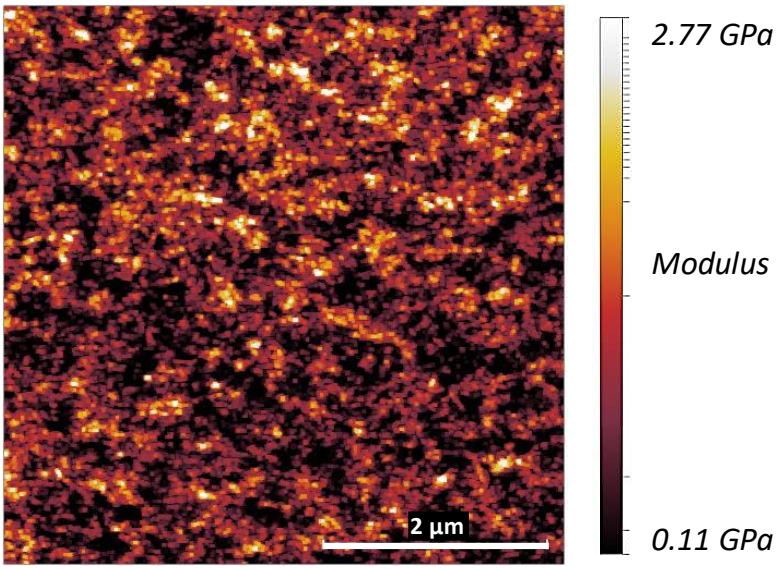

Figure IV-S7: AFM DMT image of crosslinked and liquid nitrogen quenched $PTMC_{50}$-*b*-PCL_{100}-*b*-$PTMC_{50}$ block copolymer thin film after 16 weeks.

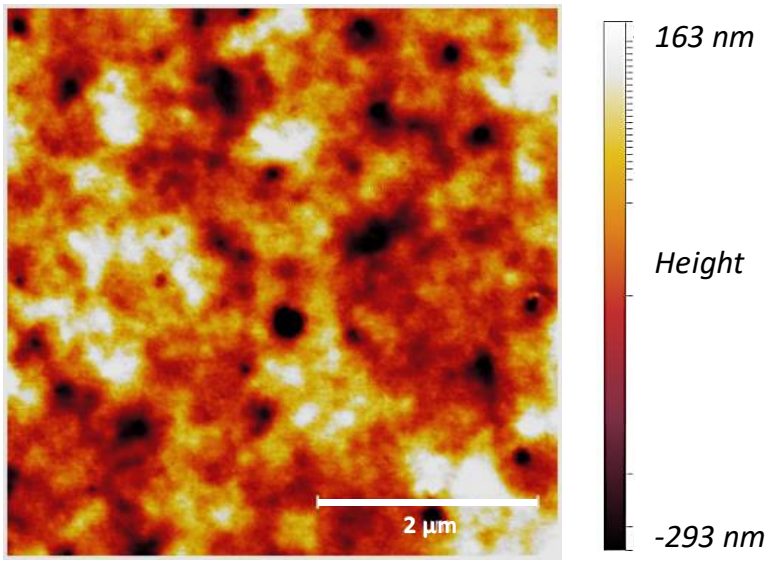

Figure IV-S8: AFM height image of liquid nitrogen quenched uncrosslinked $PTMC_{50}$-*b*-PCL_{100}-*b*-$PTMC_{50}$ block copolymer thin film, starting to retrieve the crystallinity after 4 weeks.

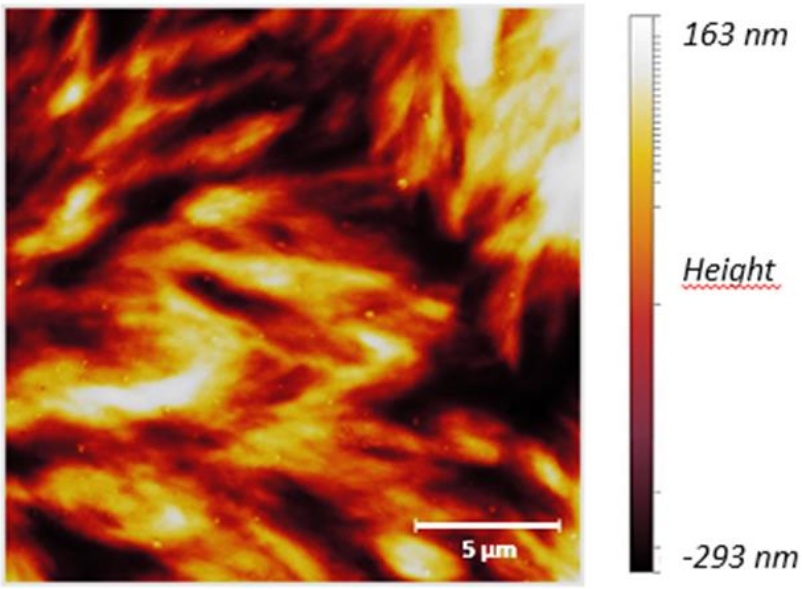

Figure IV-S9: AFM height image of crosslinked-liquid nitrogen quenched $PTMC_{50}$-*b*-PCL_{100}-*b*-$PTMC_{50}$ block copolymer thin film later heated to T > Tm (PCL).

References

[1] Doppalapudi, S.; Jain, A.; Khan, W.; Domb, A. J., *Polym Advan Technol* **2014,** *25* (5), 427-435.

[2] Mandal, P.; Shunmugam, R., *J Macromol Sci A* **2020,** *58* (2), 111-129.

[3] Malikmammadov, E.; Tanir, T. E.; Kiziltay, A.; Hasirci, V.; Hasirci, N., *J Biomat Sci-Polym E* **2018,** *29* (7-9), 863-893.

[4] Bartnikowski, M.; Dargaville, T. R.; Ivanovski, S.; Hutmacher, D. W., *Prog Polym Sci* **2019,** *96*, 1-20.

[5] Huang, W.; Zhu, N.; Liu,Y.; Wang, J.; Zhong, J.; Sun, Q.; Sun, T.; Hu, X.; Fang, Z.; Guo, K., *Chem. Eng. J.* **2019,** 356, 592-597.

[6] Yilgör, E.; Isik, M.; Söz, C. K.; Yilgör I., *Polymer* **2016,** *83*, 138-153.

[7] Li, Z.; Tan, B. H., *Mater Sci Eng C Mater Biol Appl* **2014,** *45*, 620-34.

[8] Behl, A.; Parmar, V. S.; Malhotra, S.; Chhillar, A. K., *Polymer* **2020,** *207*, 122901.

[9] Thakur, M.; Majid, I.; Hussain, S.; Nanda, V., *Packag Technol Sci* **2021,** *34* (8), 449-461.

[10] Fukushima, K., *Biomater Sci* **2016,** *4* (1), 9-24.

[11] Blanquer, S. B. G.; Gebraad, A. W. H.; Miettinen, S.; Poot, A. A.; Grijpma, D. W.; Haimi, S. P., *J Tissue Eng Regen M* **2017,** *11* (10), 2752-2762.

[12] Schappacher, M.; Fabre, T.; Mingotaud, A. F.; Soum, A., *Biomaterials* **2001,** *22* (21), 2849-2855.

[13] Yang, J. A.; Liu, F.; Tu, S.; Chen, Y. W.; Luo, X. L.; Lu, Z. Q.; Wei, J.; Li, S. M., *J Biomed Mater Res A* **2010,** *94a* (2), 396-407.

[14] Jia, Y. T.; Kim, H. Y.; Gong, J.; Lee, D. R.; Ding, B.; Bhattarai, N., *Polym Int* **2004,** *53* (3), 312-319.

[15] Guillaume, S. M., *Eur Polym J* **2013,** *49* (4), 768-779.

[16] Pego, A. P.; Zhong, Z. Y.; Dijkstra, P. J.; Grijpma, D. W.; Feijen, J., *Macromol Chem Physic* **2003,** *204* (5-6), 747-754.

[17] Labet, M.; Thielemans, W., *Chem Soc Rev* **2009,** *38* (12), 3484-3504.

[18] Muller, A. J.; Balsamo, V.; Arnal, M. L., *Adv Polym Sci* **2005,** *190*, 1-63.

[19] Muller, A. J.; Albuerne, J.; Marquez, L.; Raquez, J. M.; Degee, P.; Dubois, P.; Hobbs, J.; Hamley, I. W., *Faraday Discuss* **2005,** *128*, 231-252.

[20] Kim, J. K.; Park, D. J.; Lee, M. S.; Ihn, K. J., *Polymer* **2001,** *42* (17), 7429-7441.

[21] Cui, Y. C.; Jin, R. H.; Zhou, Y.; Yu, M. R.; Ling, Y.; Wang, L. Q., *Biomed Mater* **2021,** *16* (3), 035006.

[22] Han, W. Q.; Li, S. J.; Liao, X.; He, B.; Yang, Q.; Li, G. X., *Polym Int* **2019,** *68* (12), 1992-2003.

[23] Nandan, B.; Hsu, J. Y.; Chen, H. L., *Polym Rev* **2006,** *46* (2), 143-172.

[24] Castillo, R. V.; Fleury, G.; Navarro, C.; Couffin, A.; Bourissou, D.; Martin-Vaca, B., *Eur Polym J* **2017,** *95*, 711-727.

[25] Nojima, S.; Hashizume, K.; Rohadi, A.; Sasaki, S., *Polymer* **1997,** *38* (11), 2711-2718.

[26] Tian, G.; Zhu, G.; Ren, T.; Liu, Y.; Wei, K.; Liu, Y. X., *J Appl Polym Sci* **2019,** *136* (6), 47055.

[27] Lendlein, A.; Schmidt, A. M.; Schroeter, M.; Langer, R., *J Polym Sci Pol Chem* **2005,** *43* (7), 1369-1381.

[28] Crescenzi, V.; Manzini, G.; Calzolari, G.; Borri, C., *Eur Polym J* **1972,** *8* (3), 449-463.

[29] Zhang, X.; Peng, X.; Zhang, S. W., *Woodh Publ Ser Biom* **2017,** *117*, 217-254.

[30] Derjaguin, B. V.; Muller, V. M.; Toporov, Y. P., *J Colloid Interf Sci* **1975,** *53* (2), 314-326.

[31] Gazeau-Bureau, S.; Delcroix, D.; Martin-Vaca, B.; Bonrissou, D.; Navarro, C.; Magnet, S., *Macromolecules* **2008,** *41* (11), 3782-3784.

[32] Delcroix, D.; Martin-Vaca, B.; Bourissou, D.; Navarro, C., *Macromolecules* **2010,** *43* (21), 8828-8835.

[33] Couffin, A.; Delcroix, D.; Martin-Vaca, B.; Bourissou, D.; Navarro, C., *Macromolecules* **2013,** *46* (11), 4354-4360.

[34] Toshikj, N.; Robin, J. J.; Blanquer, S., *Eur Polym J* **2020,** *127*, 109599.

[35] Ou-Yang, W. C.; Li, L. J.; Chen, H. L.; Hwang, J. C., *Polym J* **1997,** *29* (11), 889-893.

[36] Wang, J. L.; Dong, C. M., *Polymer* **2006,** *47* (9), 3218-3228.

[37] Han, J.; Branford-White, C. J.; Zhu, L. M., *Carbohyd Polym* **2010,** *79* (1), 214-218.

[38] Mai, Y. Y.; Eisenberg, A., *Chem Soc Rev* **2012,** *41* (18), 5969-5985.

[39] Paajanen, A.; Vaari, J.; Verho, T., *Polymer* **2019,** *171*, 80-86.

[40] Sedov, I.; Magsumov, T.; Abdullin, A.; Yarko, E.; Mukhametzyanov, T.; Klimovitsky, A.; Schick, C., *Polymers* **2018,** *10* (8), 902.

[41] Lendlein, A.; Kelch, S., *Angew Chem Int Edit* **2002,** *41* (12), 2034-2057.

[42] Luo, Q.; Chen, J.; Gnanasekar, P.; Ma, X. Z.; Qin, D. D.; Na, H. N.; Zhu, J.; Yan, N., *Acs Appl Polym Mater* **2020,** *2* (11), 5259-5268.

[43] Xie, H.; Yang, K. K.; Wang, Y. Z., *Prog Polym Sci* **2019,** *95*, 32-64.

[44] Bat, E.; Kothman, B. H. M.; Higuera, G. A.; van Blitterswijk, C. A.; Feijen, J.; Grijpma, D. W., *Biomaterials* **2010,** *31* (33), 8696-8705.

[45] Zhang, X.; Tan, B. H.; Li, Z. B., *Mat Sci Eng C-Mater* **2018,** *92*, 1061-1074.

[46] Navarro-Baena, I.; Sessini, V.; Dominici, F.; Torre, L.; Kenny, J. M.; Peponi, L., *Polym Degrad Stabil* **2016,** *132*, 97-108.

[47] Pfau, M. R.; McKinzey, K. G.; Roth, A.; Grunlan, M. A., *Biomacromolecules* **2020,** *21* (6), 2493-2501.

[48] Sharifi, S.; Blanquer, S.; Grijpma, D. W., *J Appl Biomater Func* **2012,** *10* (3), 280-286.

[49] Sharifi, S.; van Kooten, T. G.; Kranenburg, H. J. C.; Meij, B. P.; Behl, M.; Lendlein, A.; Grijpma, D. W., *Biomaterials* **2013,** *34* (33), 8105-8113.

[50] Sauter, T.; Heuchel, M.; Kratz, K.; Lendlein, A., *Polym Rev* **2013,** *53* (1), 6-40.

[51] Zhu, G.; Liang, G.; Xu, Q.; Yu, Q., *J Appl Polym Sci* **2003,** *90* (6), 1589-1595.

Annexe Chapitre IV

La capacité à fabriquer des objets tridimensionnels (3D) avec une haute précision tout en utilisant une large variété de matériaux, a attiré l'attention des scientifiques sur la stéréolithographie (SLA). Il s'agit de la première forme de fabrication additive produisant des objets 3D en solidifiant sélectivement (couche par couche) une résine liquide photosensible par une réaction de photopolymérisation.[1,2] De plus, un important bouleversement est actuellement en cours dans le domaine de la fabrication 3D depuis l'arrivée de l'impression 4D. L'impression 4D peut se résumer en une approche capable d'ajouter à un objet imprimé en 3D, la possibilité de le transformer dans le temps de façon contrôlée et en réponse à une stimulation externe (température, pH, magnétique, ou électrique). Ainsi, le développement d'objets 3D fait sur mesures et programmables obtenus à partir de polymère « intelligent » permet d'apporter non seulement une nouvelle dimension mais également une perspective prometteuse dans de nombreux secteurs (santé, électronique, robotique, aérospatial, etc).

L'utilisation d'un polymère capable de générer un comportement à mémoire de forme en fabrication additive peut donc être considérée comme une perspective vers l'impression 4D. Ainsi, à titre de preuve de concept, nous avons testé la résine à base du copolymère PTMC-*b*-PCL-*b*-PTMC en stéréolithographie.[3,4]

Dans cet objectif, une résine du copolymère tribloc $PTMC_{100}$-*b*-PCL_{50}-*b*-$PTMC_{100}$ méthacrylée a été préparée. Le copolymère a été tout d'abord mis en solution dans l'anisole (80 wt. % du polymère), en présence d'un photoamorceur (Darocur 1173, 5 wt. % du polymère), photoactivable à la longueur d'onde de la machine (385 nm) ainsi que d'un photoabsorbeur (Orange G, 0,1 wt. % du polymère) afin de contrôler l'épaisseur des couches réticulées.

Dans une première partie, une étude des paramètres d'impression 3D a permis de déterminer les conditions d'impression optimales. Ainsi, une optimisation sur le temps de réticulation, l'épaisseur de la couche et la puissance de la machine a été initialement menée. Les paramètres de la machine ont été fixés à 40 $mW.cm^{-2}$ pour la puissance du rayonnement UV, accompagnée d'un temps d'exposition à la lumière UV de 50 s pour des épaisseurs de couches de 100 µm.

En parallèle, le modèle virtuel d'impression a été généré à partir de logiciels de Conception Assistée par Ordinateur (CAO) (Figure IV-B-A). Pour cette étude préliminaire, des objets tridimensionnels poreux, représentant une architecture gyroïdique, ont été dessinés.[5] Ces structures gyroïdiques ont été fabriquées avec succès par stéréolithographie (Figure IV-B-B), avec une définition de fabrication élevée, confirmant ainsi la possibilité de fabriquer des objets 3D avec les copolymères PTMC-*b*-PCL-*b*-PTMC étudiés dans ce projet de thèse.

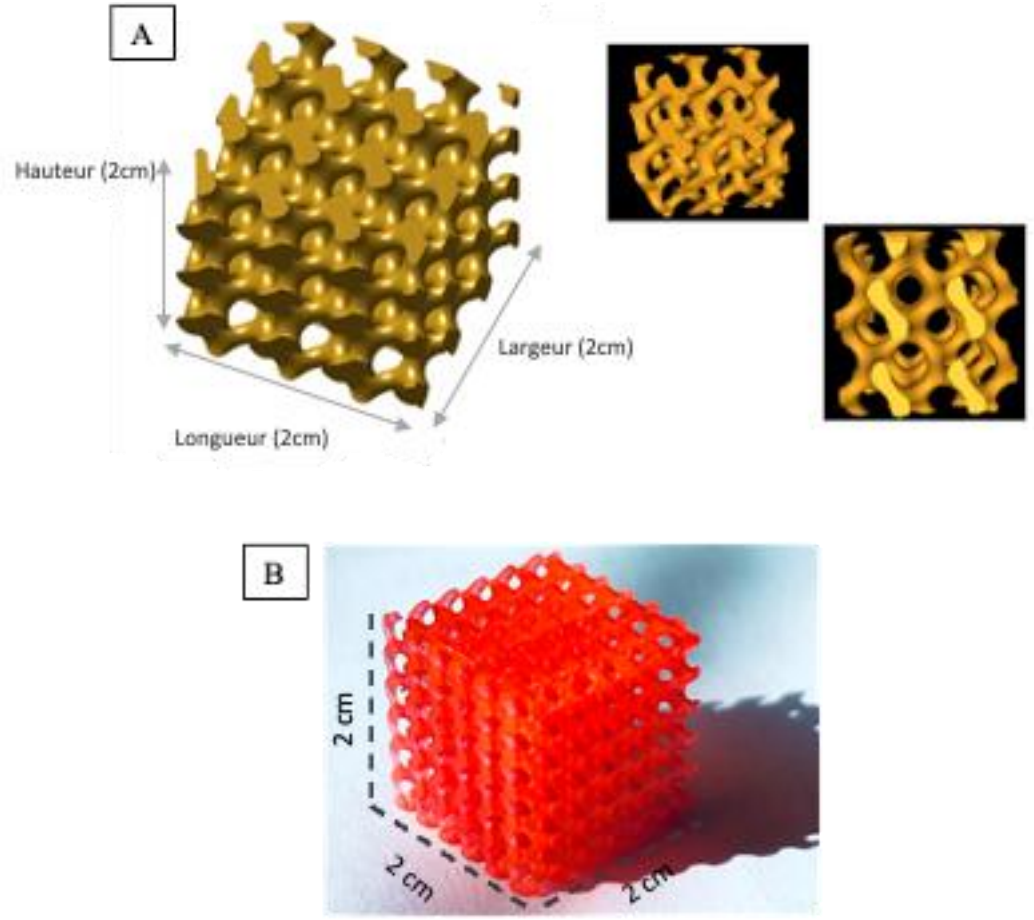

Figure IV-B: (A) Objet virtuel désigné par le logiciel CAO et (B) ensuite imprimé par la stéréolithographie.

Pour conclure, nous avons réussi à fabriquer des objets 3D macroporeux à partir de notre résine copolymère *dMa*-PTMC-*b*-PCL-*b*-PTMC-*dMa*. Ces résultats représentent un aspect très prometteur en vue de l'impression 4D de nos produits. Des essais de comportement à mémoire de forme de ces objets fabriqués en SLA sont en cours d'étude.

Références

[1] J. Huang, Q. Qin, J. Wang, *Processes* **2020**, *8*.

[2] J. Z. Manapat, Q. Chen, P. Ye, R. C. Advincula, *Macromol. Mater. Eng.* **2017**, *302*, 1.

[3] S. B. G. Blanquer, D. W. Grijpma, In *Computer-Aided Tissue Engineering: Methods and Protocols* (Eds.: Rainer, A.; Moroni, L.), Springer US, New York, NY, **2021**, pp. 19–30.

[4] T. Brossier, G. Volpi, J. Vasquez-Villegas, N. Petitjean, O. Guillaume, V. Lapinte, S. Blanquer, *Biomacromolecules* **2021**, *22*, 3873.

[5] S. B. G. Blanquer, M. Werner, M. Hannula, S. Sharifi, G. P. R. Lajoinie, D. Eglin, J. Hyttinen, A. A. Poot, D. W. Grijpma, *Biofabrication* **2017**, *9*.

CHAPTER V / CHAPITRE V

Introduction Chapitre V

Dans le Chapitre IV nous avons réussi à démontrer qu'un accès à une séparation de phase thermodynamique est possible dans le système semi-cristallin PTMC-*b*-PCL-*b*-PTMC en jouant sur sa cinétique de cristallisation. Ces études approfondies sur cette séparation de phases thermodynamique sont encourageantes et justifieraient des travaux futurs en vue de mieux comprendre ce phénomène et d'accéder à des domaines nano-séparés optimisés.

Dans ce Chapitre V, nous nous focalisons sur l'idée de générer des systèmes poreux à partir des copolymères triblocs auto-assemblés de PTMC-*b*-PCL-*b*-PTMC. La dégradabilité lente du bloc central de PCL représente un obstacle pour son élimination efficace et sélective.[1,2] Par conséquent, dans l'objectif d'anticiper la dégradation sélective de ce bloc et par la suite accéder à des systèmes poreux, nous avons fait appel à des liaisons clivables sur la base d'exemples décrits dans le chapitre bibliographique pour d'autres systèmes de copolymères à blocs (non-dégradables).[3-6] Ainsi, l'idée générale a consisté en l'élaboration d'architectures triblocs de type PTMC-*liaison clivable*-PCL-*liaison clivable*-PTMC, dont un stimulus externe serait susceptible de perturber et/ou rompre cette liaison, permettant ainsi une élimination de ce bloc central par un solvant sélectif. Pour arriver à cet objectif, plusieurs liaisons clivables ont été testées.

- **Voie 1 - Ponts disulfures**

Dans un premier temps, nous avons essayé dans une étude modèle d'établir des liaisons clivables du type ponts disulfure dans des copolymères diblocs PTMC-S-S-PCL (avant de passer par la suite à des architectures triblocs) grâce à la chimie des thiols et des disulfures.
Des polymères de PTMC et PCL ont été synthétisés par la polymérisation par ouverture de cycle (ROP), en utilisant un amorceur (le 2-mercaptoéthanol) pouvant introduire la fonction thiol en bout de chaine (Figure V-A). Par la suite, l'objectif était de faire réagir le composé 1 (Figure V-A1) avec le composé 2 (Figure V-A2), et par oxydation des thiols, arriver à un copolymère diblocs PTMC-SS-PCL.

Le spectre RMN du composé 1 (SH-PCL-OH) confirme la présence de la fonction -SH en bout de chaine (2,65 ppm) comme illustré en Figure V-B. Cependant, ceci n'était pas le cas pour le composé 2 dont le groupement -CH_2- voisin de la fonction thiol n'a pas pu être identifié sur le spectre RMN présenté en Figure V-C. Ainsi, la réaction entre les composés 1 et 2 n'était pas possible pour la création de ponts disulfure entre les deux blocs. C'est pourquoi, nous avons décidé de poursuivre sur une nouvelle voie de création de liaisons clivables.

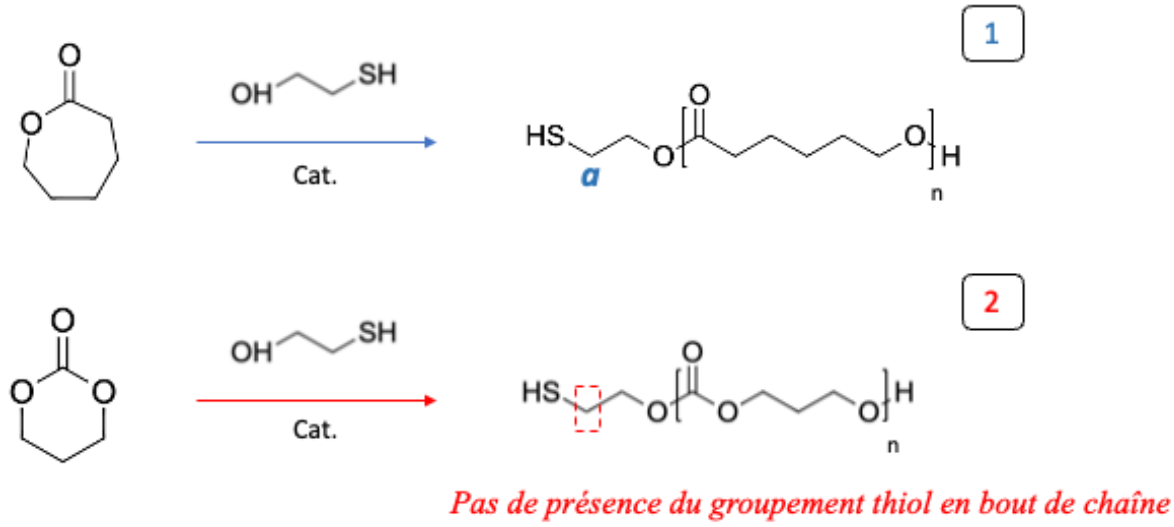

Figure V-A: Représentation schématique de la Voie 1 par création de pont disulfure.

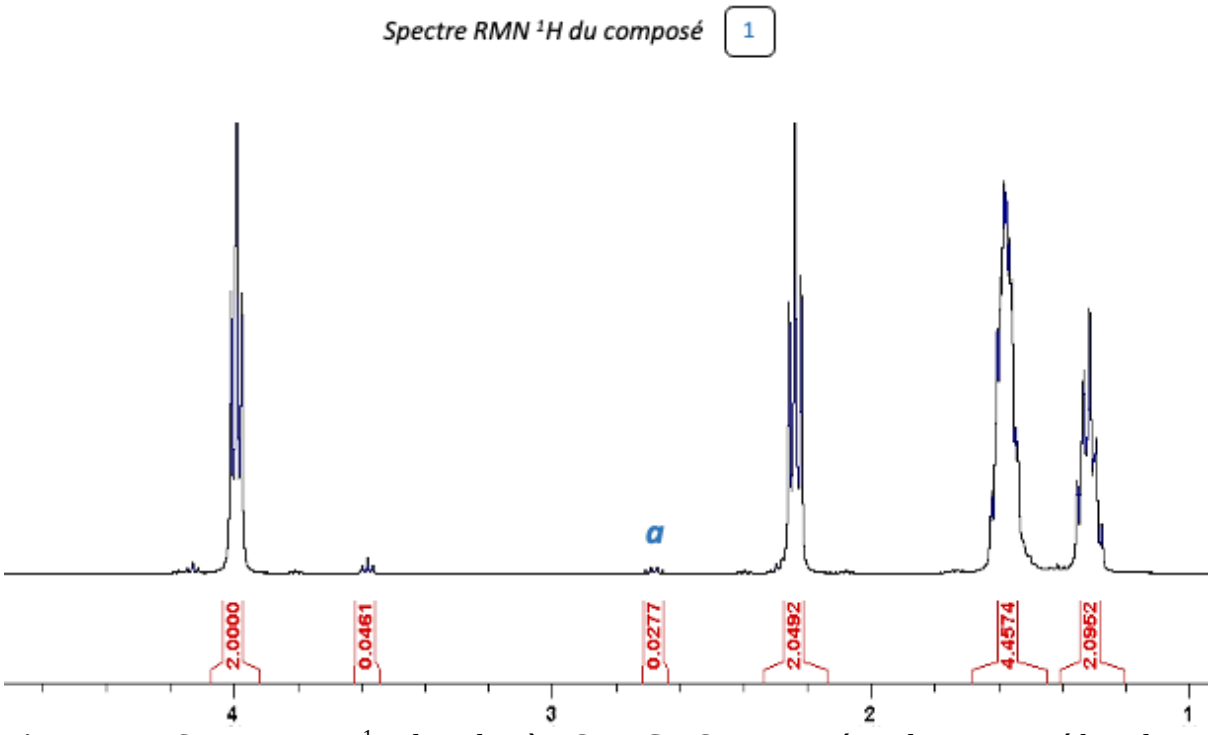

Figure V-B: Spectre RMN-^{1}H du polymère SH-PCL-OH, amorcé par le mercaptoéthanol.

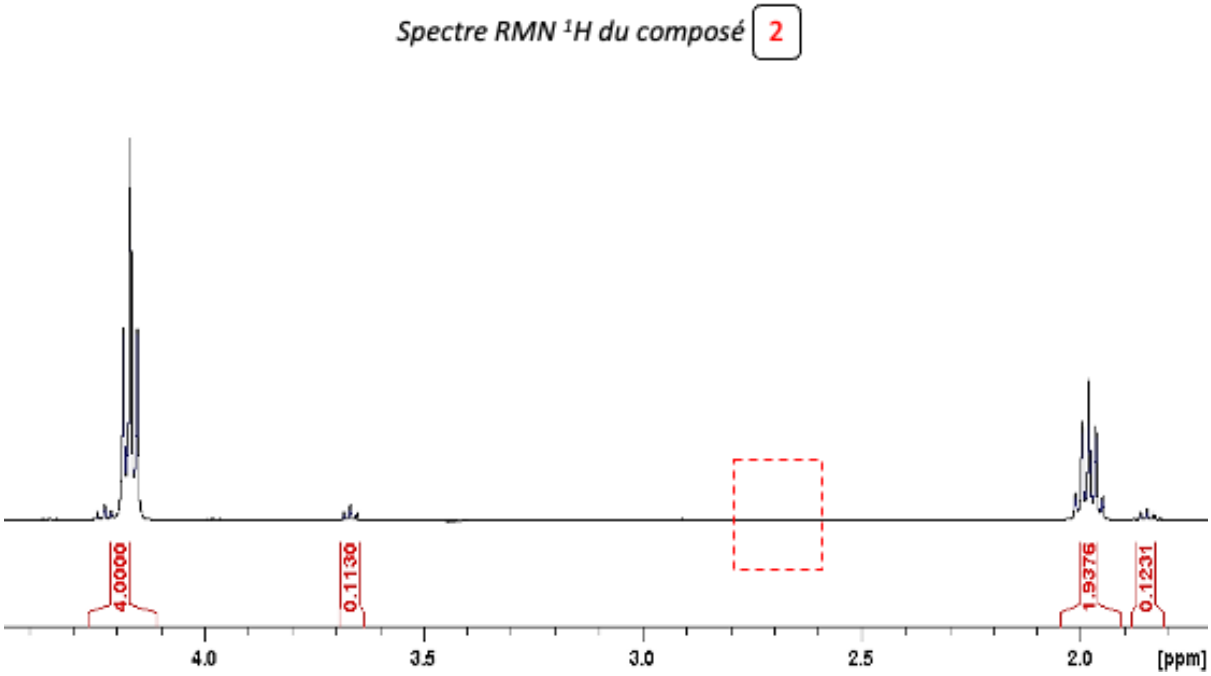

Figure V-C: Spectre RMN-^{1}H du polymère SH-PTMC-OH, amorcé par le mercaptoéthanol.

- **Voie 2 – Diels-Alder (DA)**

La liaison Diels-Alder est connue comme étant réversible par une rétro-réaction sous un stimulus de température. Deux stratégies distinctes ont été testées afin de faire réagir un PTMC portant un diène et une PCL possédant un diénophile dans l'objectif d'établir la liaison clivable de Diels-Alder entre le bloc central de PCL et les deux blocs terminaux PTMC (Figure V-D-A et V-D-B). Le PTMC, utilisé dans cette étude, a été synthétisé par ROP en utilisant l'alcool furfurylique comme amorceur. De l'autre côté, la PCL présentée en figure V-D-A a été obtenue par la réaction d'estérification de Steglich d'une PCL-diol et avec le monoéthyl fumarate, en présence d'EDC (1-éthyl-3-(3-diméthylaminopropyl) carbodiimide) et de DMAP (4-diméthyl aminopyridine). Pour la PCL utilisée pour les stratégies B et C, l'estérification a été effectuée en utilisant l'acide-6-maléimidohexanoique (avec la PCL-diol), également en présence d'EDC et de DMAP.

Les blocs PTMC et PCL portant les groupements fonctionnels antagonistes et pouvant conduire à la réaction de Diels-Alder alors ont été introduits dans un milieu réactionnel à une température de 60°C.

Aucune réactivité entre les groupements dienes et diénophiles de la voie A n'a pu être notée d'après les analyses RMN. Ce résultat pourrait être expliqué du fait de la difficulté de réaction des bouts de chaînes entre les deux types de macromolécules. De la même manière, la stratégie B qui comprend des diénophiles en bout de chaine, donc supposés être plus facilement accessibles que les diénophiles localisés dans la chaine pour la stratégie A, n'a pas abouti à un résultat positif malgré des conditions réactionnelles poussées de 480 h à des températures suffisamment élevées pour la réaction de Diels-Alder.

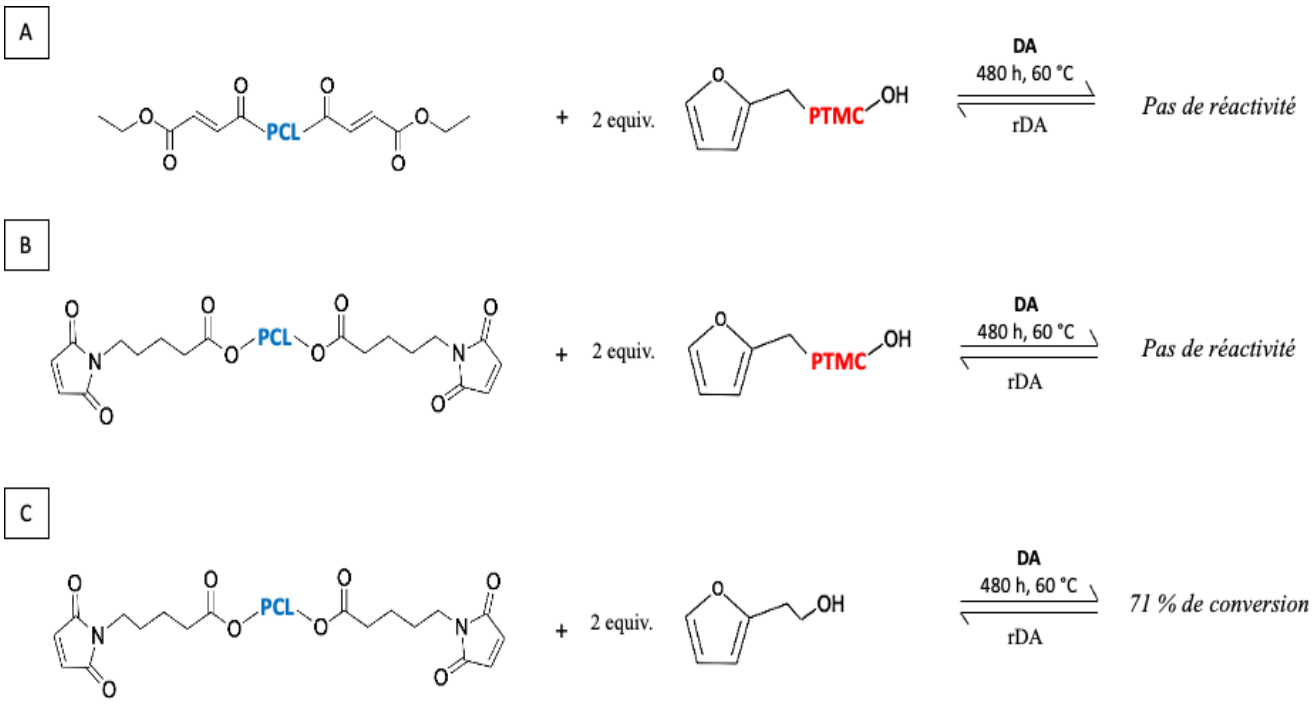

Figure V-D: Les stratégies distinctes de la voie Diels-Alder.

Enfin, la stratégie C (Figure V-D-C) a consisté dans un premier temps à réaliser la réaction de Diels-Alder (DA) sur un bloc de PCL portant le diénophile, avec un diène moléculaire, l'alcool furfurylique. Ce diéne aurait dû être plus réactif du fait de sa structure moléculaire. Dans un second temps, après cette réaction DA, les fonctions alcool libres en bouts de bloc PCL auraient pu permettre d'engager la ROP du PTMC.

Cependant, dans les mêmes conditions réactionnelles poussés, un taux de conversion de l'ordre de 71 % a été noté par les analyses RMN. Même s'il s'agit d'un taux de réactivité satisfaisant, celui-ci n'est pas convenable i) pour la génération contrôlée des architectures triblocs, ii) pour l'étude de leur auto-assemblage, et par la suite iii) pour la génération d'une porosité par ces systèmes.

- **Voie 3 – L'Approche Acétal**

En conséquence, une voie de formation de jonctions acétal a été testée. Elle correspond à une suite logique de l'approche DA testée précédemment, dans le sens où la fonction acétal est d'abord introduite dans la structure du « pré-polymère » PCL utilisée par la suite pour la ROP du TMC (Figure V-E).

Même si de nombreuses expériences de synthèse ont confirmé la formation des acétals sur le bloc PCL suivant un protocole expérimental de la littérature (Figure V-F),[7] elles ont démontré de sérieux problèmes de reproductibilité de cette réaction. En effet, la Figure V-G montre l'instabilité de cette jonction acétal attestée par une chute du taux d'acétalisation de 84 % au cours de la synthèse à 11 % au sein du polymère après purification. De plus, des analyses RMN-HSQC suggèrent la formation d'un groupement métastable d'hémiacétal (autour de 60 ppm) au lieu d'un acétal qui devrait être observable aux alentours de 80-90 ppm (Figure V-H).

Des copolymères triblocs ont pu être obtenus à partir du macroamorceur PCL supposé contenir la fonction acétal. Néanmoins, ces copolymères présentaient des dispersités élevées attestées par des analyses SEC, ce qui indique une architecture tribloc non-contrôlée. De plus, les fonctions (hémi-)acétal présentes au sein de ces copolymères étaient de l'ordre de 15 %.

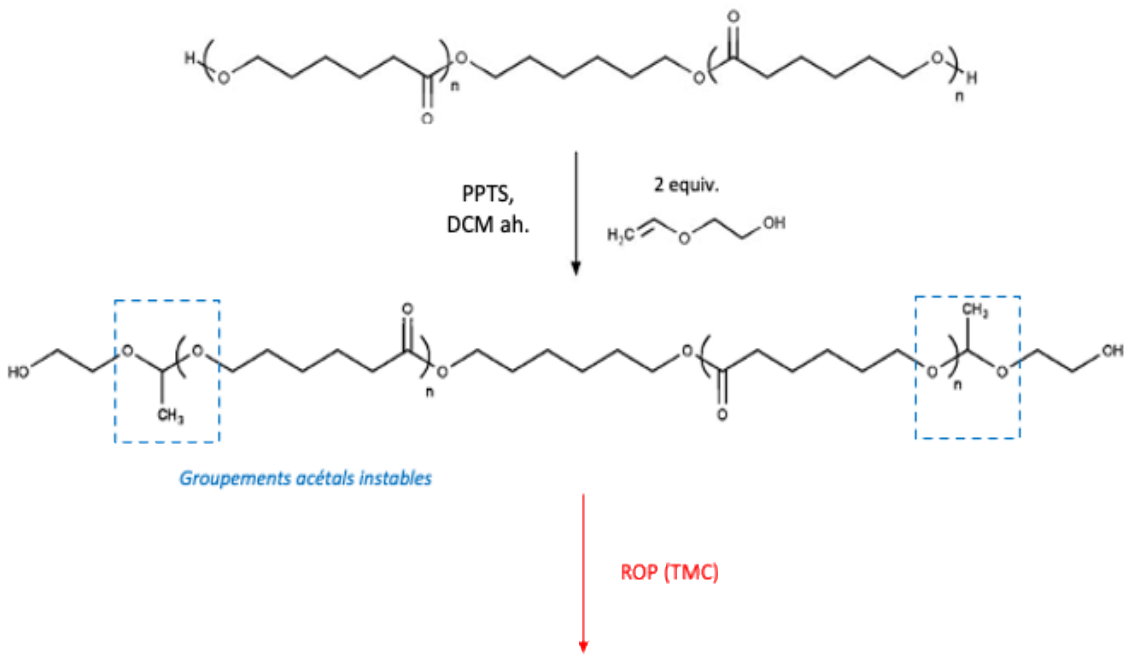

Formation d'un copolymère tribloc PTMC-b-PCL-b-PTMC contenant de 10 à 20 % de fonctions acétal

Figure V-E: La stratégie de l'approche acétal**.**

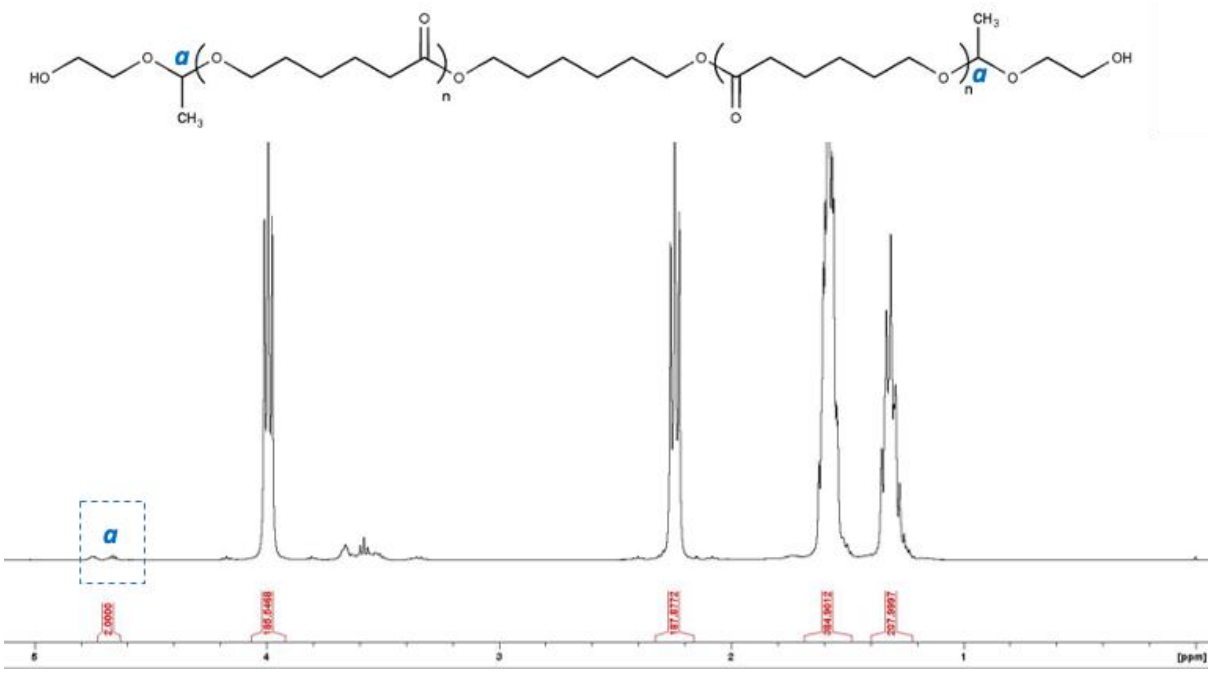

Figure V-F: Spectre RMN-^{1}H de la PCL contenant des fonctions acétals.

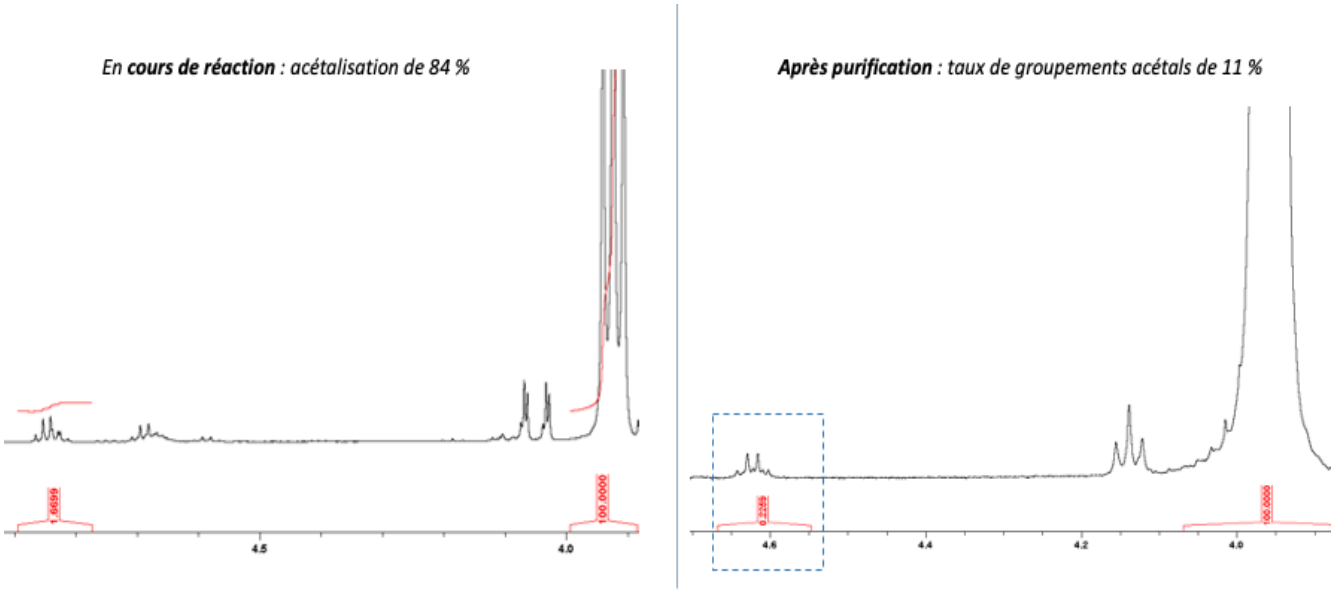

Figure V-G: Spectre RMN-^{1}H montrant la présence des fonctions acétals durant la réaction (à gauche) et après précipitation (à droite).

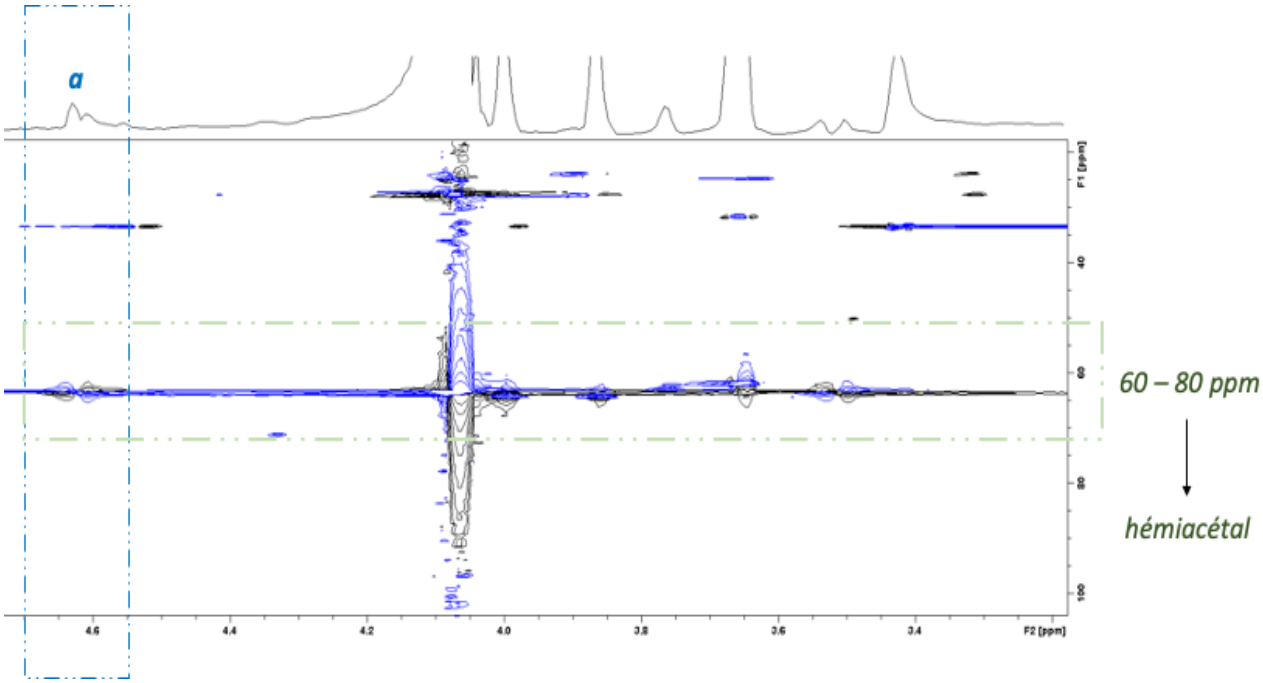

Figure V-H: Spectre RMN-HSQC du bloc PCL contenant des fonctions (hémi-)acétals.

Au terme de cette partie, nous pouvons conclure que l'introduction de liaisons clivables par une réaction de groupements fonctionnels en bout de chaînes de polymères n'a pas abouti à des résultats satisfaisants dans le cadre de notre étude. La possibilité que ces groupements réagissent ensemble dans des milieux dilués est très faible et ne conduit pas aux structures souhaitées.

D'après la littérature du Chapitre I, la quasi-majorité des liaisons clivables entre deux blocs distincts sont principalement introduites par une extension de chaine à partir d'un premier bloc obtenu par des polymérisations du type RAFT, ATRP ou NMP amenant des bouts de chaine fonctionnels halogénés facilement convertissables en une autre fonction. En revanche, dans le cas de notre étude, nos polymères se terminaient par des groupements hydroxyles, ce qui limite les possibilités de varier les réactions de conversion possibles des groupements.

Ainsi, voulant encore étudier l'impact des liaisons clivables sur la génération de porosité mais aussi sur la cristallinité de notre système, nous avons employé un amorceur qui contient au préalable une liaison clivable dans sa structure chimique – l'hydroxy éthyl disulfure. Les travaux du Chapitre V présentés sous la forme d'article à soumettre portent donc sur la synthèse contrôlée de copolymères triblocs PTMC-PCL-S-S-PCL-PTMC et sur l'étude du clivage des liaisons disulfure. Il vise également à mettre en évidence l'influence de ce clivage sur la morphologie et le comportement de films minces réticulés produits par *spin-coating* à partir de ces copolymères en vue de l'éventuelle création de porosité dans ces systèmes.

Références

[1] C. X. F. Lam, D. W. Hutmacher, J. T. Schantz, M. A. Woodruff, S. H. Teoh, *J. Biomed. Mater. Res. A* **2009**, *90*, 906.

[2] M. A. Woodruff, D. W. Hutmacher, *Prog. Polym. Sci.* **2010**, *35*, 1217.

[3] B. Le Droumaguet, R. Poupart, D. Grande, *Polym. Chem.* **2015**, *6*, 8105.

[4] M. Kang, B. Moon, *Macromolecules* **2009**, *42*, 455.

[5] M. Glassner, J. P. Blinco, C. Barner-Kowollik, *Polym. Chem.* **2011**, *2*, 83.

[6] J. T. Goldbach, K. A. Lavery, J. Penelle, T. P. Russell, *Macromolecules* **2004**, *37*, 9639.

[7] K. Satoh, J. E. Poelma, L. M. Campos, B. Stahl, C. J. Hawker, *Polym. Chem.* **2012**, *3*, 1890.

Chapter V

Synthesis of disulfide bridge interconnected PTMC-*b*-PCL-S-S-PCL-*b*-PTMC triblock copolymers and their use as smart materials

Keywords

Cleavable linkages, disulfide bridge, poly(ε-caprolactone), poly(trimethylene carbonate), crystallinity, thin film morphology

Abstract

Disulfide bonds show a growing interest in the synthesis of copolymers. Most often, these linkages are located between two distinct blocks and herein we report the synthesis of copolymers where this junction is inserted at the center of the middle block in PTMC-PCL-SS-PCL-PTMC block copolymer systems, synthesized by controlled organocatalytic ring-opening polymerization. A disruption of the disulfides by external redox stimulus using D,L-dithiothreitol as reagent provoked the conversion of the triblock copolymer architecture to diblock ones bearing free thiol functions. Pre- and post-cleavage behavior of previously spin-coated and UV-cured thin films was analyzed by Differential Scanning Calorimetry (DSC) and microscopy techniques. Curiously, as observable by Atomic Force Microscopy (AFM) analysis, the crystallinity of the system was suppressed upon the thin film chemical cleavage treatment in a selective solvent for the PCL block, allowing its collapse onto the PTMC phase. In addition, modifications of the thin films surface morphologies could be observed, as suggested by Scanning Electron Microscopy (SEM) examinations, conceivably attributable to an induced surface porosity. Moreover, the liberate thiol moieties in thicker BCP cured films were used for exploring of an induced self-healing property of such films.

1.Introduction

Biocompatible polymers are widely and increasingly used in biomedical and environmental applications.[1,2] Among them, aliphatic polyesters and polycarbonates are currently the subject of many researches related with the synthesis of innovative macromolecular structures.[3] Poly (ε-caprolactone) (PCL) as a widely used aliphatic polyester is characterized by toughness, high drug permeability, non-toxicity, and biodegradability among others.[4,5] In the meantime, poly(trimethylene carbonate) (PTMC) is one of the most studied aliphatic polycarbonates due to its unique degradability, flexibility, and hydrophobic nature.[6] Controlled ring-opening polymerization (ROP) of both polymers has enabled tailoring their features for specific applications. To that end, the interesting PTMC/PCL copolymer structures have found an interest in the field of nerve regeneration, tissue engineering or shape-memory materials.[7–9]

Porous materials with tuned functionalization or degradation rates have generated a growing interest these latest years. PTMC-PCL block copolymers (BCPs) bearing cleavable linkages in their chemical structure could widen the scope of their possible utilizations. Cleavable linkages contained in the employed polymerization initiator have been more and more implemented in block copolymer architectures by means of various polymerization techniques, leading to differing pre- and post-cleavage structures.[10]

Among the various cleavable linkages, the versatile chemistry of disulfides has aroused special interest in the extensive pharmacology, biology, and chemistry domains.[11,12] In fact, their important contribution in protein functioning and the ability to readily degrade or chemically reform within, have been the principal reason for their implementation in synthetic polymers.[13] Particularly interesting are diblock copolymer associations where the disulfide bridge was employed as a cleavable junction towards the generation of porous samples. In such perspective, copolymers based on poly(styrene)-SS-poly(ethylene oxide) and poly(styrene)-SS-(poly lactic acid) were synthesized and resulted in PS thiol-functionalized nanoporous thin films and monoliths, respectively.[14,15] Such occurrence derives from the disulfide redox sensitivity upon dithiothreitrol (DTT) treatment followed by the removal of the selective blocks (PEO and PLA) with an appropriate solvent. The thiol-end functionalization of the porous structures enabled the creation of polymer-gold composites in both cases. Moreover, copolymers containing disulfide junctions have been reported as self-healing materials thanks

to the disulfide intramolecular exchange reactions.[16] The disulfide cleavage in reductive conditions succeeded by the reformation of the resulting thiol groups by an oxidative reaction has been also reported as an original chemistry method for thermoset epoxy resins or redox-reversible hydrogels.[17,18] Tsarevsky *et al.* suggested for the first time the disulfide self-reparatory properties in polymer science from poly(styrene) structures possessing PS units connected by internal disulfide bonds.[19]

Herein, we report an investigation on fully degradable PTMC-PCL-SS-PCL-PTMC block copolymers bearing a disulfide junction (Figure V-1). Their synthesis was performed by controlled ROP starting from an initiator containing a S-S junction in its structure. The effective DTT-cleavage was studied by NMR (^{1}H and 2D-DOSY) and SEC techniques. The identical cleaving conditions were employed on photo-crosslinked block copolymer thin films obtained by spin-coating technique and its impact on the material morphology was investigated by atomic force microscopy (AFM), scanning electron microscopy (SEM) and DSC techniques. In the last part of the study, the stimulated reparatory properties in oxidative conditions of cleaved block copolymer thicker films were examined by means of tensile strength experiments.

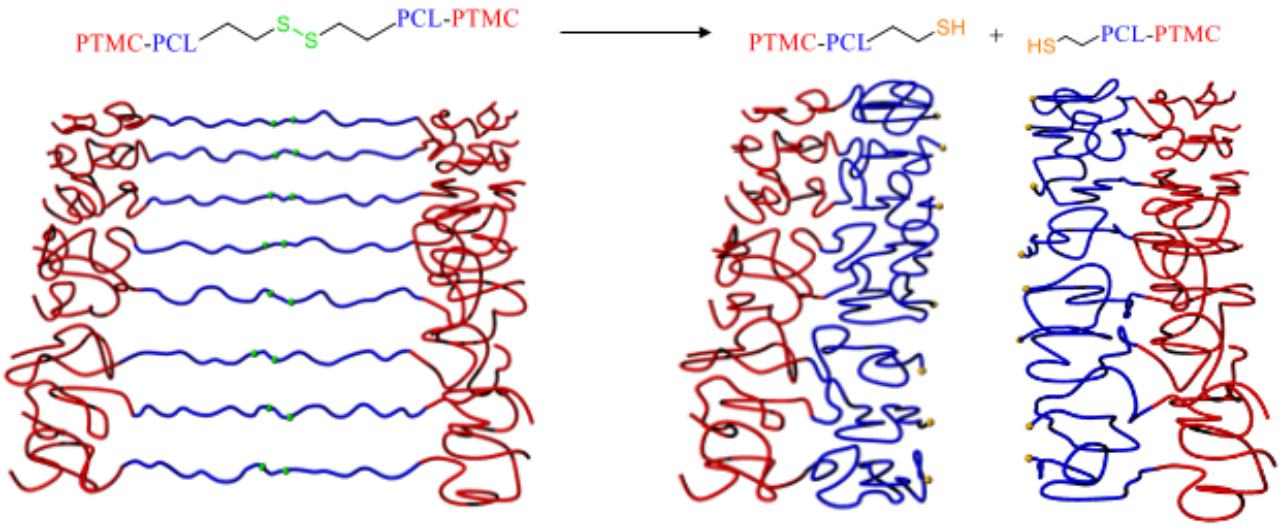

Figure V-1: Schematic representation of PTMC-b-PCL-S-S-PCL-b-PTMC block copolymers bearing disulfide linkages, before (left) and after cleavage (right).

2. Experimental section/Methods

Materials

The monomers, ε-caprolactone (ε-CL) and trimethylene carbonate (TMC) were purchased from Santa Cruz Biotechnologies (Germany) and Foryou Medical (China), respectively. The catalysts, tin (II) 2-ethyl hexanoate ($Sn(oct)_2$) and 1,5,7- triazabicyclo [4.4.0] dec-5-ene (TBD), as well as the initiator 2-hydroxyethyl disulfide (2-HEDS) and other chemicals such as tetrahydrofuran (THF), propylene carbonate (PC), dithiothreitol (DTT), iodobenzene diacetate (IBDA), acetic acid, methacrylic anhydride (MMA) and triethyl amine (TEA) were provided from Sigma Aldrich (France) and used as received. The photoinitiator, 2-hydroxy-2-methylpropiophenone (Darocur 1173) was obtained from BASF Chemicals (Germany). Anhydrous dichloromethane, used as polymerization solvent and as diluting agent for the preparation of thin films, was retrieved from solvent purificator Inert PureSolv™ (France).

Synthetic procedures

The homopolymer and triblock copolymer syntheses were performed in two-necked round bottom flasks of 100 or 250 ml, formerly dried in oven at 130 °C for 24 h and equipped with magnetic stirrer and thermometer. Prior to anhydrous solvent injection and reaction, five vacuum-dry argon cycles were performed.

Bulk synthesis of PCL by ROP of ε-CL monomer with 2-hydroxyethyl disulfide as initiator - PCL prepolymer was produced by employing $Sn(Oct)_2$ as catalyst and 2-hydroxyethyl disulfide as initiator. For the purpose of synthesizing PCL homopolymer with 100 repeating units, ε-CL monomer (10g, 87,7 mmol, 100 equiv), 2-hydroxyethyl disulfide (0,135 g, 0,877 mmol, 1 equiv) and $Sn(Oct)_2$ (0,01g, 0,0247 mmol, 0.028 equiv) were introduced in the round bottom flask and reacted in bulk for 24 h at 100°C. Once ^1H NMR analysis proved complete monomer conversion, the polymer was cooled down, then solubilized in a minimum volume (20 ml) of dichloromethane. Lastly, the polymer was purified by precipitation in cold methanol before being filtered and dried in vacuum oven at 25 °C for 24 h. A yield of 96 % was obtained. The chemical shifts of the PCL homopolymer presented in Figure S1 are designated as follows: -

$\underline{CH_2}$- (e) 1.26-1.39 ppm, 2-$\underline{CH_2}$- (d+f) 1.51-1.64 ppm, -$\underline{CH_2}$-COO (g) 2.2-2.3 ppm, $\underline{CH_2}$-S-S-$\underline{CH_2}$ (h) 2.82-2.87 ppm, -$\underline{CH_2}$OH group.

Synthetic procedure for $PTMC_{50}$-b-PCL_{50}-S-S-PCL_{50}-b-$PTMC_{50}$ triblock copolymer synthesis by step ROP of TMC with PCL macroinitiator - A typical procedure for the synthesis of a block copolymer with a PTMC/PCL 50/50 molar ratio is reported hereafter. TMC monomer (9,02 g, 87,7 mmol, 100 equiv) was introduced in a round bottom flask together with the previously synthesized PCL macroinitiator (10g, 0,877 mmol, 1 equiv). Anhydrous dichloromethane ($[TMC/\varepsilon\text{-}CL]_0$=1 mol/L) injected after the vacuum-dry argon cycles was used as polymerization solvent. TBD (0.171g, 1,228 mmol, 1,4 equiv) was selected as catalyst for the reaction performed at room temperature during 1.5 h. After full TMC conversion, as monitored by ^{1}H-NMR, an excess of acetic acid (3 equiv in respect to the catalyst) was introduced in the reaction medium in order to neutralize the TBD. Lastly, the polymers were purified by slow precipitation in cold methanol, washed several times with the same solvent before being dried in vacuum oven at 25 °C for 24 h, thus yielding 95 % of polymer. The ^{1}H-NMR chemical shifts of the synthesized triblock copolymer are presented in Figures 2, Figure S2 and Figure S3. The main peaks are: -CH_2- (e) at 1.26-1.39 ppm, 2-CH_2- (d+f) at 1.5-1.65 ppm, -CH_2-(b) at 1.95-2.05, -$\underline{CH_2}$-COO (g) at 2.20-2.29 ppm, $\underline{CH_2}$-S-S-$\underline{CH_2}$ at 2.82-2.87 ppm, $\underline{CH_2}$OH group (c) at 3.95-4.08 and O-$\underline{CH_2}$ (a) at 4.15-4.25.

Synthesis of PTMC-b-PCL-S-S-b-PCL-PTMC dimethacrylates - The triblock copolymers were end-functionalized with methacrylate groups by employing methacrylic anhydride (MMA) together with triethyl amine (TEA). For that purpose, the block copolymers were initially dissolved in anhydrous dichloromethane ($[\text{triblock copolymer}]_0$ = 0,2 g.ml^{-1}) in a round bottom flask followed by the addition of MMA and TEA (with 6 molar equivalents in respect to the polymer). The reaction was left stirring in dark, at room temperature, for 7 days. Lastly, the dimethacrylated triblock copolymers were purified in cold methanol, dried in vacuum oven at 25 °C for 24 h and stored at -18 °C until further use. The chemical shifts of the photosensitive methacrylate end groups (Figure S4) are observed at 5.55-5.59 ppm for the Ha proton and 6.08-6.12 ppm for the Hb proton.

Preparation of polymer thin films for DSC, AFM and SEM analysis

The triblock copolymer thin films were processed by spin-coating technique (4000 rpm, 90s) of 10 wt. % polymer dichloromethane solutions on previously cleaned Si-wafer substrates. In the aim of photo-crosslinking of the thin films, 5 wt. % of Darocur 1173 photoinitiator in respect to the polymer was added to the solution formulation, prior to spin-coating. The spin-coated thin films were afterwards photo-crosslinked by exposure at 100 $J.cm^{-2}$, at 10 cm of the lamps, using 365 nm wavelength within an irradiation time of 10 min, in a UV Crosslinker Bio-Link chamber (Thermo Fischer, France).

Preparation of polymer thick films for rheological analysis of self-reparatory properties

The triblock copolymer solution formulation consisted of 10 g of polymer dissolved in 35 ml of THF with 5 wt. % of Darocur 1173 photoinitiator added in respect to the polymer. The formulation was afterwards poured in molds for the preparation of thick films. The latter were photo-crosslinked in the same conditions as for the thin films. The only difference, in this case, was in the higher irradiation durations of 25 min, required for complete film curing.

Disulfide bond cleavage in block copolymer thin and thick films

Once photocrosslinked, the block copolymer films were immersed for 12 h in a 0.1 M DTT in either propylene carbonate or tetrahydrofuran. After this period, the films were washed in their respective solvent (PC or THF) for additional 12 h, before being dried in vacuum oven at room temperature for 24 h.

Induced self-healing properties of crosslinked BCP films

The reformation of the disulfide bonds, known as the induced self-healing process, was achieved when applying a solution of an oxidizing agent (IBDA) between two previously cleaved parts of the thick cured films. For that purpose, 5 wt.% in respect to the mass of the cleaved sample test of IBDA was dissolved in 50 µL of THF to prepare the oxidizing solution. The concentration of the solution depended on the mass of the cleaved sample. For example, when the mass of the cleaved thick films for induced self-healing was 2 g, 0.1 g of IBDA was

dissolved in 50 µL of THF ([IBDA] = 6.2 M). Later, this solution was applied between the cleaved parts of the cured films with an external pressure to ensure better adhesion between the parts. The process was left at room temperature for 12 h.

Instrumentations

Size exclusion chromatograms were performed by means of a triple detection (GPC Varian 390-LC viscometer detector, Varian 390-LC refractive index detector and UV detector (254 nm)) from Agilent Technologies. Tetrahydrofuran (THF) was used at a flow rate of 1.0 mL/min at 30 °C. Universal calibration was performed with PS standards from Agilent Technologies (EasiVial) using the intrinsic viscosities given by the supplier. Data acquisition and calculations were achieved with Cirrus Multi GPC/SEC software.

Nuclear Magnetic Resonance Spectrometry - ^{1}H spectra were recorded on a 400MHz Bruker Aspect Spectrometer while DOSY spectra were recorded on a 600MHz Bruker Aspect Spectrometer, where $CDCl_3$ was used as deuterated solvent. Chemical shifts were given in parts per million (ppm): the reference peak was residual $CDCl_3$ at 7.26 ppm for both ^{1}H and DOSY NMR.

Differential Scanning Calorimetry (DSC) investigations on the thermal behavior block copolymer based thin films were realized with a Mettler Toledo (Mettler Toledo, France) DSC1 calorimeter. Therein, the constant calibrations were achieved *via* biphenyl, indium, bismium, zinc and cesium chloride standards. The samples, in the range of 10 mg, after being collected from the Si-substrate, were heated between -150 °C and 100 °C with a rate of 20 °C/min while using nitrogen as a purge gas. Their thermal values were measured in the second scan of the DSC thermogram, as the midpoint of transition.

The Atomic Force Microscopy and Scanning Electron microscopy measurements were performed as detailed in the Experimental Section of Chapter III.

The mechanical properties of the polymer films, i) before and ii) after cleavage and the induced self-healing were expressed *via* their elongation at break and Young modulus, measured with aInstron3366L5885 tensile tester. The modulus was obtained at 10 % deformation by stress/strain, while the elongation at break was defined as a percentage of the original length. The crosshead speed was 5 $mm.min^{-1}$.

3. Results and discussion

3.1 Block copolymer synthesis and characterization

The overall three-step elaboration of the desired PTMC-PCL block copolymer including the final end-functionalization with photosensitive methacrylate groups, is depicted in Figure V-2.

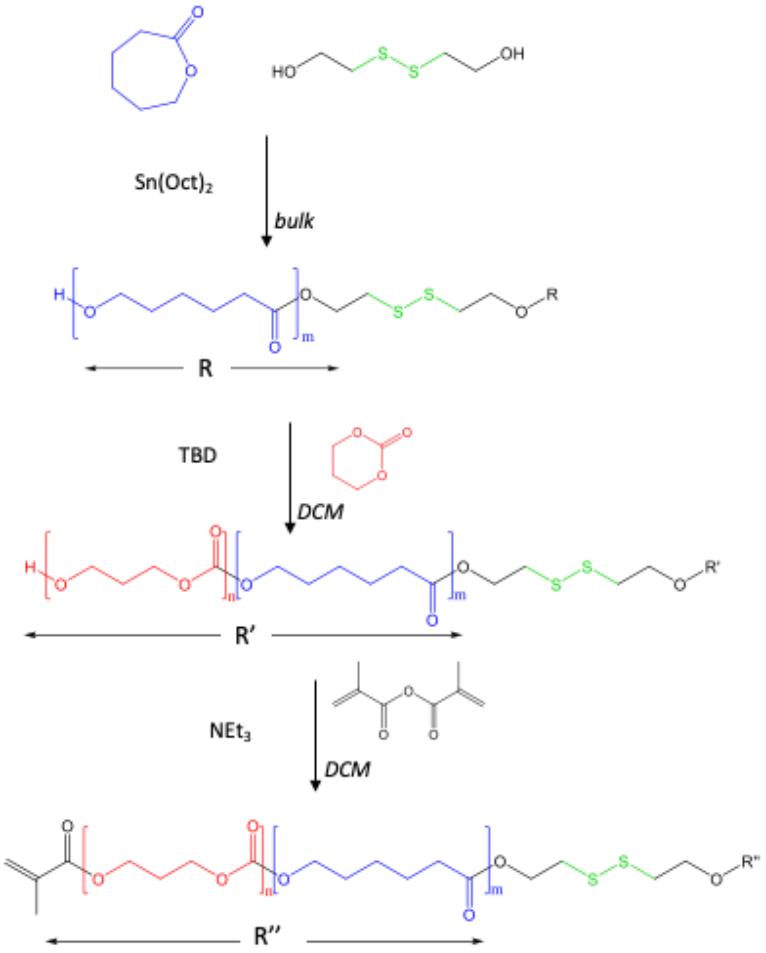

Figure V-2: Synthesis and end-functionalization of PTMC-*b*-PCL-S-S-PCL-*b*-PTMC block copolymers *via* PCL first route.

2-hydroxyethyl disulfide was used as initiator containing the disulfide bridge in its chemical structure. Due to its insolubility in the desired polymerization solvents (such as toluene or dichloromethane), the PCL "pre-polymer" was synthesized by bulk ROP using stannous octanoate as catalyst. The polymerization, performed at 100 °C, yielded PCL homopolymers with controlled architecture and desired repeating units after 24 h (Figure V-S1).

Thereupon, even though $Sn(oct)_2$ catalyst has been previously reported for the synthesis of PTMC/PCL block copolymers,[20] we selected organocatalysis instead of organometallic catalysis since it is more advantageous in terms of both environmental issues and polymerization reactivity with minimized activation energies compared to standard organometallic catalytic systems.[21] Hence, two routes have been recently developed for the organocatalytic synthesis of PTMC/PCL block copolymers: either by employing MSA catalysis as reported by Couffin et *al.*,[22] or by guanidine base (TBD) catalysis as recently published by our research group.[9]

Accordingly, using the TBD catalytic pathway for the BCP synthesis, the TMC copolymerization was initiated from the PCL macroinitiator. Full conversion was achieved under 90 min at room temperature as reported in our previous study. Block copolymers with three dissimilar lengths of the PCL middle block were synthesized for the purpose of this study. Their controlled architecture was confirmed by means of ^{1}H NMR, 2D DOSY-^{1}H NMR and SEC analyses. The molar composition ratios between the two blocks were defined by comparing the characteristic PTMC and PCL signals at 4.19 and 4.01 ppm, respectively. Thus, the ^{1}H-NMR spectra (Figure V-3, Figure V-S2 and Figure V-S3) of the three block copolymers exhibited molar proportions in agreement with the different targeted ratios. Simultaneously, the degree of polymerization was deduced by comparing the ratio of the peak integrals of the PCL chain characteristic protons with the ratio of the characteristic integral peak from the 2-HEDS initiator, located at 2.84 ppm. Moreover, the SEC analysis demonstrated a rise of the molar mass of the BCP (in red) compared to that of the initial PCL (in blue) one, together with monomodal populations (Figure V-5A) and low chain dispersities (Table V-S1).

Table V-1: Molar mass and dispersities of the block copolymers as measured by SEC.

Block copolymer	**PTMC/PCL molar ratio**	**Mn th. (g.mol^{-1})**	**Mn SEC (g.mol^{-1})**	**Mw SEC (g.mol^{-1})**	***Đ***
$PTMC_{50}$-*b*-PCL_{25}-S-S-PCL_{25}-*b*-$PTMC_{50}$	66/34	16000	13500	17300	1.28
$PTMC_{50}$-*b*-PCL_{50}-S-S-PCL_{50}-*b*-$PTMC_{50}$	50/50	21700	19800	23900	1.22
$PTMC_{50}$-*b*-PCL_{100}-S-S-PCL_{100}-*b*-$PTMC_{50}$	20/80	33100	32000	39600	1.24
$PTMC_{50}$-*b*-PCL_{50}-SH	50/50	10900	10100	12900	1.27

DOSY-NMR diffusion spectra (Figure V-5B) of the BCP (in red) remained on the same line and is distinct from that of the PCL homopolymer (in blue), indicating a controlled block copolymer architecture. At last, toward producing cross-linked thin and thick films, the BCP were end-functionalized with photosensitive groups. The methacrylation of the block copolymers was achieved in good yield and the NMR spectra of the final end-functionalized copolymer is presented Figure V-S4. The rate of conversion of OH groups in methacrylate double bonds was calculated by correlating the integrations of the protons of the double bond methacrylate units (situated at 5.6 and 6.1 ppm) with those of the PTMC or PCL blocks.

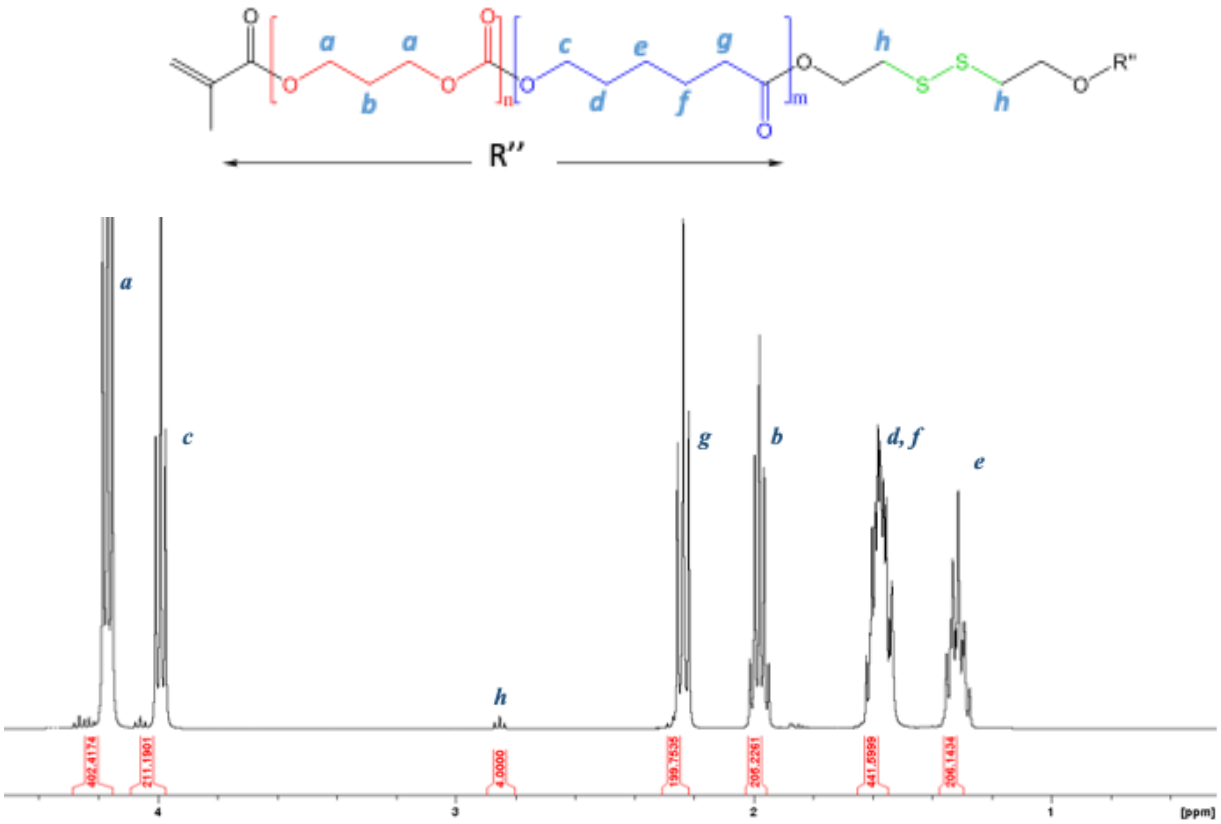

Figure V-3: ^{1}H-NMR spectrum of $PTMC_{50}$-*b*-PCL_{50}-S-S-PCL_{50}-*b*-$PTMC_{50}$ triblock copolymer with PTMC/PCL molar ratios of 50/50.

3.2 Block copolymer scission by redox stimulus

Disulfides are known to be cleavable by external redox stimulus from D,L-dithiothreitol (DTT), resulting in free thiol moieties. The latter emerge from the intermolecular hydrogen exchange and intramolecular cyclization of two consecutive thiol-disulfide reactions.[23]

Previous scientific reports on disulfide cleavage in BCPs are generally addressed on A-B diblock copolymer systems bearing the disulfide linkage between the A and the B blocks. Thus, after cleavage of the junction, which herein is positioned precisely between the two distinct blocks, one of the blocks is eliminated by selective washing procedure leading to porous structures.[14,15,24] On the other side, in our case, we aimed to prove that efficient cleavage could also occur when the disulfide linkage is located in the center of the middle block. Hence, the post-cleavage of a triblock copolymer could potentially result in a diblock copolymer architecture (Figure V-4).

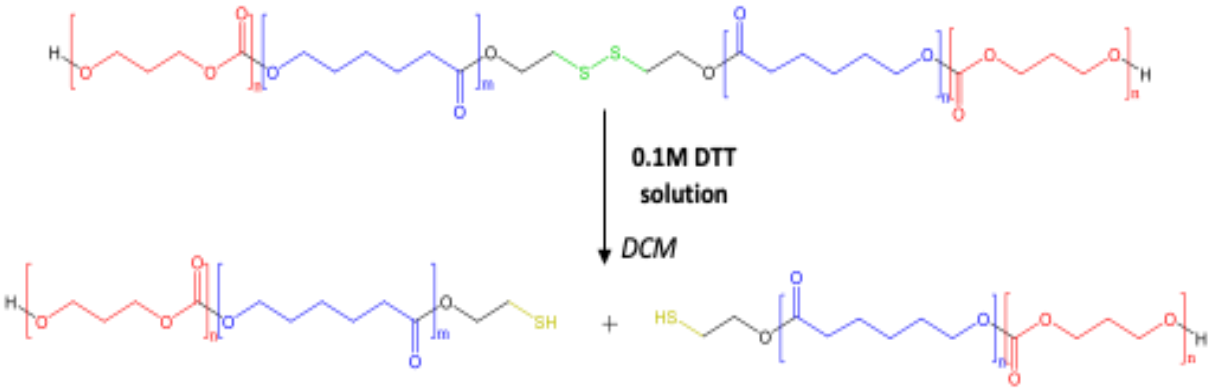

Figure V-4: Cleavage of disulfide interconnected triblock copolymers resulting into diblock copolymers with thiol end-groups.

For this purpose, the triblock copolymer was solubilized in 0.1 M DTT dichloromethane solution (a good solvent for both blocks) and stirred for 12h. After precipitation, the obtained polymer was analyzed by SEC and NMR and compared with the data of the initial triblock copolymer.

The chromatogram of the resulting copolymer HO-PTMC-PCL-SH after DTT treatment is shifted towards lower retention times and is situated in between those of the PCL homopolymer and the triblock copolymer (Figure V-5A). Moreover, the SEC analysis after cleavage with DTT pointed towards polymers with almost half molar mass than that of the initial triblock copolymer (Table V-1), showing an efficient cleavage of the disulfide bond. Simultaneously, the monomodal distribution and no variation in *Đ* proved that the cleavage occurred precisely at the disulfide junction, thus leading to a diblock copolymer structure.

The successful cleavage was also confirmed by ^{1}H NMR, where the peak at 2.84 ppm corresponding to the hydrogen atoms adjacent to the disulfide bridge of the 2-HEDS initiator, have fully disappeared in the case of the cleaved polymer (Figure V-S5). On the other hand,

the appearing quadruplet signal at 2.65 ppm can be attributed to the hydrogen atoms of CH_2 group neighboring the thiol-end group, pointing out once again at a post-cleavage resulting diblock copolymer architecture. Moreover, this statement is justified by the 2D DOSY-^{1}H NMR spectrum (Figure V-5B), where the diffusion coefficient of the cleaved polymer remains unchanged and is located in between those of the homopolymer and the triblock copolymer.

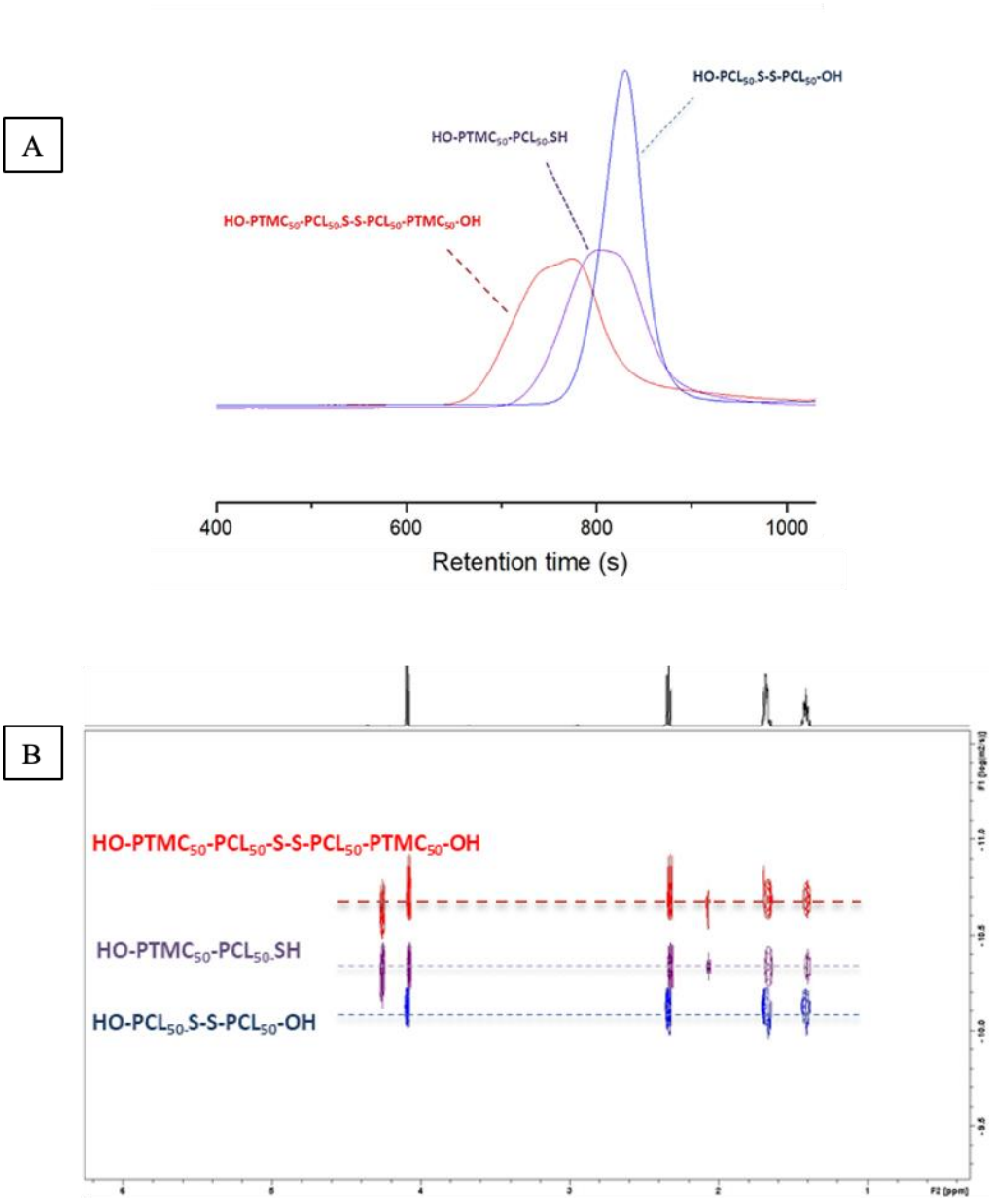

Figure V-5: (A) SEC chromatograms of: the PCL homopolymer (in blue), the triblock copolymer (in red), and the cleaved block copolymer (in violet) and (B) 2D DOSY-^{1}H NMR spectrum illustrating three dissimilar diffusion coefficients: the peaks of initial PCL homopolymer (in blue), the peaks of the triblock copolymer (in red), and the peaks of the cleaved block copolymer (in violet).

3.3 Block copolymer thin film post-cleavage behavior

Since the disulfides cleavage in the triblock copolymers has proven effective, in the following part of the study, we investigated the impact of the cleavage process on the physicochemical properties, the chain mobility and the potential generation of surface porosity by morphology investigations on PTMC-PCL BCPs thin films produced by the spin-coating technique. Prior to cleavage, the thin films were photo-crosslinked to enhance the mechanical stability of the network and to preserve its structural integrity upon the cleavage process. Moreover, the UV- treatment kept the films adhered to the substrate, unlike in the case of non-cured thin films, thus facilitating further analyses. In addition, it is important to be mentioned that the DTT cleaving process was performed in precisely selected solvent, supposed to influence the mobility of the PCL middle block chains after cleavage. For that purpose, propylene carbonate (PC), also characterized as being environmentally friendly,[25] was chosen since it is non-selective for the PCL block, expected to collapse this latter onto PTMC upon the disulfide cleavage. This occurrence is expected to modify the properties of the cleavage-resulting thin films and possibly opens the pathway to porosity creation. Therefore, the properties of cured BCP thin films before and after cleavage in DTT/PC solution were evaluated by Differential Scanning Calorimetry (DSC) while their morphology investigations were effectuated by means of Atomic Force Microscopy (AFM) and Scanning Electron Microscopy (SEM) techniques.

First, the thermal properties of the thin films of BCPs with two molar ratios, before and after cleavage with the DTT/PC solution, were investigated by DSC. The results are presented in Table V-2. Each BCP thin film (with two differing lengths of the middle PCL component) demonstrated two distinct glass transition temperatures signifying a phase-separated system. As it can be observed in Table V-2, the crystallinity rate of the system, measured by the X_c parameter, was considerably reduced upon cleavage. The melting points of the cleaved BCP thin films are noticeably lower as well. Hence, cleaving the triblock copolymers at their mid-point results in modified physico-chemical properties and loss of crystallinity once they are in the form of thin films of diblock copolymers. Thus, it can be concluded that simple DTT/solvent treatment alters the behavior of the resulting thin films. Such phenomenon is attractive for microscopy investigations of pre- and post-treated thin films of $PTMC_{50}$-*b*-PCL_{50}-S-S-PCL_{50}-*b*-$PTMC_{50}$ BCP.

Table V-2: Thermal properties of BCP thin films provided by DSC analyses.

*After DTT cleavage in propylene carbonate (PC); *ND: not determinable on our apparatus*

Block copolymer thin films	**Tg (PCL) (°C)**	**Tg (PTMC) (°C)**	**Tm (PCL) (°C)**	**$\|\Delta H_f$ (Tm)$\|$ ($J.g^{-1}$)**	**X_c (%)**
$PTMC_{100}$-PCL_{50}-S-S-PCL_{50}-$PTMC_{100}$	-42	-9	56	35	26
$PTMC_{100}$-PCL_{50}-S-S-PCL_{50}-$PTMC_{100}$*	-42	*ND*	32	17	13
$PTMC_{100}$-PCL_{100}-S-S-PCL_{100}-$PTMC_{100}$	-43	-17	57	42	31
$PTMC_{100}$-PCL_{100}-S-S-PCL_{100}-$PTMC_{100}$*	-61	*ND*	31	4	2

Therefore, in the first part of microscopy analyses, we tried to confirm the suppression of crystallinity upon DTT cleavage, as precedently suggested by DSC. Hence, Figure V-5 depicts AFM height images of $PTMC_{50}$-*b*-PCL_{50}-S-S-PCL_{50}-*b*-$PTMC_{50}$ BCP thin film before (A) and after cleavage (B). As it can be concluded, the cleaved film does not display the characteristic spherulites to the PCL phase widely observable in the pre-cleaved thin film. However, even though the crystallinity of the system is noticeably suppressed upon cleavage, clear visualization on the thin film morphology is not discernible in this case.

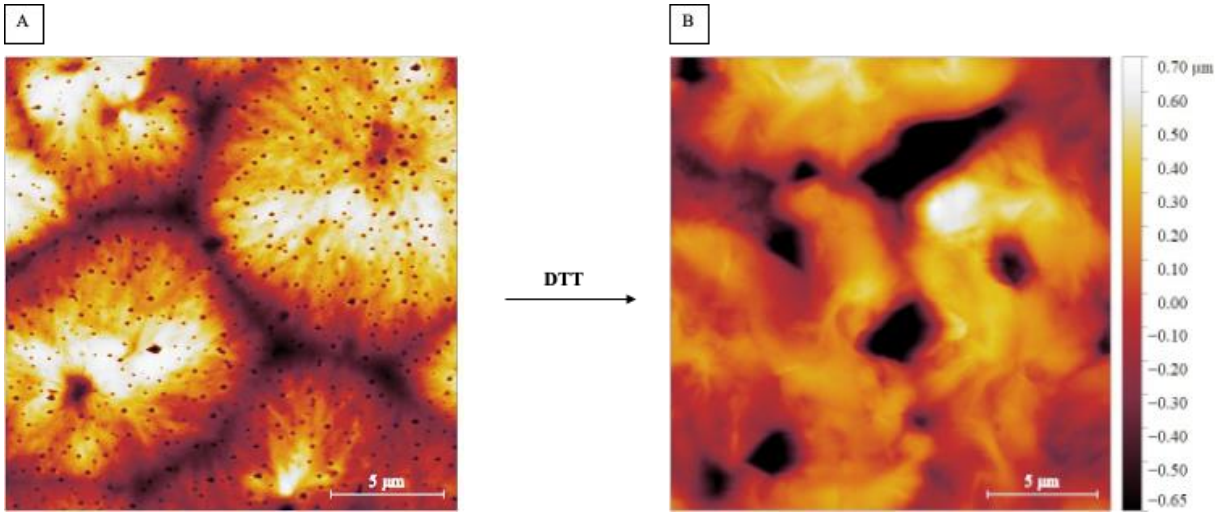

Figure V-5: AFM height image of A) spin-coated $PTMC_{50}$-*b*-PCL_{50}-S-S-PCL_{50}-*b*-$PTMC_{50}$ thin film and B) thin film exposed to disulfide bridge cleavage by DTT on 20 x 20 µm length scale.

As reported in our previous study,[9] a thermal treatment consisting of exposing the cured films at temperatures higher than the PCL melting point, followed by rapid liquid nitrogen (LN_2) quenching of the melt state, allowed the access to thermodynamical phase separation and better understanding of the surface morphology. Similarly, the same procedure (consisting of thermal annealing of the cured thin film at 80°C for 4h followed by LN_2 quenching) was applied for the BCP thin films analyzed in the following part of the study. Hence, in Figure V-6A, AFM stiffness image of a thermally annealed and quenched BCP thin film before cleavage is presented, leading to the characteristic thermodynamic phase separation, as demonstrated in Chapter IV. Interestingly, as observable in Figure V-6B, upon DTT/PC cleavage, the collapse of the PCL chains onto the PTMC phase, led to further modification of the surface morphology. The top-film surface modification could possibly lead to unlocked pores upon collapsing of one phase on the other, alike the generation of cavities resulting from the non-solvent induced phase-separation (NIPS) method.[25–27]

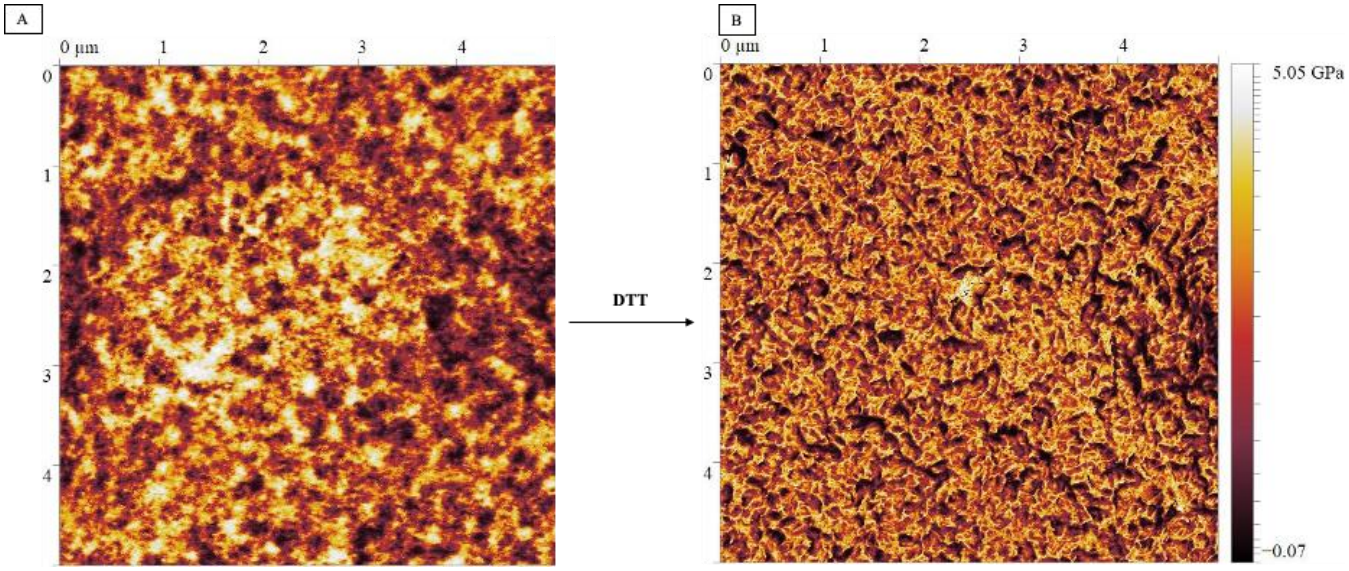

Figure V-6: AFM top surface stiffness image of thermally annealed and LN_2 quenched A) spin-coated $PTMC_{50}$-*b*-PCL_{50}-S-S-PCL_{50}-*b*-$PTMC_{50}$ thin film and B) thin film exposed to disulfide bridge cleavage by DTT on 5 x 5 µm length scale.

Since a clear conclusion on such occurrence could not be made on only AFM analyzed thin films, we proceeded with SEM investigations of post-cleavage thin films. In the Figure V-7A, the pre-cleavage thin film demonstrates predominantly homogeneous surface. However, as observable in Figure V-7B, a creation of surface roughness is clearly discernible which could possibly implicate open cavities on the top surface of the thin film (further investigations of

this phenomenon are currently being overtook, notably an experiment of reoxidation of the thin film surface in order to observe if the thin film could return to the initial homogeneous state).

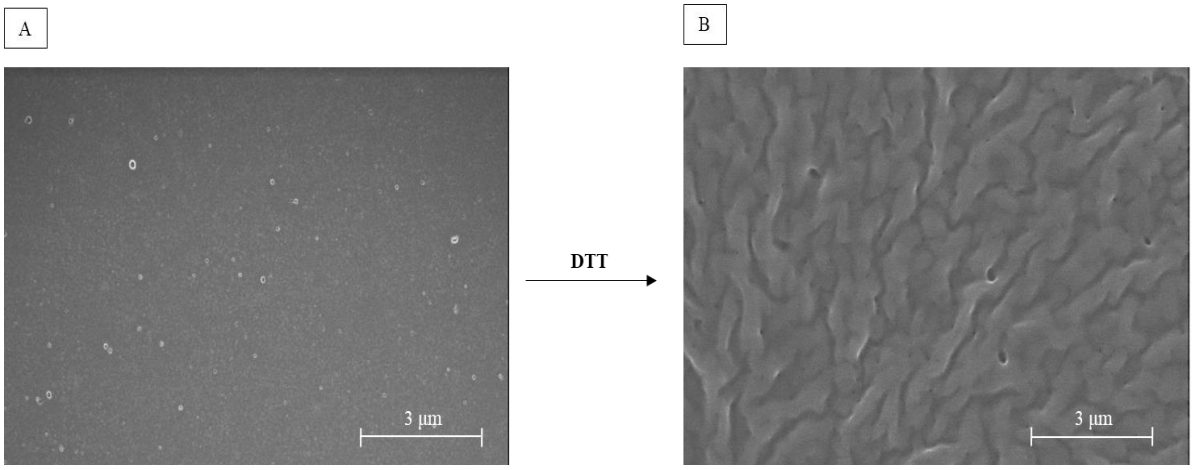

Figure V-7: SEM image of A) spin-coated $PTMC_{50}$-*b*-PCL_{50}-S-S-PCL_{50}-*b*-$PTMC_{50}$ thin film and B) BCP thin film after DTT redox stimuli.

3.4 Self-healing properties of BCP thick films

In the last part of the study, we investigated the capacity of the reversible disulfide bridge to generate self-healing properties of photo-crosslinked BCP thick films. For that purpose, the disulfide bridge in cured films of $PTMC_{50}$-PCL_{25}-S-S-PCL_{25}-$PTMC_{50}$ BCP was firstly cleaved by placing the specimens in 0.1 M DTT solution. After washing and drying, the resulting SH-functionalized polymer films were oxidized with the aid of a IBDA reagent, hence allowed to reform the disulfide bridge. Thus, following a similar experimental procedure as in the study by Yu *et al.*,[28] the IBDA solution was applied, at ambient temperature, in between the films previously subjected to cleavage. External pressure maintained permanent contact between the two films.

The mechanism of thiol oxidation with IBDA is represented in Figure V-8. In the first step, a sulfenyl iodide intermediate is formed upon ligand exchange of thiols and IBDA. Another thiol group afterwards interacts with the intermediate, leading to disulfide formation and liberation of iodobenzene and acetate group.[29,30]

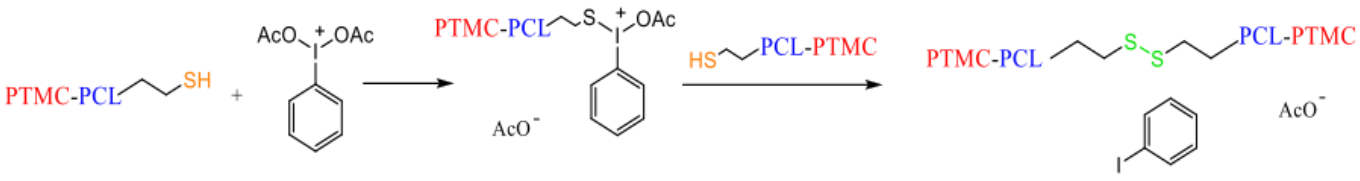

Figure V-8: Mechanism of thiol oxidation with IBDA.

The induced self-healing properties, visible by the established permanent contact of the two previously cleaved film parts, were verified by mechanical analyses. Tensile tests were performed on these films and the results were compared to those of the original BCP thin films. The non-cleaved films demonstrated elongation at break of 185 % at an external applied strain of 3 MPa. However, the cleavage and induced self-healing properties being performed in a solution, tend to decrease the mechanical resistance of such films. However, the films subjected to self-healing with IBDA demonstrated an ability to self-heal, even at ambient temperature. In the Figure V-9, the stress-strain curve of the firstly cleaved and then self-healed BCP experimental film is presented with an elongation at break of 40 % at an external stress of 0.6 MPa, thus confirming the ability of the disulfides to reform.

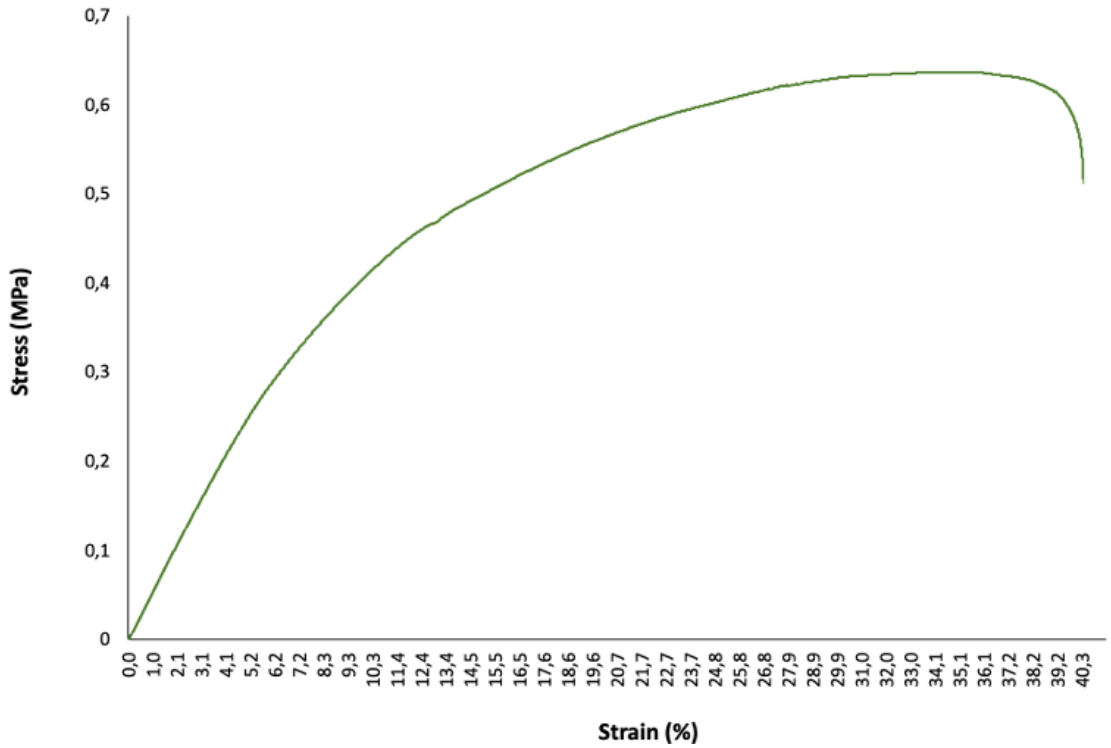

Figure V-9: Stress-strain curve of cleaved and auto-repaired $PTMC_{50}$-PCL_{25}-S-S-PCL_{25}-$PTMC_{50}$ BCP experimental film.

4. Conclusion

In this study, the use of the disulfide bridge as a cleavable linkage has been investigated in the aim to open pathways of various possible applications of PTMC-*b*-PCL-S-S-*b*-PCL-*b*-PTMC triblock copolymers. The interesting emplacement of the junction, as the mid-point of the central block, enabled a fluctuation from a triblock to PTMC-PCL-SH diblock copolymer architecture bearing thiol end-groups upon DTT employment. The same treatment resulted in block copolymer thin films demonstrating i/modification of the surface rugosity, possibly indicating a creation of surface pores, upon the precipitation of the PCL block on PTMC using selective solvent (PC) and ii/ suppression of the semi-crystalline nature of the block copolymer, observable by AFM, SEM and DSC. Mechanical analysis the block copolymer films, presenting cleaved then reformed S-S bonds in a redox process, also demonstrated an ability of the block copolymer to partially self-heal.

Supplementary Information

Synthesis of disulfide bridge interconnected PTMC-*b*-PCL-S-S-PCL-*b*-PTMC triblock copolymers and their use as smart materials

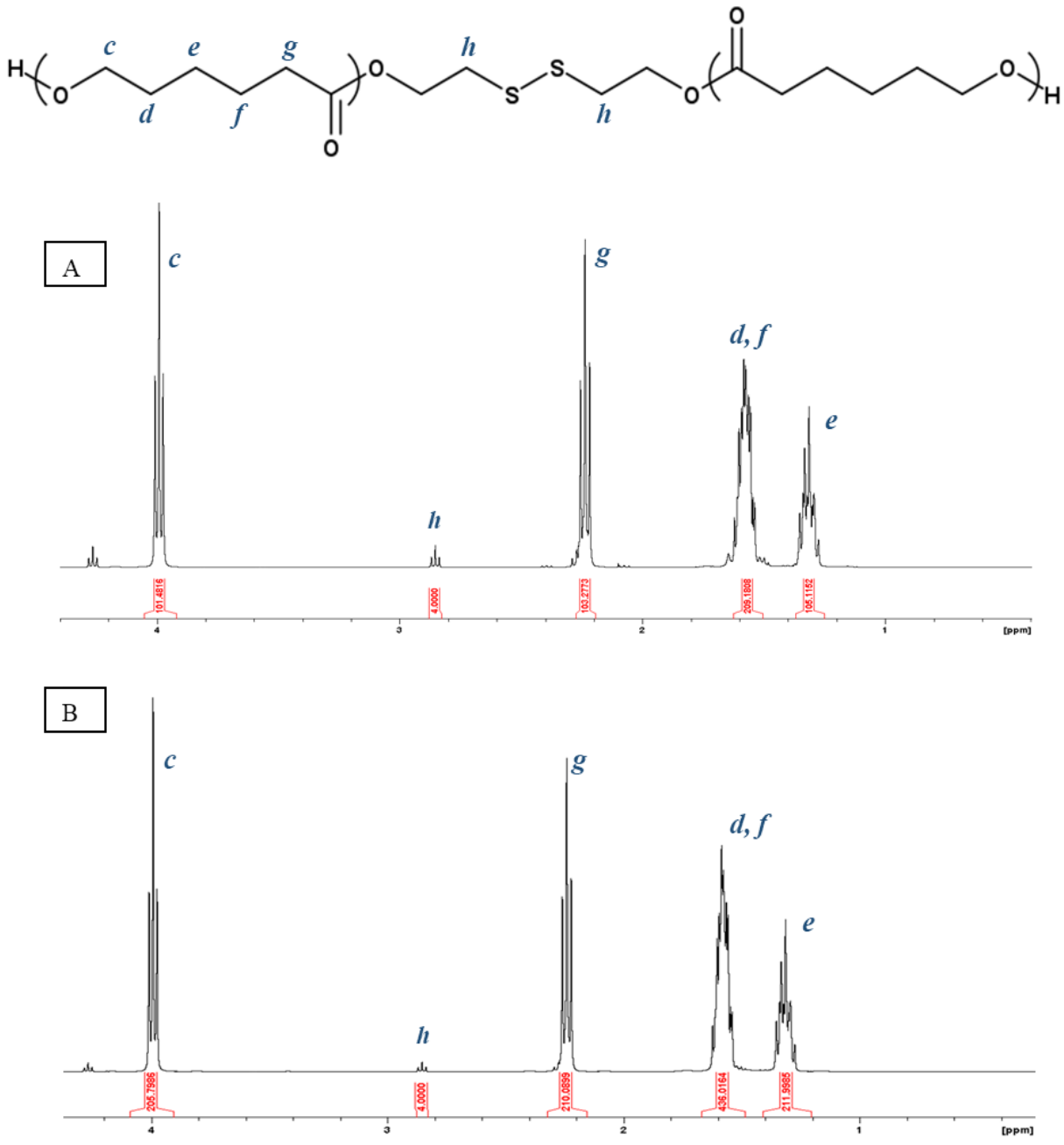

Figure V-S1: ^{1}H-NMR spectrum of PCL_{25}-S-S-PCL_{25} (A) and PCL_{50}-S-S-PCL_{50} (B) homopolymers.

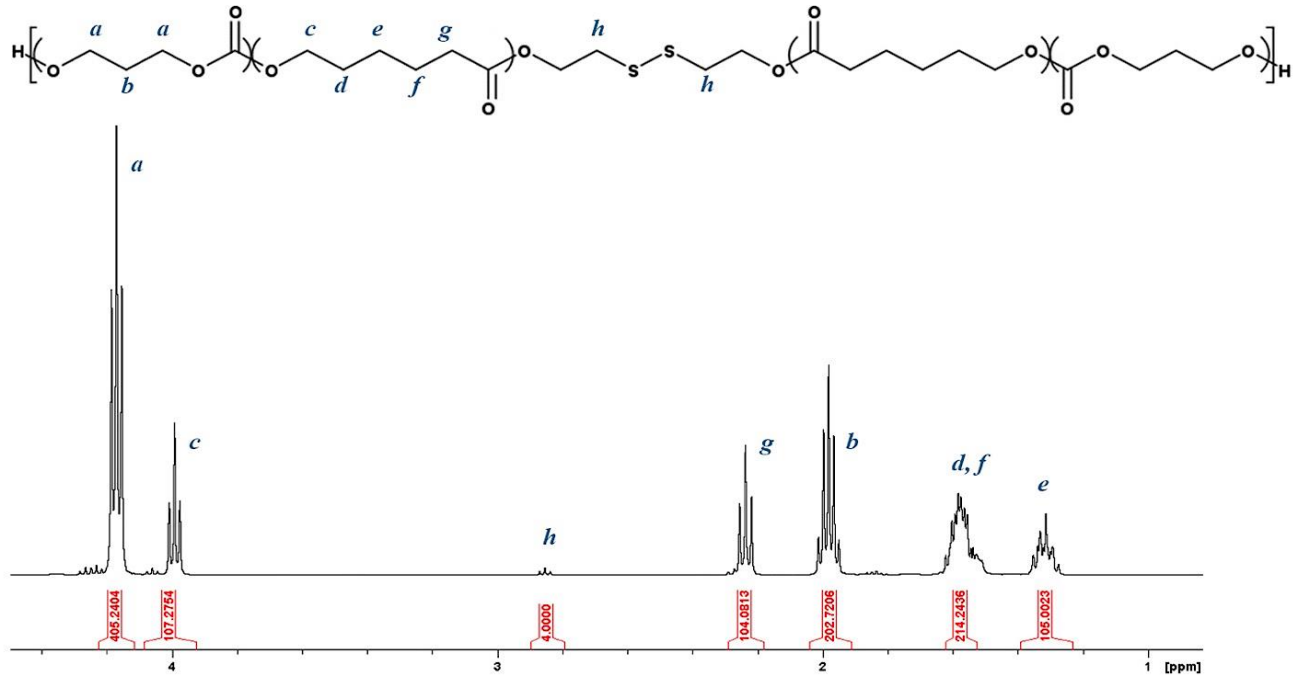

Figure V-S2: ^{1}H-NMR spectrum of $PTMC_{50}$-*b*-PCL_{25}-S-S-PCL_{25}-*b*-$PTMC_{50}$ triblock copolymer with PTMC/PCL molar ratios of 66/34.

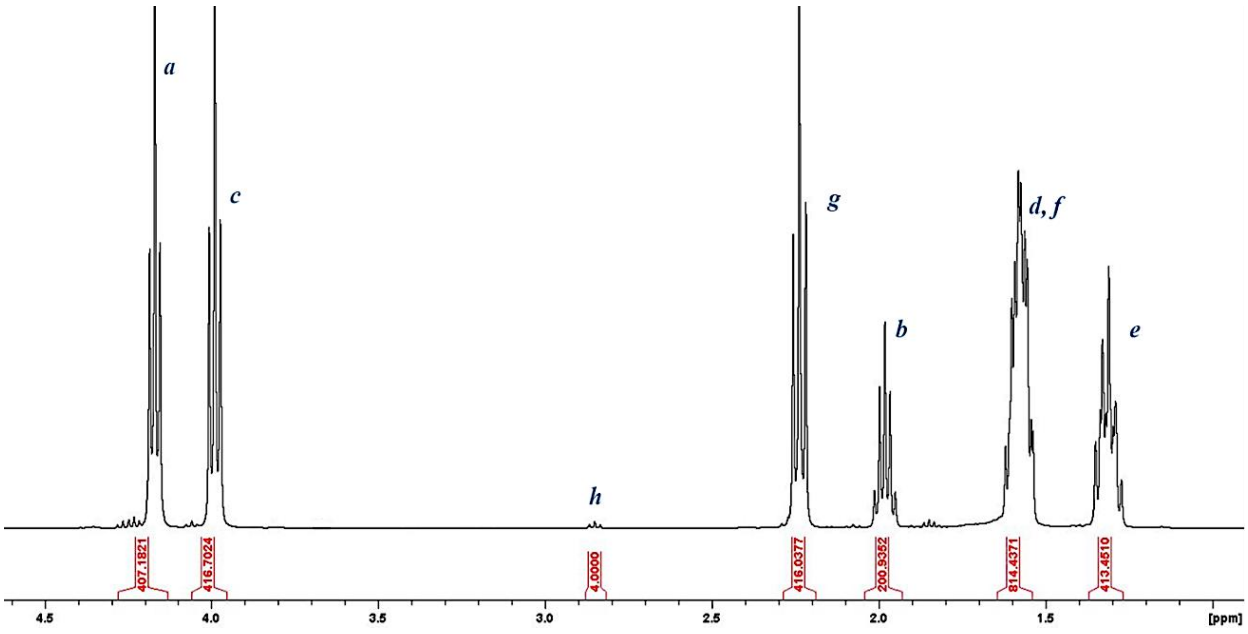

Figure V-S3: ^{1}H-NMR spectrum of $PTMC_{50}$-*b*-PCL_{100}-S-S-PCL_{100}-*b*-$PTMC_{50}$ triblock copolymer with PTMC/PCL molar ratios of 20/80.

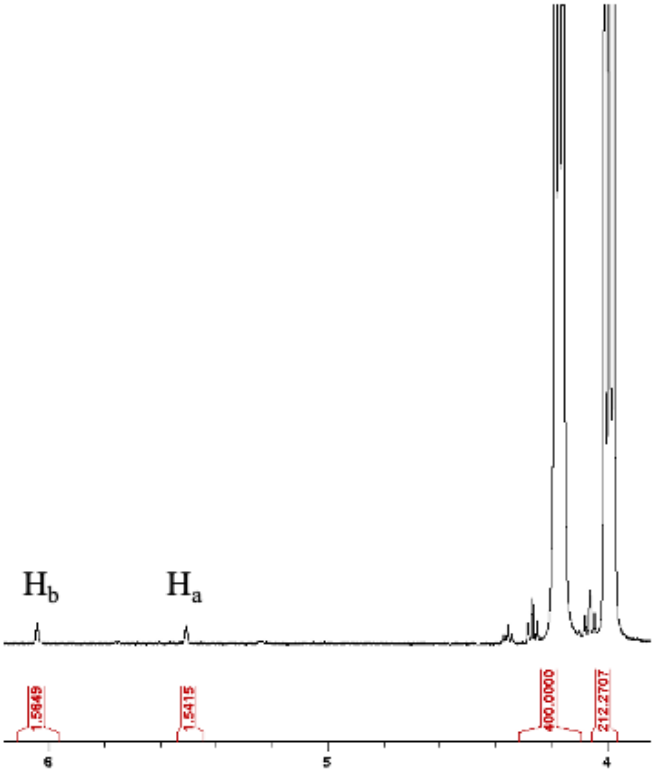

Figure V-S4: ^{1}H-NMR spectrum (4-6 ppm) of end-functionalized PTMC$_{50}$-*b*-PCL$_{50}$-S-S-PCL$_{50}$-*b*-PTMC$_{50}$ dimethacrylate triblock copolymer.

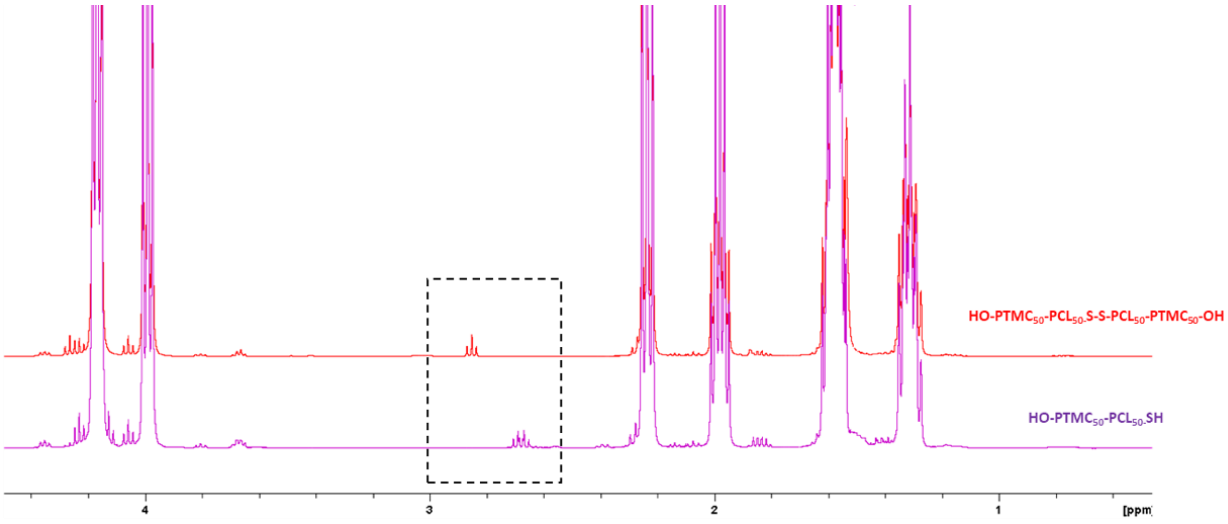

Figure V-S5: ^{1}H-NMR spectrum of PTMC$_{50}$-*b*-PCL$_{50}$-S-S-PCL$_{50}$-*b*-PTMC$_{50}$ BCP (reference, in red) and cleaved PTMC$_{50}$-*b*-PCL$_{50}$-SH BCP (in violet).

References

[1] F. Asghari, M. Samiei, K. Adibkia, A. Akbarzadeh, S. Davaran, *Artif. Cells, Nanomedicine Biotechnol.* **2017**, *45*, 185.

[2] Y. Zhong, P. Godwin, Y. Jin, H. Xiao, *Adv. Ind. Eng. Polym. Res.* **2020**, *3*, 27.

[3] R. P. Brannigan, A. P. Dove, *Biomater. Sci.* **2017**, *5*, 9.

[4] R. Dwivedi, S. Kumar, R. Pandey, A. Mahajan, D. Nandana, D. S. Katti, D. Mehrotra, *J. Oral Biol. Craniofacial Res.* **2020**, *10*, 381.

[5] S. H. Chang, H. J. Lee, S. Park, Y. Kim, B. Jeong, *Biomacromolecules* **2018**, *19*, 2302.

[6] K. Fukushima, *Biomater. Sci.* **2016**, *4*, 9.

[7] D. N. Rocha, P. Brites, C. Fonseca, A. P. Pêgo, *PLoS One* **2014**, *9*.

[8] A. Güney, J. Malda, W. J. A. Dhert, D. W. Grijpma, *Int. J. Artif. Organs* **2017**, *40*, 176.

[9] N. Toshikj, J.-J. Robin, M. Ramonda, S. Catrouillet, S. Blanquer, *ACS Appl. Polym. Mater.* **2021**.

[10] M. D. Rikkou, C. S. Patrickios, *Prog. Polym. Sci.* **2011**, *36*, 1079.

[11] P. J. Hogg, **2003**, *28*, 210.

[12] V. I. Abkevich, E. I. Shakhnovich, **2000**, 975.

[13] L. Mcdowall, M. H. Stenzel, **2014**, 1772.

[14] B. Le Droumaguet, R. Poupart, D. Grande, *Polym. Chem.* **2015**, *6*, 8105.

[15] J. H. Ryu, S. Park, B. Kim, A. Klaikherd, T. P. Russell, S. Thayumanavan, *J. Am. Chem. Soc.* **2009**, *131*, 9870.

[16] M. Pepels, I. Filot, B. Klumperman, H. Goossens, *Polym. Chem.* **2013**, *4*, 4955.

[17] Y. Chujo, K. Sada, A. Naka, R. Nomura, T. Saegusa, *Macromolecules* **1993**, *26*, 883.

[18] G. C. Tesoro, V. Sastri, *J. Appl. Polym. Sci.* **1990**, *39*, 1425.

[19] N. V. Tsarevsky, K. Matyjaszewski, *Macromolecules* **2002**, *35*, 9009.

[20] Y. T. Jia, H. Y. Kim, J. Gong, D. R. Lee, B. Ding, N. Bhattarai, *Polym. Int.* **2004**, *53*, 312.

[21] V. da G. Oliveira, M. F. D. C. Cardoso, L. da S. M. Forezi, *Catalysts* **2018**, *8*.

[22] A. Couffin, D. Delcroix, B. Martín-Vaca, D. Bourissou, C. Navarro, *Macromolecules* **2013**, *46*, 4354.

[23] W. Konigsberg, *Methods Enzymol.* **1972**, *25*, 185.

[24] A. Klaikherd, S. Ghosh, S. Thayumanavan, *Macromolecules* **2007**, *40*, 8518.

[25] J. Bayardon, J. Holz, B. Schäffner, V. Andrushko, S. Verevkin, A. Preetz, A. Börner, *Angew. Chemie - Int. Ed.* **2007**, *46*, 5971.

[26] H. H. Wang, J. T. Jung, J. F. Kim, S. Kim, E. Drioli, Y. M. Lee, *J. Memb. Sci.* **2019**, *574*, 44.

[27] M. Gallei, S. Rangou, V. Filiz, K. Buhr, S. Bolmer, C. Abetz, V. Abetz, *Macromol. Chem. Phys.* **2013**, *214*, 1037.

[28] K. Yu, A. Xin, H. Du, Y. Li, Q. Wang, *NPG Asia Mater.* **2019**, *11*.

[29] R. A. Ortiz, O. A. Berlanga, A. E. G. Valdez, R. A. Flores, J. G. T. Padilla, M. G. M. Padilla, *Adv. Mater. Sci. Eng.* **2016**, *2016*.

[30] E. Rattanangkool, W. Krailat, T. Vilaivan, P. Phuwapraisirisan, M. Sukwattanasinitt, S. Wacharasindhu, *European J. Org. Chem.* **2014**, *2014*, 4795.

CONCLUSION GENERALE

Conclusion générale

Ce travail de thèse fait partie d'un concept élargi de développement de structures à porosités hiérarchiques et contrôlées à base de copolymères à blocs dégradables. Le concept est basé sur la synergie de deux stratégies distinctes, d'un côté l'auto-assemblage de copolymères à blocs pouvant conduire à une porosité nanométrique après une dégradation sélective d'une des phases, et de l'autre côté, le secteur en pleine croissance de la fabrication additive tridimensionnelle produisant des structures poreuses macrométriques. Ce thème suscite actuellement des recherches approfondies pour chacune de ces approches. Étant donné que la première approche d'auto-assemblage des copolymères à blocs dégradables a été très peu explorée jusqu'à maintenant et représente une approche scientifique importante, ce projet de thèse est principalement dédié à cette thématique.

Dans un premier temps, dans le **Chapitre II**, la synthèse parfaitement contrôlée de copolymères triblocs avec des architectures propres, c'est-à-dire sans erreurs d'enchainements, était indispensable pour pouvoir étudier, par la suite, la séparation de phases au sein de ces copolymères triblocs. Des études poussées sur les mécanismes réactionnels différents de la polymérisation par ouverture de cycle nous ont conduit à mettre au point un procédé de synthèse optimal par l'emploi de catalyseurs organiques modernes. Celle-ci est effectuée d'une manière assez rapide sans la présence de réactions secondaires tels que la transestérification, et conduit à une approche généralisée de la production des copolymères triblocs poly(ester) et poly(carbonate) à partir d'un macroamorceur poly(lactide) (Figure A).

Par la suite, les travaux présentés dans le **chapitre III** ont permis de mettre en évidence la première étude avancée sur la séparation de phases de copolymères à blocs entièrement dégradables. Préalablement, **le chapitre (I) bibliographique** a démontré la forte croissance de l'intérêt scientifique pour ce domaine dans les dernières années. Les améliorations apportées à de nombreuses associations de copolymères en vue de la génération de structures auto-assemblées pouvant conduire à des systèmes à porosités contrôlées sont clairement mises en évidence dans ce chapitre. Néanmoins, il s'agit dans tous les cas de copolymères à blocs non-dégradables ou bien, dans le meilleur des cas, présentant un seul des blocs dégradable (le poly(acide lactique) le plus souvent). Les travaux du Chapitre III s'inscrivent dans l'auto-assemblage de copolymères dont les deux blocs sont dégradables, ce qui constitue le caractère innovant de ce travail.

Ainsi, les copolymères triblocs PTMC-*b*-PDLLA-*b*-PTMC, caractérisés comme étant entièrement amorphes, ont conduit à une matrice nanoporeuse de PTMC lors de la dégradation sélective du bloc central de PDLLA (Figure A). En prenant en considération la sensibilité enzymatique du PTMC, cette découverte pourrait être particulièrement utile dans le domaine biomédical. En effet, notamment dans l'ingénierie tissulaire, ce type de porosité contrôlée et nanométrique est particulièrement recherché pour permettre le flux de nutriments nécessaire à la survie cellulaire dans une matrice polymère. Egalement dans le domaine de l'absorption, ce type de système pourrait avoir un grand intérêt, avec comme avancée, cette idée de biodégrader facilement la matrice polymère après utilisation.

Il est reconnu que la séparation de phases de copolymères à blocs est largement plus étudiée sur des structures amorphes afin de se dédouaner des effets de cristallinité. Pour autant, par la maitrise de la cristallinité, l'étude de copolymères semi-cristallins peut apporter son lot de comportements spécifiques et intéressants. C'est pourquoi, en parallèle à l'étude sur les assemblages de copolymères amorphes, un système semi-cristallin de PTMC-*b*-PCL-*b*-PTMC (avec un produit de ségrégation (χN) élevé) a également été exploré. Ainsi, nous avons montré que dans ce cas, deux mécanismes d'organisation macromoléculaire concurrents sont mis en jeu : l'organisation due à la cristallinité et l'auto-assemblage dû à l'incompatibilité thermodynamique des blocs.

Dans le **Chapitre IV**, lors des études morphologiques de ces systèmes, l'impact de la cristallinité sur la séparation de phases thermodynamique est directement visible. Néanmoins, en jouant sur la cinétique de cristallisation, cette séparation de phases thermodynamique prédomine sur la cristallinité permettant ainsi l'accès aux structures de PTMC et PCL auto-assemblées. L'étape de photo-réticulation, largement utilisée dans le chapitre précédent (III) pour conférer une stabilité mécanique aux films minces poreux, s'est avérée aussi utile pour l'implémentation des propriétés à mémoire de forme dans ces copolymères (Figure A). Ce comportement dû à la présence simultanée de réseaux cristallins et réticulés, peut être également une autre ouverture vers des applications biomédicales, notamment dans la conception de dispositifs obtenus par fabrication additive 3D. C'est pourquoi, une preuve de concept de l'imprimabilité 3D par stéréolithographie des résines photosensibles de ce copolymère triblocs dégradable a été apportée.

L'étude du contrôle de la séparation de phases de système semi-cristallin à base de copolymère de PTMC et PCL a permis de mettre en évidence un intérêt non négligeable dans ces matériaux. Néanmoins la PCL pourtant hydrolysable est reconnue pour avoir une cinétique de dégradation très lente, rendant ainsi difficile la génération de porosité par dégradation sélective. Ainsi le **Chapitre V** s'est focalisé sur une stratégie visant à incorporer des liaisons clivables entre les blocs de PTMC et PCL et en vue de pallier la faible dégradabilité du bloc central PCL. Plusieurs types de liaisons clivables ont donc été étudiés sur ces copolymères et seule la stratégie d'incorporation d'un pont disulfure sur la chaine a été fructueuse. Lors du clivage de cette liaison, des propriétés intéressantes peuvent être observées, tels que le passage d'une architecture copolymère triblocs à une structuration diblocs, une perte de la cristallinité ainsi que des changements morphologiques à la surface des films minces pouvant être un indicateur de la création d'un autre type de structures poreuses. Néanmoins, le développement d'une liaison clivable située précisément entre les blocs PTMC et PCL serait indispensable pour aller vers la génération facilitée de porosité. Ceci représente une des **perspectives** majeures de ce projet.

D'autres perspectives sont également envisageables pour la suite de cette thèse, comme par exemple, des études complémentaires sur l'auto-assemblage du copolymère triblocs PTMC-*b*-PDLLA-*b*-PTMC. Il s'agirait d'améliorer les nombreux paramètres du procédé de mise en œuvre des copolymères, comme le choix du solvant, les conditions de *spin-coating* et *d'annealing*, la modification chimique du support de *spin-coating*, etc… Ceci permettrait de générer des architectures à séparation de phases plus variées. Enfin, changer de dimension pour atteindre des structures tridimensionnelles, en couplant la séparation de phases de ces copolymères triblocs avec une technique d'impression 3D par photopolymérisation (comme la stéréolithographie), suivi par une dégradation sélective du bloc central du copolymère pour ainsi générer des systèmes 3D à porosité hiérarchique, serait un aspect intéressant à développer à l'avenir.

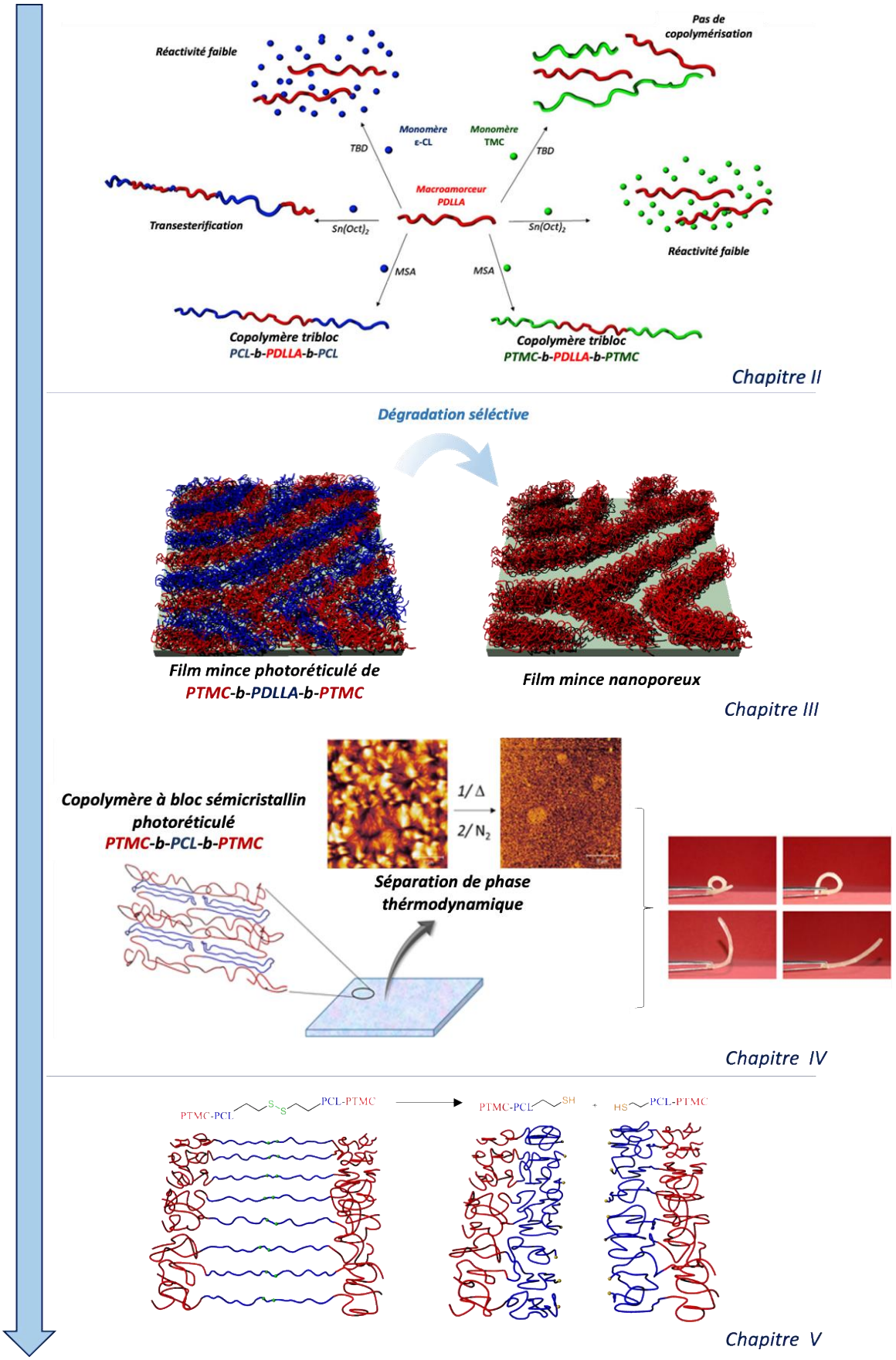

Figure A: Schématisation des travaux effectués dans le projet de thèse.

Synthesis of degradable copolymers and study of their nanostructuration in the view of obtaining porous multifunctional materials

Porous polymers are receiving considerable attention in various disciplines such as energy, biomedical domains, or the environment. Their structure-property relationship must be perfectly mastered and defined in order to achieve the performances required in these fields of application. However, very few techniques allow an achievement of such structures in a controlled and reproductible manner. The **block copolymer phase-separation** represents a serious asset in this perspective, with its ability to generate nanoscale pores by a sacrificial block approach. Nevertheless, the phase-separation of degradable block copolymers remains under-researched, and it represents one of the key points of this study. In addition, responding to the need of developing non-toxic materials with low environmental impact, the use of **degradable structures** is a major requirement of the modern polymer science. Therefore, the objective of this PhD thesis is to develop degradable porous materials based on precisely selected block copolymer associations: one **amorphous (PTMC-*b*-PDLLA-*b*-PTMC)** and the other **semi-crystalline (PTMC-*b*-PCL-*b*-PTMC)**, where both present an interaction parameter (χN) suitable for phase separation.

Since the perfect control and the purity of the block copolymer architectures are being crucial for an efficient phase separation, the initial part of the study was devoted to a **controlled ring-opening polymerization** of these block copolymers while employing modern **organocatalytic** routes. In a second part, an in-depth theoretical and experimental study of the amorphous system self-assembly led to separate **PTMC and PDLLA domains in bicontinuous nanophases**. Selective hydrolysis of the PDLLA block resulted in **nanometer-size porous PTMC matrix** in the form of a **thin film** produced by the spin-coating technique. An additional step of **photo-crosslinking** of the methacrylate end-chain groups allowed a mechanical reinforcement of the porous matrix. It is precisely the photo-crosslinking step, combined with rapid liquid nitrogen quenching, that enabled a suppression of crystallinity and further access to a thermodynamical phase separation in the semi-crystalline system. In addition, the **coexistence of both crystalline and crosslinked** networks in the same structure, has allowed the establishment of advanced **shape memory properties** in these PTMC/PCL block copolymers. The last part of the study was devoted to the use of **cleavable junctions** in the aim to anticipate the slow degradability of the PCL phase. Hence, a cleavage of disulfides, initially located in the middle of the central PCL block, led to materials with interesting physicochemical properties.

Synthèse de copolymères dégradables et étude de leur nanostructuration en vue de l'obtention de matériaux poreux multifonctionnels

Les polymères poreux suscitent une attention considérable dans diverses disciplines comme l'énergie, les applications biomédicales ou l'environnement. Les relations structure-propriétés doivent être parfaitement définies et maîtrisées pour pouvoir atteindre les performances requises dans ces domaines d'applications. Cependant, très peu de techniques permettent d'obtenir de telles structures contrôlées et de façon reproductible. La **séparation de phases de copolymères à blocs** est un atout dans cette perspective avec sa capacité à générer des pores à l'échelle nanométrique par une approche de bloc sacrificiel. Pour autant, la séparation de phases de copolymères à blocs dégradables reste encore trop peu étudiée, et elle représente un des points clés de ce travail. De plus, répondant à la nécessité de développer des matériaux à faible impact environnemental et non toxiques, l'exploitation de **structures dégradables** est une exigence majeure de la science des polymères actuelle. Par conséquent, l'objectif de cette thèse est de développer des polymères poreux dégradables à base de copolymères à blocs précisément sélectionnés : l'un **amorphe (PTMC-*b*-PDLLA-*b*-PTMC)** et l'autre **semi-cristallin (PTMC-*b*-PCL-*b*-PTMC)**, où les deux présentent un paramètre d'interaction (χN) adapté à la séparation de phases.

La parfaite maîtrise et la pureté des architectures des copolymères à blocs étant cruciales pour une séparation de phases efficace, la première partie de l'étude a été consacrée à une **polymérisation par ouverture de cycle maîtrisée** de ces copolymères tout en utilisant des voies **organocatalytiques** modernes. Dans une deuxième partie, une étude théorique et expérimentale approfondie de l'auto-assemblage du système amorphe a conduit à des **domaines PTMC et PDLLA séparés dans des nanophases bicontinues**. L'hydrolyse sélective du bloc PDLLA a abouti à une **matrice de PTMC poreuse** de dimension nanométrique sous la forme d'un **film mince** produit par *spin-coating*. Une étape supplémentaire de **photoréticulation** des groupes méthacrylates en bouts de chaîne a permis le renforcement mécanique de la matrice poreuse. C'est précisément l'étape de photoréticulation, combinée à une trempe rapide à l'azote liquide, qui a permis une suppression de la cristallinité et un accès à la séparation de phases thermodynamique dans les systèmes semi-cristallins. De plus, la **coexistence d'un réseau cristallin et réticulé** a permis l'établissement de propriétés avancées de **mémoire de forme** dans ces copolymères PTMC/PCL. La dernière partie de l'étude a été consacrée à l'utilisation de **liaisons clivables** pour anticiper la lente dégradabilité de la phase PCL. Un clivage de la jonction disulfure, initialement située au milieu du bloc PCL central, a permis d'obtenir des matériaux aux propriétés physico-chimiques intéressantes.